

Deep Learning

Ian Goodfellow
Yoshua Bengio
Aaron Courville

Part II

Contents

Website	vii
Acknowledgments	viii
Notation	xi
1 Introduction	1
1.1 Who Should Read This Book?	8
1.2 Historical Trends in Deep Learning	11
I Applied Math and Machine Learning Basics	29
2 Linear Algebra	31
2.1 Scalars, Vectors, Matrices and Tensors	31
2.2 Multiplying Matrices and Vectors	34
2.3 Identity and Inverse Matrices	36
2.4 Linear Dependence and Span	37
2.5 Norms	39
2.6 Special Kinds of Matrices and Vectors	40
2.7 Eigendecomposition	42
2.8 Singular Value Decomposition	44
2.9 The Moore-Penrose Pseudoinverse	45
2.10 The Trace Operator	46
2.11 The Determinant	47
2.12 Example: Principal Components Analysis	48
3 Probability and Information Theory	53
3.1 Why Probability?	54

3.2	Random Variables	56
3.3	Probability Distributions	56
3.4	Marginal Probability	58
3.5	Conditional Probability	59
3.6	The Chain Rule of Conditional Probabilities	59
3.7	Independence and Conditional Independence	60
3.8	Expectation, Variance and Covariance	60
3.9	Common Probability Distributions	62
3.10	Useful Properties of Common Functions	67
3.11	Bayes' Rule	70
3.12	Technical Details of Continuous Variables	71
3.13	Information Theory	73
3.14	Structured Probabilistic Models	75
4	Numerical Computation	80
4.1	Overflow and Underflow	80
4.2	Poor Conditioning	82
4.3	Gradient-Based Optimization	82
4.4	Constrained Optimization	93
4.5	Example: Linear Least Squares	96
5	Machine Learning Basics	98
5.1	Learning Algorithms	99
5.2	Capacity, Overfitting and Underfitting	110
5.3	Hyperparameters and Validation Sets	120
5.4	Estimators, Bias and Variance	122
5.5	Maximum Likelihood Estimation	131
5.6	Bayesian Statistics	135
5.7	Supervised Learning Algorithms	140
5.8	Unsupervised Learning Algorithms	146
5.9	Stochastic Gradient Descent	151
5.10	Building a Machine Learning Algorithm	153
5.11	Challenges Motivating Deep Learning	155
II	Deep Networks: Modern Practices	166
6	Deep Feedforward Networks	168
6.1	Example: Learning XOR	171
6.2	Gradient-Based Learning	177

6.3	Hidden Units	191
6.4	Architecture Design	197
6.5	Back-Propagation and Other Differentiation Algorithms	204
6.6	Historical Notes	224
7	Regularization for Deep Learning	228
7.1	Parameter Norm Penalties	230
7.2	Norm Penalties as Constrained Optimization	237
7.3	Regularization and Under-Constrained Problems	239
7.4	Dataset Augmentation	240
7.5	Noise Robustness	242
7.6	Semi-Supervised Learning	243
7.7	Multi-Task Learning	244
7.8	Early Stopping	246
7.9	Parameter Tying and Parameter Sharing	253
7.10	Sparse Representations	254
7.11	Bagging and Other Ensemble Methods	256
7.12	Dropout	258
7.13	Adversarial Training	268
7.14	Tangent Distance, Tangent Prop, and Manifold Tangent Classifier	270
8	Optimization for Training Deep Models	274
8.1	How Learning Differs from Pure Optimization	275
8.2	Challenges in Neural Network Optimization	282
8.3	Basic Algorithms	294
8.4	Parameter Initialization Strategies	301
8.5	Algorithms with Adaptive Learning Rates	306
8.6	Approximate Second-Order Methods	310
8.7	Optimization Strategies and Meta-Algorithms	317
9	Convolutional Networks	330
9.1	The Convolution Operation	331
9.2	Motivation	335
9.3	Pooling	339
9.4	Convolution and Pooling as an Infinitely Strong Prior	345
9.5	Variants of the Basic Convolution Function	347
9.6	Structured Outputs	358
9.7	Data Types	360
9.8	Efficient Convolution Algorithms	362
9.9	Random or Unsupervised Features	363

9.10	The Neuroscientific Basis for Convolutional Networks	364
9.11	Convolutional Networks and the History of Deep Learning	371
10	Sequence Modeling: Recurrent and Recursive Nets	373
10.1	Unfolding Computational Graphs	375
10.2	Recurrent Neural Networks	378
10.3	Bidirectional RNNs	394
10.4	Encoder-Decoder Sequence-to-Sequence Architectures	396
10.5	Deep Recurrent Networks	398
10.6	Recursive Neural Networks	400
10.7	The Challenge of Long-Term Dependencies	401
10.8	Echo State Networks	404
10.9	Leaky Units and Other Strategies for Multiple Time Scales	406
10.10	The Long Short-Term Memory and Other Gated RNNs	408
10.11	Optimization for Long-Term Dependencies	413
10.12	Explicit Memory	416
11	Practical Methodology	421
11.1	Performance Metrics	422
11.2	Default Baseline Models	425
11.3	Determining Whether to Gather More Data	426
11.4	Selecting Hyperparameters	427
11.5	Debugging Strategies	436
11.6	Example: Multi-Digit Number Recognition	440
12	Applications	443
12.1	Large-Scale Deep Learning	443
12.2	Computer Vision	452
12.3	Speech Recognition	458
12.4	Natural Language Processing	461
12.5	Other Applications	478
III	Deep Learning Research	486
13	Linear Factor Models	489
13.1	Probabilistic PCA and Factor Analysis	490
13.2	Independent Component Analysis (ICA)	491
13.3	Slow Feature Analysis	493
13.4	Sparse Coding	496

13.5	Manifold Interpretation of PCA	499
14	Autoencoders	502
14.1	Undercomplete Autoencoders	503
14.2	Regularized Autoencoders	504
14.3	Representational Power, Layer Size and Depth	508
14.4	Stochastic Encoders and Decoders	509
14.5	Denoising Autoencoders	510
14.6	Learning Manifolds with Autoencoders	515
14.7	Contractive Autoencoders	521
14.8	Predictive Sparse Decomposition	523
14.9	Applications of Autoencoders	524
15	Representation Learning	526
15.1	Greedy Layer-Wise Unsupervised Pretraining	528
15.2	Transfer Learning and Domain Adaptation	536
15.3	Semi-Supervised Disentangling of Causal Factors	541
15.4	Distributed Representation	546
15.5	Exponential Gains from Depth	553
15.6	Providing Clues to Discover Underlying Causes	554
16	Structured Probabilistic Models for Deep Learning	558
16.1	The Challenge of Unstructured Modeling	559
16.2	Using Graphs to Describe Model Structure	563
16.3	Sampling from Graphical Models	580
16.4	Advantages of Structured Modeling	582
16.5	Learning about Dependencies	582
16.6	Inference and Approximate Inference	584
16.7	The Deep Learning Approach to Structured Probabilistic Models	585
17	Monte Carlo Methods	590
17.1	Sampling and Monte Carlo Methods	590
17.2	Importance Sampling	592
17.3	Markov Chain Monte Carlo Methods	595
17.4	Gibbs Sampling	599
17.5	The Challenge of Mixing between Separated Modes	599
18	Confronting the Partition Function	605
18.1	The Log-Likelihood Gradient	606
18.2	Stochastic Maximum Likelihood and Contrastive Divergence	607

18.3	Pseudolikelihood	615
18.4	Score Matching and Ratio Matching	617
18.5	Denoising Score Matching	619
18.6	Noise-Contrastive Estimation	620
18.7	Estimating the Partition Function	623
19	Approximate Inference	631
19.1	Inference as Optimization	633
19.2	Expectation Maximization	634
19.3	MAP Inference and Sparse Coding	635
19.4	Variational Inference and Learning	638
19.5	Learned Approximate Inference	651
20	Deep Generative Models	654
20.1	Boltzmann Machines	654
20.2	Restricted Boltzmann Machines	656
20.3	Deep Belief Networks	660
20.4	Deep Boltzmann Machines	663
20.5	Boltzmann Machines for Real-Valued Data	676
20.6	Convolutional Boltzmann Machines	683
20.7	Boltzmann Machines for Structured or Sequential Outputs	685
20.8	Other Boltzmann Machines	686
20.9	Back-Propagation through Random Operations	687
20.10	Directed Generative Nets	692
20.11	Drawing Samples from Autoencoders	711
20.12	Generative Stochastic Networks	714
20.13	Other Generation Schemes	716
20.14	Evaluating Generative Models	717
20.15	Conclusion	720
	Bibliography	721
	Index	777

Website

www.deeplearningbook.org

This book is accompanied by the above website. The website provides a variety of supplementary material, including exercises, lecture slides, corrections of mistakes, and other resources that should be useful to both readers and instructors.

Acknowledgments

This book would not have been possible without the contributions of many people.

We would like to thank those who commented on our proposal for the book and helped plan its contents and organization: Guillaume Alain, Kyunghyun Cho, Çağlar Gülcöhre, David Krueger, Hugo Larochelle, Razvan Pascanu and Thomas Rohée.

We would like to thank the people who offered feedback on the content of the book itself. Some offered feedback on many chapters: Martín Abadi, Guillaume Alain, Ion Androutsopoulos, Fred Bertsch, Olexa Bilaniuk, Ufuk Can Biçici, Matko Bošnjak, John Boersma, Greg Brockman, Alexandre de Brébisson, Pierre Luc Carrier, Sarath Chandar, Paweł Chilinski, Mark Daoust, Oleg Dashevskii, Laurent Dinh, Stephan Dreseitl, Jim Fan, Miao Fan, Meire Fortunato, Frédéric Francis, Nando de Freitas, Çağlar Gülcöhre, Jurgen Van Gael, Javier Alonso García, Jonathan Hunt, Gopi Jeyaram, Chingiz Kabytayev, Lukasz Kaiser, Varun Kanade, Asifullah Khan, Akiel Khan, John King, Diederik P. Kingma, Yann LeCun, Rudolf Mathey, Matías Mattamala, Abhinav Maurya, Kevin Murphy, Oleg Mürk, Roman Novak, Augustus Q. Odena, Simon Pavlik, Karl Pichotta, Eddie Pierce, Kari Pulli, Roussel Rahman, Tapani Raiko, Anurag Ranjan, Johannes Roith, Mihaela Rosca, Halis Sak, César Salgado, Grigory Sapunov, Yoshinori Sasaki, Mike Schuster, Julian Serban, Nir Shabat, Ken Shirriff, Andre Simpelo, Scott Stanley, David Sussillo, Ilya Sutskever, Carles Gelada Sáez, Graham Taylor, Valentin Tolmer, Massimiliano Tomassoli, An Tran, Shubhendu Trivedi, Alexey Umnov, Vincent Vanhoucke, Marco Visentini-Scarzanella, Martin Vita, David Warde-Farley, Dustin Webb, Kelvin Xu, Wei Xue, Ke Yang, Li Yao, Zygmunt Zajac and Ozan Çağlayan.

We would also like to thank those who provided us with useful feedback on individual chapters:

- **Notation:** Zhang Yuanhang.
- **Chapter 1, Introduction:** Yusuf Akgul, Sébastien Bratieres, Samira Ebrahimi,

Charlie Gorichanaz, Brendan Loudermilk, Eric Morris, Cosmin Pârvulescu and Alfredo Solano.

- Chapter 2, **Linear Algebra**: Amjad Almahairi, Nikola Banić, Kevin Bennett, Philippe Castonguay, Oscar Chang, Eric Fosler-Lussier, Andrey Khalyavin, Sergey Oreshkov, István Petrás, Dennis Prangle, Thomas Rohée, Gitanjali Gulve Sehgal, Colby Toland, Alessandro Vitale and Bob Welland.
- Chapter 3, **Probability and Information Theory**: John Philip Anderson, Kai Arulkumaran, Vincent Dumoulin, Rui Fa, Stephan Gouws, Artem Oboturov, Antti Rasmus, Alexey Surkov and Volker Tresp.
- Chapter 4, **Numerical Computation**: Tran Lam An Ian Fischer and Hu Yuhuang.
- Chapter 5, **Machine Learning Basics**: Dzmitry Bahdanau, Justin Domingue, Nikhil Garg, Makoto Otsuka, Bob Pepin, Philip Popien, Emmanuel Rayner, Peter Shepard, Kee-Bong Song, Zheng Sun and Andy Wu.
- Chapter 6, **Deep Feedforward Networks**: Uriel Berdugo, Fabrizio Bottarel, Elizabeth Burl, Ishan Durugkar, Jeff Hlywa, Jong Wook Kim, David Krueger and Aditya Kumar Praharaj.
- Chapter 7, **Regularization for Deep Learning**: Morten Kolbæk, Kshitij Lauria, Inkyu Lee, Sunil Mohan, Hai Phong Phan and Joshua Salisbury.
- Chapter 8, **Optimization for Training Deep Models**: Marcel Ackermann, Peter Armitage, Rowel Atienza, Andrew Brock, Tegan Maharaj, James Martens, Kashif Rasul, Klaus Strobl and Nicholas Turner.
- Chapter 9, **Convolutional Networks**: Martín Arjovsky, Eugene Brevdo, Konstantin Divilov, Eric Jensen, Mehdi Mirza, Alex Paino, Marjorie Sayer, Ryan Stout and Wentao Wu.
- Chapter 10, **Sequence Modeling: Recurrent and Recursive Nets**: Gökçen Eraslan, Steven Hickson, Razvan Pascanu, Lorenzo von Ritter, Rui Rodrigues, Dmitriy Serdyuk, Dongyu Shi and Kaiyu Yang.
- Chapter 11, **Practical Methodology**: Daniel Beckstein.
- Chapter 12, **Applications**: George Dahl, Vladimir Nekrasov and Ribana Roscher.
- Chapter 13, **Linear Factor Models**: Jayanth Koushik.

- Chapter 15, **Representation Learning**: Kunal Ghosh.
- Chapter 16, **Structured Probabilistic Models for Deep Learning**: Minh Lê and Anton Varfolom.
- Chapter 18, **Confronting the Partition Function**: Sam Bowman.
- Chapter 19, **Approximate Inference**: Yujia Bao.
- Chapter 20, **Deep Generative Models**: Nicolas Chapados, Daniel Galvez, Wenming Ma, Fady Medhat, Shakir Mohamed and Grégoire Montavon.
- Bibliography: Lukas Michelbacher and Leslie N. Smith.

We also want to thank those who allowed us to reproduce images, figures or data from their publications. We indicate their contributions in the figure captions throughout the text.

We would like to thank Lu Wang for writing pdf2htmlEX, which we used to make the web version of the book, and for offering support to improve the quality of the resulting HTML.

We would like to thank Ian’s wife Daniela Flori Goodfellow for patiently supporting Ian during the writing of the book as well as for help with proofreading.

We would like to thank the Google Brain team for providing an intellectual environment where Ian could devote a tremendous amount of time to writing this book and receive feedback and guidance from colleagues. We would especially like to thank Ian’s former manager, Greg Corrado, and his current manager, Samy Bengio, for their support of this project. Finally, we would like to thank Geoffrey Hinton for encouragement when writing was difficult.

Notation

This section provides a concise reference describing the notation used throughout this book. If you are unfamiliar with any of the corresponding mathematical concepts, we describe most of these ideas in chapters 2–4.

Numbers and Arrays

a	A scalar (integer or real)
\mathbf{a}	A vector
\mathbf{A}	A matrix
\mathbf{A}	A tensor
\mathbf{I}_n	Identity matrix with n rows and n columns
\mathbf{I}	Identity matrix with dimensionality implied by context
$\mathbf{e}^{(i)}$	Standard basis vector $[0, \dots, 0, 1, 0, \dots, 0]$ with a 1 at position i
$\text{diag}(\mathbf{a})$	A square, diagonal matrix with diagonal entries given by \mathbf{a}
\mathbf{a}	A scalar random variable
\mathbf{a}	A vector-valued random variable
\mathbf{A}	A matrix-valued random variable

Sets and Graphs

\mathbb{A}	A set
\mathbb{R}	The set of real numbers
$\{0, 1\}$	The set containing 0 and 1
$\{0, 1, \dots, n\}$	The set of all integers between 0 and n
$[a, b]$	The real interval including a and b
$(a, b]$	The real interval excluding a but including b
$\mathbb{A} \setminus \mathbb{B}$	Set subtraction, i.e., the set containing the elements of \mathbb{A} that are not in \mathbb{B}
\mathcal{G}	A graph
$Pa_{\mathcal{G}}(x_i)$	The parents of x_i in \mathcal{G}

Indexing

a_i	Element i of vector \mathbf{a} , with indexing starting at 1
a_{-i}	All elements of vector \mathbf{a} except for element i
$A_{i,j}$	Element i, j of matrix \mathbf{A}
$\mathbf{A}_{i,:}$	Row i of matrix \mathbf{A}
$\mathbf{A}_{:,i}$	Column i of matrix \mathbf{A}
$A_{i,j,k}$	Element (i, j, k) of a 3-D tensor \mathbf{A}
$\mathbf{A}_{(:,:,i)}$	2-D slice of a 3-D tensor
a_i	Element i of the random vector \mathbf{a}

Linear Algebra Operations

\mathbf{A}^\top	Transpose of matrix \mathbf{A}
\mathbf{A}^+	Moore-Penrose pseudoinverse of \mathbf{A}
$\mathbf{A} \odot \mathbf{B}$	Element-wise (Hadamard) product of \mathbf{A} and \mathbf{B}
$\det(\mathbf{A})$	Determinant of \mathbf{A}

Calculus

$\frac{dy}{dx}$	Derivative of y with respect to x
$\frac{\partial y}{\partial x}$	Partial derivative of y with respect to x
$\nabla_{\mathbf{x}} y$	Gradient of y with respect to \mathbf{x}
$\nabla_{\mathbf{X}} y$	Matrix derivatives of y with respect to \mathbf{X}
$\nabla_{\mathbf{X}} \mathbf{y}$	Tensor containing derivatives of y with respect to \mathbf{X}
$\frac{\partial f}{\partial \mathbf{x}}$	Jacobian matrix $\mathbf{J} \in \mathbb{R}^{m \times n}$ of $f : \mathbb{R}^n \rightarrow \mathbb{R}^m$
$\nabla_{\mathbf{x}}^2 f(\mathbf{x})$ or $\mathbf{H}(f)(\mathbf{x})$	The Hessian matrix of f at input point \mathbf{x}
$\int f(\mathbf{x}) d\mathbf{x}$	Definite integral over the entire domain of \mathbf{x}
$\int_{\mathbb{S}} f(\mathbf{x}) d\mathbf{x}$	Definite integral with respect to \mathbf{x} over the set \mathbb{S}

Probability and Information Theory

$a \perp b$	The random variables a and b are independent
$a \perp b \mid c$	They are conditionally independent given c
$P(a)$	A probability distribution over a discrete variable
$p(a)$	A probability distribution over a continuous variable, or over a variable whose type has not been specified
$a \sim P$	Random variable a has distribution P
$\mathbb{E}_{x \sim P}[f(x)]$ or $\mathbb{E}f(x)$	Expectation of $f(x)$ with respect to $P(x)$
$\text{Var}(f(x))$	Variance of $f(x)$ under $P(x)$
$\text{Cov}(f(x), g(x))$	Covariance of $f(x)$ and $g(x)$ under $P(x)$
$H(x)$	Shannon entropy of the random variable x
$D_{\text{KL}}(P \parallel Q)$	Kullback-Leibler divergence of P and Q
$\mathcal{N}(\mathbf{x}; \boldsymbol{\mu}, \boldsymbol{\Sigma})$	Gaussian distribution over \mathbf{x} with mean $\boldsymbol{\mu}$ and covariance $\boldsymbol{\Sigma}$

Functions

$f : \mathbb{A} \rightarrow \mathbb{B}$	The function f with domain \mathbb{A} and range \mathbb{B}
$f \circ g$	Composition of the functions f and g
$f(\mathbf{x}; \boldsymbol{\theta})$	A function of \mathbf{x} parametrized by $\boldsymbol{\theta}$. (Sometimes we write $f(\mathbf{x})$ and omit the argument $\boldsymbol{\theta}$ to lighten notation)
$\log x$	Natural logarithm of x
$\sigma(x)$	Logistic sigmoid, $\frac{1}{1 + \exp(-x)}$
$\zeta(x)$	Softplus, $\log(1 + \exp(x))$
$\ \mathbf{x}\ _p$	L^p norm of \mathbf{x}
$\ \mathbf{x}\ $	L^2 norm of \mathbf{x}
x^+	Positive part of x , i.e., $\max(0, x)$
$\mathbf{1}_{\text{condition}}$	is 1 if the condition is true, 0 otherwise

Sometimes we use a function f whose argument is a scalar but apply it to a vector, matrix, or tensor: $f(\mathbf{x})$, $f(\mathbf{X})$, or $f(\mathbf{X})$. This denotes the application of f to the array element-wise. For example, if $\mathbf{C} = \sigma(\mathbf{X})$, then $C_{i,j,k} = \sigma(X_{i,j,k})$ for all valid values of i , j and k .

Datasets and Distributions

p_{data}	The data generating distribution
\hat{p}_{data}	The empirical distribution defined by the training set
\mathbb{X}	A set of training examples
$\mathbf{x}^{(i)}$	The i -th example (input) from a dataset
$y^{(i)}$ or $\mathbf{y}^{(i)}$	The target associated with $\mathbf{x}^{(i)}$ for supervised learning
\mathbf{X}	The $m \times n$ matrix with input example $\mathbf{x}^{(i)}$ in row $\mathbf{X}_{i,:}$

Part II

Deep Networks: Modern Practices

This part of the book summarizes the state of modern deep learning as it is used to solve practical applications.

Deep learning has a long history and many aspirations. Several approaches have been proposed that have yet to entirely bear fruit. Several ambitious goals have yet to be realized. These less-developed branches of deep learning appear in the final part of the book.

This part focuses only on those approaches that are essentially working technologies that are already used heavily in industry.

Modern deep learning provides a very powerful framework for supervised learning. By adding more layers and more units within a layer, a deep network can represent functions of increasing complexity. Most tasks that consist of mapping an input vector to an output vector, and that are easy for a person to do rapidly, can be accomplished via deep learning, given sufficiently large models and sufficiently large datasets of labeled training examples. Other tasks, that can not be described as associating one vector to another, or that are difficult enough that a person would require time to think and reflect in order to accomplish the task, remain beyond the scope of deep learning for now.

This part of the book describes the core parametric function approximation technology that is behind nearly all modern practical applications of deep learning. We begin by describing the feedforward deep network model that is used to represent these functions. Next, we present advanced techniques for regularization and optimization of such models. Scaling these models to large inputs such as high resolution images or long temporal sequences requires specialization. We introduce the convolutional network for scaling to large images and the recurrent neural network for processing temporal sequences. Finally, we present general guidelines for the practical methodology involved in designing, building, and configuring an application involving deep learning, and review some of the applications of deep learning.

These chapters are the most important for a practitioner—someone who wants to begin implementing and using deep learning algorithms to solve real-world problems today.

Chapter 6

Deep Feedforward Networks

Deep feedforward networks, also often called **feedforward neural networks**, or **multilayer perceptrons** (MLPs), are the quintessential deep learning models. The goal of a feedforward network is to approximate some function f^* . For example, for a classifier, $y = f^*(\mathbf{x})$ maps an input \mathbf{x} to a category y . A feedforward network defines a mapping $\mathbf{y} = f(\mathbf{x}; \boldsymbol{\theta})$ and learns the value of the parameters $\boldsymbol{\theta}$ that result in the best function approximation.

These models are called **feedforward** because information flows through the function being evaluated from \mathbf{x} , through the intermediate computations used to define f , and finally to the output \mathbf{y} . There are no **feedback** connections in which outputs of the model are fed back into itself. When feedforward neural networks are extended to include feedback connections, they are called **recurrent neural networks**, presented in chapter 10.

Feedforward networks are of extreme importance to machine learning practitioners. They form the basis of many important commercial applications. For example, the convolutional networks used for object recognition from photos are a specialized kind of feedforward network. Feedforward networks are a conceptual stepping stone on the path to recurrent networks, which power many natural language applications.

Feedforward neural networks are called **networks** because they are typically represented by composing together many different functions. The model is associated with a directed acyclic graph describing how the functions are composed together. For example, we might have three functions $f^{(1)}$, $f^{(2)}$, and $f^{(3)}$ connected in a chain, to form $f(\mathbf{x}) = f^{(3)}(f^{(2)}(f^{(1)}(\mathbf{x})))$. These chain structures are the most commonly used structures of neural networks. In this case, $f^{(1)}$ is called the **first layer** of the network, $f^{(2)}$ is called the **second layer**, and so on. The overall

length of the chain gives the **depth** of the model. It is from this terminology that the name “deep learning” arises. The final layer of a feedforward network is called the **output layer**. During neural network training, we drive $f(\mathbf{x})$ to match $f^*(\mathbf{x})$. The training data provides us with noisy, approximate examples of $f^*(\mathbf{x})$ evaluated at different training points. Each example \mathbf{x} is accompanied by a label $y \approx f^*(\mathbf{x})$. The training examples specify directly what the output layer must do at each point \mathbf{x} ; it must produce a value that is close to y . The behavior of the other layers is not directly specified by the training data. The learning algorithm must decide how to use those layers to produce the desired output, but the training data does not say what each individual layer should do. Instead, the learning algorithm must decide how to use these layers to best implement an approximation of f^* . Because the training data does not show the desired output for each of these layers, these layers are called **hidden layers**.

Finally, these networks are called *neural* because they are loosely inspired by neuroscience. Each hidden layer of the network is typically vector-valued. The dimensionality of these hidden layers determines the **width** of the model. Each element of the vector may be interpreted as playing a role analogous to a neuron. Rather than thinking of the layer as representing a single vector-to-vector function, we can also think of the layer as consisting of many **units** that act in parallel, each representing a vector-to-scalar function. Each unit resembles a neuron in the sense that it receives input from many other units and computes its own activation value. The idea of using many layers of vector-valued representation is drawn from neuroscience. The choice of the functions $f^{(i)}(\mathbf{x})$ used to compute these representations is also loosely guided by neuroscientific observations about the functions that biological neurons compute. However, modern neural network research is guided by many mathematical and engineering disciplines, and the goal of neural networks is not to perfectly model the brain. It is best to think of feedforward networks as function approximation machines that are designed to achieve statistical generalization, occasionally drawing some insights from what we know about the brain, rather than as models of brain function.

One way to understand feedforward networks is to begin with linear models and consider how to overcome their limitations. Linear models, such as logistic regression and linear regression, are appealing because they may be fit efficiently and reliably, either in closed form or with convex optimization. Linear models also have the obvious defect that the model capacity is limited to linear functions, so the model cannot understand the interaction between any two input variables.

To extend linear models to represent nonlinear functions of \mathbf{x} , we can apply the linear model not to \mathbf{x} itself but to a transformed input $\phi(\mathbf{x})$, where ϕ is a

nonlinear transformation. Equivalently, we can apply the kernel trick described in section 5.7.2, to obtain a nonlinear learning algorithm based on implicitly applying the ϕ mapping. We can think of ϕ as providing a set of features describing \mathbf{x} , or as providing a new representation for \mathbf{x} .

The question is then how to choose the mapping ϕ .

1. One option is to use a very generic ϕ , such as the infinite-dimensional ϕ that is implicitly used by kernel machines based on the RBF kernel. If $\phi(\mathbf{x})$ is of high enough dimension, we can always have enough capacity to fit the training set, but generalization to the test set often remains poor. Very generic feature mappings are usually based only on the principle of local smoothness and do not encode enough prior information to solve advanced problems.
2. Another option is to manually engineer ϕ . Until the advent of deep learning, this was the dominant approach. This approach requires decades of human effort for each separate task, with practitioners specializing in different domains such as speech recognition or computer vision, and with little transfer between domains.
3. The strategy of deep learning is to learn ϕ . In this approach, we have a model $y = f(\mathbf{x}; \boldsymbol{\theta}, \mathbf{w}) = \phi(\mathbf{x}; \boldsymbol{\theta})^\top \mathbf{w}$. We now have parameters $\boldsymbol{\theta}$ that we use to learn ϕ from a broad class of functions, and parameters \mathbf{w} that map from $\phi(\mathbf{x})$ to the desired output. This is an example of a deep feedforward network, with ϕ defining a hidden layer. This approach is the only one of the three that gives up on the convexity of the training problem, but the benefits outweigh the harms. In this approach, we parametrize the representation as $\phi(\mathbf{x}; \boldsymbol{\theta})$ and use the optimization algorithm to find the $\boldsymbol{\theta}$ that corresponds to a good representation. If we wish, this approach can capture the benefit of the first approach by being highly generic—we do so by using a very broad family $\phi(\mathbf{x}; \boldsymbol{\theta})$. This approach can also capture the benefit of the second approach. Human practitioners can encode their knowledge to help generalization by designing families $\phi(\mathbf{x}; \boldsymbol{\theta})$ that they expect will perform well. The advantage is that the human designer only needs to find the right general function family rather than finding precisely the right function.

This general principle of improving models by learning features extends beyond the feedforward networks described in this chapter. It is a recurring theme of deep learning that applies to all of the kinds of models described throughout this book. Feedforward networks are the application of this principle to learning deterministic

mappings from \mathbf{x} to \mathbf{y} that lack feedback connections. Other models presented later will apply these principles to learning stochastic mappings, learning functions with feedback, and learning probability distributions over a single vector.

We begin this chapter with a simple example of a feedforward network. Next, we address each of the design decisions needed to deploy a feedforward network. First, training a feedforward network requires making many of the same design decisions as are necessary for a linear model: choosing the optimizer, the cost function, and the form of the output units. We review these basics of gradient-based learning, then proceed to confront some of the design decisions that are unique to feedforward networks. Feedforward networks have introduced the concept of a hidden layer, and this requires us to choose the **activation functions** that will be used to compute the hidden layer values. We must also design the architecture of the network, including how many layers the network should contain, how these layers should be connected to each other, and how many units should be in each layer. Learning in deep neural networks requires computing the gradients of complicated functions. We present the **back-propagation** algorithm and its modern generalizations, which can be used to efficiently compute these gradients. Finally, we close with some historical perspective.

6.1 Example: Learning XOR

To make the idea of a feedforward network more concrete, we begin with an example of a fully functioning feedforward network on a very simple task: learning the XOR function.

The XOR function (“exclusive or”) is an operation on two binary values, x_1 and x_2 . When exactly one of these binary values is equal to 1, the XOR function returns 1. Otherwise, it returns 0. The XOR function provides the target function $y = f^*(\mathbf{x})$ that we want to learn. Our model provides a function $y = f(\mathbf{x}; \boldsymbol{\theta})$ and our learning algorithm will adapt the parameters $\boldsymbol{\theta}$ to make f as similar as possible to f^* .

In this simple example, we will not be concerned with statistical generalization. We want our network to perform correctly on the four points $\mathbb{X} = \{[0, 0]^\top, [0, 1]^\top, [1, 0]^\top, [1, 1]^\top\}$. We will train the network on all four of these points. The only challenge is to fit the training set.

We can treat this problem as a regression problem and use a mean squared error loss function. We choose this loss function to simplify the math for this example as much as possible. In practical applications, MSE is usually not an

appropriate cost function for modeling binary data. More appropriate approaches are described in section 6.2.2.2.

Evaluated on our whole training set, the MSE loss function is

$$J(\boldsymbol{\theta}) = \frac{1}{4} \sum_{\mathbf{x} \in \mathbb{X}} (f^*(\mathbf{x}) - f(\mathbf{x}; \boldsymbol{\theta}))^2. \quad (6.1)$$

Now we must choose the form of our model, $f(\mathbf{x}; \boldsymbol{\theta})$. Suppose that we choose a linear model, with $\boldsymbol{\theta}$ consisting of \mathbf{w} and b . Our model is defined to be

$$f(\mathbf{x}; \mathbf{w}, b) = \mathbf{x}^\top \mathbf{w} + b. \quad (6.2)$$

We can minimize $J(\boldsymbol{\theta})$ in closed form with respect to \mathbf{w} and b using the normal equations.

After solving the normal equations, we obtain $\mathbf{w} = \mathbf{0}$ and $b = \frac{1}{2}$. The linear model simply outputs 0.5 everywhere. Why does this happen? Figure 6.1 shows how a linear model is not able to represent the XOR function. One way to solve this problem is to use a model that learns a different feature space in which a linear model is able to represent the solution.

Specifically, we will introduce a very simple feedforward network with one hidden layer containing two hidden units. See figure 6.2 for an illustration of this model. This feedforward network has a vector of hidden units \mathbf{h} that are computed by a function $f^{(1)}(\mathbf{x}; \mathbf{W}, \mathbf{c})$. The values of these hidden units are then used as the input for a second layer. The second layer is the output layer of the network. The output layer is still just a linear regression model, but now it is applied to \mathbf{h} rather than to \mathbf{x} . The network now contains two functions chained together: $\mathbf{h} = f^{(1)}(\mathbf{x}; \mathbf{W}, \mathbf{c})$ and $y = f^{(2)}(\mathbf{h}; \mathbf{w}, b)$, with the complete model being $f(\mathbf{x}; \mathbf{W}, \mathbf{c}, \mathbf{w}, b) = f^{(2)}(f^{(1)}(\mathbf{x}))$.

What function should $f^{(1)}$ compute? Linear models have served us well so far, and it may be tempting to make $f^{(1)}$ be linear as well. Unfortunately, if $f^{(1)}$ were linear, then the feedforward network as a whole would remain a linear function of its input. Ignoring the intercept terms for the moment, suppose $f^{(1)}(\mathbf{x}) = \mathbf{W}^\top \mathbf{x}$ and $f^{(2)}(\mathbf{h}) = \mathbf{h}^\top \mathbf{w}$. Then $f(\mathbf{x}) = \mathbf{w}^\top \mathbf{W}^\top \mathbf{x}$. We could represent this function as $f(\mathbf{x}) = \mathbf{x}^\top \mathbf{w}'$ where $\mathbf{w}' = \mathbf{W}\mathbf{w}$.

Clearly, we must use a nonlinear function to describe the features. Most neural networks do so using an affine transformation controlled by learned parameters, followed by a fixed, nonlinear function called an activation function. We use that strategy here, by defining $\mathbf{h} = g(\mathbf{W}^\top \mathbf{x} + \mathbf{c})$, where \mathbf{W} provides the weights of a linear transformation and \mathbf{c} the biases. Previously, to describe a linear regression

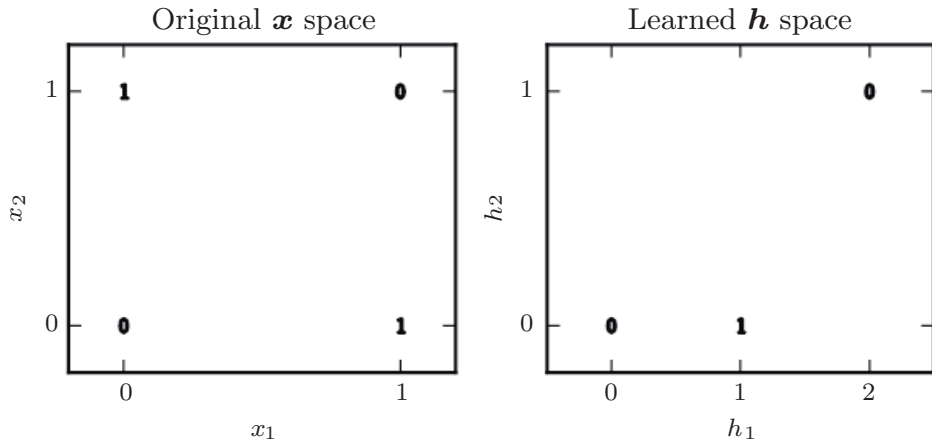


Figure 6.1: Solving the XOR problem by learning a representation. The bold numbers printed on the plot indicate the value that the learned function must output at each point. (*Left*) A linear model applied directly to the original input cannot implement the XOR function. When $x_1 = 0$, the model's output must increase as x_2 increases. When $x_1 = 1$, the model's output must decrease as x_2 increases. A linear model must apply a fixed coefficient w_2 to x_2 . The linear model therefore cannot use the value of x_1 to change the coefficient on x_2 and cannot solve this problem. (*Right*) In the transformed space represented by the features extracted by a neural network, a linear model can now solve the problem. In our example solution, the two points that must have output 1 have been collapsed into a single point in feature space. In other words, the nonlinear features have mapped both $\mathbf{x} = [1, 0]^\top$ and $\mathbf{x} = [0, 1]^\top$ to a single point in feature space, $\mathbf{h} = [1, 0]^\top$. The linear model can now describe the function as increasing in h_1 and decreasing in h_2 . In this example, the motivation for learning the feature space is only to make the model capacity greater so that it can fit the training set. In more realistic applications, learned representations can also help the model to generalize.

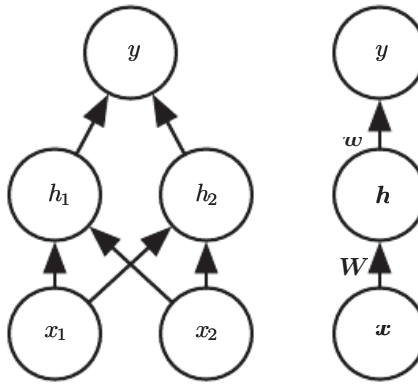


Figure 6.2: An example of a feedforward network, drawn in two different styles. Specifically, this is the feedforward network we use to solve the XOR example. It has a single hidden layer containing two units. (*Left*) In this style, we draw every unit as a node in the graph. This style is very explicit and unambiguous but for networks larger than this example it can consume too much space. (*Right*) In this style, we draw a node in the graph for each entire vector representing a layer’s activations. This style is much more compact. Sometimes we annotate the edges in this graph with the name of the parameters that describe the relationship between two layers. Here, we indicate that a matrix \mathbf{W} describes the mapping from \mathbf{x} to \mathbf{h} , and a vector \mathbf{w} describes the mapping from \mathbf{h} to y . We typically omit the intercept parameters associated with each layer when labeling this kind of drawing.

model, we used a vector of weights and a scalar bias parameter to describe an affine transformation from an input vector to an output scalar. Now, we describe an affine transformation from a vector \mathbf{x} to a vector \mathbf{h} , so an entire vector of bias parameters is needed. The activation function g is typically chosen to be a function that is applied element-wise, with $h_i = g(\mathbf{x}^\top \mathbf{W}_{:,i} + c_i)$. In modern neural networks, the default recommendation is to use the **rectified linear unit** or ReLU (Jarrett *et al.*, 2009; Nair and Hinton, 2010; Glorot *et al.*, 2011a) defined by the activation function $g(z) = \max\{0, z\}$ depicted in figure 6.3.

We can now specify our complete network as

$$f(\mathbf{x}; \mathbf{W}, \mathbf{c}, \mathbf{w}, b) = \mathbf{w}^\top \max\{0, \mathbf{W}^\top \mathbf{x} + \mathbf{c}\} + b. \quad (6.3)$$

We can now specify a solution to the XOR problem. Let

$$\mathbf{W} = \begin{bmatrix} 1 & 1 \\ 1 & 1 \end{bmatrix}, \quad (6.4)$$

$$\mathbf{c} = \begin{bmatrix} 0 \\ -1 \end{bmatrix}, \quad (6.5)$$

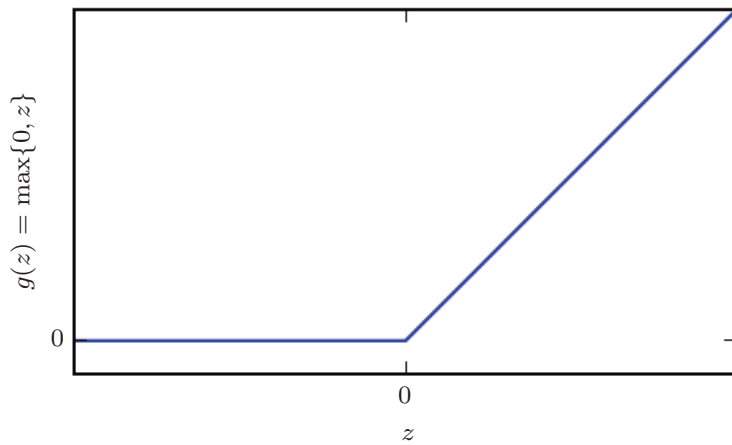


Figure 6.3: The rectified linear activation function. This activation function is the default activation function recommended for use with most feedforward neural networks. Applying this function to the output of a linear transformation yields a nonlinear transformation. However, the function remains very close to linear, in the sense that it is a piecewise linear function with two linear pieces. Because rectified linear units are nearly linear, they preserve many of the properties that make linear models easy to optimize with gradient-based methods. They also preserve many of the properties that make linear models generalize well. A common principle throughout computer science is that we can build complicated systems from minimal components. Much as a Turing machine's memory needs only to be able to store 0 or 1 states, we can build a universal function approximator from rectified linear functions.

$$\mathbf{w} = \begin{bmatrix} 1 \\ -2 \end{bmatrix}, \quad (6.6)$$

and $b = 0$.

We can now walk through the way that the model processes a batch of inputs. Let \mathbf{X} be the design matrix containing all four points in the binary input space, with one example per row:

$$\mathbf{X} = \begin{bmatrix} 0 & 0 \\ 0 & 1 \\ 1 & 0 \\ 1 & 1 \end{bmatrix}. \quad (6.7)$$

The first step in the neural network is to multiply the input matrix by the first layer's weight matrix:

$$\mathbf{XW} = \begin{bmatrix} 0 & 0 \\ 1 & 1 \\ 1 & 1 \\ 2 & 2 \end{bmatrix}. \quad (6.8)$$

Next, we add the bias vector \mathbf{c} , to obtain

$$\begin{bmatrix} 0 & -1 \\ 1 & 0 \\ 1 & 0 \\ 2 & 1 \end{bmatrix}. \quad (6.9)$$

In this space, all of the examples lie along a line with slope 1. As we move along this line, the output needs to begin at 0, then rise to 1, then drop back down to 0. A linear model cannot implement such a function. To finish computing the value of \mathbf{h} for each example, we apply the rectified linear transformation:

$$\begin{bmatrix} 0 & 0 \\ 1 & 0 \\ 1 & 0 \\ 2 & 1 \end{bmatrix}. \quad (6.10)$$

This transformation has changed the relationship between the examples. They no longer lie on a single line. As shown in figure 6.1, they now lie in a space where a linear model can solve the problem.

We finish by multiplying by the weight vector \mathbf{w} :

$$\begin{bmatrix} 0 \\ 1 \\ 1 \\ 0 \end{bmatrix}. \quad (6.11)$$

The neural network has obtained the correct answer for every example in the batch.

In this example, we simply specified the solution, then showed that it obtained zero error. In a real situation, there might be billions of model parameters and billions of training examples, so one cannot simply guess the solution as we did here. Instead, a gradient-based optimization algorithm can find parameters that produce very little error. The solution we described to the XOR problem is at a global minimum of the loss function, so gradient descent could converge to this point. There are other equivalent solutions to the XOR problem that gradient descent could also find. The convergence point of gradient descent depends on the initial values of the parameters. In practice, gradient descent would usually not find clean, easily understood, integer-valued solutions like the one we presented here.

6.2 Gradient-Based Learning

Designing and training a neural network is not much different from training any other machine learning model with gradient descent. In section 5.10, we described how to build a machine learning algorithm by specifying an optimization procedure, a cost function, and a model family.

The largest difference between the linear models we have seen so far and neural networks is that the nonlinearity of a neural network causes most interesting loss functions to become non-convex. This means that neural networks are usually trained by using iterative, gradient-based optimizers that merely drive the cost function to a very low value, rather than the linear equation solvers used to train linear regression models or the convex optimization algorithms with global convergence guarantees used to train logistic regression or SVMs. Convex optimization converges starting from any initial parameters (in theory—in practice it is very robust but can encounter numerical problems). Stochastic gradient descent applied to non-convex loss functions has no such convergence guarantee, and is sensitive to the values of the initial parameters. For feedforward neural networks, it is important to initialize all weights to small random values. The biases may be initialized to zero or to small positive values. The iterative gradient-based optimization algorithms used to train feedforward networks and almost all other deep models will be described in detail in chapter 8, with parameter initialization in particular discussed in section 8.4. For the moment, it suffices to understand that the training algorithm is almost always based on using the gradient to descend the cost function in one way or another. The specific algorithms are improvements and refinements on the ideas of gradient descent, introduced in section 4.3, and,

more specifically, are most often improvements of the stochastic gradient descent algorithm, introduced in section 5.9.

We can of course, train models such as linear regression and support vector machines with gradient descent too, and in fact this is common when the training set is extremely large. From this point of view, training a neural network is not much different from training any other model. Computing the gradient is slightly more complicated for a neural network, but can still be done efficiently and exactly. Section 6.5 will describe how to obtain the gradient using the back-propagation algorithm and modern generalizations of the back-propagation algorithm.

As with other machine learning models, to apply gradient-based learning we must choose a cost function, and we must choose how to represent the output of the model. We now revisit these design considerations with special emphasis on the neural networks scenario.

6.2.1 Cost Functions

An important aspect of the design of a deep neural network is the choice of the cost function. Fortunately, the cost functions for neural networks are more or less the same as those for other parametric models, such as linear models.

In most cases, our parametric model defines a distribution $p(\mathbf{y} \mid \mathbf{x}; \boldsymbol{\theta})$ and we simply use the principle of maximum likelihood. This means we use the cross-entropy between the training data and the model's predictions as the cost function.

Sometimes, we take a simpler approach, where rather than predicting a complete probability distribution over \mathbf{y} , we merely predict some statistic of \mathbf{y} conditioned on \mathbf{x} . Specialized loss functions allow us to train a predictor of these estimates.

The total cost function used to train a neural network will often combine one of the primary cost functions described here with a regularization term. We have already seen some simple examples of regularization applied to linear models in section 5.2.2. The weight decay approach used for linear models is also directly applicable to deep neural networks and is among the most popular regularization strategies. More advanced regularization strategies for neural networks will be described in chapter 7.

6.2.1.1 Learning Conditional Distributions with Maximum Likelihood

Most modern neural networks are trained using maximum likelihood. This means that the cost function is simply the negative log-likelihood, equivalently described

as the cross-entropy between the training data and the model distribution. This cost function is given by

$$J(\boldsymbol{\theta}) = -\mathbb{E}_{\mathbf{x}, \mathbf{y} \sim \hat{p}_{\text{data}}} \log p_{\text{model}}(\mathbf{y} \mid \mathbf{x}). \quad (6.12)$$

The specific form of the cost function changes from model to model, depending on the specific form of $\log p_{\text{model}}$. The expansion of the above equation typically yields some terms that do not depend on the model parameters and may be discarded. For example, as we saw in section 5.5.1, if $p_{\text{model}}(\mathbf{y} \mid \mathbf{x}) = \mathcal{N}(\mathbf{y}; f(\mathbf{x}; \boldsymbol{\theta}), \mathbf{I})$, then we recover the mean squared error cost,

$$J(\boldsymbol{\theta}) = \frac{1}{2} \mathbb{E}_{\mathbf{x}, \mathbf{y} \sim \hat{p}_{\text{data}}} \|\mathbf{y} - f(\mathbf{x}; \boldsymbol{\theta})\|^2 + \text{const}, \quad (6.13)$$

up to a scaling factor of $\frac{1}{2}$ and a term that does not depend on $\boldsymbol{\theta}$. The discarded constant is based on the variance of the Gaussian distribution, which in this case we chose not to parametrize. Previously, we saw that the equivalence between maximum likelihood estimation with an output distribution and minimization of mean squared error holds for a linear model, but in fact, the equivalence holds regardless of the $f(\mathbf{x}; \boldsymbol{\theta})$ used to predict the mean of the Gaussian.

An advantage of this approach of deriving the cost function from maximum likelihood is that it removes the burden of designing cost functions for each model. Specifying a model $p(\mathbf{y} \mid \mathbf{x})$ automatically determines a cost function $\log p(\mathbf{y} \mid \mathbf{x})$.

One recurring theme throughout neural network design is that the gradient of the cost function must be large and predictable enough to serve as a good guide for the learning algorithm. Functions that saturate (become very flat) undermine this objective because they make the gradient become very small. In many cases this happens because the activation functions used to produce the output of the hidden units or the output units saturate. The negative log-likelihood helps to avoid this problem for many models. Many output units involve an \exp function that can saturate when its argument is very negative. The \log function in the negative log-likelihood cost function undoes the \exp of some output units. We will discuss the interaction between the cost function and the choice of output unit in section 6.2.2.

One unusual property of the cross-entropy cost used to perform maximum likelihood estimation is that it usually does not have a minimum value when applied to the models commonly used in practice. For discrete output variables, most models are parametrized in such a way that they cannot represent a probability of zero or one, but can come arbitrarily close to doing so. Logistic regression is an example of such a model. For real-valued output variables, if the model

can control the density of the output distribution (for example, by learning the variance parameter of a Gaussian output distribution) then it becomes possible to assign extremely high density to the correct training set outputs, resulting in cross-entropy approaching negative infinity. Regularization techniques described in chapter 7 provide several different ways of modifying the learning problem so that the model cannot reap unlimited reward in this way.

6.2.1.2 Learning Conditional Statistics

Instead of learning a full probability distribution $p(\mathbf{y} | \mathbf{x}; \boldsymbol{\theta})$ we often want to learn just one conditional statistic of \mathbf{y} given \mathbf{x} .

For example, we may have a predictor $f(\mathbf{x}; \boldsymbol{\theta})$ that we wish to predict the mean of \mathbf{y} .

If we use a sufficiently powerful neural network, we can think of the neural network as being able to represent any function f from a wide class of functions, with this class being limited only by features such as continuity and boundedness rather than by having a specific parametric form. From this point of view, we can view the cost function as being a **functional** rather than just a function. A functional is a mapping from functions to real numbers. We can thus think of learning as choosing a function rather than merely choosing a set of parameters. We can design our cost functional to have its minimum occur at some specific function we desire. For example, we can design the cost functional to have its minimum lie on the function that maps \mathbf{x} to the expected value of \mathbf{y} given \mathbf{x} . Solving an optimization problem with respect to a function requires a mathematical tool called **calculus of variations**, described in section 19.4.2. It is not necessary to understand calculus of variations to understand the content of this chapter. At the moment, it is only necessary to understand that calculus of variations may be used to derive the following two results.

Our first result derived using calculus of variations is that solving the optimization problem

$$f^* = \arg \min_f \mathbb{E}_{\mathbf{x}, \mathbf{y} \sim p_{\text{data}}} \|\mathbf{y} - f(\mathbf{x})\|^2 \quad (6.14)$$

yields

$$f^*(\mathbf{x}) = \mathbb{E}_{\mathbf{y} \sim p_{\text{data}}(\mathbf{y} | \mathbf{x})} [\mathbf{y}], \quad (6.15)$$

so long as this function lies within the class we optimize over. In other words, if we could train on infinitely many samples from the true data generating distribution, minimizing the mean squared error cost function gives a function that predicts the mean of \mathbf{y} for each value of \mathbf{x} .

Different cost functions give different statistics. A second result derived using calculus of variations is that

$$f^* = \arg \min_f \mathbb{E}_{\mathbf{x}, \mathbf{y} \sim p_{\text{data}}} \|\mathbf{y} - f(\mathbf{x})\|_1 \quad (6.16)$$

yields a function that predicts the *median* value of \mathbf{y} for each \mathbf{x} , so long as such a function may be described by the family of functions we optimize over. This cost function is commonly called **mean absolute error**.

Unfortunately, mean squared error and mean absolute error often lead to poor results when used with gradient-based optimization. Some output units that saturate produce very small gradients when combined with these cost functions. This is one reason that the cross-entropy cost function is more popular than mean squared error or mean absolute error, even when it is not necessary to estimate an entire distribution $p(\mathbf{y} | \mathbf{x})$.

6.2.2 Output Units

The choice of cost function is tightly coupled with the choice of output unit. Most of the time, we simply use the cross-entropy between the data distribution and the model distribution. The choice of how to represent the output then determines the form of the cross-entropy function.

Any kind of neural network unit that may be used as an output can also be used as a hidden unit. Here, we focus on the use of these units as outputs of the model, but in principle they can be used internally as well. We revisit these units with additional detail about their use as hidden units in section 6.3.

Throughout this section, we suppose that the feedforward network provides a set of hidden features defined by $\mathbf{h} = f(\mathbf{x}; \boldsymbol{\theta})$. The role of the output layer is then to provide some additional transformation from the features to complete the task that the network must perform.

6.2.2.1 Linear Units for Gaussian Output Distributions

One simple kind of output unit is an output unit based on an affine transformation with no nonlinearity. These are often just called linear units.

Given features \mathbf{h} , a layer of linear output units produces a vector $\hat{\mathbf{y}} = \mathbf{W}^\top \mathbf{h} + \mathbf{b}$.

Linear output layers are often used to produce the mean of a conditional Gaussian distribution:

$$p(\mathbf{y} | \mathbf{x}) = \mathcal{N}(\mathbf{y}; \hat{\mathbf{y}}, \mathbf{I}). \quad (6.17)$$

Maximizing the log-likelihood is then equivalent to minimizing the mean squared error.

The maximum likelihood framework makes it straightforward to learn the covariance of the Gaussian too, or to make the covariance of the Gaussian be a function of the input. However, the covariance must be constrained to be a positive definite matrix for all inputs. It is difficult to satisfy such constraints with a linear output layer, so typically other output units are used to parametrize the covariance. Approaches to modeling the covariance are described shortly, in section 6.2.2.4.

Because linear units do not saturate, they pose little difficulty for gradient-based optimization algorithms and may be used with a wide variety of optimization algorithms.

6.2.2.2 Sigmoid Units for Bernoulli Output Distributions

Many tasks require predicting the value of a binary variable y . Classification problems with two classes can be cast in this form.

The maximum-likelihood approach is to define a Bernoulli distribution over y conditioned on \mathbf{x} .

A Bernoulli distribution is defined by just a single number. The neural net needs to predict only $P(y = 1 | \mathbf{x})$. For this number to be a valid probability, it must lie in the interval $[0, 1]$.

Satisfying this constraint requires some careful design effort. Suppose we were to use a linear unit, and threshold its value to obtain a valid probability:

$$P(y = 1 | \mathbf{x}) = \max \left\{ 0, \min \left\{ 1, \mathbf{w}^\top \mathbf{h} + b \right\} \right\}. \quad (6.18)$$

This would indeed define a valid conditional distribution, but we would not be able to train it very effectively with gradient descent. Any time that $\mathbf{w}^\top \mathbf{h} + b$ strayed outside the unit interval, the gradient of the output of the model with respect to its parameters would be $\mathbf{0}$. A gradient of $\mathbf{0}$ is typically problematic because the learning algorithm no longer has a guide for how to improve the corresponding parameters.

Instead, it is better to use a different approach that ensures there is always a strong gradient whenever the model has the wrong answer. This approach is based on using sigmoid output units combined with maximum likelihood.

A sigmoid output unit is defined by

$$\hat{y} = \sigma(\mathbf{w}^\top \mathbf{h} + b) \quad (6.19)$$

where σ is the logistic sigmoid function described in section 3.10.

We can think of the sigmoid output unit as having two components. First, it uses a linear layer to compute $z = \mathbf{w}^\top \mathbf{h} + b$. Next, it uses the sigmoid activation function to convert z into a probability.

We omit the dependence on \mathbf{x} for the moment to discuss how to define a probability distribution over y using the value z . The sigmoid can be motivated by constructing an unnormalized probability distribution $\tilde{P}(y)$, which does not sum to 1. We can then divide by an appropriate constant to obtain a valid probability distribution. If we begin with the assumption that the unnormalized log probabilities are linear in y and z , we can exponentiate to obtain the unnormalized probabilities. We then normalize to see that this yields a Bernoulli distribution controlled by a sigmoidal transformation of z :

$$\log \tilde{P}(y) = yz \quad (6.20)$$

$$\tilde{P}(y) = \exp(yz) \quad (6.21)$$

$$P(y) = \frac{\exp(yz)}{\sum_{y'=0}^1 \exp(y'z)} \quad (6.22)$$

$$P(y) = \sigma((2y - 1)z). \quad (6.23)$$

Probability distributions based on exponentiation and normalization are common throughout the statistical modeling literature. The z variable defining such a distribution over binary variables is called a **logit**.

This approach to predicting the probabilities in log-space is natural to use with maximum likelihood learning. Because the cost function used with maximum likelihood is $-\log P(y | \mathbf{x})$, the log in the cost function undoes the \exp of the sigmoid. Without this effect, the saturation of the sigmoid could prevent gradient-based learning from making good progress. The loss function for maximum likelihood learning of a Bernoulli parametrized by a sigmoid is

$$J(\boldsymbol{\theta}) = -\log P(y | \mathbf{x}) \quad (6.24)$$

$$= -\log \sigma((2y - 1)z) \quad (6.25)$$

$$= \zeta((1 - 2y)z). \quad (6.26)$$

This derivation makes use of some properties from section 3.10. By rewriting the loss in terms of the softplus function, we can see that it saturates only when $(1 - 2y)z$ is very negative. Saturation thus occurs only when the model already has the right answer—when $y = 1$ and z is very positive, or $y = 0$ and z is very negative. When z has the wrong sign, the argument to the softplus function,

$(1 - 2y)z$, may be simplified to $|z|$. As $|z|$ becomes large while z has the wrong sign, the softplus function asymptotes toward simply returning its argument $|z|$. The derivative with respect to z asymptotes to $\text{sign}(z)$, so, in the limit of extremely incorrect z , the softplus function does not shrink the gradient at all. This property is very useful because it means that gradient-based learning can act to quickly correct a mistaken z .

When we use other loss functions, such as mean squared error, the loss can saturate anytime $\sigma(z)$ saturates. The sigmoid activation function saturates to 0 when z becomes very negative and saturates to 1 when z becomes very positive. The gradient can shrink too small to be useful for learning whenever this happens, whether the model has the correct answer or the incorrect answer. For this reason, maximum likelihood is almost always the preferred approach to training sigmoid output units.

Analytically, the logarithm of the sigmoid is always defined and finite, because the sigmoid returns values restricted to the open interval $(0, 1)$, rather than using the entire closed interval of valid probabilities $[0, 1]$. In software implementations, to avoid numerical problems, it is best to write the negative log-likelihood as a function of z , rather than as a function of $\hat{y} = \sigma(z)$. If the sigmoid function underflows to zero, then taking the logarithm of \hat{y} yields negative infinity.

6.2.2.3 Softmax Units for Multinoulli Output Distributions

Any time we wish to represent a probability distribution over a discrete variable with n possible values, we may use the softmax function. This can be seen as a generalization of the sigmoid function which was used to represent a probability distribution over a binary variable.

Softmax functions are most often used as the output of a classifier, to represent the probability distribution over n different classes. More rarely, softmax functions can be used inside the model itself, if we wish the model to choose between one of n different options for some internal variable.

In the case of binary variables, we wished to produce a single number

$$\hat{y} = P(y = 1 \mid \mathbf{x}). \quad (6.27)$$

Because this number needed to lie between 0 and 1, and because we wanted the logarithm of the number to be well-behaved for gradient-based optimization of the log-likelihood, we chose to instead predict a number $z = \log \tilde{P}(y = 1 \mid \mathbf{x})$. Exponentiating and normalizing gave us a Bernoulli distribution controlled by the sigmoid function.

To generalize to the case of a discrete variable with n values, we now need to produce a vector $\hat{\mathbf{y}}$, with $\hat{y}_i = P(y = i \mid \mathbf{x})$. We require not only that each element of \hat{y}_i be between 0 and 1, but also that the entire vector sums to 1 so that it represents a valid probability distribution. The same approach that worked for the Bernoulli distribution generalizes to the multinoulli distribution. First, a linear layer predicts unnormalized log probabilities:

$$\mathbf{z} = \mathbf{W}^\top \mathbf{h} + \mathbf{b}, \quad (6.28)$$

where $z_i = \log \tilde{P}(y = i \mid \mathbf{x})$. The softmax function can then exponentiate and normalize \mathbf{z} to obtain the desired $\hat{\mathbf{y}}$. Formally, the softmax function is given by

$$\text{softmax}(\mathbf{z})_i = \frac{\exp(z_i)}{\sum_j \exp(z_j)}. \quad (6.29)$$

As with the logistic sigmoid, the use of the \exp function works very well when training the softmax to output a target value y using maximum log-likelihood. In this case, we wish to maximize $\log P(y = i; \mathbf{z}) = \log \text{softmax}(\mathbf{z})_i$. Defining the softmax in terms of \exp is natural because the \log in the log-likelihood can undo the \exp of the softmax:

$$\log \text{softmax}(\mathbf{z})_i = z_i - \log \sum_j \exp(z_j). \quad (6.30)$$

The first term of equation 6.30 shows that the input z_i always has a direct contribution to the cost function. Because this term cannot saturate, we know that learning can proceed, even if the contribution of z_i to the second term of equation 6.30 becomes very small. When maximizing the log-likelihood, the first term encourages z_i to be pushed up, while the second term encourages all of \mathbf{z} to be pushed down. To gain some intuition for the second term, $\log \sum_j \exp(z_j)$, observe that this term can be roughly approximated by $\max_j z_j$. This approximation is based on the idea that $\exp(z_k)$ is insignificant for any z_k that is noticeably less than $\max_j z_j$. The intuition we can gain from this approximation is that the negative log-likelihood cost function always strongly penalizes the most active incorrect prediction. If the correct answer already has the largest input to the softmax, then the $-z_i$ term and the $\log \sum_j \exp(z_j) \approx \max_j z_j = z_i$ terms will roughly cancel. This example will then contribute little to the overall training cost, which will be dominated by other examples that are not yet correctly classified.

So far we have discussed only a single example. Overall, unregularized maximum likelihood will drive the model to learn parameters that drive the softmax to predict

the fraction of counts of each outcome observed in the training set:

$$\text{softmax}(\mathbf{z}(\mathbf{x}; \boldsymbol{\theta}))_i \approx \frac{\sum_{j=1}^m \mathbf{1}_{y^{(j)}=i, \mathbf{x}^{(j)}=\mathbf{x}}}{\sum_{j=1}^m \mathbf{1}_{\mathbf{x}^{(j)}=\mathbf{x}}}. \quad (6.31)$$

Because maximum likelihood is a consistent estimator, this is guaranteed to happen so long as the model family is capable of representing the training distribution. In practice, limited model capacity and imperfect optimization will mean that the model is only able to approximate these fractions.

Many objective functions other than the log-likelihood do not work as well with the softmax function. Specifically, objective functions that do not use a log to undo the exp of the softmax fail to learn when the argument to the exp becomes very negative, causing the gradient to vanish. In particular, squared error is a poor loss function for softmax units, and can fail to train the model to change its output, even when the model makes highly confident incorrect predictions (Bridle, 1990). To understand why these other loss functions can fail, we need to examine the softmax function itself.

Like the sigmoid, the softmax activation can saturate. The sigmoid function has a single output that saturates when its input is extremely negative or extremely positive. In the case of the softmax, there are multiple output values. These output values can saturate when the differences between input values become extreme. When the softmax saturates, many cost functions based on the softmax also saturate, unless they are able to invert the saturating activating function.

To see that the softmax function responds to the difference between its inputs, observe that the softmax output is invariant to adding the same scalar to all of its inputs:

$$\text{softmax}(\mathbf{z}) = \text{softmax}(\mathbf{z} + c). \quad (6.32)$$

Using this property, we can derive a numerically stable variant of the softmax:

$$\text{softmax}(\mathbf{z}) = \text{softmax}(\mathbf{z} - \max_i z_i). \quad (6.33)$$

The reformulated version allows us to evaluate softmax with only small numerical errors even when \mathbf{z} contains extremely large or extremely negative numbers. Examining the numerically stable variant, we see that the softmax function is driven by the amount that its arguments deviate from $\max_i z_i$.

An output $\text{softmax}(\mathbf{z})_i$ saturates to 1 when the corresponding input is maximal ($z_i = \max_i z_i$) and z_i is much greater than all of the other inputs. The output $\text{softmax}(\mathbf{z})_i$ can also saturate to 0 when z_i is not maximal and the maximum is much greater. This is a generalization of the way that sigmoid units saturate, and

can cause similar difficulties for learning if the loss function is not designed to compensate for it.

The argument \mathbf{z} to the softmax function can be produced in two different ways. The most common is simply to have an earlier layer of the neural network output every element of \mathbf{z} , as described above using the linear layer $\mathbf{z} = \mathbf{W}^\top \mathbf{h} + \mathbf{b}$. While straightforward, this approach actually overparametrizes the distribution. The constraint that the n outputs must sum to 1 means that only $n - 1$ parameters are necessary; the probability of the n -th value may be obtained by subtracting the first $n - 1$ probabilities from 1. We can thus impose a requirement that one element of \mathbf{z} be fixed. For example, we can require that $z_n = 0$. Indeed, this is exactly what the sigmoid unit does. Defining $P(y = 1 | \mathbf{x}) = \sigma(z)$ is equivalent to defining $P(y = 1 | \mathbf{x}) = \text{softmax}(\mathbf{z})_1$ with a two-dimensional \mathbf{z} and $z_1 = 0$. Both the $n - 1$ argument and the n argument approaches to the softmax can describe the same set of probability distributions, but have different learning dynamics. In practice, there is rarely much difference between using the overparametrized version or the restricted version, and it is simpler to implement the overparametrized version.

From a neuroscientific point of view, it is interesting to think of the softmax as a way to create a form of competition between the units that participate in it: the softmax outputs always sum to 1 so an increase in the value of one unit necessarily corresponds to a decrease in the value of others. This is analogous to the lateral inhibition that is believed to exist between nearby neurons in the cortex. At the extreme (when the difference between the maximal a_i and the others is large in magnitude) it becomes a form of **winner-take-all** (one of the outputs is nearly 1 and the others are nearly 0).

The name “softmax” can be somewhat confusing. The function is more closely related to the arg max function than the max function. The term “soft” derives from the fact that the softmax function is continuous and differentiable. The arg max function, with its result represented as a one-hot vector, is not continuous or differentiable. The softmax function thus provides a “softened” version of the arg max. The corresponding soft version of the maximum function is $\text{softmax}(\mathbf{z})^\top \mathbf{z}$. It would perhaps be better to call the softmax function “softargmax,” but the current name is an entrenched convention.

6.2.2.4 Other Output Types

The linear, sigmoid, and softmax output units described above are the most common. Neural networks can generalize to almost any kind of output layer that we wish. The principle of maximum likelihood provides a guide for how to design

a good cost function for nearly any kind of output layer.

In general, if we define a conditional distribution $p(\mathbf{y} | \mathbf{x}; \boldsymbol{\theta})$, the principle of maximum likelihood suggests we use $-\log p(\mathbf{y} | \mathbf{x}; \boldsymbol{\theta})$ as our cost function.

In general, we can think of the neural network as representing a function $f(\mathbf{x}; \boldsymbol{\theta})$. The outputs of this function are not direct predictions of the value \mathbf{y} . Instead, $f(\mathbf{x}; \boldsymbol{\theta}) = \boldsymbol{\omega}$ provides the parameters for a distribution over y . Our loss function can then be interpreted as $-\log p(\mathbf{y}; \boldsymbol{\omega}(\mathbf{x}))$.

For example, we may wish to learn the variance of a conditional Gaussian for \mathbf{y} , given \mathbf{x} . In the simple case, where the variance σ^2 is a constant, there is a closed form expression because the maximum likelihood estimator of variance is simply the empirical mean of the squared difference between observations \mathbf{y} and their expected value. A computationally more expensive approach that does not require writing special-case code is to simply include the variance as one of the properties of the distribution $p(\mathbf{y} | \mathbf{x})$ that is controlled by $\boldsymbol{\omega} = f(\mathbf{x}; \boldsymbol{\theta})$. The negative log-likelihood $-\log p(\mathbf{y}; \boldsymbol{\omega}(\mathbf{x}))$ will then provide a cost function with the appropriate terms necessary to make our optimization procedure incrementally learn the variance. In the simple case where the standard deviation does not depend on the input, we can make a new parameter in the network that is copied directly into $\boldsymbol{\omega}$. This new parameter might be σ itself or could be a parameter v representing σ^2 or it could be a parameter β representing $\frac{1}{\sigma^2}$, depending on how we choose to parametrize the distribution. We may wish our model to predict a different amount of variance in \mathbf{y} for different values of \mathbf{x} . This is called a **heteroscedastic** model. In the heteroscedastic case, we simply make the specification of the variance be one of the values output by $f(\mathbf{x}; \boldsymbol{\theta})$. A typical way to do this is to formulate the Gaussian distribution using precision, rather than variance, as described in equation 3.22. In the multivariate case it is most common to use a diagonal precision matrix

$$\text{diag}(\boldsymbol{\beta}). \quad (6.34)$$

This formulation works well with gradient descent because the formula for the log-likelihood of the Gaussian distribution parametrized by $\boldsymbol{\beta}$ involves only multiplication by β_i and addition of $\log \beta_i$. The gradient of multiplication, addition, and logarithm operations is well-behaved. By comparison, if we parametrized the output in terms of variance, we would need to use division. The division function becomes arbitrarily steep near zero. While large gradients can help learning, arbitrarily large gradients usually result in instability. If we parametrized the output in terms of standard deviation, the log-likelihood would still involve division, and would also involve squaring. The gradient through the squaring operation can vanish near zero, making it difficult to learn parameters that are squared.

Regardless of whether we use standard deviation, variance, or precision, we must ensure that the covariance matrix of the Gaussian is positive definite. Because the eigenvalues of the precision matrix are the reciprocals of the eigenvalues of the covariance matrix, this is equivalent to ensuring that the precision matrix is positive definite. If we use a diagonal matrix, or a scalar times the diagonal matrix, then the only condition we need to enforce on the output of the model is positivity. If we suppose that \mathbf{a} is the raw activation of the model used to determine the diagonal precision, we can use the softplus function to obtain a positive precision vector: $\boldsymbol{\beta} = \zeta(\mathbf{a})$. This same strategy applies equally if using variance or standard deviation rather than precision or if using a scalar times identity rather than diagonal matrix.

It is rare to learn a covariance or precision matrix with richer structure than diagonal. If the covariance is full and conditional, then a parametrization must be chosen that guarantees positive-definiteness of the predicted covariance matrix. This can be achieved by writing $\boldsymbol{\Sigma}(\mathbf{x}) = \mathbf{B}(\mathbf{x})\mathbf{B}^\top(\mathbf{x})$, where \mathbf{B} is an unconstrained square matrix. One practical issue if the matrix is full rank is that computing the likelihood is expensive, with a $d \times d$ matrix requiring $O(d^3)$ computation for the determinant and inverse of $\boldsymbol{\Sigma}(\mathbf{x})$ (or equivalently, and more commonly done, its eigendecomposition or that of $\mathbf{B}(\mathbf{x})$).

We often want to perform multimodal regression, that is, to predict real values that come from a conditional distribution $p(\mathbf{y} | \mathbf{x})$ that can have several different peaks in \mathbf{y} space for the same value of \mathbf{x} . In this case, a Gaussian mixture is a natural representation for the output (Jacobs *et al.*, 1991; Bishop, 1994). Neural networks with Gaussian mixtures as their output are often called **mixture density networks**. A Gaussian mixture output with n components is defined by the conditional probability distribution

$$p(\mathbf{y} | \mathbf{x}) = \sum_{i=1}^n p(c = i | \mathbf{x}) \mathcal{N}(\mathbf{y}; \boldsymbol{\mu}^{(i)}(\mathbf{x}), \boldsymbol{\Sigma}^{(i)}(\mathbf{x})). \quad (6.35)$$

The neural network must have three outputs: a vector defining $p(c = i | \mathbf{x})$, a matrix providing $\boldsymbol{\mu}^{(i)}(\mathbf{x})$ for all i , and a tensor providing $\boldsymbol{\Sigma}^{(i)}(\mathbf{x})$ for all i . These outputs must satisfy different constraints:

1. Mixture components $p(c = i | \mathbf{x})$: these form a multinoulli distribution over the n different components associated with latent variable¹ c , and can

¹We consider c to be latent because we do not observe it in the data: given input \mathbf{x} and target \mathbf{y} , it is not possible to know with certainty which Gaussian component was responsible for \mathbf{y} , but we can imagine that \mathbf{y} was generated by picking one of them, and make that unobserved choice a random variable.

typically be obtained by a softmax over an n -dimensional vector, to guarantee that these outputs are positive and sum to 1.

2. Means $\boldsymbol{\mu}^{(i)}(\mathbf{x})$: these indicate the center or mean associated with the i -th Gaussian component, and are unconstrained (typically with no nonlinearity at all for these output units). If \mathbf{y} is a d -vector, then the network must output an $n \times d$ matrix containing all n of these d -dimensional vectors. Learning these means with maximum likelihood is slightly more complicated than learning the means of a distribution with only one output mode. We only want to update the mean for the component that actually produced the observation. In practice, we do not know which component produced each observation. The expression for the negative log-likelihood naturally weights each example's contribution to the loss for each component by the probability that the component produced the example.
3. Covariances $\boldsymbol{\Sigma}^{(i)}(\mathbf{x})$: these specify the covariance matrix for each component i . As when learning a single Gaussian component, we typically use a diagonal matrix to avoid needing to compute determinants. As with learning the means of the mixture, maximum likelihood is complicated by needing to assign partial responsibility for each point to each mixture component. Gradient descent will automatically follow the correct process if given the correct specification of the negative log-likelihood under the mixture model.

It has been reported that gradient-based optimization of conditional Gaussian mixtures (on the output of neural networks) can be unreliable, in part because one gets divisions (by the variance) which can be numerically unstable (when some variance gets to be small for a particular example, yielding very large gradients). One solution is to **clip gradients** (see section 10.11.1) while another is to scale the gradients heuristically ([Murray and Larochelle, 2014](#)).

Gaussian mixture outputs are particularly effective in generative models of speech ([Schuster, 1999](#)) or movements of physical objects ([Graves, 2013](#)). The mixture density strategy gives a way for the network to represent multiple output modes and to control the variance of its output, which is crucial for obtaining a high degree of quality in these real-valued domains. An example of a mixture density network is shown in figure 6.4.

In general, we may wish to continue to model larger vectors \mathbf{y} containing more variables, and to impose richer and richer structures on these output variables. For example, we may wish for our neural network to output a sequence of characters that forms a sentence. In these cases, we may continue to use the principle of maximum likelihood applied to our model $p(\mathbf{y}; \boldsymbol{\omega}(\mathbf{x}))$, but the model we use

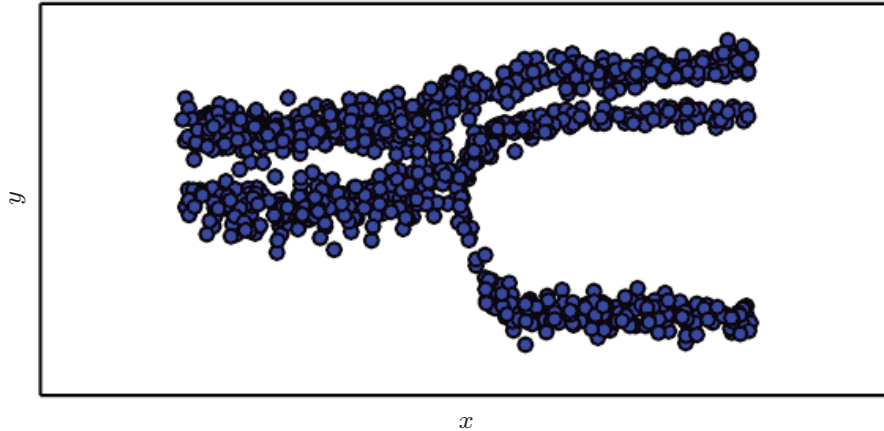


Figure 6.4: Samples drawn from a neural network with a mixture density output layer. The input x is sampled from a uniform distribution and the output y is sampled from $p_{\text{model}}(y | x)$. The neural network is able to learn nonlinear mappings from the input to the parameters of the output distribution. These parameters include the probabilities governing which of three mixture components will generate the output as well as the parameters for each mixture component. Each mixture component is Gaussian with predicted mean and variance. All of these aspects of the output distribution are able to vary with respect to the input x , and to do so in nonlinear ways.

to describe \mathbf{y} becomes complex enough to be beyond the scope of this chapter. Chapter 10 describes how to use recurrent neural networks to define such models over sequences, and part III describes advanced techniques for modeling arbitrary probability distributions.

6.3 Hidden Units

So far we have focused our discussion on design choices for neural networks that are common to most parametric machine learning models trained with gradient-based optimization. Now we turn to an issue that is unique to feedforward neural networks: how to choose the type of hidden unit to use in the hidden layers of the model.

The design of hidden units is an extremely active area of research and does not yet have many definitive guiding theoretical principles.

Rectified linear units are an excellent default choice of hidden unit. Many other types of hidden units are available. It can be difficult to determine when to use which kind (though rectified linear units are usually an acceptable choice). We

describe here some of the basic intuitions motivating each type of hidden units. These intuitions can help decide when to try out each of these units. It is usually impossible to predict in advance which will work best. The design process consists of trial and error, intuiting that a kind of hidden unit may work well, and then training a network with that kind of hidden unit and evaluating its performance on a validation set.

Some of the hidden units included in this list are not actually differentiable at all input points. For example, the rectified linear function $g(z) = \max\{0, z\}$ is not differentiable at $z = 0$. This may seem like it invalidates g for use with a gradient-based learning algorithm. In practice, gradient descent still performs well enough for these models to be used for machine learning tasks. This is in part because neural network training algorithms do not usually arrive at a local minimum of the cost function, but instead merely reduce its value significantly, as shown in figure 4.3. These ideas will be described further in chapter 8. Because we do not expect training to actually reach a point where the gradient is $\mathbf{0}$, it is acceptable for the minima of the cost function to correspond to points with undefined gradient. Hidden units that are not differentiable are usually non-differentiable at only a small number of points. In general, a function $g(z)$ has a left derivative defined by the slope of the function immediately to the left of z and a right derivative defined by the slope of the function immediately to the right of z . A function is differentiable at z only if both the left derivative and the right derivative are defined and equal to each other. The functions used in the context of neural networks usually have defined left derivatives and defined right derivatives. In the case of $g(z) = \max\{0, z\}$, the left derivative at $z = 0$ is 0 and the right derivative is 1. Software implementations of neural network training usually return one of the one-sided derivatives rather than reporting that the derivative is undefined or raising an error. This may be heuristically justified by observing that gradient-based optimization on a digital computer is subject to numerical error anyway. When a function is asked to evaluate $g(0)$, it is very unlikely that the underlying value truly was 0. Instead, it was likely to be some small value ϵ that was rounded to 0. In some contexts, more theoretically pleasing justifications are available, but these usually do not apply to neural network training. The important point is that in practice one can safely disregard the non-differentiability of the hidden unit activation functions described below.

Unless indicated otherwise, most hidden units can be described as accepting a vector of inputs \mathbf{x} , computing an affine transformation $\mathbf{z} = \mathbf{W}^\top \mathbf{x} + \mathbf{b}$, and then applying an element-wise nonlinear function $g(\mathbf{z})$. Most hidden units are distinguished from each other only by the choice of the form of the activation function $g(\mathbf{z})$.

6.3.1 Rectified Linear Units and Their Generalizations

Rectified linear units use the activation function $g(z) = \max\{0, z\}$.

Rectified linear units are easy to optimize because they are so similar to linear units. The only difference between a linear unit and a rectified linear unit is that a rectified linear unit outputs zero across half its domain. This makes the derivatives through a rectified linear unit remain large whenever the unit is active. The gradients are not only large but also consistent. The second derivative of the rectifying operation is 0 almost everywhere, and the derivative of the rectifying operation is 1 everywhere that the unit is active. This means that the gradient direction is far more useful for learning than it would be with activation functions that introduce second-order effects.

Rectified linear units are typically used on top of an affine transformation:

$$\mathbf{h} = g(\mathbf{W}^\top \mathbf{x} + \mathbf{b}). \quad (6.36)$$

When initializing the parameters of the affine transformation, it can be a good practice to set all elements of \mathbf{b} to a small, positive value, such as 0.1. This makes it very likely that the rectified linear units will be initially active for most inputs in the training set and allow the derivatives to pass through.

Several generalizations of rectified linear units exist. Most of these generalizations perform comparably to rectified linear units and occasionally perform better.

One drawback to rectified linear units is that they cannot learn via gradient-based methods on examples for which their activation is zero. A variety of generalizations of rectified linear units guarantee that they receive gradient everywhere.

Three generalizations of rectified linear units are based on using a non-zero slope α_i when $z_i < 0$: $h_i = g(\mathbf{z}, \boldsymbol{\alpha})_i = \max(0, z_i) + \alpha_i \min(0, z_i)$. **Absolute value rectification** fixes $\alpha_i = -1$ to obtain $g(z) = |z|$. It is used for object recognition from images (Jarrett *et al.*, 2009), where it makes sense to seek features that are invariant under a polarity reversal of the input illumination. Other generalizations of rectified linear units are more broadly applicable. A **leaky ReLU** (Maas *et al.*, 2013) fixes α_i to a small value like 0.01 while a **parametric ReLU** or **PReLU** treats α_i as a learnable parameter (He *et al.*, 2015).

Maxout units (Goodfellow *et al.*, 2013a) generalize rectified linear units further. Instead of applying an element-wise function $g(z)$, maxout units divide \mathbf{z} into groups of k values. Each maxout unit then outputs the maximum element of

one of these groups:

$$g(\mathbf{z})_i = \max_{j \in \mathbb{G}^{(i)}} z_j \quad (6.37)$$

where $\mathbb{G}^{(i)}$ is the set of indices into the inputs for group i , $\{(i-1)k+1, \dots, ik\}$. This provides a way of learning a piecewise linear function that responds to multiple directions in the input \mathbf{x} space.

A maxout unit can learn a piecewise linear, convex function with up to k pieces. Maxout units can thus be seen as *learning the activation function* itself rather than just the relationship between units. With large enough k , a maxout unit can learn to approximate any convex function with arbitrary fidelity. In particular, a maxout layer with two pieces can learn to implement the same function of the input \mathbf{x} as a traditional layer using the rectified linear activation function, absolute value rectification function, or the leaky or parametric ReLU, or can learn to implement a totally different function altogether. The maxout layer will of course be parametrized differently from any of these other layer types, so the learning dynamics will be different even in the cases where maxout learns to implement the same function of \mathbf{x} as one of the other layer types.

Each maxout unit is now parametrized by k weight vectors instead of just one, so maxout units typically need more regularization than rectified linear units. They can work well without regularization if the training set is large and the number of pieces per unit is kept low ([Cai et al., 2013](#)).

Maxout units have a few other benefits. In some cases, one can gain some statistical and computational advantages by requiring fewer parameters. Specifically, if the features captured by n different linear filters can be summarized without losing information by taking the max over each group of k features, then the next layer can get by with k times fewer weights.

Because each unit is driven by multiple filters, maxout units have some redundancy that helps them to resist a phenomenon called **catastrophic forgetting** in which neural networks forget how to perform tasks that they were trained on in the past ([Goodfellow et al., 2014a](#)).

Rectified linear units and all of these generalizations of them are based on the principle that models are easier to optimize if their behavior is closer to linear. This same general principle of using linear behavior to obtain easier optimization also applies in other contexts besides deep linear networks. Recurrent networks can learn from sequences and produce a sequence of states and outputs. When training them, one needs to propagate information through several time steps, which is much easier when some linear computations (with some directional derivatives being of magnitude near 1) are involved. One of the best-performing recurrent network

architectures, the LSTM, propagates information through time via summation—a particular straightforward kind of such linear activation. This is discussed further in section 10.10.

6.3.2 Logistic Sigmoid and Hyperbolic Tangent

Prior to the introduction of rectified linear units, most neural networks used the logistic sigmoid activation function

$$g(z) = \sigma(z) \quad (6.38)$$

or the hyperbolic tangent activation function

$$g(z) = \tanh(z). \quad (6.39)$$

These activation functions are closely related because $\tanh(z) = 2\sigma(2z) - 1$.

We have already seen sigmoid units as output units, used to predict the probability that a binary variable is 1. Unlike piecewise linear units, sigmoidal units saturate across most of their domain—they saturate to a high value when z is very positive, saturate to a low value when z is very negative, and are only strongly sensitive to their input when z is near 0. The widespread saturation of sigmoidal units can make gradient-based learning very difficult. For this reason, their use as hidden units in feedforward networks is now discouraged. Their use as output units is compatible with the use of gradient-based learning when an appropriate cost function can undo the saturation of the sigmoid in the output layer.

When a sigmoidal activation function must be used, the hyperbolic tangent activation function typically performs better than the logistic sigmoid. It resembles the identity function more closely, in the sense that $\tanh(0) = 0$ while $\sigma(0) = \frac{1}{2}$. Because \tanh is similar to the identity function near 0, training a deep neural network $\hat{y} = \mathbf{w}^\top \tanh(\mathbf{U}^\top \tanh(\mathbf{V}^\top \mathbf{x}))$ resembles training a linear model $\hat{y} = \mathbf{w}^\top \mathbf{U}^\top \mathbf{V}^\top \mathbf{x}$ so long as the activations of the network can be kept small. This makes training the \tanh network easier.

Sigmoidal activation functions are more common in settings other than feed-forward networks. Recurrent networks, many probabilistic models, and some autoencoders have additional requirements that rule out the use of piecewise linear activation functions and make sigmoidal units more appealing despite the drawbacks of saturation.

6.3.3 Other Hidden Units

Many other types of hidden units are possible, but are used less frequently.

In general, a wide variety of differentiable functions perform perfectly well. Many unpublished activation functions perform just as well as the popular ones. To provide a concrete example, the authors tested a feedforward network using $\mathbf{h} = \cos(\mathbf{W}\mathbf{x} + \mathbf{b})$ on the MNIST dataset and obtained an error rate of less than 1%, which is competitive with results obtained using more conventional activation functions. During research and development of new techniques, it is common to test many different activation functions and find that several variations on standard practice perform comparably. This means that usually new hidden unit types are published only if they are clearly demonstrated to provide a significant improvement. New hidden unit types that perform roughly comparably to known types are so common as to be uninteresting.

It would be impractical to list all of the hidden unit types that have appeared in the literature. We highlight a few especially useful and distinctive ones.

One possibility is to not have an activation $g(z)$ at all. One can also think of this as using the identity function as the activation function. We have already seen that a linear unit can be useful as the output of a neural network. It may also be used as a hidden unit. If every layer of the neural network consists of only linear transformations, then the network as a whole will be linear. However, it is acceptable for some layers of the neural network to be purely linear. Consider a neural network layer with n inputs and p outputs, $\mathbf{h} = g(\mathbf{W}^\top \mathbf{x} + \mathbf{b})$. We may replace this with two layers, with one layer using weight matrix \mathbf{U} and the other using weight matrix \mathbf{V} . If the first layer has no activation function, then we have essentially factored the weight matrix of the original layer based on \mathbf{W} . The factored approach is to compute $\mathbf{h} = g(\mathbf{V}^\top \mathbf{U}^\top \mathbf{x} + \mathbf{b})$. If \mathbf{U} produces q outputs, then \mathbf{U} and \mathbf{V} together contain only $(n+p)q$ parameters, while \mathbf{W} contains np parameters. For small q , this can be a considerable saving in parameters. It comes at the cost of constraining the linear transformation to be low-rank, but these low-rank relationships are often sufficient. Linear hidden units thus offer an effective way of reducing the number of parameters in a network.

Softmax units are another kind of unit that is usually used as an output (as described in section 6.2.2.3) but may sometimes be used as a hidden unit. Softmax units naturally represent a probability distribution over a discrete variable with k possible values, so they may be used as a kind of switch. These kinds of hidden units are usually only used in more advanced architectures that explicitly learn to manipulate memory, described in section 10.12.

A few other reasonably common hidden unit types include:

- **Radial basis function** or RBF unit: $h_i = \exp\left(-\frac{1}{\sigma_i^2} \|\mathbf{W}_{:,i} - \mathbf{x}\|^2\right)$. This function becomes more active as \mathbf{x} approaches a template $\mathbf{W}_{:,i}$. Because it saturates to 0 for most \mathbf{x} , it can be difficult to optimize.
- **Softplus**: $g(a) = \zeta(a) = \log(1 + e^a)$. This is a smooth version of the rectifier, introduced by [Dugas et al. \(2001\)](#) for function approximation and by [Nair and Hinton \(2010\)](#) for the conditional distributions of undirected probabilistic models. [Glorot et al. \(2011a\)](#) compared the softplus and rectifier and found better results with the latter. The use of the softplus is generally discouraged. The softplus demonstrates that the performance of hidden unit types can be very counterintuitive—one might expect it to have an advantage over the rectifier due to being differentiable everywhere or due to saturating less completely, but empirically it does not.
- **Hard** tanh: this is shaped similarly to the tanh and the rectifier but unlike the latter, it is bounded, $g(a) = \max(-1, \min(1, a))$. It was introduced by [Collobert \(2004\)](#).

Hidden unit design remains an active area of research and many useful hidden unit types remain to be discovered.

6.4 Architecture Design

Another key design consideration for neural networks is determining the architecture. The word **architecture** refers to the overall structure of the network: how many units it should have and how these units should be connected to each other.

Most neural networks are organized into groups of units called layers. Most neural network architectures arrange these layers in a chain structure, with each layer being a function of the layer that preceded it. In this structure, the first layer is given by

$$\mathbf{h}^{(1)} = g^{(1)} \left(\mathbf{W}^{(1)\top} \mathbf{x} + \mathbf{b}^{(1)} \right), \quad (6.40)$$

the second layer is given by

$$\mathbf{h}^{(2)} = g^{(2)} \left(\mathbf{W}^{(2)\top} \mathbf{h}^{(1)} + \mathbf{b}^{(2)} \right), \quad (6.41)$$

and so on.

In these chain-based architectures, the main architectural considerations are to choose the depth of the network and the width of each layer. As we will see, a network with even one hidden layer is sufficient to fit the training set. Deeper networks often are able to use far fewer units per layer and far fewer parameters and often generalize to the test set, but are also often harder to optimize. The ideal network architecture for a task must be found via experimentation guided by monitoring the validation set error.

6.4.1 Universal Approximation Properties and Depth

A linear model, mapping from features to outputs via matrix multiplication, can by definition represent only linear functions. It has the advantage of being easy to train because many loss functions result in convex optimization problems when applied to linear models. Unfortunately, we often want to learn nonlinear functions.

At first glance, we might presume that learning a nonlinear function requires designing a specialized model family for the kind of nonlinearity we want to learn. Fortunately, feedforward networks with hidden layers provide a universal approximation framework. Specifically, the **universal approximation theorem** (Hornik *et al.*, 1989; Cybenko, 1989) states that a feedforward network with a linear output layer and at least one hidden layer with any “squashing” activation function (such as the logistic sigmoid activation function) can approximate any Borel measurable function from one finite-dimensional space to another with any desired non-zero amount of error, provided that the network is given enough hidden units. The derivatives of the feedforward network can also approximate the derivatives of the function arbitrarily well (Hornik *et al.*, 1990). The concept of Borel measurability is beyond the scope of this book; for our purposes it suffices to say that any continuous function on a closed and bounded subset of \mathbb{R}^n is Borel measurable and therefore may be approximated by a neural network. A neural network may also approximate any function mapping from any finite dimensional discrete space to another. While the original theorems were first stated in terms of units with activation functions that saturate both for very negative and for very positive arguments, universal approximation theorems have also been proved for a wider class of activation functions, which includes the now commonly used rectified linear unit (Leshno *et al.*, 1993).

The universal approximation theorem means that regardless of what function we are trying to learn, we know that a large MLP will be able to *represent* this function. However, we are not guaranteed that the training algorithm will be able to *learn* that function. Even if the MLP is able to represent the function, learning can fail for two different reasons. First, the optimization algorithm used for training

may not be able to find the value of the parameters that corresponds to the desired function. Second, the training algorithm might choose the wrong function due to overfitting. Recall from section 5.2.1 that the “no free lunch” theorem shows that there is no universally superior machine learning algorithm. Feedforward networks provide a universal system for representing functions, in the sense that, given a function, there exists a feedforward network that approximates the function. There is no universal procedure for examining a training set of specific examples and choosing a function that will generalize to points not in the training set.

The universal approximation theorem says that there exists a network large enough to achieve any degree of accuracy we desire, but the theorem does not say how large this network will be. [Barron \(1993\)](#) provides some bounds on the size of a single-layer network needed to approximate a broad class of functions. Unfortunately, in the worse case, an exponential number of hidden units (possibly with one hidden unit corresponding to each input configuration that needs to be distinguished) may be required. This is easiest to see in the binary case: the number of possible binary functions on vectors $\mathbf{v} \in \{0, 1\}^n$ is 2^{2^n} and selecting one such function requires 2^n bits, which will in general require $O(2^n)$ degrees of freedom.

In summary, a feedforward network with a single layer is sufficient to represent any function, but the layer may be infeasibly large and may fail to learn and generalize correctly. In many circumstances, using deeper models can reduce the number of units required to represent the desired function and can reduce the amount of generalization error.

There exist families of functions which can be approximated efficiently by an architecture with depth greater than some value d , but which require a much larger model if depth is restricted to be less than or equal to d . In many cases, the number of hidden units required by the shallow model is exponential in n . Such results were first proved for models that do not resemble the continuous, differentiable neural networks used for machine learning, but have since been extended to these models. The first results were for circuits of logic gates ([Håstad, 1986](#)). Later work extended these results to linear threshold units with non-negative weights ([Håstad and Goldmann, 1991](#); [Hajnal et al., 1993](#)), and then to networks with continuous-valued activations ([Maass, 1992](#); [Maass et al., 1994](#)). Many modern neural networks use rectified linear units. [Leshno et al. \(1993\)](#) demonstrated that shallow networks with a broad family of non-polynomial activation functions, including rectified linear units, have universal approximation properties, but these results do not address the questions of depth or efficiency—they specify only that a sufficiently wide rectifier network could represent any function. [Montufar et al.](#)

(2014) showed that functions representable with a deep rectifier net can require an exponential number of hidden units with a shallow (one hidden layer) network. More precisely, they showed that piecewise linear networks (which can be obtained from rectifier nonlinearities or maxout units) can represent functions with a number of regions that is exponential in the depth of the network. Figure 6.5 illustrates how a network with absolute value rectification creates mirror images of the function computed on top of some hidden unit, with respect to the input of that hidden unit. Each hidden unit specifies where to fold the input space in order to create mirror responses (on both sides of the absolute value nonlinearity). By composing these folding operations, we obtain an exponentially large number of piecewise linear regions which can capture all kinds of regular (e.g., repeating) patterns.

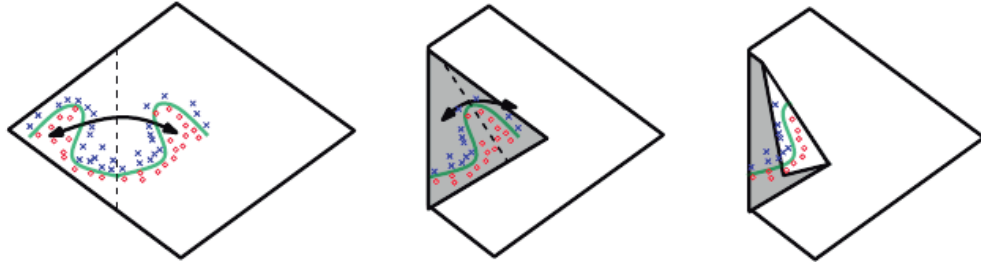


Figure 6.5: An intuitive, geometric explanation of the exponential advantage of deeper rectifier networks formally by Montufar *et al.* (2014). (*Left*) An absolute value rectification unit has the same output for every pair of mirror points in its input. The mirror axis of symmetry is given by the hyperplane defined by the weights and bias of the unit. A function computed on top of that unit (the green decision surface) will be a mirror image of a simpler pattern across that axis of symmetry. (*Center*) The function can be obtained by folding the space around the axis of symmetry. (*Right*) Another repeating pattern can be folded on top of the first (by another downstream unit) to obtain another symmetry (which is now repeated four times, with two hidden layers). Figure reproduced with permission from Montufar *et al.* (2014).

More precisely, the main theorem in Montufar *et al.* (2014) states that the number of linear regions carved out by a deep rectifier network with d inputs, depth l , and n units per hidden layer, is

$$O\left(\binom{n}{d}^{d(l-1)} n^d\right), \quad (6.42)$$

i.e., exponential in the depth l . In the case of maxout networks with k filters per unit, the number of linear regions is

$$O\left(k^{(l-1)+d}\right). \quad (6.43)$$

Of course, there is no guarantee that the kinds of functions we want to learn in applications of machine learning (and in particular for AI) share such a property.

We may also want to choose a deep model for statistical reasons. Any time we choose a specific machine learning algorithm, we are implicitly stating some set of prior beliefs we have about what kind of function the algorithm should learn. Choosing a deep model encodes a very general belief that the function we want to learn should involve composition of several simpler functions. This can be interpreted from a representation learning point of view as saying that we believe the learning problem consists of discovering a set of underlying factors of variation that can in turn be described in terms of other, simpler underlying factors of variation. Alternately, we can interpret the use of a deep architecture as expressing a belief that the function we want to learn is a computer program consisting of multiple steps, where each step makes use of the previous step’s output. These intermediate outputs are not necessarily factors of variation, but can instead be analogous to counters or pointers that the network uses to organize its internal processing. Empirically, greater depth does seem to result in better generalization for a wide variety of tasks (Bengio *et al.*, 2007; Erhan *et al.*, 2009; Bengio, 2009; Mesnil *et al.*, 2011; Ciresan *et al.*, 2012; Krizhevsky *et al.*, 2012; Sermanet *et al.*, 2013; Farabet *et al.*, 2013; Couprie *et al.*, 2013; Kahou *et al.*, 2013; Goodfellow *et al.*, 2014d; Szegedy *et al.*, 2014a). See figure 6.6 and figure 6.7 for examples of some of these empirical results. This suggests that using deep architectures does indeed express a useful prior over the space of functions the model learns.

6.4.2 Other Architectural Considerations

So far we have described neural networks as being simple chains of layers, with the main considerations being the depth of the network and the width of each layer. In practice, neural networks show considerably more diversity.

Many neural network architectures have been developed for specific tasks. Specialized architectures for computer vision called convolutional networks are described in chapter 9. Feedforward networks may also be generalized to the recurrent neural networks for sequence processing, described in chapter 10, which have their own architectural considerations.

In general, the layers need not be connected in a chain, even though this is the most common practice. Many architectures build a main chain but then add extra architectural features to it, such as skip connections going from layer i to layer $i + 2$ or higher. These skip connections make it easier for the gradient to flow from output layers to layers nearer the input.

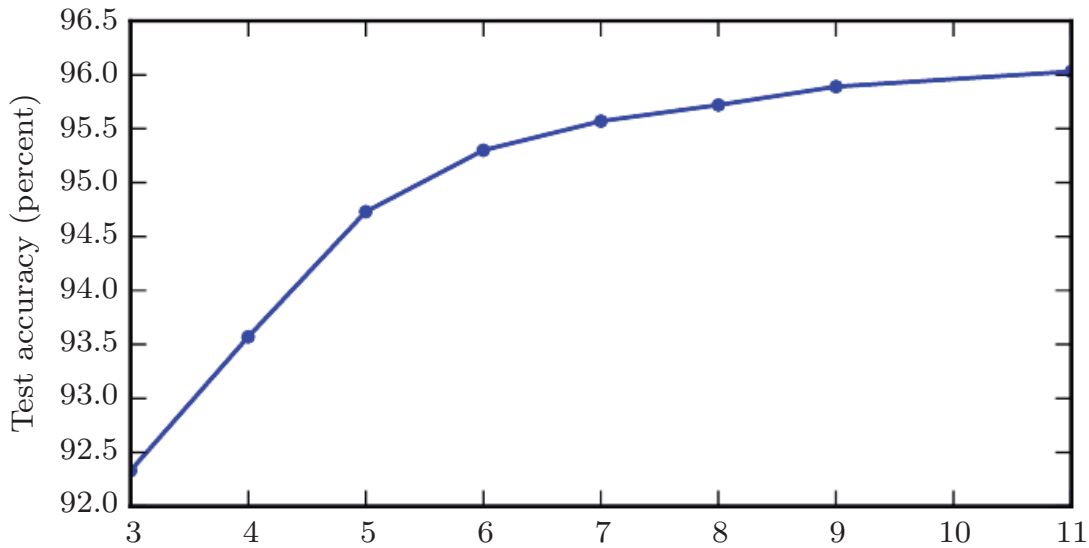


Figure 6.6: Empirical results showing that deeper networks generalize better when used to transcribe multi-digit numbers from photographs of addresses. Data from [Goodfellow et al. \(2014d\)](#). The test set accuracy consistently increases with increasing depth. See figure 6.7 for a control experiment demonstrating that other increases to the model size do not yield the same effect.

Another key consideration of architecture design is exactly how to connect a pair of layers to each other. In the default neural network layer described by a linear transformation via a matrix \mathbf{W} , every input unit is connected to every output unit. Many specialized networks in the chapters ahead have fewer connections, so that each unit in the input layer is connected to only a small subset of units in the output layer. These strategies for reducing the number of connections reduce the number of parameters and the amount of computation required to evaluate the network, but are often highly problem-dependent. For example, convolutional networks, described in chapter 9, use specialized patterns of sparse connections that are very effective for computer vision problems. In this chapter, it is difficult to give much more specific advice concerning the architecture of a generic neural network. Subsequent chapters develop the particular architectural strategies that have been found to work well for different application domains.

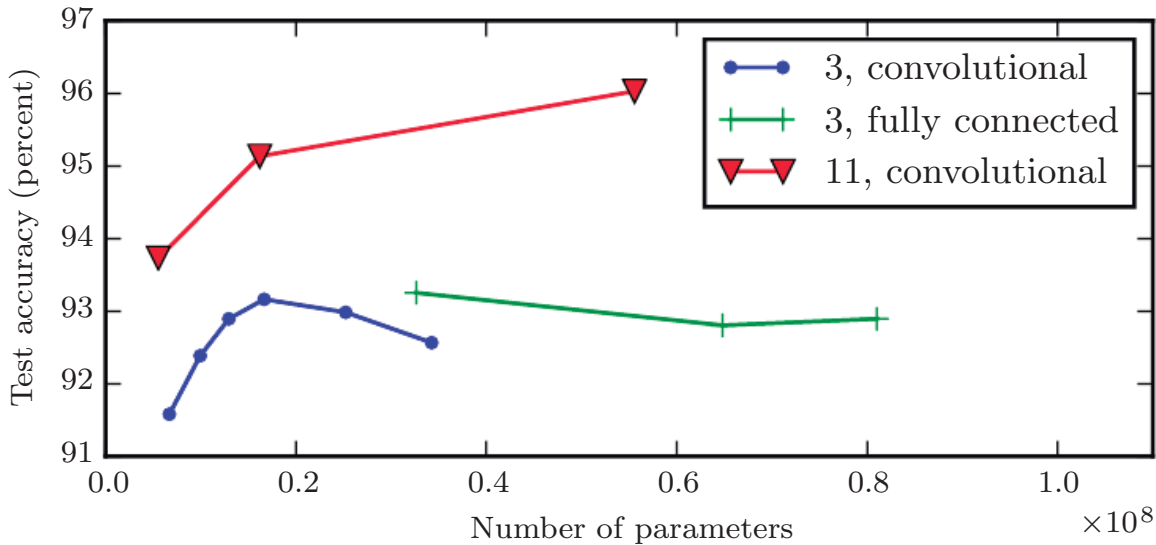


Figure 6.7: Deeper models tend to perform better. This is not merely because the model is larger. This experiment from Goodfellow *et al.* (2014d) shows that increasing the number of parameters in layers of convolutional networks without increasing their depth is not nearly as effective at increasing test set performance. The legend indicates the depth of network used to make each curve and whether the curve represents variation in the size of the convolutional or the fully connected layers. We observe that shallow models in this context overfit at around 20 million parameters while deep ones can benefit from having over 60 million. This suggests that using a deep model expresses a useful preference over the space of functions the model can learn. Specifically, it expresses a belief that the function should consist of many simpler functions composed together. This could result either in learning a representation that is composed in turn of simpler representations (e.g., corners defined in terms of edges) or in learning a program with sequentially dependent steps (e.g., first locate a set of objects, then segment them from each other, then recognize them).

6.5 Back-Propagation and Other Differentiation Algorithms

When we use a feedforward neural network to accept an input \mathbf{x} and produce an output $\hat{\mathbf{y}}$, information flows forward through the network. The inputs \mathbf{x} provide the initial information that then propagates up to the hidden units at each layer and finally produces $\hat{\mathbf{y}}$. This is called **forward propagation**. During training, forward propagation can continue onward until it produces a scalar cost $J(\boldsymbol{\theta})$. The **back-propagation** algorithm (Rumelhart *et al.*, 1986a), often simply called **backprop**, allows the information from the cost to then flow backwards through the network, in order to compute the gradient.

Computing an analytical expression for the gradient is straightforward, but numerically evaluating such an expression can be computationally expensive. The back-propagation algorithm does so using a simple and inexpensive procedure.

The term back-propagation is often misunderstood as meaning the whole learning algorithm for multi-layer neural networks. Actually, back-propagation refers only to the method for computing the gradient, while another algorithm, such as stochastic gradient descent, is used to perform learning using this gradient. Furthermore, back-propagation is often misunderstood as being specific to multi-layer neural networks, but in principle it can compute derivatives of any function (for some functions, the correct response is to report that the derivative of the function is undefined). Specifically, we will describe how to compute the gradient $\nabla_{\mathbf{x}} f(\mathbf{x}, \mathbf{y})$ for an arbitrary function f , where \mathbf{x} is a set of variables whose derivatives are desired, and \mathbf{y} is an additional set of variables that are inputs to the function but whose derivatives are not required. In learning algorithms, the gradient we most often require is the gradient of the cost function with respect to the parameters, $\nabla_{\boldsymbol{\theta}} J(\boldsymbol{\theta})$. Many machine learning tasks involve computing other derivatives, either as part of the learning process, or to analyze the learned model. The back-propagation algorithm can be applied to these tasks as well, and is not restricted to computing the gradient of the cost function with respect to the parameters. The idea of computing derivatives by propagating information through a network is very general, and can be used to compute values such as the Jacobian of a function f with multiple outputs. We restrict our description here to the most commonly used case where f has a single output.

6.5.1 Computational Graphs

So far we have discussed neural networks with a relatively informal graph language. To describe the back-propagation algorithm more precisely, it is helpful to have a more precise **computational graph** language.

Many ways of formalizing computation as graphs are possible.

Here, we use each node in the graph to indicate a variable. The variable may be a scalar, vector, matrix, tensor, or even a variable of another type.

To formalize our graphs, we also need to introduce the idea of an **operation**. An operation is a simple function of one or more variables. Our graph language is accompanied by a set of allowable operations. Functions more complicated than the operations in this set may be described by composing many operations together.

Without loss of generality, we define an operation to return only a single output variable. This does not lose generality because the output variable can have multiple entries, such as a vector. Software implementations of back-propagation usually support operations with multiple outputs, but we avoid this case in our description because it introduces many extra details that are not important to conceptual understanding.

If a variable y is computed by applying an operation to a variable x , then we draw a directed edge from x to y . We sometimes annotate the output node with the name of the operation applied, and other times omit this label when the operation is clear from context.

Examples of computational graphs are shown in figure 6.8.

6.5.2 Chain Rule of Calculus

The chain rule of calculus (not to be confused with the chain rule of probability) is used to compute the derivatives of functions formed by composing other functions whose derivatives are known. Back-propagation is an algorithm that computes the chain rule, with a specific order of operations that is highly efficient.

Let x be a real number, and let f and g both be functions mapping from a real number to a real number. Suppose that $y = g(x)$ and $z = f(g(x)) = f(y)$. Then the chain rule states that

$$\frac{dz}{dx} = \frac{dz}{dy} \frac{dy}{dx}. \quad (6.44)$$

We can generalize this beyond the scalar case. Suppose that $\mathbf{x} \in \mathbb{R}^m$, $\mathbf{y} \in \mathbb{R}^n$,

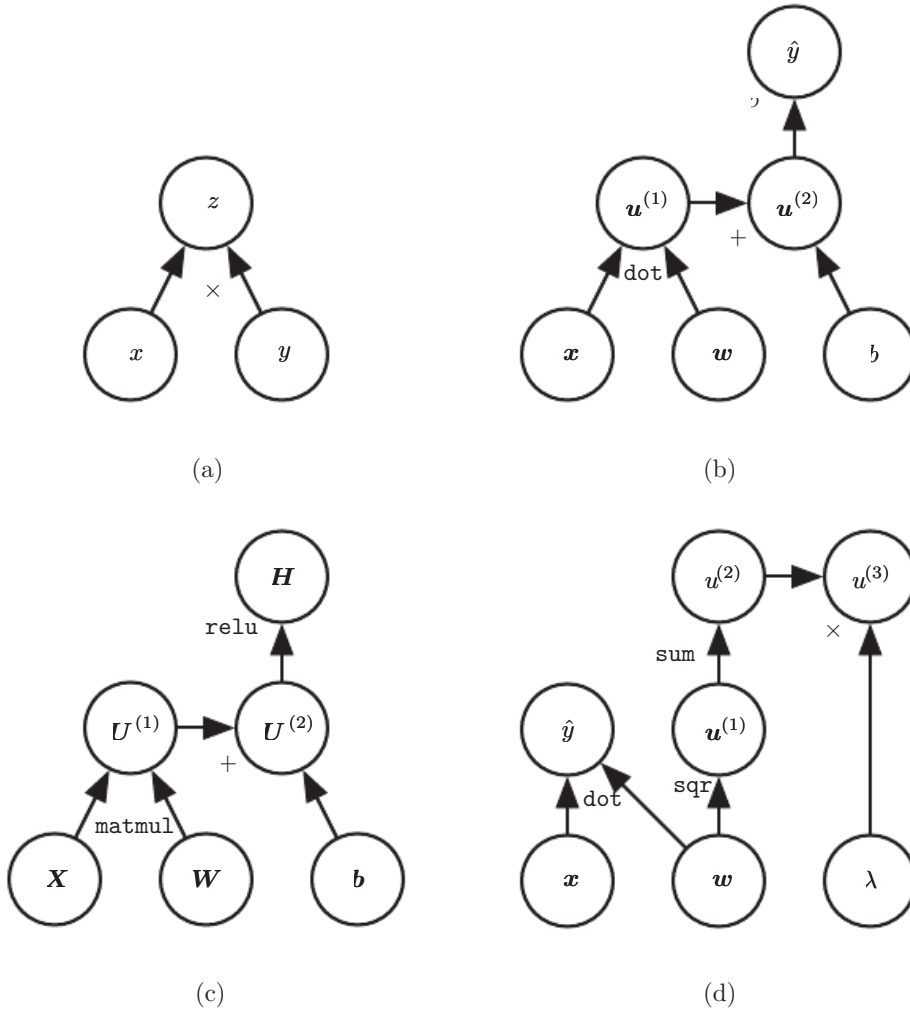


Figure 6.8: Examples of computational graphs. (a) The graph using the \times operation to compute $z = xy$. (b) The graph for the logistic regression prediction $\hat{y} = \sigma(\mathbf{x}^\top \mathbf{w} + b)$. Some of the intermediate expressions do not have names in the algebraic expression but need names in the graph. We simply name the i -th such variable $\mathbf{u}^{(i)}$. (c) The computational graph for the expression $\mathbf{H} = \max\{0, \mathbf{X}\mathbf{W} + \mathbf{b}\}$, which computes a design matrix of rectified linear unit activations \mathbf{H} given a design matrix containing a minibatch of inputs \mathbf{X} . (d) Examples a–c applied at most one operation to each variable, but it is possible to apply more than one operation. Here we show a computation graph that applies more than one operation to the weights \mathbf{w} of a linear regression model. The weights are used to make both the prediction \hat{y} and the weight decay penalty $\lambda \sum_i w_i^2$.

g maps from \mathbb{R}^m to \mathbb{R}^n , and f maps from \mathbb{R}^n to \mathbb{R} . If $\mathbf{y} = g(\mathbf{x})$ and $z = f(\mathbf{y})$, then

$$\frac{\partial z}{\partial x_i} = \sum_j \frac{\partial z}{\partial y_j} \frac{\partial y_j}{\partial x_i}. \quad (6.45)$$

In vector notation, this may be equivalently written as

$$\nabla_{\mathbf{x}} z = \left(\frac{\partial \mathbf{y}}{\partial \mathbf{x}} \right)^\top \nabla_{\mathbf{y}} z, \quad (6.46)$$

where $\frac{\partial \mathbf{y}}{\partial \mathbf{x}}$ is the $n \times m$ Jacobian matrix of g .

From this we see that the gradient of a variable \mathbf{x} can be obtained by multiplying a Jacobian matrix $\frac{\partial \mathbf{y}}{\partial \mathbf{x}}$ by a gradient $\nabla_{\mathbf{y}} z$. The back-propagation algorithm consists of performing such a Jacobian-gradient product for each operation in the graph.

Usually we do not apply the back-propagation algorithm merely to vectors, but rather to tensors of arbitrary dimensionality. Conceptually, this is exactly the same as back-propagation with vectors. The only difference is how the numbers are arranged in a grid to form a tensor. We could imagine flattening each tensor into a vector before we run back-propagation, computing a vector-valued gradient, and then reshaping the gradient back into a tensor. In this rearranged view, back-propagation is still just multiplying Jacobians by gradients.

To denote the gradient of a value z with respect to a tensor \mathbf{X} , we write $\nabla_{\mathbf{X}} z$, just as if \mathbf{X} were a vector. The indices into \mathbf{X} now have multiple coordinates—for example, a 3-D tensor is indexed by three coordinates. We can abstract this away by using a single variable i to represent the complete tuple of indices. For all possible index tuples i , $(\nabla_{\mathbf{X}} z)_i$ gives $\frac{\partial z}{\partial X_i}$. This is exactly the same as how for all possible integer indices i into a vector, $(\nabla_{\mathbf{x}} z)_i$ gives $\frac{\partial z}{\partial x_i}$. Using this notation, we can write the chain rule as it applies to tensors. If $\mathbf{Y} = g(\mathbf{X})$ and $z = f(\mathbf{Y})$, then

$$\nabla_{\mathbf{X}} z = \sum_j (\nabla_{\mathbf{X}} Y_j) \frac{\partial z}{\partial Y_j}. \quad (6.47)$$

6.5.3 Recursively Applying the Chain Rule to Obtain Backprop

Using the chain rule, it is straightforward to write down an algebraic expression for the gradient of a scalar with respect to any node in the computational graph that produced that scalar. However, actually evaluating that expression in a computer introduces some extra considerations.

Specifically, many subexpressions may be repeated several times within the overall expression for the gradient. Any procedure that computes the gradient

will need to choose whether to store these subexpressions or to recompute them several times. An example of how these repeated subexpressions arise is given in figure 6.9. In some cases, computing the same subexpression twice would simply be wasteful. For complicated graphs, there can be exponentially many of these wasted computations, making a naive implementation of the chain rule infeasible. In other cases, computing the same subexpression twice could be a valid way to reduce memory consumption at the cost of higher runtime.

We first begin by a version of the back-propagation algorithm that specifies the actual gradient computation directly (algorithm 6.2 along with algorithm 6.1 for the associated forward computation), in the order it will actually be done and according to the recursive application of chain rule. One could either directly perform these computations or view the description of the algorithm as a symbolic specification of the computational graph for computing the back-propagation. However, this formulation does not make explicit the manipulation and the construction of the symbolic graph that performs the gradient computation. Such a formulation is presented below in section 6.5.6, with algorithm 6.5, where we also generalize to nodes that contain arbitrary tensors.

First consider a computational graph describing how to compute a single scalar $u^{(n)}$ (say the loss on a training example). This scalar is the quantity whose gradient we want to obtain, with respect to the n_i input nodes $u^{(1)}$ to $u^{(n_i)}$. In other words we wish to compute $\frac{\partial u^{(n)}}{\partial u^{(i)}}$ for all $i \in \{1, 2, \dots, n_i\}$. In the application of back-propagation to computing gradients for gradient descent over parameters, $u^{(n)}$ will be the cost associated with an example or a minibatch, while $u^{(1)}$ to $u^{(n_i)}$ correspond to the parameters of the model.

We will assume that the nodes of the graph have been ordered in such a way that we can compute their output one after the other, starting at $u^{(n_i+1)}$ and going up to $u^{(n)}$. As defined in algorithm 6.1, each node $u^{(i)}$ is associated with an operation $f^{(i)}$ and is computed by evaluating the function

$$u^{(i)} = f(\mathbb{A}^{(i)}) \quad (6.48)$$

where $\mathbb{A}^{(i)}$ is the set of all nodes that are parents of $u^{(i)}$.

That algorithm specifies the forward propagation computation, which we could put in a graph \mathcal{G} . In order to perform back-propagation, we can construct a computational graph that depends on \mathcal{G} and adds to it an extra set of nodes. These form a subgraph \mathcal{B} with one node per node of \mathcal{G} . Computation in \mathcal{B} proceeds in exactly the reverse of the order of computation in \mathcal{G} , and each node of \mathcal{B} computes the derivative $\frac{\partial u^{(n)}}{\partial u^{(i)}}$ associated with the forward graph node $u^{(i)}$. This is done

Algorithm 6.1 A procedure that performs the computations mapping n_i inputs $u^{(1)}$ to $u^{(n_i)}$ to an output $u^{(n)}$. This defines a computational graph where each node computes numerical value $u^{(i)}$ by applying a function $f^{(i)}$ to the set of arguments $\mathbb{A}^{(i)}$ that comprises the values of previous nodes $u^{(j)}$, $j < i$, with $j \in Pa(u^{(i)})$. The input to the computational graph is the vector \mathbf{x} , and is set into the first n_i nodes $u^{(1)}$ to $u^{(n_i)}$. The output of the computational graph is read off the last (output) node $u^{(n)}$.

```
for  $i = 1, \dots, n_i$  do
     $u^{(i)} \leftarrow x_i$ 
end for
for  $i = n_i + 1, \dots, n$  do
     $\mathbb{A}^{(i)} \leftarrow \{u^{(j)} \mid j \in Pa(u^{(i)})\}$ 
     $u^{(i)} \leftarrow f^{(i)}(\mathbb{A}^{(i)})$ 
end for
return  $u^{(n)}$ 
```

using the chain rule with respect to scalar output $u^{(n)}$:

$$\frac{\partial u^{(n)}}{\partial u^{(j)}} = \sum_{i:j \in Pa(u^{(i)})} \frac{\partial u^{(n)}}{\partial u^{(i)}} \frac{\partial u^{(i)}}{\partial u^{(j)}} \quad (6.49)$$

as specified by algorithm 6.2. The subgraph \mathcal{B} contains exactly one edge for each edge from node $u^{(j)}$ to node $u^{(i)}$ of \mathcal{G} . The edge from $u^{(j)}$ to $u^{(i)}$ is associated with the computation of $\frac{\partial u^{(i)}}{\partial u^{(j)}}$. In addition, a dot product is performed for each node, between the gradient already computed with respect to nodes $u^{(i)}$ that are children of $u^{(j)}$ and the vector containing the partial derivatives $\frac{\partial u^{(i)}}{\partial u^{(j)}}$ for the same children nodes $u^{(i)}$. To summarize, the amount of computation required for performing the back-propagation scales linearly with the number of edges in \mathcal{G} , where the computation for each edge corresponds to computing a partial derivative (of one node with respect to one of its parents) as well as performing one multiplication and one addition. Below, we generalize this analysis to tensor-valued nodes, which is just a way to group multiple scalar values in the same node and enable more efficient implementations.

The back-propagation algorithm is designed to reduce the number of common subexpressions without regard to memory. Specifically, it performs on the order of one Jacobian product per node in the graph. This can be seen from the fact that backprop (algorithm 6.2) visits each edge from node $u^{(j)}$ to node $u^{(i)}$ of the graph exactly once in order to obtain the associated partial derivative $\frac{\partial u^{(i)}}{\partial u^{(j)}}$.

Algorithm 6.2 Simplified version of the back-propagation algorithm for computing the derivatives of $u^{(n)}$ with respect to the variables in the graph. This example is intended to further understanding by showing a simplified case where all variables are scalars, and we wish to compute the derivatives with respect to $u^{(1)}, \dots, u^{(n_i)}$. This simplified version computes the derivatives of all nodes in the graph. The computational cost of this algorithm is proportional to the number of edges in the graph, assuming that the partial derivative associated with each edge requires a constant time. This is of the same order as the number of computations for the forward propagation. Each $\frac{\partial u^{(i)}}{\partial u^{(j)}}$ is a function of the parents $u^{(j)}$ of $u^{(i)}$, thus linking the nodes of the forward graph to those added for the back-propagation graph.

Run forward propagation (algorithm 6.1 for this example) to obtain the activations of the network

Initialize `grad_table`, a data structure that will store the derivatives that have been computed. The entry `grad_table`[$u^{(i)}$] will store the computed value of $\frac{\partial u^{(n)}}{\partial u^{(i)}}$.

`grad_table`[$u^{(n)}$] $\leftarrow 1$

for $j = n - 1$ down to 1 **do**

The next line computes $\frac{\partial u^{(n)}}{\partial u^{(j)}} = \sum_{i:j \in Pa(u^{(i)})} \frac{\partial u^{(n)}}{\partial u^{(i)}} \frac{\partial u^{(i)}}{\partial u^{(j)}}$ using stored values:

`grad_table`[$u^{(j)}$] $\leftarrow \sum_{i:j \in Pa(u^{(i)})} \text{grad_table}[u^{(i)}] \frac{\partial u^{(i)}}{\partial u^{(j)}}$

end for

return {`grad_table`[$u^{(i)}$] | $i = 1, \dots, n_i$ }

Back-propagation thus avoids the exponential explosion in repeated subexpressions. However, other algorithms may be able to avoid more subexpressions by performing simplifications on the computational graph, or may be able to conserve memory by recomputing rather than storing some subexpressions. We will revisit these ideas after describing the back-propagation algorithm itself.

6.5.4 Back-Propagation Computation in Fully-Connected MLP

To clarify the above definition of the back-propagation computation, let us consider the specific graph associated with a fully-connected multi-layer MLP.

Algorithm 6.3 first shows the forward propagation, which maps parameters to the supervised loss $L(\hat{\mathbf{y}}, \mathbf{y})$ associated with a single (input,target) training example (\mathbf{x}, \mathbf{y}) , with $\hat{\mathbf{y}}$ the output of the neural network when \mathbf{x} is provided in input.

Algorithm 6.4 then shows the corresponding computation to be done for

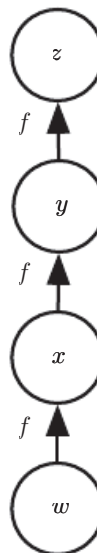


Figure 6.9: A computational graph that results in repeated subexpressions when computing the gradient. Let $w \in \mathbb{R}$ be the input to the graph. We use the same function $f : \mathbb{R} \rightarrow \mathbb{R}$ as the operation that we apply at every step of a chain: $x = f(w)$, $y = f(x)$, $z = f(y)$. To compute $\frac{\partial z}{\partial w}$, we apply equation 6.44 and obtain:

$$\frac{\partial z}{\partial w} \quad (6.50)$$

$$= \frac{\partial z}{\partial y} \frac{\partial y}{\partial x} \frac{\partial x}{\partial w} \quad (6.51)$$

$$= f'(y) f'(x) f'(w) \quad (6.52)$$

$$= f'(f(f(w))) f'(f(w)) f'(w) \quad (6.53)$$

Equation 6.52 suggests an implementation in which we compute the value of $f(w)$ only once and store it in the variable x . This is the approach taken by the back-propagation algorithm. An alternative approach is suggested by equation 6.53, where the subexpression $f(w)$ appears more than once. In the alternative approach, $f(w)$ is recomputed each time it is needed. When the memory required to store the value of these expressions is low, the back-propagation approach of equation 6.52 is clearly preferable because of its reduced runtime. However, equation 6.53 is also a valid implementation of the chain rule, and is useful when memory is limited.

applying the back-propagation algorithm to this graph.

Algorithms 6.3 and 6.4 are demonstrations that are chosen to be simple and straightforward to understand. However, they are specialized to one specific problem.

Modern software implementations are based on the generalized form of back-propagation described in section 6.5.6 below, which can accommodate any computational graph by explicitly manipulating a data structure for representing symbolic computation.

Algorithm 6.3 Forward propagation through a typical deep neural network and the computation of the cost function. The loss $L(\hat{\mathbf{y}}, \mathbf{y})$ depends on the output $\hat{\mathbf{y}}$ and on the target \mathbf{y} (see section 6.2.1.1 for examples of loss functions). To obtain the total cost J , the loss may be added to a regularizer $\Omega(\theta)$, where θ contains all the parameters (weights and biases). Algorithm 6.4 shows how to compute gradients of J with respect to parameters \mathbf{W} and \mathbf{b} . For simplicity, this demonstration uses only a single input example \mathbf{x} . Practical applications should use a minibatch. See section 6.5.7 for a more realistic demonstration.

Require: Network depth, l

Require: $\mathbf{W}^{(i)}, i \in \{1, \dots, l\}$, the weight matrices of the model

Require: $\mathbf{b}^{(i)}, i \in \{1, \dots, l\}$, the bias parameters of the model

Require: \mathbf{x} , the input to process

Require: \mathbf{y} , the target output

$$\mathbf{h}^{(0)} = \mathbf{x}$$

for $k = 1, \dots, l$ **do**

$$\mathbf{a}^{(k)} = \mathbf{b}^{(k)} + \mathbf{W}^{(k)} \mathbf{h}^{(k-1)}$$

$$\mathbf{h}^{(k)} = f(\mathbf{a}^{(k)})$$

end for

$$\hat{\mathbf{y}} = \mathbf{h}^{(l)}$$

$$J = L(\hat{\mathbf{y}}, \mathbf{y}) + \lambda \Omega(\theta)$$

6.5.5 Symbol-to-Symbol Derivatives

Algebraic expressions and computational graphs both operate on **symbols**, or variables that do not have specific values. These algebraic and graph-based representations are called **symbolic** representations. When we actually use or train a neural network, we must assign specific values to these symbols. We replace a symbolic input to the network \mathbf{x} with a specific **numeric** value, such as $[1.2, 3.765, -1.8]^\top$.

Algorithm 6.4 Backward computation for the deep neural network of algorithm 6.3, which uses in addition to the input \mathbf{x} a target \mathbf{y} . This computation yields the gradients on the activations $\mathbf{a}^{(k)}$ for each layer k , starting from the output layer and going backwards to the first hidden layer. From these gradients, which can be interpreted as an indication of how each layer's output should change to reduce error, one can obtain the gradient on the parameters of each layer. The gradients on weights and biases can be immediately used as part of a stochastic gradient update (performing the update right after the gradients have been computed) or used with other gradient-based optimization methods.

After the forward computation, compute the gradient on the output layer:

$$\mathbf{g} \leftarrow \nabla_{\hat{\mathbf{y}}} J = \nabla_{\hat{\mathbf{y}}} L(\hat{\mathbf{y}}, \mathbf{y})$$

for $k = l, l - 1, \dots, 1$ **do**

Convert the gradient on the layer's output into a gradient into the pre-nonlinearity activation (element-wise multiplication if f is element-wise):

$$\mathbf{g} \leftarrow \nabla_{\mathbf{a}^{(k)}} J = \mathbf{g} \odot f'(\mathbf{a}^{(k)})$$

Compute gradients on weights and biases (including the regularization term, where needed):

$$\nabla_{\mathbf{b}^{(k)}} J = \mathbf{g} + \lambda \nabla_{\mathbf{b}^{(k)}} \Omega(\theta)$$

$$\nabla_{\mathbf{W}^{(k)}} J = \mathbf{g} \mathbf{h}^{(k-1)\top} + \lambda \nabla_{\mathbf{W}^{(k)}} \Omega(\theta)$$

Propagate the gradients w.r.t. the next lower-level hidden layer's activations:

$$\mathbf{g} \leftarrow \nabla_{\mathbf{h}^{(k-1)}} J = \mathbf{W}^{(k)\top} \mathbf{g}$$

end for

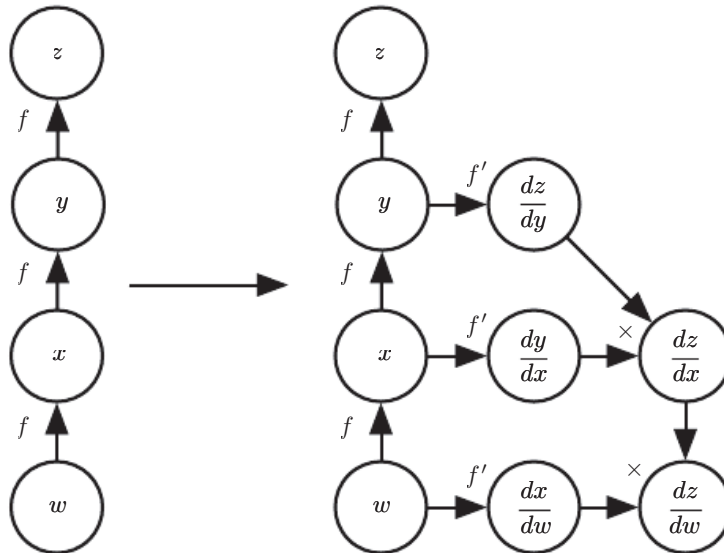


Figure 6.10: An example of the symbol-to-symbol approach to computing derivatives. In this approach, the back-propagation algorithm does not need to ever access any actual specific numeric values. Instead, it adds nodes to a computational graph describing how to compute these derivatives. A generic graph evaluation engine can later compute the derivatives for any specific numeric values. (*Left*) In this example, we begin with a graph representing $z = f(f(f(w)))$. (*Right*) We run the back-propagation algorithm, instructing it to construct the graph for the expression corresponding to $\frac{dz}{dw}$. In this example, we do not explain how the back-propagation algorithm works. The purpose is only to illustrate what the desired result is: a computational graph with a symbolic description of the derivative.

Some approaches to back-propagation take a computational graph and a set of numerical values for the inputs to the graph, then return a set of numerical values describing the gradient at those input values. We call this approach “symbol-to-number” differentiation. This is the approach used by libraries such as Torch (Collobert *et al.*, 2011b) and Caffe (Jia, 2013).

Another approach is to take a computational graph and add additional nodes to the graph that provide a symbolic description of the desired derivatives. This is the approach taken by Theano (Bergstra *et al.*, 2010; Bastien *et al.*, 2012) and TensorFlow (Abadi *et al.*, 2015). An example of how this approach works is illustrated in figure 6.10. The primary advantage of this approach is that the derivatives are described in the same language as the original expression. Because the derivatives are just another computational graph, it is possible to run back-propagation again, differentiating the derivatives in order to obtain higher derivatives. Computation of higher-order derivatives is described in section 6.5.10.

We will use the latter approach and describe the back-propagation algorithm in

terms of constructing a computational graph for the derivatives. Any subset of the graph may then be evaluated using specific numerical values at a later time. This allows us to avoid specifying exactly when each operation should be computed. Instead, a generic graph evaluation engine can evaluate every node as soon as its parents' values are available.

The description of the symbol-to-symbol based approach subsumes the symbol-to-number approach. The symbol-to-number approach can be understood as performing exactly the same computations as are done in the graph built by the symbol-to-symbol approach. The key difference is that the symbol-to-number approach does not expose the graph.

6.5.6 General Back-Propagation

The back-propagation algorithm is very simple. To compute the gradient of some scalar z with respect to one of its ancestors \mathbf{x} in the graph, we begin by observing that the gradient with respect to z is given by $\frac{dz}{dz} = 1$. We can then compute the gradient with respect to each parent of z in the graph by multiplying the current gradient by the Jacobian of the operation that produced z . We continue multiplying by Jacobians traveling backwards through the graph in this way until we reach \mathbf{x} . For any node that may be reached by going backwards from z through two or more paths, we simply sum the gradients arriving from different paths at that node.

More formally, each node in the graph \mathcal{G} corresponds to a variable. To achieve maximum generality, we describe this variable as being a tensor \mathbf{V} . Tensor can in general have any number of dimensions. They subsume scalars, vectors, and matrices.

We assume that each variable \mathbf{V} is associated with the following subroutines:

- **get_operation(\mathbf{V})**: This returns the operation that computes \mathbf{V} , represented by the edges coming into \mathbf{V} in the computational graph. For example, there may be a Python or C++ class representing the matrix multiplication operation, and the `get_operation` function. Suppose we have a variable that is created by matrix multiplication, $\mathbf{C} = \mathbf{A}\mathbf{B}$. Then `get_operation(\mathbf{V})` returns a pointer to an instance of the corresponding C++ class.
- **get_consumers(\mathbf{V}, \mathcal{G})**: This returns the list of variables that are children of \mathbf{V} in the computational graph \mathcal{G} .
- **get_inputs(\mathbf{V}, \mathcal{G})**: This returns the list of variables that are parents of \mathbf{V} in the computational graph \mathcal{G} .

Each operation `op` is also associated with a `bprop` operation. This `bprop` operation can compute a Jacobian-vector product as described by equation 6.47. This is how the back-propagation algorithm is able to achieve great generality. Each operation is responsible for knowing how to back-propagate through the edges in the graph that it participates in. For example, we might use a matrix multiplication operation to create a variable $\mathbf{C} = \mathbf{AB}$. Suppose that the gradient of a scalar z with respect to \mathbf{C} is given by \mathbf{G} . The matrix multiplication operation is responsible for defining two back-propagation rules, one for each of its input arguments. If we call the `bprop` method to request the gradient with respect to \mathbf{A} given that the gradient on the output is \mathbf{G} , then the `bprop` method of the matrix multiplication operation must state that the gradient with respect to \mathbf{A} is given by \mathbf{GB}^\top . Likewise, if we call the `bprop` method to request the gradient with respect to \mathbf{B} , then the matrix operation is responsible for implementing the `bprop` method and specifying that the desired gradient is given by $\mathbf{A}^\top \mathbf{G}$. The back-propagation algorithm itself does not need to know any differentiation rules. It only needs to call each operation's `bprop` rules with the right arguments. Formally, `op.bprop(inputs, X, G)` must return

$$\sum_i (\nabla_{\mathbf{X}} \text{op.f(inputs)}_i) G_i, \quad (6.54)$$

which is just an implementation of the chain rule as expressed in equation 6.47. Here, `inputs` is a list of inputs that are supplied to the operation, `op.f` is the mathematical function that the operation implements, \mathbf{X} is the input whose gradient we wish to compute, and \mathbf{G} is the gradient on the output of the operation.

The `op.bprop` method should always pretend that all of its inputs are distinct from each other, even if they are not. For example, if the `mul` operator is passed two copies of x to compute x^2 , the `op.bprop` method should still return x as the derivative with respect to both inputs. The back-propagation algorithm will later add both of these arguments together to obtain $2x$, which is the correct total derivative on x .

Software implementations of back-propagation usually provide both the operations and their `bprop` methods, so that users of deep learning software libraries are able to back-propagate through graphs built using common operations like matrix multiplication, exponents, logarithms, and so on. Software engineers who build a new implementation of back-propagation or advanced users who need to add their own operation to an existing library must usually derive the `op.bprop` method for any new operations manually.

The back-propagation algorithm is formally described in algorithm 6.5.

Algorithm 6.5 The outermost skeleton of the back-propagation algorithm. This portion does simple setup and cleanup work. Most of the important work happens in the `build_grad` subroutine of algorithm 6.6

Require: \mathbb{T} , the target set of variables whose gradients must be computed.

Require: \mathcal{G} , the computational graph

Require: z , the variable to be differentiated

Let \mathcal{G}' be \mathcal{G} pruned to contain only nodes that are ancestors of z and descendants of nodes in \mathbb{T} .

Initialize `grad_table`, a data structure associating tensors to their gradients

`grad_table`[z] $\leftarrow 1$

for \mathbf{V} in \mathbb{T} **do**

`build_grad`($\mathbf{V}, \mathcal{G}, \mathcal{G}', \text{grad_table}$)

end for

Return `grad_table` restricted to \mathbb{T}

In section 6.5.2, we explained that back-propagation was developed in order to avoid computing the same subexpression in the chain rule multiple times. The naive algorithm could have exponential runtime due to these repeated subexpressions. Now that we have specified the back-propagation algorithm, we can understand its computational cost. If we assume that each operation evaluation has roughly the same cost, then we may analyze the computational cost in terms of the number of operations executed. Keep in mind here that we refer to an operation as the fundamental unit of our computational graph, which might actually consist of very many arithmetic operations (for example, we might have a graph that treats matrix multiplication as a single operation). Computing a gradient in a graph with n nodes will never execute more than $O(n^2)$ operations or store the output of more than $O(n^2)$ operations. Here we are counting operations in the computational graph, not individual operations executed by the underlying hardware, so it is important to remember that the runtime of each operation may be highly variable. For example, multiplying two matrices that each contain millions of entries might correspond to a single operation in the graph. We can see that computing the gradient requires at most $O(n^2)$ operations because the forward propagation stage will at worst execute all n nodes in the original graph (depending on which values we want to compute, we may not need to execute the entire graph). The back-propagation algorithm adds one Jacobian-vector product, which should be expressed with $O(1)$ nodes, per edge in the original graph. Because the computational graph is a directed acyclic graph it has at most $O(n^2)$ edges. For the kinds of graphs that are commonly used in practice, the situation is even better. Most neural network cost functions are

Algorithm 6.6 The inner loop subroutine `build_grad(V, G, G', grad_table)` of the back-propagation algorithm, called by the back-propagation algorithm defined in algorithm 6.5.

Require: \mathbf{V} , the variable whose gradient should be added to \mathcal{G} and `grad_table`.
Require: \mathcal{G} , the graph to modify.
Require: \mathcal{G}' , the restriction of \mathcal{G} to nodes that participate in the gradient.
Require: `grad_table`, a data structure mapping nodes to their gradients

```
if  $\mathbf{V}$  is in grad_table then
    Return grad_table[ $\mathbf{V}$ ]
end if
 $i \leftarrow 1$ 
for  $\mathbf{C}$  in get_consumers( $\mathbf{V}, \mathcal{G}'$ ) do
     $\text{op} \leftarrow \text{get_operation}(\mathbf{C})$ 
     $\mathbf{D} \leftarrow \text{build_grad}(\mathbf{C}, \mathcal{G}, \mathcal{G}', \text{grad\_table})$ 
     $\mathbf{G}^{(i)} \leftarrow \text{op.bprop}(\text{get_inputs}(\mathbf{C}, \mathcal{G}'), \mathbf{V}, \mathbf{D})$ 
     $i \leftarrow i + 1$ 
end for
 $\mathbf{G} \leftarrow \sum_i \mathbf{G}^{(i)}$ 
grad_table[ $\mathbf{V}$ ] =  $\mathbf{G}$ 
Insert  $\mathbf{G}$  and the operations creating it into  $\mathcal{G}$ 
Return  $\mathbf{G}$ 
```

roughly chain-structured, causing back-propagation to have $O(n)$ cost. This is far better than the naive approach, which might need to execute exponentially many nodes. This potentially exponential cost can be seen by expanding and rewriting the recursive chain rule (equation 6.49) non-recursively:

$$\frac{\partial u^{(n)}}{\partial u^{(j)}} = \sum_{\substack{\text{path } (u^{(\pi_1)}, u^{(\pi_2)}, \dots, u^{(\pi_t)}), \\ \text{from } \pi_1=j \text{ to } \pi_t=n}} \prod_{k=2}^t \frac{\partial u^{(\pi_k)}}{\partial u^{(\pi_{k-1})}}. \quad (6.55)$$

Since the number of paths from node j to node n can grow exponentially in the length of these paths, the number of terms in the above sum, which is the number of such paths, can grow exponentially with the depth of the forward propagation graph. This large cost would be incurred because the same computation for $\frac{\partial u^{(i)}}{\partial u^{(j)}}$ would be redone many times. To avoid such recomputation, we can think of back-propagation as a table-filling algorithm that takes advantage of storing intermediate results $\frac{\partial u^{(n)}}{\partial u^{(i)}}$. Each node in the graph has a corresponding slot in a table to store the gradient for that node. By filling in these table entries in order,

back-propagation avoids repeating many common subexpressions. This table-filling strategy is sometimes called **dynamic programming**.

6.5.7 Example: Back-Propagation for MLP Training

As an example, we walk through the back-propagation algorithm as it is used to train a multilayer perceptron.

Here we develop a very simple multilayer perception with a single hidden layer. To train this model, we will use minibatch stochastic gradient descent. The back-propagation algorithm is used to compute the gradient of the cost on a single minibatch. Specifically, we use a minibatch of examples from the training set formatted as a design matrix \mathbf{X} and a vector of associated class labels \mathbf{y} . The network computes a layer of hidden features $\mathbf{H} = \max\{0, \mathbf{X}\mathbf{W}^{(1)}\}$. To simplify the presentation we do not use biases in this model. We assume that our graph language includes a `relu` operation that can compute $\max\{0, \mathbf{Z}\}$ element-wise. The predictions of the unnormalized log probabilities over classes are then given by $\mathbf{HW}^{(2)}$. We assume that our graph language includes a `cross_entropy` operation that computes the cross-entropy between the targets \mathbf{y} and the probability distribution defined by these unnormalized log probabilities. The resulting cross-entropy defines the cost J_{MLE} . Minimizing this cross-entropy performs maximum likelihood estimation of the classifier. However, to make this example more realistic, we also include a regularization term. The total cost

$$J = J_{\text{MLE}} + \lambda \left(\sum_{i,j} \left(W_{i,j}^{(1)} \right)^2 + \sum_{i,j} \left(W_{i,j}^{(2)} \right)^2 \right) \quad (6.56)$$

consists of the cross-entropy and a weight decay term with coefficient λ . The computational graph is illustrated in figure 6.11.

The computational graph for the gradient of this example is large enough that it would be tedious to draw or to read. This demonstrates one of the benefits of the back-propagation algorithm, which is that it can automatically generate gradients that would be straightforward but tedious for a software engineer to derive manually.

We can roughly trace out the behavior of the back-propagation algorithm by looking at the forward propagation graph in figure 6.11. To train, we wish to compute both $\nabla_{\mathbf{W}^{(1)}} J$ and $\nabla_{\mathbf{W}^{(2)}} J$. There are two different paths leading backward from J to the weights: one through the cross-entropy cost, and one through the weight decay cost. The weight decay cost is relatively simple; it will always contribute $2\lambda \mathbf{W}^{(i)}$ to the gradient on $\mathbf{W}^{(i)}$.

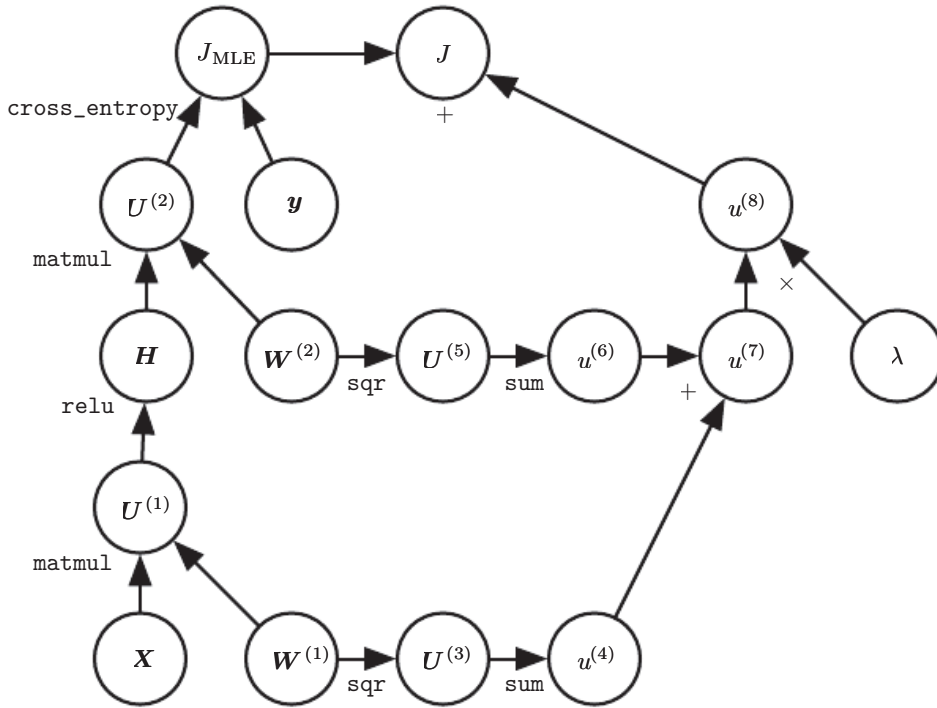


Figure 6.11: The computational graph used to compute the cost used to train our example of a single-layer MLP using the cross-entropy loss and weight decay.

The other path through the cross-entropy cost is slightly more complicated. Let \mathbf{G} be the gradient on the unnormalized log probabilities $\mathbf{U}^{(2)}$ provided by the `cross_entropy` operation. The back-propagation algorithm now needs to explore two different branches. On the shorter branch, it adds $\mathbf{H}^\top \mathbf{G}$ to the gradient on $\mathbf{W}^{(2)}$, using the back-propagation rule for the second argument to the matrix multiplication operation. The other branch corresponds to the longer chain descending further along the network. First, the back-propagation algorithm computes $\nabla_{\mathbf{H}} J = \mathbf{G} \mathbf{W}^{(2)\top}$ using the back-propagation rule for the first argument to the matrix multiplication operation. Next, the `relu` operation uses its back-propagation rule to zero out components of the gradient corresponding to entries of $\mathbf{U}^{(1)}$ that were less than 0. Let the result be called \mathbf{G}' . The last step of the back-propagation algorithm is to use the back-propagation rule for the second argument of the `matmul` operation to add $\mathbf{X}^\top \mathbf{G}'$ to the gradient on $\mathbf{W}^{(1)}$.

After these gradients have been computed, it is the responsibility of the gradient descent algorithm, or another optimization algorithm, to use these gradients to update the parameters.

For the MLP, the computational cost is dominated by the cost of matrix multiplication. During the forward propagation stage, we multiply by each weight

matrix, resulting in $O(w)$ multiply-adds, where w is the number of weights. During the backward propagation stage, we multiply by the transpose of each weight matrix, which has the same computational cost. The main memory cost of the algorithm is that we need to store the input to the nonlinearity of the hidden layer. This value is stored from the time it is computed until the backward pass has returned to the same point. The memory cost is thus $O(mn_h)$, where m is the number of examples in the minibatch and n_h is the number of hidden units.

6.5.8 Complications

Our description of the back-propagation algorithm here is simpler than the implementations actually used in practice.

As noted above, we have restricted the definition of an operation to be a function that returns a single tensor. Most software implementations need to support operations that can return more than one tensor. For example, if we wish to compute both the maximum value in a tensor and the index of that value, it is best to compute both in a single pass through memory, so it is most efficient to implement this procedure as a single operation with two outputs.

We have not described how to control the memory consumption of back-propagation. Back-propagation often involves summation of many tensors together. In the naive approach, each of these tensors would be computed separately, then all of them would be added in a second step. The naive approach has an overly high memory bottleneck that can be avoided by maintaining a single buffer and adding each value to that buffer as it is computed.

Real-world implementations of back-propagation also need to handle various data types, such as 32-bit floating point, 64-bit floating point, and integer values. The policy for handling each of these types takes special care to design.

Some operations have undefined gradients, and it is important to track these cases and determine whether the gradient requested by the user is undefined.

Various other technicalities make real-world differentiation more complicated. These technicalities are not insurmountable, and this chapter has described the key intellectual tools needed to compute derivatives, but it is important to be aware that many more subtleties exist.

6.5.9 Differentiation outside the Deep Learning Community

The deep learning community has been somewhat isolated from the broader computer science community and has largely developed its own cultural attitudes

concerning how to perform differentiation. More generally, the field of **automatic differentiation** is concerned with how to compute derivatives algorithmically. The back-propagation algorithm described here is only one approach to automatic differentiation. It is a special case of a broader class of techniques called **reverse mode accumulation**. Other approaches evaluate the subexpressions of the chain rule in different orders. In general, determining the order of evaluation that results in the lowest computational cost is a difficult problem. Finding the optimal sequence of operations to compute the gradient is NP-complete (Naumann, 2008), in the sense that it may require simplifying algebraic expressions into their least expensive form.

For example, suppose we have variables p_1, p_2, \dots, p_n representing probabilities and variables z_1, z_2, \dots, z_n representing unnormalized log probabilities. Suppose we define

$$q_i = \frac{\exp(z_i)}{\sum_i \exp(z_i)}, \quad (6.57)$$

where we build the softmax function out of exponentiation, summation and division operations, and construct a cross-entropy loss $J = -\sum_i p_i \log q_i$. A human mathematician can observe that the derivative of J with respect to z_i takes a very simple form: $q_i - p_i$. The back-propagation algorithm is not capable of simplifying the gradient this way, and will instead explicitly propagate gradients through all of the logarithm and exponentiation operations in the original graph. Some software libraries such as Theano (Bergstra *et al.*, 2010; Bastien *et al.*, 2012) are able to perform some kinds of algebraic substitution to improve over the graph proposed by the pure back-propagation algorithm.

When the forward graph \mathcal{G} has a single output node and each partial derivative $\frac{\partial u^{(i)}}{\partial u^{(j)}}$ can be computed with a constant amount of computation, back-propagation guarantees that the number of computations for the gradient computation is of the same order as the number of computations for the forward computation: this can be seen in algorithm 6.2 because each local partial derivative $\frac{\partial u^{(i)}}{\partial u^{(j)}}$ needs to be computed only once along with an associated multiplication and addition for the recursive chain-rule formulation (equation 6.49). The overall computation is therefore $O(\# \text{ edges})$. However, it can potentially be reduced by simplifying the computational graph constructed by back-propagation, and this is an NP-complete task. Implementations such as Theano and TensorFlow use heuristics based on matching known simplification patterns in order to iteratively attempt to simplify the graph. We defined back-propagation only for the computation of a gradient of a scalar output but back-propagation can be extended to compute a Jacobian (either of k different scalar nodes in the graph, or of a tensor-valued node containing k values). A naive implementation may then need k times more computation: for

each scalar internal node in the original forward graph, the naive implementation computes k gradients instead of a single gradient. When the number of outputs of the graph is larger than the number of inputs, it is sometimes preferable to use another form of automatic differentiation called **forward mode accumulation**. Forward mode computation has been proposed for obtaining real-time computation of gradients in recurrent networks, for example (Williams and Zipser, 1989). This also avoids the need to store the values and gradients for the whole graph, trading off computational efficiency for memory. The relationship between forward mode and backward mode is analogous to the relationship between left-multiplying versus right-multiplying a sequence of matrices, such as

$$\mathbf{A}\mathbf{B}\mathbf{C}\mathbf{D}, \quad (6.58)$$

where the matrices can be thought of as Jacobian matrices. For example, if \mathbf{D} is a column vector while \mathbf{A} has many rows, this corresponds to a graph with a single output and many inputs, and starting the multiplications from the end and going backwards only requires matrix-vector products. This corresponds to the backward mode. Instead, starting to multiply from the left would involve a series of matrix-matrix products, which makes the whole computation much more expensive. However, if \mathbf{A} has fewer rows than \mathbf{D} has columns, it is cheaper to run the multiplications left-to-right, corresponding to the forward mode.

In many communities outside of machine learning, it is more common to implement differentiation software that acts directly on traditional programming language code, such as Python or C code, and automatically generates programs that differentiate functions written in these languages. In the deep learning community, computational graphs are usually represented by explicit data structures created by specialized libraries. The specialized approach has the drawback of requiring the library developer to define the `bprop` methods for every operation and limiting the user of the library to only those operations that have been defined. However, the specialized approach also has the benefit of allowing customized back-propagation rules to be developed for each operation, allowing the developer to improve speed or stability in non-obvious ways that an automatic procedure would presumably be unable to replicate.

Back-propagation is therefore not the only way or the optimal way of computing the gradient, but it is a very practical method that continues to serve the deep learning community very well. In the future, differentiation technology for deep networks may improve as deep learning practitioners become more aware of advances in the broader field of automatic differentiation.

6.5.10 Higher-Order Derivatives

Some software frameworks support the use of higher-order derivatives. Among the deep learning software frameworks, this includes at least Theano and TensorFlow. These libraries use the same kind of data structure to describe the expressions for derivatives as they use to describe the original function being differentiated. This means that the symbolic differentiation machinery can be applied to derivatives.

In the context of deep learning, it is rare to compute a single second derivative of a scalar function. Instead, we are usually interested in properties of the Hessian matrix. If we have a function $f : \mathbb{R}^n \rightarrow \mathbb{R}$, then the Hessian matrix is of size $n \times n$. In typical deep learning applications, n will be the number of parameters in the model, which could easily number in the billions. The entire Hessian matrix is thus infeasible to even represent.

Instead of explicitly computing the Hessian, the typical deep learning approach is to use **Krylov methods**. Krylov methods are a set of iterative techniques for performing various operations like approximately inverting a matrix or finding approximations to its eigenvectors or eigenvalues, without using any operation other than matrix-vector products.

In order to use Krylov methods on the Hessian, we only need to be able to compute the product between the Hessian matrix \mathbf{H} and an arbitrary vector \mathbf{v} . A straightforward technique (Christianson, 1992) for doing so is to compute

$$\mathbf{H}\mathbf{v} = \nabla_{\mathbf{x}} \left[(\nabla_{\mathbf{x}} f(\mathbf{x}))^\top \mathbf{v} \right]. \quad (6.59)$$

Both of the gradient computations in this expression may be computed automatically by the appropriate software library. Note that the outer gradient expression takes the gradient of a function of the inner gradient expression.

If \mathbf{v} is itself a vector produced by a computational graph, it is important to specify that the automatic differentiation software should not differentiate through the graph that produced \mathbf{v} .

While computing the Hessian is usually not advisable, it is possible to do with Hessian vector products. One simply computes $\mathbf{H}\mathbf{e}^{(i)}$ for all $i = 1, \dots, n$, where $\mathbf{e}^{(i)}$ is the one-hot vector with $e_i^{(i)} = 1$ and all other entries equal to 0.

6.6 Historical Notes

Feedforward networks can be seen as efficient nonlinear function approximators based on using gradient descent to minimize the error in a function approximation.

From this point of view, the modern feedforward network is the culmination of centuries of progress on the general function approximation task.

The chain rule that underlies the back-propagation algorithm was invented in the 17th century ([Leibniz, 1676](#); [L'Hôpital, 1696](#)). Calculus and algebra have long been used to solve optimization problems in closed form, but gradient descent was not introduced as a technique for iteratively approximating the solution to optimization problems until the 19th century ([Cauchy, 1847](#)).

Beginning in the 1940s, these function approximation techniques were used to motivate machine learning models such as the perceptron. However, the earliest models were based on linear models. Critics including Marvin Minsky pointed out several of the flaws of the linear model family, such as its inability to learn the XOR function, which led to a backlash against the entire neural network approach.

Learning nonlinear functions required the development of a multilayer perceptron and a means of computing the gradient through such a model. Efficient applications of the chain rule based on dynamic programming began to appear in the 1960s and 1970s, mostly for control applications ([Kelley, 1960](#); [Bryson and Denham, 1961](#); [Dreyfus, 1962](#); [Bryson and Ho, 1969](#); [Dreyfus, 1973](#)) but also for sensitivity analysis ([Linnainmaa, 1976](#)). [Werbos \(1981\)](#) proposed applying these techniques to training artificial neural networks. The idea was finally developed in practice after being independently rediscovered in different ways ([LeCun, 1985](#); [Parker, 1985](#); [Rumelhart *et al.*, 1986a](#)). The book **Parallel Distributed Processing** presented the results of some of the first successful experiments with back-propagation in a chapter ([Rumelhart *et al.*, 1986b](#)) that contributed greatly to the popularization of back-propagation and initiated a very active period of research in multi-layer neural networks. However, the ideas put forward by the authors of that book and in particular by Rumelhart and Hinton go much beyond back-propagation. They include crucial ideas about the possible computational implementation of several central aspects of cognition and learning, which came under the name of “connectionism” because of the importance this school of thought places on the connections between neurons as the locus of learning and memory. In particular, these ideas include the notion of distributed representation ([Hinton *et al.*, 1986](#)).

Following the success of back-propagation, neural network research gained popularity and reached a peak in the early 1990s. Afterwards, other machine learning techniques became more popular until the modern deep learning renaissance that began in 2006.

The core ideas behind modern feedforward networks have not changed substantially since the 1980s. The same back-propagation algorithm and the same

approaches to gradient descent are still in use. Most of the improvement in neural network performance from 1986 to 2015 can be attributed to two factors. First, larger datasets have reduced the degree to which statistical generalization is a challenge for neural networks. Second, neural networks have become much larger, due to more powerful computers, and better software infrastructure. However, a small number of algorithmic changes have improved the performance of neural networks noticeably.

One of these algorithmic changes was the replacement of mean squared error with the cross-entropy family of loss functions. Mean squared error was popular in the 1980s and 1990s, but was gradually replaced by cross-entropy losses and the principle of maximum likelihood as ideas spread between the statistics community and the machine learning community. The use of cross-entropy losses greatly improved the performance of models with sigmoid and softmax outputs, which had previously suffered from saturation and slow learning when using the mean squared error loss.

The other major algorithmic change that has greatly improved the performance of feedforward networks was the replacement of sigmoid hidden units with piecewise linear hidden units, such as rectified linear units. Rectification using the $\max\{0, z\}$ function was introduced in early neural network models and dates back at least as far as the Cognitron and Neocognitron (Fukushima, 1975, 1980). These early models did not use rectified linear units, but instead applied rectification to nonlinear functions. Despite the early popularity of rectification, rectification was largely replaced by sigmoids in the 1980s, perhaps because sigmoids perform better when neural networks are very small. As of the early 2000s, rectified linear units were avoided due to a somewhat superstitious belief that activation functions with non-differentiable points must be avoided. This began to change in about 2009. Jarrett *et al.* (2009) observed that “using a rectifying nonlinearity is the single most important factor in improving the performance of a recognition system” among several different factors of neural network architecture design.

For small datasets, Jarrett *et al.* (2009) observed that using rectifying nonlinearities is even more important than learning the weights of the hidden layers. Random weights are sufficient to propagate useful information through a rectified linear network, allowing the classifier layer at the top to learn how to map different feature vectors to class identities.

When more data is available, learning begins to extract enough useful knowledge to exceed the performance of randomly chosen parameters. Glorot *et al.* (2011a) showed that learning is far easier in deep rectified linear networks than in deep networks that have curvature or two-sided saturation in their activation functions.

Rectified linear units are also of historical interest because they show that neuroscience has continued to have an influence on the development of deep learning algorithms. Glorot *et al.* (2011a) motivate rectified linear units from biological considerations. The half-rectifying nonlinearity was intended to capture these properties of biological neurons: 1) For some inputs, biological neurons are completely inactive. 2) For some inputs, a biological neuron’s output is proportional to its input. 3) Most of the time, biological neurons operate in the regime where they are inactive (i.e., they should have **sparse activations**).

When the modern resurgence of deep learning began in 2006, feedforward networks continued to have a bad reputation. From about 2006-2012, it was widely believed that feedforward networks would not perform well unless they were assisted by other models, such as probabilistic models. Today, it is now known that with the right resources and engineering practices, feedforward networks perform very well. Today, gradient-based learning in feedforward networks is used as a tool to develop probabilistic models, such as the variational autoencoder and generative adversarial networks, described in chapter 20. Rather than being viewed as an unreliable technology that must be supported by other techniques, gradient-based learning in feedforward networks has been viewed since 2012 as a powerful technology that may be applied to many other machine learning tasks. In 2006, the community used unsupervised learning to support supervised learning, and now, ironically, it is more common to use supervised learning to support unsupervised learning.

Feedforward networks continue to have unfulfilled potential. In the future, we expect they will be applied to many more tasks, and that advances in optimization algorithms and model design will improve their performance even further. This chapter has primarily described the neural network family of models. In the subsequent chapters, we turn to how to use these models—how to regularize and train them.

Chapter 7

Regularization for Deep Learning

A central problem in machine learning is how to make an algorithm that will perform well not just on the training data, but also on new inputs. Many strategies used in machine learning are explicitly designed to reduce the test error, possibly at the expense of increased training error. These strategies are known collectively as regularization. As we will see there are a great many forms of regularization available to the deep learning practitioner. In fact, developing more effective regularization strategies has been one of the major research efforts in the field.

Chapter 5 introduced the basic concepts of generalization, underfitting, overfitting, bias, variance and regularization. If you are not already familiar with these notions, please refer to that chapter before continuing with this one.

In this chapter, we describe regularization in more detail, focusing on regularization strategies for deep models or models that may be used as building blocks to form deep models.

Some sections of this chapter deal with standard concepts in machine learning. If you are already familiar with these concepts, feel free to skip the relevant sections. However, most of this chapter is concerned with the extension of these basic concepts to the particular case of neural networks.

In section 5.2.2, we defined regularization as “any modification we make to a learning algorithm that is intended to reduce its generalization error but not its training error.” There are many regularization strategies. Some put extra constraints on a machine learning model, such as adding restrictions on the parameter values. Some add extra terms in the objective function that can be thought of as corresponding to a soft constraint on the parameter values. If chosen carefully, these extra constraints and penalties can lead to improved performance

on the test set. Sometimes these constraints and penalties are designed to encode specific kinds of prior knowledge. Other times, these constraints and penalties are designed to express a generic preference for a simpler model class in order to promote generalization. Sometimes penalties and constraints are necessary to make an underdetermined problem determined. Other forms of regularization, known as ensemble methods, combine multiple hypotheses that explain the training data.

In the context of deep learning, most regularization strategies are based on regularizing estimators. Regularization of an estimator works by trading increased bias for reduced variance. An effective regularizer is one that makes a profitable trade, reducing variance significantly while not overly increasing the bias. When we discussed generalization and overfitting in chapter 5, we focused on three situations, where the model family being trained either (1) excluded the true data generating process—corresponding to underfitting and inducing bias, or (2) matched the true data generating process, or (3) included the generating process but also many other possible generating processes—the overfitting regime where variance rather than bias dominates the estimation error. The goal of regularization is to take a model from the third regime into the second regime.

In practice, an overly complex model family does not necessarily include the target function or the true data generating process, or even a close approximation of either. We almost never have access to the true data generating process so we can never know for sure if the model family being estimated includes the generating process or not. However, most applications of deep learning algorithms are to domains where the true data generating process is almost certainly outside the model family. Deep learning algorithms are typically applied to extremely complicated domains such as images, audio sequences and text, for which the true generation process essentially involves simulating the entire universe. To some extent, we are always trying to fit a square peg (the data generating process) into a round hole (our model family).

What this means is that controlling the complexity of the model is not a simple matter of finding the model of the right size, with the right number of parameters. Instead, we might find—and indeed in practical deep learning scenarios, we almost always do find—that the best fitting model (in the sense of minimizing generalization error) is a large model that has been regularized appropriately.

We now review several strategies for how to create such a large, deep, regularized model.

7.1 Parameter Norm Penalties

Regularization has been used for decades prior to the advent of deep learning. Linear models such as linear regression and logistic regression allow simple, straightforward, and effective regularization strategies.

Many regularization approaches are based on limiting the capacity of models, such as neural networks, linear regression, or logistic regression, by adding a parameter norm penalty $\Omega(\boldsymbol{\theta})$ to the objective function J . We denote the regularized objective function by \tilde{J} :

$$\tilde{J}(\boldsymbol{\theta}; \mathbf{X}, \mathbf{y}) = J(\boldsymbol{\theta}; \mathbf{X}, \mathbf{y}) + \alpha\Omega(\boldsymbol{\theta}) \quad (7.1)$$

where $\alpha \in [0, \infty)$ is a hyperparameter that weights the relative contribution of the norm penalty term, Ω , relative to the standard objective function J . Setting α to 0 results in no regularization. Larger values of α correspond to more regularization.

When our training algorithm minimizes the regularized objective function \tilde{J} it will decrease both the original objective J on the training data and some measure of the size of the parameters $\boldsymbol{\theta}$ (or some subset of the parameters). Different choices for the parameter norm Ω can result in different solutions being preferred. In this section, we discuss the effects of the various norms when used as penalties on the model parameters.

Before delving into the regularization behavior of different norms, we note that for neural networks, we typically choose to use a parameter norm penalty Ω that penalizes *only the weights* of the affine transformation at each layer and leaves the biases unregularized. The biases typically require less data to fit accurately than the weights. Each weight specifies how two variables interact. Fitting the weight well requires observing both variables in a variety of conditions. Each bias controls only a single variable. This means that we do not induce too much variance by leaving the biases unregularized. Also, regularizing the bias parameters can introduce a significant amount of underfitting. We therefore use the vector \mathbf{w} to indicate all of the weights that should be affected by a norm penalty, while the vector $\boldsymbol{\theta}$ denotes all of the parameters, including both \mathbf{w} and the unregularized parameters.

In the context of neural networks, it is sometimes desirable to use a separate penalty with a different α coefficient for each layer of the network. Because it can be expensive to search for the correct value of multiple hyperparameters, it is still reasonable to use the same weight decay at all layers just to reduce the size of search space.

7.1.1 L^2 Parameter Regularization

We have already seen, in section 5.2.2, one of the simplest and most common kinds of parameter norm penalty: the L^2 parameter norm penalty commonly known as **weight decay**. This regularization strategy drives the weights closer to the origin¹ by adding a regularization term $\Omega(\boldsymbol{\theta}) = \frac{1}{2}\|\boldsymbol{\theta}\|_2^2$ to the objective function. In other academic communities, L^2 regularization is also known as **ridge regression** or **Tikhonov regularization**.

We can gain some insight into the behavior of weight decay regularization by studying the gradient of the regularized objective function. To simplify the presentation, we assume no bias parameter, so $\boldsymbol{\theta}$ is just \mathbf{w} . Such a model has the following total objective function:

$$\tilde{J}(\mathbf{w}; \mathbf{X}, \mathbf{y}) = \frac{\alpha}{2} \mathbf{w}^\top \mathbf{w} + J(\mathbf{w}; \mathbf{X}, \mathbf{y}), \quad (7.2)$$

with the corresponding parameter gradient

$$\nabla_{\mathbf{w}} \tilde{J}(\mathbf{w}; \mathbf{X}, \mathbf{y}) = \alpha \mathbf{w} + \nabla_{\mathbf{w}} J(\mathbf{w}; \mathbf{X}, \mathbf{y}). \quad (7.3)$$

To take a single gradient step to update the weights, we perform this update:

$$\mathbf{w} \leftarrow \mathbf{w} - \epsilon (\alpha \mathbf{w} + \nabla_{\mathbf{w}} J(\mathbf{w}; \mathbf{X}, \mathbf{y})). \quad (7.4)$$

Written another way, the update is:

$$\mathbf{w} \leftarrow (1 - \epsilon \alpha) \mathbf{w} - \epsilon \nabla_{\mathbf{w}} J(\mathbf{w}; \mathbf{X}, \mathbf{y}). \quad (7.5)$$

We can see that the addition of the weight decay term has modified the learning rule to multiplicatively shrink the weight vector by a constant factor on each step, just before performing the usual gradient update. This describes what happens in a single step. But what happens over the entire course of training?

We will further simplify the analysis by making a quadratic approximation to the objective function in the neighborhood of the value of the weights that obtains minimal unregularized training cost, $\mathbf{w}^* = \arg \min_{\mathbf{w}} J(\mathbf{w})$. If the objective function is truly quadratic, as in the case of fitting a linear regression model with

¹More generally, we could regularize the parameters to be near any specific point in space and, surprisingly, still get a regularization effect, but better results will be obtained for a value closer to the true one, with zero being a default value that makes sense when we do not know if the correct value should be positive or negative. Since it is far more common to regularize the model parameters towards zero, we will focus on this special case in our exposition.

mean squared error, then the approximation is perfect. The approximation \hat{J} is given by

$$\hat{J}(\boldsymbol{\theta}) = J(\mathbf{w}^*) + \frac{1}{2}(\mathbf{w} - \mathbf{w}^*)^\top \mathbf{H}(\mathbf{w} - \mathbf{w}^*), \quad (7.6)$$

where \mathbf{H} is the Hessian matrix of J with respect to \mathbf{w} evaluated at \mathbf{w}^* . There is no first-order term in this quadratic approximation, because \mathbf{w}^* is defined to be a minimum, where the gradient vanishes. Likewise, because \mathbf{w}^* is the location of a minimum of J , we can conclude that \mathbf{H} is positive semidefinite.

The minimum of \hat{J} occurs where its gradient

$$\nabla_{\mathbf{w}} \hat{J}(\mathbf{w}) = \mathbf{H}(\mathbf{w} - \mathbf{w}^*) \quad (7.7)$$

is equal to $\mathbf{0}$.

To study the effect of weight decay, we modify equation 7.7 by adding the weight decay gradient. We can now solve for the minimum of the regularized version of \hat{J} . We use the variable $\tilde{\mathbf{w}}$ to represent the location of the minimum.

$$\alpha \tilde{\mathbf{w}} + \mathbf{H}(\tilde{\mathbf{w}} - \mathbf{w}^*) = 0 \quad (7.8)$$

$$(\mathbf{H} + \alpha \mathbf{I})\tilde{\mathbf{w}} = \mathbf{H}\mathbf{w}^* \quad (7.9)$$

$$\tilde{\mathbf{w}} = (\mathbf{H} + \alpha \mathbf{I})^{-1} \mathbf{H}\mathbf{w}^*. \quad (7.10)$$

As α approaches 0, the regularized solution $\tilde{\mathbf{w}}$ approaches \mathbf{w}^* . But what happens as α grows? Because \mathbf{H} is real and symmetric, we can decompose it into a diagonal matrix Λ and an orthonormal basis of eigenvectors, \mathbf{Q} , such that $\mathbf{H} = \mathbf{Q}\Lambda\mathbf{Q}^\top$. Applying the decomposition to equation 7.10, we obtain:

$$\tilde{\mathbf{w}} = (\mathbf{Q}\Lambda\mathbf{Q}^\top + \alpha \mathbf{I})^{-1} \mathbf{Q}\Lambda\mathbf{Q}^\top \mathbf{w}^* \quad (7.11)$$

$$= [\mathbf{Q}(\Lambda + \alpha \mathbf{I})\mathbf{Q}^\top]^{-1} \mathbf{Q}\Lambda\mathbf{Q}^\top \mathbf{w}^* \quad (7.12)$$

$$= \mathbf{Q}(\Lambda + \alpha \mathbf{I})^{-1} \Lambda \mathbf{Q}^\top \mathbf{w}^*. \quad (7.13)$$

We see that the effect of weight decay is to rescale \mathbf{w}^* along the axes defined by the eigenvectors of \mathbf{H} . Specifically, the component of \mathbf{w}^* that is aligned with the i -th eigenvector of \mathbf{H} is rescaled by a factor of $\frac{\lambda_i}{\lambda_i + \alpha}$. (You may wish to review how this kind of scaling works, first explained in figure 2.3).

Along the directions where the eigenvalues of \mathbf{H} are relatively large, for example, where $\lambda_i \gg \alpha$, the effect of regularization is relatively small. However, components with $\lambda_i \ll \alpha$ will be shrunk to have nearly zero magnitude. This effect is illustrated in figure 7.1.

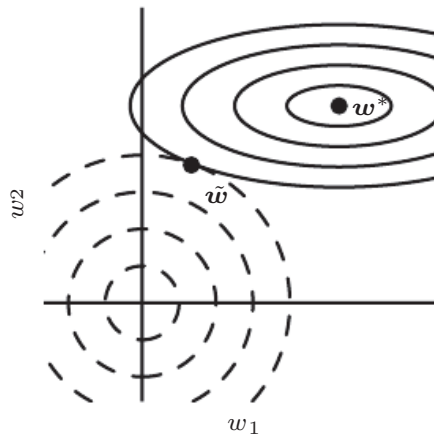


Figure 7.1: An illustration of the effect of L^2 (or weight decay) regularization on the value of the optimal \mathbf{w} . The solid ellipses represent contours of equal value of the unregularized objective. The dotted circles represent contours of equal value of the L^2 regularizer. At the point $\tilde{\mathbf{w}}$, these competing objectives reach an equilibrium. In the first dimension, the eigenvalue of the Hessian of J is small. The objective function does not increase much when moving horizontally away from \mathbf{w}^* . Because the objective function does not express a strong preference along this direction, the regularizer has a strong effect on this axis. The regularizer pulls w_1 close to zero. In the second dimension, the objective function is very sensitive to movements away from \mathbf{w}^* . The corresponding eigenvalue is large, indicating high curvature. As a result, weight decay affects the position of w_2 relatively little.

Only directions along which the parameters contribute significantly to reducing the objective function are preserved relatively intact. In directions that do not contribute to reducing the objective function, a small eigenvalue of the Hessian tells us that movement in this direction will not significantly increase the gradient. Components of the weight vector corresponding to such unimportant directions are decayed away through the use of the regularization throughout training.

So far we have discussed weight decay in terms of its effect on the optimization of an abstract, general, quadratic cost function. How do these effects relate to machine learning in particular? We can find out by studying linear regression, a model for which the true cost function is quadratic and therefore amenable to the same kind of analysis we have used so far. Applying the analysis again, we will be able to obtain a special case of the same results, but with the solution now phrased in terms of the training data. For linear regression, the cost function is

the sum of squared errors:

$$(\mathbf{X}\mathbf{w} - \mathbf{y})^\top (\mathbf{X}\mathbf{w} - \mathbf{y}). \quad (7.14)$$

When we add L^2 regularization, the objective function changes to

$$(\mathbf{X}\mathbf{w} - \mathbf{y})^\top (\mathbf{X}\mathbf{w} - \mathbf{y}) + \frac{1}{2}\alpha\mathbf{w}^\top \mathbf{w}. \quad (7.15)$$

This changes the normal equations for the solution from

$$\mathbf{w} = (\mathbf{X}^\top \mathbf{X})^{-1} \mathbf{X}^\top \mathbf{y} \quad (7.16)$$

to

$$\mathbf{w} = (\mathbf{X}^\top \mathbf{X} + \alpha \mathbf{I})^{-1} \mathbf{X}^\top \mathbf{y}. \quad (7.17)$$

The matrix $\mathbf{X}^\top \mathbf{X}$ in equation 7.16 is proportional to the covariance matrix $\frac{1}{m} \mathbf{X}^\top \mathbf{X}$. Using L^2 regularization replaces this matrix with $(\mathbf{X}^\top \mathbf{X} + \alpha \mathbf{I})^{-1}$ in equation 7.17. The new matrix is the same as the original one, but with the addition of α to the diagonal. The diagonal entries of this matrix correspond to the variance of each input feature. We can see that L^2 regularization causes the learning algorithm to “perceive” the input \mathbf{X} as having higher variance, which makes it shrink the weights on features whose covariance with the output target is low compared to this added variance.

7.1.2 L^1 Regularization

While L^2 weight decay is the most common form of weight decay, there are other ways to penalize the size of the model parameters. Another option is to use L^1 regularization.

Formally, L^1 regularization on the model parameter \mathbf{w} is defined as:

$$\Omega(\boldsymbol{\theta}) = \|\mathbf{w}\|_1 = \sum_i |w_i|, \quad (7.18)$$

that is, as the sum of absolute values of the individual parameters.² We will now discuss the effect of L^1 regularization on the simple linear regression model, with no bias parameter, that we studied in our analysis of L^2 regularization. In particular, we are interested in delineating the differences between L^1 and L^2 forms

²As with L^2 regularization, we could regularize the parameters towards a value that is not zero, but instead towards some parameter value $\mathbf{w}^{(o)}$. In that case the L^1 regularization would introduce the term $\Omega(\boldsymbol{\theta}) = \|\mathbf{w} - \mathbf{w}^{(o)}\|_1 = \sum_i |w_i - w_i^{(o)}|$.

of regularization. As with L^2 weight decay, L^1 weight decay controls the strength of the regularization by scaling the penalty Ω using a positive hyperparameter α . Thus, the regularized objective function $\tilde{J}(\mathbf{w}; \mathbf{X}, \mathbf{y})$ is given by

$$\tilde{J}(\mathbf{w}; \mathbf{X}, \mathbf{y}) = \alpha \|\mathbf{w}\|_1 + J(\mathbf{w}; \mathbf{X}, \mathbf{y}), \quad (7.19)$$

with the corresponding gradient (actually, sub-gradient):

$$\nabla_{\mathbf{w}} \tilde{J}(\mathbf{w}; \mathbf{X}, \mathbf{y}) = \alpha \text{sign}(\mathbf{w}) + \nabla_{\mathbf{w}} J(\mathbf{X}, \mathbf{y}; \mathbf{w}) \quad (7.20)$$

where $\text{sign}(\mathbf{w})$ is simply the sign of \mathbf{w} applied element-wise.

By inspecting equation 7.20, we can see immediately that the effect of L^1 regularization is quite different from that of L^2 regularization. Specifically, we can see that the regularization contribution to the gradient no longer scales linearly with each w_i ; instead it is a constant factor with a sign equal to $\text{sign}(w_i)$. One consequence of this form of the gradient is that we will not necessarily see clean algebraic solutions to quadratic approximations of $J(\mathbf{X}, \mathbf{y}; \mathbf{w})$ as we did for L^2 regularization.

Our simple linear model has a quadratic cost function that we can represent via its Taylor series. Alternately, we could imagine that this is a truncated Taylor series approximating the cost function of a more sophisticated model. The gradient in this setting is given by

$$\nabla_{\mathbf{w}} \hat{J}(\mathbf{w}) = \mathbf{H}(\mathbf{w} - \mathbf{w}^*), \quad (7.21)$$

where, again, \mathbf{H} is the Hessian matrix of J with respect to \mathbf{w} evaluated at \mathbf{w}^* .

Because the L^1 penalty does not admit clean algebraic expressions in the case of a fully general Hessian, we will also make the further simplifying assumption that the Hessian is diagonal, $\mathbf{H} = \text{diag}([H_{1,1}, \dots, H_{n,n}])$, where each $H_{i,i} > 0$. This assumption holds if the data for the linear regression problem has been preprocessed to remove all correlation between the input features, which may be accomplished using PCA.

Our quadratic approximation of the L^1 regularized objective function decomposes into a sum over the parameters:

$$\hat{J}(\mathbf{w}; \mathbf{X}, \mathbf{y}) = J(\mathbf{w}^*; \mathbf{X}, \mathbf{y}) + \sum_i \left[\frac{1}{2} H_{i,i} (\mathbf{w}_i - \mathbf{w}_i^*)^2 + \alpha |w_i| \right]. \quad (7.22)$$

The problem of minimizing this approximate cost function has an analytical solution (for each dimension i), with the following form:

$$w_i = \text{sign}(w_i^*) \max \left\{ |w_i^*| - \frac{\alpha}{H_{i,i}}, 0 \right\}. \quad (7.23)$$

Consider the situation where $w_i^* > 0$ for all i . There are two possible outcomes:

1. The case where $w_i^* \leq \frac{\alpha}{H_{i,i}}$. Here the optimal value of w_i under the regularized objective is simply $w_i = 0$. This occurs because the contribution of $J(\mathbf{w}; \mathbf{X}, \mathbf{y})$ to the regularized objective $\tilde{J}(\mathbf{w}; \mathbf{X}, \mathbf{y})$ is overwhelmed—in direction i —by the L^1 regularization which pushes the value of w_i to zero.
2. The case where $w_i^* > \frac{\alpha}{H_{i,i}}$. In this case, the regularization does not move the optimal value of w_i to zero but instead it just shifts it in that direction by a distance equal to $\frac{\alpha}{H_{i,i}}$.

A similar process happens when $w_i^* < 0$, but with the L^1 penalty making w_i less negative by $\frac{\alpha}{H_{i,i}}$, or 0.

In comparison to L^2 regularization, L^1 regularization results in a solution that is more **sparse**. Sparsity in this context refers to the fact that some parameters have an optimal value of zero. The sparsity of L^1 regularization is a qualitatively different behavior than arises with L^2 regularization. Equation 7.13 gave the solution \tilde{w} for L^2 regularization. If we revisit that equation using the assumption of a diagonal and positive definite Hessian \mathbf{H} that we introduced for our analysis of L^1 regularization, we find that $\tilde{w}_i = \frac{H_{i,i}}{H_{i,i} + \alpha} w_i^*$. If w_i^* was nonzero, then \tilde{w}_i remains nonzero. This demonstrates that L^2 regularization does not cause the parameters to become sparse, while L^1 regularization may do so for large enough α .

The sparsity property induced by L^1 regularization has been used extensively as a **feature selection** mechanism. Feature selection simplifies a machine learning problem by choosing which subset of the available features should be used. In particular, the well known LASSO ([Tibshirani, 1995](#)) (least absolute shrinkage and selection operator) model integrates an L^1 penalty with a linear model and a least squares cost function. The L^1 penalty causes a subset of the weights to become zero, suggesting that the corresponding features may safely be discarded.

In section 5.6.1, we saw that many regularization strategies can be interpreted as MAP Bayesian inference, and that in particular, L^2 regularization is equivalent to MAP Bayesian inference with a Gaussian prior on the weights. For L^1 regularization, the penalty $\alpha\Omega(\mathbf{w}) = \alpha\sum_i |w_i|$ used to regularize a cost function is equivalent to the log-prior term that is maximized by MAP Bayesian inference when the prior is an isotropic Laplace distribution (equation 3.26) over $\mathbf{w} \in \mathbb{R}^n$:

$$\log p(\mathbf{w}) = \sum_i \log \text{Laplace}(w_i; 0, \frac{1}{\alpha}) = -\alpha\|\mathbf{w}\|_1 + n \log \alpha - n \log 2. \quad (7.24)$$

From the point of view of learning via maximization with respect to \mathbf{w} , we can ignore the $\log \alpha - \log 2$ terms because they do not depend on \mathbf{w} .

7.2 Norm Penalties as Constrained Optimization

Consider the cost function regularized by a parameter norm penalty:

$$\tilde{J}(\boldsymbol{\theta}; \mathbf{X}, \mathbf{y}) = J(\boldsymbol{\theta}; \mathbf{X}, \mathbf{y}) + \alpha \Omega(\boldsymbol{\theta}). \quad (7.25)$$

Recall from section 4.4 that we can minimize a function subject to constraints by constructing a generalized Lagrange function, consisting of the original objective function plus a set of penalties. Each penalty is a product between a coefficient, called a Karush–Kuhn–Tucker (KKT) multiplier, and a function representing whether the constraint is satisfied. If we wanted to constrain $\Omega(\boldsymbol{\theta})$ to be less than some constant k , we could construct a generalized Lagrange function

$$\mathcal{L}(\boldsymbol{\theta}, \alpha; \mathbf{X}, \mathbf{y}) = J(\boldsymbol{\theta}; \mathbf{X}, \mathbf{y}) + \alpha(\Omega(\boldsymbol{\theta}) - k). \quad (7.26)$$

The solution to the constrained problem is given by

$$\boldsymbol{\theta}^* = \arg \min_{\boldsymbol{\theta}} \max_{\alpha, \alpha \geq 0} \mathcal{L}(\boldsymbol{\theta}, \alpha). \quad (7.27)$$

As described in section 4.4, solving this problem requires modifying both $\boldsymbol{\theta}$ and α . Section 4.5 provides a worked example of linear regression with an L^2 constraint. Many different procedures are possible—some may use gradient descent, while others may use analytical solutions for where the gradient is zero—but in all procedures α must increase whenever $\Omega(\boldsymbol{\theta}) > k$ and decrease whenever $\Omega(\boldsymbol{\theta}) < k$. All positive α encourage $\Omega(\boldsymbol{\theta})$ to shrink. The optimal value α^* will encourage $\Omega(\boldsymbol{\theta})$ to shrink, but not so strongly to make $\Omega(\boldsymbol{\theta})$ become less than k .

To gain some insight into the effect of the constraint, we can fix α^* and view the problem as just a function of $\boldsymbol{\theta}$:

$$\boldsymbol{\theta}^* = \arg \min_{\boldsymbol{\theta}} \mathcal{L}(\boldsymbol{\theta}, \alpha^*) = \arg \min_{\boldsymbol{\theta}} J(\boldsymbol{\theta}; \mathbf{X}, \mathbf{y}) + \alpha^* \Omega(\boldsymbol{\theta}). \quad (7.28)$$

This is exactly the same as the regularized training problem of minimizing \tilde{J} . We can thus think of a parameter norm penalty as imposing a constraint on the weights. If Ω is the L^2 norm, then the weights are constrained to lie in an L^2 ball. If Ω is the L^1 norm, then the weights are constrained to lie in a region of

limited L^1 norm. Usually we do not know the size of the constraint region that we impose by using weight decay with coefficient α^* because the value of α^* does not directly tell us the value of k . In principle, one can solve for k , but the relationship between k and α^* depends on the form of J . While we do not know the exact size of the constraint region, we can control it roughly by increasing or decreasing α in order to grow or shrink the constraint region. Larger α will result in a smaller constraint region. Smaller α will result in a larger constraint region.

Sometimes we may wish to use explicit constraints rather than penalties. As described in section 4.4, we can modify algorithms such as stochastic gradient descent to take a step downhill on $J(\theta)$ and then project θ back to the nearest point that satisfies $\Omega(\theta) < k$. This can be useful if we have an idea of what value of k is appropriate and do not want to spend time searching for the value of α that corresponds to this k .

Another reason to use explicit constraints and reprojection rather than enforcing constraints with penalties is that penalties can cause non-convex optimization procedures to get stuck in local minima corresponding to small θ . When training neural networks, this usually manifests as neural networks that train with several “dead units.” These are units that do not contribute much to the behavior of the function learned by the network because the weights going into or out of them are all very small. When training with a penalty on the norm of the weights, these configurations can be locally optimal, even if it is possible to significantly reduce J by making the weights larger. Explicit constraints implemented by re-projection can work much better in these cases because they do not encourage the weights to approach the origin. Explicit constraints implemented by re-projection only have an effect when the weights become large and attempt to leave the constraint region.

Finally, explicit constraints with reprojection can be useful because they impose some stability on the optimization procedure. When using high learning rates, it is possible to encounter a positive feedback loop in which large weights induce large gradients which then induce a large update to the weights. If these updates consistently increase the size of the weights, then θ rapidly moves away from the origin until numerical overflow occurs. Explicit constraints with reprojection prevent this feedback loop from continuing to increase the magnitude of the weights without bound. Hinton *et al.* (2012c) recommend using constraints combined with a high learning rate to allow rapid exploration of parameter space while maintaining some stability.

In particular, Hinton *et al.* (2012c) recommend a strategy introduced by Srebro and Shraibman (2005): constraining the norm of each *column* of the weight matrix

of a neural net layer, rather than constraining the Frobenius norm of the entire weight matrix. Constraining the norm of each column separately prevents any one hidden unit from having very large weights. If we converted this constraint into a penalty in a Lagrange function, it would be similar to L^2 weight decay but with a separate KKT multiplier for the weights of each hidden unit. Each of these KKT multipliers would be dynamically updated separately to make each hidden unit obey the constraint. In practice, column norm limitation is always implemented as an explicit constraint with reprojection.

7.3 Regularization and Under-Constrained Problems

In some cases, regularization is necessary for machine learning problems to be properly defined. Many linear models in machine learning, including linear regression and PCA, depend on inverting the matrix $\mathbf{X}^\top \mathbf{X}$. This is not possible whenever $\mathbf{X}^\top \mathbf{X}$ is singular. This matrix can be singular whenever the data generating distribution truly has no variance in some direction, or when no variance is *observed* in some direction because there are fewer examples (rows of \mathbf{X}) than input features (columns of \mathbf{X}). In this case, many forms of regularization correspond to inverting $\mathbf{X}^\top \mathbf{X} + \alpha \mathbf{I}$ instead. This regularized matrix is guaranteed to be invertible.

These linear problems have closed form solutions when the relevant matrix is invertible. It is also possible for a problem with no closed form solution to be underdetermined. An example is logistic regression applied to a problem where the classes are linearly separable. If a weight vector \mathbf{w} is able to achieve perfect classification, then $2\mathbf{w}$ will also achieve perfect classification and higher likelihood. An iterative optimization procedure like stochastic gradient descent will continually increase the magnitude of \mathbf{w} and, in theory, will never halt. In practice, a numerical implementation of gradient descent will eventually reach sufficiently large weights to cause numerical overflow, at which point its behavior will depend on how the programmer has decided to handle values that are not real numbers.

Most forms of regularization are able to guarantee the convergence of iterative methods applied to underdetermined problems. For example, weight decay will cause gradient descent to quit increasing the magnitude of the weights when the slope of the likelihood is equal to the weight decay coefficient.

The idea of using regularization to solve underdetermined problems extends beyond machine learning. The same idea is useful for several basic linear algebra problems.

As we saw in section 2.9, we can solve underdetermined linear equations using

the Moore-Penrose pseudoinverse. Recall that one definition of the pseudoinverse \mathbf{X}^+ of a matrix \mathbf{X} is

$$\mathbf{X}^+ = \lim_{\alpha \searrow 0} (\mathbf{X}^\top \mathbf{X} + \alpha \mathbf{I})^{-1} \mathbf{X}^\top. \quad (7.29)$$

We can now recognize equation 7.29 as performing linear regression with weight decay. Specifically, equation 7.29 is the limit of equation 7.17 as the regularization coefficient shrinks to zero. We can thus interpret the pseudoinverse as stabilizing underdetermined problems using regularization.

7.4 Dataset Augmentation

The best way to make a machine learning model generalize better is to train it on more data. Of course, in practice, the amount of data we have is limited. One way to get around this problem is to create fake data and add it to the training set. For some machine learning tasks, it is reasonably straightforward to create new fake data.

This approach is easiest for classification. A classifier needs to take a complicated, high dimensional input \mathbf{x} and summarize it with a single category identity y . This means that the main task facing a classifier is to be invariant to a wide variety of transformations. We can generate new (\mathbf{x}, y) pairs easily just by transforming the \mathbf{x} inputs in our training set.

This approach is not as readily applicable to many other tasks. For example, it is difficult to generate new fake data for a density estimation task unless we have already solved the density estimation problem.

Dataset augmentation has been a particularly effective technique for a specific classification problem: object recognition. Images are high dimensional and include an enormous variety of factors of variation, many of which can be easily simulated. Operations like translating the training images a few pixels in each direction can often greatly improve generalization, even if the model has already been designed to be partially translation invariant by using the convolution and pooling techniques described in chapter 9. Many other operations such as rotating the image or scaling the image have also proven quite effective.

One must be careful not to apply transformations that would change the correct class. For example, optical character recognition tasks require recognizing the difference between ‘b’ and ‘d’ and the difference between ‘6’ and ‘9’, so horizontal flips and 180° rotations are not appropriate ways of augmenting datasets for these tasks.

There are also transformations that we would like our classifiers to be invariant to, but which are not easy to perform. For example, out-of-plane rotation can not be implemented as a simple geometric operation on the input pixels.

Dataset augmentation is effective for speech recognition tasks as well ([Jaity and Hinton, 2013](#)).

Injecting noise in the input to a neural network ([Sietsma and Dow, 1991](#)) can also be seen as a form of data augmentation. For many classification and even some regression tasks, the task should still be possible to solve even if small random noise is added to the input. Neural networks prove not to be very robust to noise, however ([Tang and Eliasmith, 2010](#)). One way to improve the robustness of neural networks is simply to train them with random noise applied to their inputs. Input noise injection is part of some unsupervised learning algorithms such as the denoising autoencoder ([Vincent et al., 2008](#)). Noise injection also works when the noise is applied to the hidden units, which can be seen as doing dataset augmentation at multiple levels of abstraction. [Poole et al. \(2014\)](#) recently showed that this approach can be highly effective provided that the magnitude of the noise is carefully tuned. Dropout, a powerful regularization strategy that will be described in section [7.12](#), can be seen as a process of constructing new inputs by *multiplying* by noise.

When comparing machine learning benchmark results, it is important to take the effect of dataset augmentation into account. Often, hand-designed dataset augmentation schemes can dramatically reduce the generalization error of a machine learning technique. To compare the performance of one machine learning algorithm to another, it is necessary to perform controlled experiments. When comparing machine learning algorithm A and machine learning algorithm B, it is necessary to make sure that both algorithms were evaluated using the same hand-designed dataset augmentation schemes. Suppose that algorithm A performs poorly with no dataset augmentation and algorithm B performs well when combined with numerous synthetic transformations of the input. In such a case it is likely the synthetic transformations caused the improved performance, rather than the use of machine learning algorithm B. Sometimes deciding whether an experiment has been properly controlled requires subjective judgment. For example, machine learning algorithms that inject noise into the input are performing a form of dataset augmentation. Usually, operations that are generally applicable (such as adding Gaussian noise to the input) are considered part of the machine learning algorithm, while operations that are specific to one application domain (such as randomly cropping an image) are considered to be separate pre-processing steps.

7.5 Noise Robustness

Section 7.4 has motivated the use of noise applied to the inputs as a dataset augmentation strategy. For some models, the addition of noise with infinitesimal variance at the input of the model is equivalent to imposing a penalty on the norm of the weights (Bishop, 1995a,b). In the general case, it is important to remember that noise injection can be much more powerful than simply shrinking the parameters, especially when the noise is added to the hidden units. Noise applied to the hidden units is such an important topic that it merit its own separate discussion; the dropout algorithm described in section 7.12 is the main development of that approach.

Another way that noise has been used in the service of regularizing models is by adding it to the weights. This technique has been used primarily in the context of recurrent neural networks (Jim *et al.*, 1996; Graves, 2011). This can be interpreted as a stochastic implementation of Bayesian inference over the weights. The Bayesian treatment of learning would consider the model weights to be uncertain and representable via a probability distribution that reflects this uncertainty. Adding noise to the weights is a practical, stochastic way to reflect this uncertainty.

Noise applied to the weights can also be interpreted as equivalent (under some assumptions) to a more traditional form of regularization, encouraging stability of the function to be learned. Consider the regression setting, where we wish to train a function $\hat{y}(\mathbf{x})$ that maps a set of features \mathbf{x} to a scalar using the least-squares cost function between the model predictions $\hat{y}(\mathbf{x})$ and the true values y :

$$J = \mathbb{E}_{p(x,y)} [(\hat{y}(\mathbf{x}) - y)^2]. \quad (7.30)$$

The training set consists of m labeled examples $\{(\mathbf{x}^{(1)}, y^{(1)}), \dots, (\mathbf{x}^{(m)}, y^{(m)})\}$.

We now assume that with each input presentation we also include a random perturbation $\epsilon_{\mathbf{W}} \sim \mathcal{N}(\mathbf{\epsilon}, \mathbf{0}, \eta \mathbf{I})$ of the network weights. Let us imagine that we have a standard l -layer MLP. We denote the perturbed model as $\hat{y}_{\epsilon_{\mathbf{W}}}(\mathbf{x})$. Despite the injection of noise, we are still interested in minimizing the squared error of the output of the network. The objective function thus becomes:

$$\tilde{J}_{\mathbf{W}} = \mathbb{E}_{p(\mathbf{x}, y, \epsilon_{\mathbf{W}})} [(\hat{y}_{\epsilon_{\mathbf{W}}}(\mathbf{x}) - y)^2] \quad (7.31)$$

$$= \mathbb{E}_{p(\mathbf{x}, y, \epsilon_{\mathbf{W}})} [\hat{y}_{\epsilon_{\mathbf{W}}}^2(\mathbf{x}) - 2y\hat{y}_{\epsilon_{\mathbf{W}}}(\mathbf{x}) + y^2]. \quad (7.32)$$

For small η , the minimization of J with added weight noise (with covariance $\eta \mathbf{I}$) is equivalent to minimization of J with an additional regularization term:

$\eta \mathbb{E}_{p(\mathbf{x}, y)} [\|\nabla_{\mathbf{w}} \hat{y}(\mathbf{x})\|^2]$. This form of regularization encourages the parameters to go to regions of parameter space where small perturbations of the weights have a relatively small influence on the output. In other words, it pushes the model into regions where the model is relatively insensitive to small variations in the weights, finding points that are not merely minima, but minima surrounded by flat regions (Hochreiter and Schmidhuber, 1995). In the simplified case of linear regression (where, for instance, $\hat{y}(\mathbf{x}) = \mathbf{w}^\top \mathbf{x} + b$), this regularization term collapses into $\eta \mathbb{E}_{p(\mathbf{x})} [\|\mathbf{x}\|^2]$, which is not a function of parameters and therefore does not contribute to the gradient of $\tilde{J}_{\mathbf{W}}$ with respect to the model parameters.

7.5.1 Injecting Noise at the Output Targets

Most datasets have some amount of mistakes in the y labels. It can be harmful to maximize $\log p(y | \mathbf{x})$ when y is a mistake. One way to prevent this is to explicitly model the noise on the labels. For example, we can assume that for some small constant ϵ , the training set label y is correct with probability $1 - \epsilon$, and otherwise any of the other possible labels might be correct. This assumption is easy to incorporate into the cost function analytically, rather than by explicitly drawing noise samples. For example, **label smoothing** regularizes a model based on a softmax with k output values by replacing the hard 0 and 1 classification targets with targets of $\frac{\epsilon}{k-1}$ and $1 - \epsilon$, respectively. The standard cross-entropy loss may then be used with these soft targets. Maximum likelihood learning with a softmax classifier and hard targets may actually never converge—the softmax can never predict a probability of exactly 0 or exactly 1, so it will continue to learn larger and larger weights, making more extreme predictions forever. It is possible to prevent this scenario using other regularization strategies like weight decay. Label smoothing has the advantage of preventing the pursuit of hard probabilities without discouraging correct classification. This strategy has been used since the 1980s and continues to be featured prominently in modern neural networks (Szegedy *et al.*, 2015).

7.6 Semi-Supervised Learning

In the paradigm of semi-supervised learning, both unlabeled examples from $P(\mathbf{x})$ and labeled examples from $P(\mathbf{x}, \mathbf{y})$ are used to estimate $P(\mathbf{y} | \mathbf{x})$ or predict \mathbf{y} from \mathbf{x} .

In the context of deep learning, semi-supervised learning usually refers to learning a representation $\mathbf{h} = f(\mathbf{x})$. The goal is to learn a representation so

that examples from the same class have similar representations. Unsupervised learning can provide useful cues for how to group examples in representation space. Examples that cluster tightly in the input space should be mapped to similar representations. A linear classifier in the new space may achieve better generalization in many cases (Belkin and Niyogi, 2002; Chapelle *et al.*, 2003). A long-standing variant of this approach is the application of principal components analysis as a pre-processing step before applying a classifier (on the projected data).

Instead of having separate unsupervised and supervised components in the model, one can construct models in which a generative model of either $P(\mathbf{x})$ or $P(\mathbf{x}, \mathbf{y})$ shares parameters with a discriminative model of $P(\mathbf{y} | \mathbf{x})$. One can then trade-off the supervised criterion $-\log P(\mathbf{y} | \mathbf{x})$ with the unsupervised or generative one (such as $-\log P(\mathbf{x})$ or $-\log P(\mathbf{x}, \mathbf{y})$). The generative criterion then expresses a particular form of prior belief about the solution to the supervised learning problem (Lasserre *et al.*, 2006), namely that the structure of $P(\mathbf{x})$ is connected to the structure of $P(\mathbf{y} | \mathbf{x})$ in a way that is captured by the shared parametrization. By controlling how much of the generative criterion is included in the total criterion, one can find a better trade-off than with a purely generative or a purely discriminative training criterion (Lasserre *et al.*, 2006; Larochelle and Bengio, 2008).

Salakhutdinov and Hinton (2008) describe a method for learning the kernel function of a kernel machine used for regression, in which the usage of unlabeled examples for modeling $P(\mathbf{x})$ improves $P(\mathbf{y} | \mathbf{x})$ quite significantly.

See Chapelle *et al.* (2006) for more information about semi-supervised learning.

7.7 Multi-Task Learning

Multi-task learning (Caruana, 1993) is a way to improve generalization by pooling the examples (which can be seen as soft constraints imposed on the parameters) arising out of several tasks. In the same way that additional training examples put more pressure on the parameters of the model towards values that generalize well, when part of a model is shared across tasks, that part of the model is more constrained towards good values (assuming the sharing is justified), often yielding better generalization.

Figure 7.2 illustrates a very common form of multi-task learning, in which different supervised tasks (predicting $\mathbf{y}^{(i)}$ given \mathbf{x}) share the same input \mathbf{x} , as well as some intermediate-level representation $\mathbf{h}^{(\text{shared})}$ capturing a common pool of

factors. The model can generally be divided into two kinds of parts and associated parameters:

1. Task-specific parameters (which only benefit from the examples of their task to achieve good generalization). These are the upper layers of the neural network in figure 7.2.
2. Generic parameters, shared across all the tasks (which benefit from the pooled data of all the tasks). These are the lower layers of the neural network in figure 7.2.

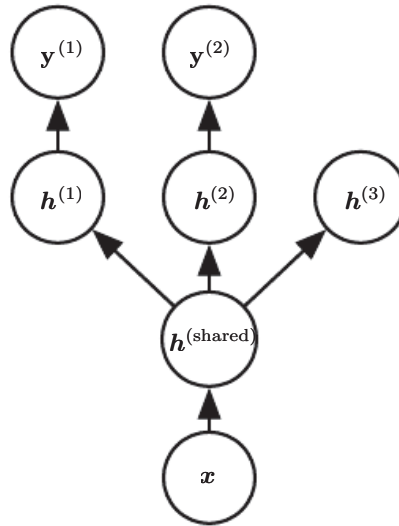


Figure 7.2: Multi-task learning can be cast in several ways in deep learning frameworks and this figure illustrates the common situation where the tasks share a common input but involve different target random variables. The lower layers of a deep network (whether it is supervised and feedforward or includes a generative component with downward arrows) can be shared across such tasks, while task-specific parameters (associated respectively with the weights into and from $\mathbf{h}^{(1)}$ and $\mathbf{h}^{(2)}$) can be learned on top of those yielding a shared representation $\mathbf{h}^{(\text{shared})}$. The underlying assumption is that there exists a common pool of factors that explain the variations in the input \mathbf{x} , while each task is associated with a subset of these factors. In this example, it is additionally assumed that top-level hidden units $\mathbf{h}^{(1)}$ and $\mathbf{h}^{(2)}$ are specialized to each task (respectively predicting $\mathbf{y}^{(1)}$ and $\mathbf{y}^{(2)}$) while some intermediate-level representation $\mathbf{h}^{(\text{shared})}$ is shared across all tasks. In the unsupervised learning context, it makes sense for some of the top-level factors to be associated with none of the output tasks ($\mathbf{h}^{(3)}$): these are the factors that explain some of the input variations but are not relevant for predicting $\mathbf{y}^{(1)}$ or $\mathbf{y}^{(2)}$.

Improved generalization and generalization error bounds (Baxter, 1995) can be achieved because of the shared parameters, for which statistical strength can be

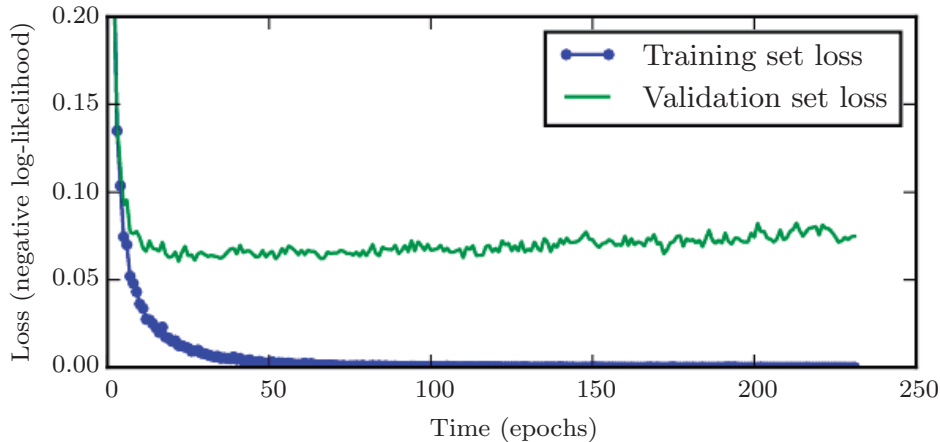


Figure 7.3: Learning curves showing how the negative log-likelihood loss changes over time (indicated as number of training iterations over the dataset, or **epochs**). In this example, we train a maxout network on MNIST. Observe that the training objective decreases consistently over time, but the validation set average loss eventually begins to increase again, forming an asymmetric U-shaped curve.

greatly improved (in proportion with the increased number of examples for the shared parameters, compared to the scenario of single-task models). Of course this will happen only if some assumptions about the statistical relationship between the different tasks are valid, meaning that there is something shared across some of the tasks.

From the point of view of deep learning, the underlying prior belief is the following: *among the factors that explain the variations observed in the data associated with the different tasks, some are shared across two or more tasks.*

7.8 Early Stopping

When training large models with sufficient representational capacity to overfit the task, we often observe that training error decreases steadily over time, but validation set error begins to rise again. See figure 7.3 for an example of this behavior. This behavior occurs very reliably.

This means we can obtain a model with better validation set error (and thus, hopefully better test set error) by returning to the parameter setting at the point in time with the lowest validation set error. Every time the error on the validation set improves, we store a copy of the model parameters. When the training algorithm terminates, we return these parameters, rather than the latest parameters. The

algorithm terminates when no parameters have improved over the best recorded validation error for some pre-specified number of iterations. This procedure is specified more formally in algorithm 7.1.

Algorithm 7.1 The early stopping meta-algorithm for determining the best amount of time to train. This meta-algorithm is a general strategy that works well with a variety of training algorithms and ways of quantifying error on the validation set.

Let n be the number of steps between evaluations.

Let p be the “patience,” the number of times to observe worsening validation set error before giving up.

Let θ_o be the initial parameters.

$\theta \leftarrow \theta_o$

$i \leftarrow 0$

$j \leftarrow 0$

$v \leftarrow \infty$

$\theta^* \leftarrow \theta$

$i^* \leftarrow i$

while $j < p$ **do**

 Update θ by running the training algorithm for n steps.

$i \leftarrow i + n$

$v' \leftarrow \text{ValidationSetError}(\theta)$

if $v' < v$ **then**

$j \leftarrow 0$

$\theta^* \leftarrow \theta$

$i^* \leftarrow i$

$v \leftarrow v'$

else

$j \leftarrow j + 1$

end if

end while

Best parameters are θ^* , best number of training steps is i^*

This strategy is known as **early stopping**. It is probably the most commonly used form of regularization in deep learning. Its popularity is due both to its effectiveness and its simplicity.

One way to think of early stopping is as a very efficient hyperparameter selection algorithm. In this view, the number of training steps is just another hyperparameter. We can see in figure 7.3 that this hyperparameter has a U-shaped validation set

performance curve. Most hyperparameters that control model capacity have such a U-shaped validation set performance curve, as illustrated in figure 5.3. In the case of early stopping, we are controlling the effective capacity of the model by determining how many steps it can take to fit the training set. Most hyperparameters must be chosen using an expensive guess and check process, where we set a hyperparameter at the start of training, then run training for several steps to see its effect. The “training time” hyperparameter is unique in that by definition a single run of training tries out many values of the hyperparameter. The only significant cost to choosing this hyperparameter automatically via early stopping is running the validation set evaluation periodically during training. Ideally, this is done in parallel to the training process on a separate machine, separate CPU, or separate GPU from the main training process. If such resources are not available, then the cost of these periodic evaluations may be reduced by using a validation set that is small compared to the training set or by evaluating the validation set error less frequently and obtaining a lower resolution estimate of the optimal training time.

An additional cost to early stopping is the need to maintain a copy of the best parameters. This cost is generally negligible, because it is acceptable to store these parameters in a slower and larger form of memory (for example, training in GPU memory, but storing the optimal parameters in host memory or on a disk drive). Since the best parameters are written to infrequently and never read during training, these occasional slow writes have little effect on the total training time.

Early stopping is a very unobtrusive form of regularization, in that it requires almost no change in the underlying training procedure, the objective function, or the set of allowable parameter values. This means that it is easy to use early stopping without damaging the learning dynamics. This is in contrast to weight decay, where one must be careful not to use too much weight decay and trap the network in a bad local minimum corresponding to a solution with pathologically small weights.

Early stopping may be used either alone or in conjunction with other regularization strategies. Even when using regularization strategies that modify the objective function to encourage better generalization, it is rare for the best generalization to occur at a local minimum of the training objective.

Early stopping requires a validation set, which means some training data is not fed to the model. To best exploit this extra data, one can perform extra training after the initial training with early stopping has completed. In the second, extra training step, all of the training data is included. There are two basic strategies one can use for this second training procedure.

One strategy (algorithm 7.2) is to initialize the model again and retrain on all

of the data. In this second training pass, we train for the same number of steps as the early stopping procedure determined was optimal in the first pass. There are some subtleties associated with this procedure. For example, there is not a good way of knowing whether to retrain for the same number of parameter updates or the same number of passes through the dataset. On the second round of training, each pass through the dataset will require more parameter updates because the training set is bigger.

Algorithm 7.2 A meta-algorithm for using early stopping to determine how long to train, then retraining on all the data.

Let $\mathbf{X}^{(\text{train})}$ and $\mathbf{y}^{(\text{train})}$ be the training set.

Split $\mathbf{X}^{(\text{train})}$ and $\mathbf{y}^{(\text{train})}$ into $(\mathbf{X}^{(\text{subtrain})}, \mathbf{X}^{(\text{valid})})$ and $(\mathbf{y}^{(\text{subtrain})}, \mathbf{y}^{(\text{valid})})$ respectively.

Run early stopping (algorithm 7.1) starting from random $\boldsymbol{\theta}$ using $\mathbf{X}^{(\text{subtrain})}$ and $\mathbf{y}^{(\text{subtrain})}$ for training data and $\mathbf{X}^{(\text{valid})}$ and $\mathbf{y}^{(\text{valid})}$ for validation data. This returns i^* , the optimal number of steps.

Set $\boldsymbol{\theta}$ to random values again.

Train on $\mathbf{X}^{(\text{train})}$ and $\mathbf{y}^{(\text{train})}$ for i^* steps.

Another strategy for using all of the data is to keep the parameters obtained from the first round of training and then *continue* training but now using all of the data. At this stage, we now no longer have a guide for when to stop in terms of a number of steps. Instead, we can monitor the average loss function on the validation set, and continue training until it falls below the value of the training set objective at which the early stopping procedure halted. This strategy avoids the high cost of retraining the model from scratch, but is not as well-behaved. For example, there is not any guarantee that the objective on the validation set will ever reach the target value, so this strategy is not even guaranteed to terminate. This procedure is presented more formally in algorithm 7.3.

Early stopping is also useful because it reduces the computational cost of the training procedure. Besides the obvious reduction in cost due to limiting the number of training iterations, it also has the benefit of providing regularization without requiring the addition of penalty terms to the cost function or the computation of the gradients of such additional terms.

How early stopping acts as a regularizer: So far we have stated that early stopping *is* a regularization strategy, but we have supported this claim only by showing learning curves where the validation set error has a U-shaped curve. What

Algorithm 7.3 Meta-algorithm using early stopping to determine at what objective value we start to overfit, then continue training until that value is reached.

Let $\mathbf{X}^{(\text{train})}$ and $\mathbf{y}^{(\text{train})}$ be the training set.

Split $\mathbf{X}^{(\text{train})}$ and $\mathbf{y}^{(\text{train})}$ into $(\mathbf{X}^{(\text{subtrain})}, \mathbf{X}^{(\text{valid})})$ and $(\mathbf{y}^{(\text{subtrain})}, \mathbf{y}^{(\text{valid})})$ respectively.

Run early stopping (algorithm 7.1) starting from random $\boldsymbol{\theta}$ using $\mathbf{X}^{(\text{subtrain})}$ and $\mathbf{y}^{(\text{subtrain})}$ for training data and $\mathbf{X}^{(\text{valid})}$ and $\mathbf{y}^{(\text{valid})}$ for validation data. This updates $\boldsymbol{\theta}$.

$$\epsilon \leftarrow J(\boldsymbol{\theta}, \mathbf{X}^{(\text{subtrain})}, \mathbf{y}^{(\text{subtrain})})$$

while $J(\boldsymbol{\theta}, \mathbf{X}^{(\text{valid})}, \mathbf{y}^{(\text{valid})}) > \epsilon$ **do**

 Train on $\mathbf{X}^{(\text{train})}$ and $\mathbf{y}^{(\text{train})}$ for n steps.

end while

is the actual mechanism by which early stopping regularizes the model? Bishop (1995a) and Sjöberg and Ljung (1995) argued that early stopping has the effect of restricting the optimization procedure to a relatively small volume of parameter space in the neighborhood of the initial parameter value $\boldsymbol{\theta}_o$, as illustrated in figure 7.4. More specifically, imagine taking τ optimization steps (corresponding to τ training iterations) and with learning rate ϵ . We can view the product $\epsilon\tau$ as a measure of effective capacity. Assuming the gradient is bounded, restricting both the number of iterations and the learning rate limits the volume of parameter space reachable from $\boldsymbol{\theta}_o$. In this sense, $\epsilon\tau$ behaves as if it were the reciprocal of the coefficient used for weight decay.

Indeed, we can show how—in the case of a simple linear model with a quadratic error function and simple gradient descent—early stopping is equivalent to L^2 regularization.

In order to compare with classical L^2 regularization, we examine a simple setting where the only parameters are linear weights ($\boldsymbol{\theta} = \mathbf{w}$). We can model the cost function J with a quadratic approximation in the neighborhood of the empirically optimal value of the weights \mathbf{w}^* :

$$\hat{J}(\boldsymbol{\theta}) = J(\mathbf{w}^*) + \frac{1}{2}(\mathbf{w} - \mathbf{w}^*)^\top \mathbf{H}(\mathbf{w} - \mathbf{w}^*), \quad (7.33)$$

where \mathbf{H} is the Hessian matrix of J with respect to \mathbf{w} evaluated at \mathbf{w}^* . Given the assumption that \mathbf{w}^* is a minimum of $J(\mathbf{w})$, we know that \mathbf{H} is positive semidefinite. Under a local Taylor series approximation, the gradient is given by:

$$\nabla_{\mathbf{w}} \hat{J}(\mathbf{w}) = \mathbf{H}(\mathbf{w} - \mathbf{w}^*). \quad (7.34)$$

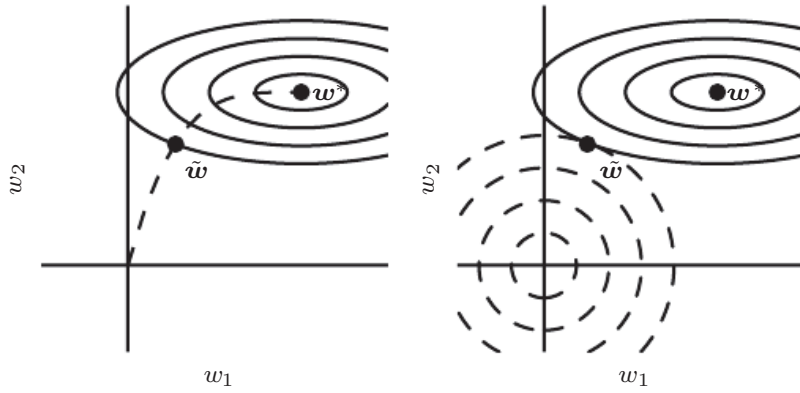


Figure 7.4: An illustration of the effect of early stopping. (*Left*)The solid contour lines indicate the contours of the negative log-likelihood. The dashed line indicates the trajectory taken by SGD beginning from the origin. Rather than stopping at the point \mathbf{w}^* that minimizes the cost, early stopping results in the trajectory stopping at an earlier point $\tilde{\mathbf{w}}$. (*Right*)An illustration of the effect of L^2 regularization for comparison. The dashed circles indicate the contours of the L^2 penalty, which causes the minimum of the total cost to lie nearer the origin than the minimum of the unregularized cost.

We are going to study the trajectory followed by the parameter vector during training. For simplicity, let us set the initial parameter vector to the origin,³ that is $\mathbf{w}^{(0)} = \mathbf{0}$. Let us study the approximate behavior of gradient descent on J by analyzing gradient descent on \hat{J} :

$$\mathbf{w}^{(\tau)} = \mathbf{w}^{(\tau-1)} - \epsilon \nabla_{\mathbf{w}} \hat{J}(\mathbf{w}^{(\tau-1)}) \quad (7.35)$$

$$= \mathbf{w}^{(\tau-1)} - \epsilon \mathbf{H}(\mathbf{w}^{(\tau-1)} - \mathbf{w}^*) \quad (7.36)$$

$$\mathbf{w}^{(\tau)} - \mathbf{w}^* = (\mathbf{I} - \epsilon \mathbf{H})(\mathbf{w}^{(\tau-1)} - \mathbf{w}^*). \quad (7.37)$$

Let us now rewrite this expression in the space of the eigenvectors of \mathbf{H} , exploiting the eigendecomposition of \mathbf{H} : $\mathbf{H} = \mathbf{Q}\Lambda\mathbf{Q}^\top$, where Λ is a diagonal matrix and \mathbf{Q} is an orthonormal basis of eigenvectors.

$$\mathbf{w}^{(\tau)} - \mathbf{w}^* = (\mathbf{I} - \epsilon \mathbf{Q}\Lambda\mathbf{Q}^\top)(\mathbf{w}^{(\tau-1)} - \mathbf{w}^*) \quad (7.38)$$

$$\mathbf{Q}^\top(\mathbf{w}^{(\tau)} - \mathbf{w}^*) = (\mathbf{I} - \epsilon \Lambda)\mathbf{Q}^\top(\mathbf{w}^{(\tau-1)} - \mathbf{w}^*) \quad (7.39)$$

³For neural networks, to obtain symmetry breaking between hidden units, we cannot initialize all the parameters to $\mathbf{0}$, as discussed in section 6.2. However, the argument holds for any other initial value $\mathbf{w}^{(0)}$.

Assuming that $\mathbf{w}^{(0)} = 0$ and that ϵ is chosen to be small enough to guarantee $|1 - \epsilon\lambda_i| < 1$, the parameter trajectory during training after τ parameter updates is as follows:

$$\mathbf{Q}^\top \mathbf{w}^{(\tau)} = [\mathbf{I} - (\mathbf{I} - \epsilon\Lambda)^\tau] \mathbf{Q}^\top \mathbf{w}^*. \quad (7.40)$$

Now, the expression for $\mathbf{Q}^\top \tilde{\mathbf{w}}$ in equation 7.13 for L^2 regularization can be rearranged as:

$$\mathbf{Q}^\top \tilde{\mathbf{w}} = (\Lambda + \alpha\mathbf{I})^{-1} \Lambda \mathbf{Q}^\top \mathbf{w}^* \quad (7.41)$$

$$\mathbf{Q}^\top \tilde{\mathbf{w}} = [\mathbf{I} - (\Lambda + \alpha\mathbf{I})^{-1} \alpha] \mathbf{Q}^\top \mathbf{w}^* \quad (7.42)$$

Comparing equation 7.40 and equation 7.42, we see that if the hyperparameters ϵ , α , and τ are chosen such that

$$(\mathbf{I} - \epsilon\Lambda)^\tau = (\Lambda + \alpha\mathbf{I})^{-1} \alpha, \quad (7.43)$$

then L^2 regularization and early stopping can be seen to be equivalent (at least under the quadratic approximation of the objective function). Going even further, by taking logarithms and using the series expansion for $\log(1+x)$, we can conclude that if all λ_i are small (that is, $\epsilon\lambda_i \ll 1$ and $\lambda_i/\alpha \ll 1$) then

$$\tau \approx \frac{1}{\epsilon\alpha}, \quad (7.44)$$

$$\alpha \approx \frac{1}{\tau\epsilon}. \quad (7.45)$$

That is, under these assumptions, the number of training iterations τ plays a role inversely proportional to the L^2 regularization parameter, and the inverse of $\tau\epsilon$ plays the role of the weight decay coefficient.

Parameter values corresponding to directions of significant curvature (of the objective function) are regularized less than directions of less curvature. Of course, in the context of early stopping, this really means that parameters that correspond to directions of significant curvature tend to learn early relative to parameters corresponding to directions of less curvature.

The derivations in this section have shown that a trajectory of length τ ends at a point that corresponds to a minimum of the L^2 -regularized objective. Early stopping is of course more than the mere restriction of the trajectory length; instead, early stopping typically involves monitoring the validation set error in order to stop the trajectory at a particularly good point in space. Early stopping therefore has the advantage over weight decay that early stopping automatically determines the correct amount of regularization while weight decay requires many training experiments with different values of its hyperparameter.

7.9 Parameter Tying and Parameter Sharing

Thus far, in this chapter, when we have discussed adding constraints or penalties to the parameters, we have always done so with respect to a fixed region or point. For example, L^2 regularization (or weight decay) penalizes model parameters for deviating from the fixed value of zero. However, sometimes we may need other ways to express our prior knowledge about suitable values of the model parameters. Sometimes we might not know precisely what values the parameters should take but we know, from knowledge of the domain and model architecture, that there should be some dependencies between the model parameters.

A common type of dependency that we often want to express is that certain parameters should be close to one another. Consider the following scenario: we have two models performing the same classification task (with the same set of classes) but with somewhat different input distributions. Formally, we have model A with parameters $\mathbf{w}^{(A)}$ and model B with parameters $\mathbf{w}^{(B)}$. The two models map the input to two different, but related outputs: $\hat{y}^{(A)} = f(\mathbf{w}^{(A)}, \mathbf{x})$ and $\hat{y}^{(B)} = g(\mathbf{w}^{(B)}, \mathbf{x})$.

Let us imagine that the tasks are similar enough (perhaps with similar input and output distributions) that we believe the model parameters should be close to each other: $\forall i, w_i^{(A)}$ should be close to $w_i^{(B)}$. We can leverage this information through regularization. Specifically, we can use a parameter norm penalty of the form: $\Omega(\mathbf{w}^{(A)}, \mathbf{w}^{(B)}) = \|\mathbf{w}^{(A)} - \mathbf{w}^{(B)}\|_2^2$. Here we used an L^2 penalty, but other choices are also possible.

This kind of approach was proposed by [Lasserre et al. \(2006\)](#), who regularized the parameters of one model, trained as a classifier in a supervised paradigm, to be close to the parameters of another model, trained in an unsupervised paradigm (to capture the distribution of the observed input data). The architectures were constructed such that many of the parameters in the classifier model could be paired to corresponding parameters in the unsupervised model.

While a parameter norm penalty is one way to regularize parameters to be close to one another, the more popular way is to use constraints: *to force sets of parameters to be equal*. This method of regularization is often referred to as **parameter sharing**, because we interpret the various models or model components as sharing a unique set of parameters. A significant advantage of parameter sharing over regularizing the parameters to be close (via a norm penalty) is that only a subset of the parameters (the unique set) need to be stored in memory. In certain models—such as the convolutional neural network—this can lead to significant reduction in the memory footprint of the model.

Convolutional Neural Networks By far the most popular and extensive use of parameter sharing occurs in **convolutional neural networks** (CNNs) applied to computer vision.

Natural images have many statistical properties that are invariant to translation. For example, a photo of a cat remains a photo of a cat if it is translated one pixel to the right. CNNs take this property into account by sharing parameters across multiple image locations. The same feature (a hidden unit with the same weights) is computed over different locations in the input. This means that we can find a cat with the same cat detector whether the cat appears at column i or column $i + 1$ in the image.

Parameter sharing has allowed CNNs to dramatically lower the number of unique model parameters and to significantly increase network sizes without requiring a corresponding increase in training data. It remains one of the best examples of how to effectively incorporate domain knowledge into the network architecture.

CNNs will be discussed in more detail in chapter 9.

7.10 Sparse Representations

Weight decay acts by placing a penalty directly on the model parameters. Another strategy is to place a penalty on the activations of the units in a neural network, encouraging their activations to be sparse. This indirectly imposes a complicated penalty on the model parameters.

We have already discussed (in section 7.1.2) how L^1 penalization induces a sparse parametrization—meaning that many of the parameters become zero (or close to zero). Representational sparsity, on the other hand, describes a representation where many of the elements of the representation are zero (or close to zero). A simplified view of this distinction can be illustrated in the context of linear regression:

$$\begin{bmatrix} 18 \\ 5 \\ 15 \\ -9 \\ -3 \end{bmatrix} = \begin{bmatrix} 4 & 0 & 0 & -2 & 0 & 0 \\ 0 & 0 & -1 & 0 & 3 & 0 \\ 0 & 5 & 0 & 0 & 0 & 0 \\ 1 & 0 & 0 & -1 & 0 & -4 \\ 1 & 0 & 0 & 0 & -5 & 0 \end{bmatrix} \begin{bmatrix} 2 \\ 3 \\ -2 \\ -5 \\ 1 \\ 4 \end{bmatrix} \quad (7.46)$$
$$\mathbf{y} \in \mathbb{R}^m \qquad \mathbf{A} \in \mathbb{R}^{m \times n} \qquad \mathbf{x} \in \mathbb{R}^n$$

$$\begin{bmatrix} -14 \\ 1 \\ 19 \\ 2 \\ 23 \end{bmatrix} = \begin{bmatrix} 3 & -1 & 2 & -5 & 4 & 1 \\ 4 & 2 & -3 & -1 & 1 & 3 \\ -1 & 5 & 4 & 2 & -3 & -2 \\ 3 & 1 & 2 & -3 & 0 & -3 \\ -5 & 4 & -2 & 2 & -5 & -1 \end{bmatrix} \begin{bmatrix} 0 \\ 2 \\ 0 \\ 0 \\ -3 \\ 0 \end{bmatrix} \quad (7.47)$$

$\mathbf{y} \in \mathbb{R}^m \qquad \mathbf{B} \in \mathbb{R}^{m \times n} \qquad \mathbf{h} \in \mathbb{R}^n$

In the first expression, we have an example of a sparsely parametrized linear regression model. In the second, we have linear regression with a sparse representation \mathbf{h} of the data \mathbf{x} . That is, \mathbf{h} is a function of \mathbf{x} that, in some sense, represents the information present in \mathbf{x} , but does so with a sparse vector.

Representational regularization is accomplished by the same sorts of mechanisms that we have used in parameter regularization.

Norm penalty regularization of representations is performed by adding to the loss function J a norm penalty on the *representation*. This penalty is denoted $\Omega(\mathbf{h})$. As before, we denote the regularized loss function by \tilde{J} :

$$\tilde{J}(\boldsymbol{\theta}; \mathbf{X}, \mathbf{y}) = J(\boldsymbol{\theta}; \mathbf{X}, \mathbf{y}) + \alpha \Omega(\mathbf{h}) \quad (7.48)$$

where $\alpha \in [0, \infty)$ weights the relative contribution of the norm penalty term, with larger values of α corresponding to more regularization.

Just as an L^1 penalty on the parameters induces parameter sparsity, an L^1 penalty on the elements of the representation induces representational sparsity: $\Omega(\mathbf{h}) = \|\mathbf{h}\|_1 = \sum_i |h_i|$. Of course, the L^1 penalty is only one choice of penalty that can result in a sparse representation. Others include the penalty derived from a Student- t prior on the representation (Olshausen and Field, 1996; Bergstra, 2011) and KL divergence penalties (Larochelle and Bengio, 2008) that are especially useful for representations with elements constrained to lie on the unit interval. Lee *et al.* (2008) and Goodfellow *et al.* (2009) both provide examples of strategies based on regularizing the average activation across several examples, $\frac{1}{m} \sum_i \mathbf{h}^{(i)}$, to be near some target value, such as a vector with .01 for each entry.

Other approaches obtain representational sparsity with a hard constraint on the activation values. For example, **orthogonal matching pursuit** (Pati *et al.*, 1993) encodes an input \mathbf{x} with the representation \mathbf{h} that solves the constrained optimization problem

$$\arg \min_{\mathbf{h}, \|\mathbf{h}\|_0 \leq k} \|\mathbf{x} - \mathbf{W}\mathbf{h}\|^2, \quad (7.49)$$

where $\|\mathbf{h}\|_0$ is the number of non-zero entries of \mathbf{h} . This problem can be solved efficiently when \mathbf{W} is constrained to be orthogonal. This method is often called

OMP- k with the value of k specified to indicate the number of non-zero features allowed. Coates and Ng (2011) demonstrated that OMP-1 can be a very effective feature extractor for deep architectures.

Essentially any model that has hidden units can be made sparse. Throughout this book, we will see many examples of sparsity regularization used in a variety of contexts.

7.11 Bagging and Other Ensemble Methods

Bagging (short for **bootstrap aggregating**) is a technique for reducing generalization error by combining several models (Breiman, 1994). The idea is to train several different models separately, then have all of the models vote on the output for test examples. This is an example of a general strategy in machine learning called **model averaging**. Techniques employing this strategy are known as **ensemble methods**.

The reason that model averaging works is that different models will usually not make all the same errors on the test set.

Consider for example a set of k regression models. Suppose that each model makes an error ϵ_i on each example, with the errors drawn from a zero-mean multivariate normal distribution with variances $\mathbb{E}[\epsilon_i^2] = v$ and covariances $\mathbb{E}[\epsilon_i \epsilon_j] = c$. Then the error made by the average prediction of all the ensemble models is $\frac{1}{k} \sum_i \epsilon_i$. The expected squared error of the ensemble predictor is

$$\mathbb{E} \left[\left(\frac{1}{k} \sum_i \epsilon_i \right)^2 \right] = \frac{1}{k^2} \mathbb{E} \left[\sum_i \left(\epsilon_i^2 + \sum_{j \neq i} \epsilon_i \epsilon_j \right) \right] \quad (7.50)$$

$$= \frac{1}{k} v + \frac{k-1}{k} c. \quad (7.51)$$

In the case where the errors are perfectly correlated and $c = v$, the mean squared error reduces to v , so the model averaging does not help at all. In the case where the errors are perfectly uncorrelated and $c = 0$, the expected squared error of the ensemble is only $\frac{1}{k} v$. This means that the expected squared error of the ensemble decreases linearly with the ensemble size. In other words, on average, the ensemble will perform at least as well as any of its members, and if the members make independent errors, the ensemble will perform significantly better than its members.

Different ensemble methods construct the ensemble of models in different ways. For example, each member of the ensemble could be formed by training a completely

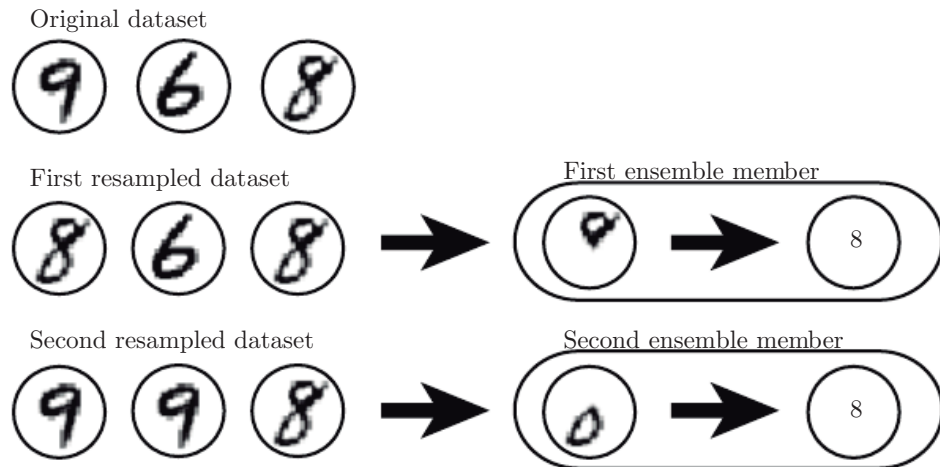


Figure 7.5: A cartoon depiction of how bagging works. Suppose we train an 8 detector on the dataset depicted above, containing an 8, a 6 and a 9. Suppose we make two different resampled datasets. The bagging training procedure is to construct each of these datasets by sampling with replacement. The first dataset omits the 9 and repeats the 8. On this dataset, the detector learns that a loop on top of the digit corresponds to an 8. On the second dataset, we repeat the 9 and omit the 6. In this case, the detector learns that a loop on the bottom of the digit corresponds to an 8. Each of these individual classification rules is brittle, but if we average their output then the detector is robust, achieving maximal confidence only when both loops of the 8 are present.

different kind of model using a different algorithm or objective function. Bagging is a method that allows the same kind of model, training algorithm and objective function to be reused several times.

Specifically, bagging involves constructing k different datasets. Each dataset has the same number of examples as the original dataset, but each dataset is constructed by sampling with replacement from the original dataset. This means that, with high probability, each dataset is missing some of the examples from the original dataset and also contains several duplicate examples (on average around $2/3$ of the examples from the original dataset are found in the resulting training set, if it has the same size as the original). Model i is then trained on dataset i . The differences between which examples are included in each dataset result in differences between the trained models. See figure 7.5 for an example.

Neural networks reach a wide enough variety of solution points that they can often benefit from model averaging even if all of the models are trained on the same dataset. Differences in random initialization, random selection of minibatches, differences in hyperparameters, or different outcomes of non-deterministic implementations of neural networks are often enough to cause different members of the

ensemble to make partially independent errors.

Model averaging is an extremely powerful and reliable method for reducing generalization error. Its use is usually discouraged when benchmarking algorithms for scientific papers, because any machine learning algorithm can benefit substantially from model averaging at the price of increased computation and memory. For this reason, benchmark comparisons are usually made using a single model.

Machine learning contests are usually won by methods using model averaging over dozens of models. A recent prominent example is the Netflix Grand Prize (Koren, 2009).

Not all techniques for constructing ensembles are designed to make the ensemble more regularized than the individual models. For example, a technique called **boosting** (Freund and Schapire, 1996b,a) constructs an ensemble with higher capacity than the individual models. Boosting has been applied to build ensembles of neural networks (Schwenk and Bengio, 1998) by incrementally adding neural networks to the ensemble. Boosting has also been applied interpreting an individual neural network as an ensemble (Bengio *et al.*, 2006a), incrementally adding hidden units to the neural network.

7.12 Dropout

Dropout (Srivastava *et al.*, 2014) provides a computationally inexpensive but powerful method of regularizing a broad family of models. To a first approximation, dropout can be thought of as a method of making bagging practical for ensembles of very many large neural networks. Bagging involves training multiple models, and evaluating multiple models on each test example. This seems impractical when each model is a large neural network, since training and evaluating such networks is costly in terms of runtime and memory. It is common to use ensembles of five to ten neural networks—Szegedy *et al.* (2014a) used six to win the ILSVRC—but more than this rapidly becomes unwieldy. Dropout provides an inexpensive approximation to training and evaluating a bagged ensemble of exponentially many neural networks.

Specifically, dropout trains the ensemble consisting of all sub-networks that can be formed by removing non-output units from an underlying base network, as illustrated in figure 7.6. In most modern neural networks, based on a series of affine transformations and nonlinearities, we can effectively remove a unit from a network by multiplying its output value by zero. This procedure requires some slight modification for models such as radial basis function networks, which take

the difference between the unit’s state and some reference value. Here, we present the dropout algorithm in terms of multiplication by zero for simplicity, but it can be trivially modified to work with other operations that remove a unit from the network.

Recall that to learn with bagging, we define k different models, construct k different datasets by sampling from the training set with replacement, and then train model i on dataset i . Dropout aims to approximate this process, but with an exponentially large number of neural networks. Specifically, to train with dropout, we use a minibatch-based learning algorithm that makes small steps, such as stochastic gradient descent. Each time we load an example into a minibatch, we randomly sample a different binary mask to apply to all of the input and hidden units in the network. The mask for each unit is sampled independently from all of the others. The probability of sampling a mask value of one (causing a unit to be included) is a hyperparameter fixed before training begins. It is not a function of the current value of the model parameters or the input example. Typically, an input unit is included with probability 0.8 and a hidden unit is included with probability 0.5. We then run forward propagation, back-propagation, and the learning update as usual. Figure 7.7 illustrates how to run forward propagation with dropout.

More formally, suppose that a mask vector μ specifies which units to include, and $J(\theta, \mu)$ defines the cost of the model defined by parameters θ and mask μ . Then dropout training consists in minimizing $\mathbb{E}_\mu J(\theta, \mu)$. The expectation contains exponentially many terms but we can obtain an unbiased estimate of its gradient by sampling values of μ .

Dropout training is not quite the same as bagging training. In the case of bagging, the models are all independent. In the case of dropout, the models share parameters, with each model inheriting a different subset of parameters from the parent neural network. This parameter sharing makes it possible to represent an exponential number of models with a tractable amount of memory. In the case of bagging, each model is trained to convergence on its respective training set. In the case of dropout, typically most models are not explicitly trained at all—usually, the model is large enough that it would be infeasible to sample all possible sub-networks within the lifetime of the universe. Instead, a tiny fraction of the possible sub-networks are each trained for a single step, and the parameter sharing causes the remaining sub-networks to arrive at good settings of the parameters. These are the only differences. Beyond these, dropout follows the bagging algorithm. For example, the training set encountered by each sub-network is indeed a subset of the original training set sampled with replacement.

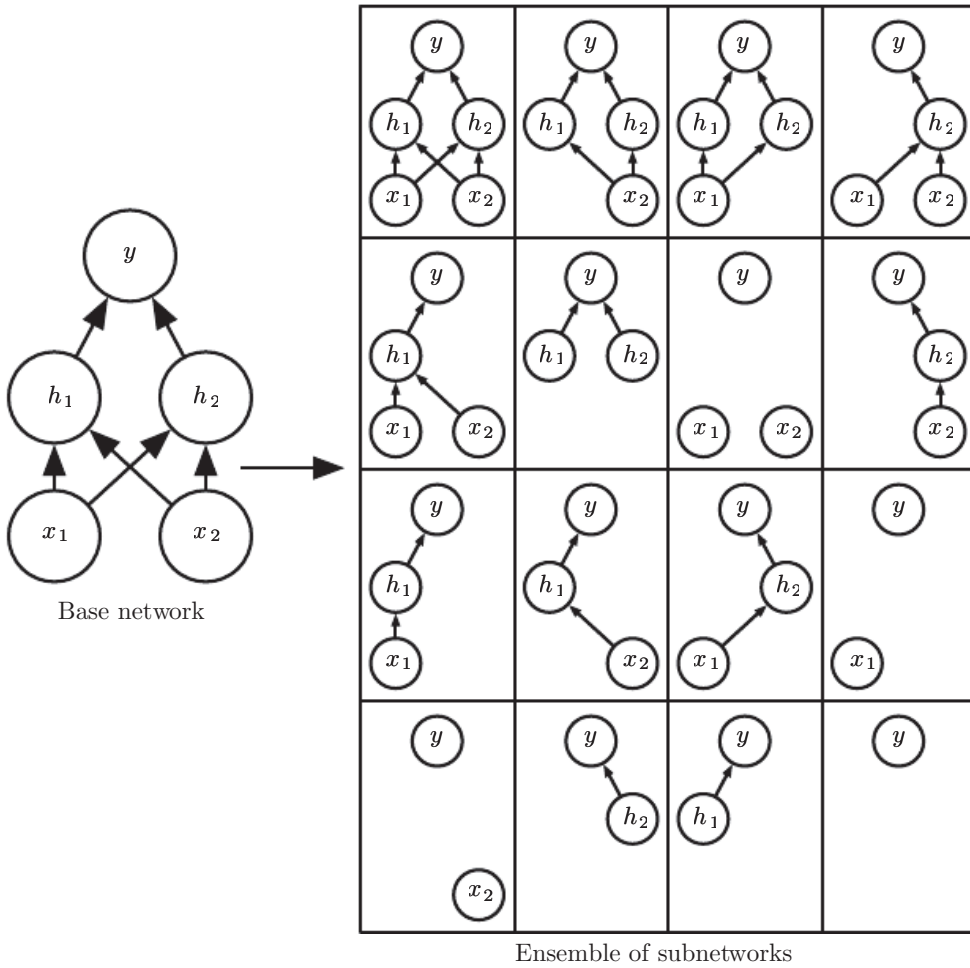


Figure 7.6: Dropout trains an ensemble consisting of all sub-networks that can be constructed by removing non-output units from an underlying base network. Here, we begin with a base network with two visible units and two hidden units. There are sixteen possible subsets of these four units. We show all sixteen subnetworks that may be formed by dropping out different subsets of units from the original network. In this small example, a large proportion of the resulting networks have no input units or no path connecting the input to the output. This problem becomes insignificant for networks with wider layers, where the probability of dropping all possible paths from inputs to outputs becomes smaller.

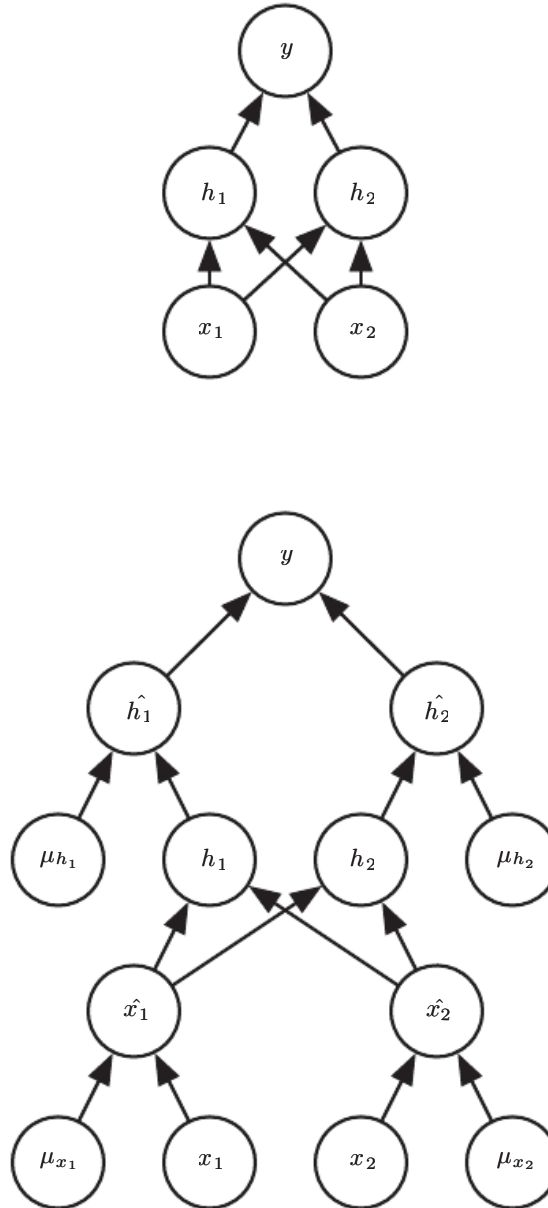


Figure 7.7: An example of forward propagation through a feedforward network using dropout. (*Top*) In this example, we use a feedforward network with two input units, one hidden layer with two hidden units, and one output unit. (*Bottom*) To perform forward propagation with dropout, we randomly sample a vector μ with one entry for each input or hidden unit in the network. The entries of μ are binary and are sampled independently from each other. The probability of each entry being 1 is a hyperparameter, usually 0.5 for the hidden layers and 0.8 for the input. Each unit in the network is multiplied by the corresponding mask, and then forward propagation continues through the rest of the network as usual. This is equivalent to randomly selecting one of the sub-networks from figure 7.6 and running forward propagation through it.

To make a prediction, a bagged ensemble must accumulate votes from all of its members. We refer to this process as **inference** in this context. So far, our description of bagging and dropout has not required that the model be explicitly probabilistic. Now, we assume that the model’s role is to output a probability distribution. In the case of bagging, each model i produces a probability distribution $p^{(i)}(y | \mathbf{x})$. The prediction of the ensemble is given by the arithmetic mean of all of these distributions,

$$\frac{1}{k} \sum_{i=1}^k p^{(i)}(y | \mathbf{x}). \quad (7.52)$$

In the case of dropout, each sub-model defined by mask vector $\boldsymbol{\mu}$ defines a probability distribution $p(y | \mathbf{x}, \boldsymbol{\mu})$. The arithmetic mean over all masks is given by

$$\sum_{\boldsymbol{\mu}} p(\boldsymbol{\mu}) p(y | \mathbf{x}, \boldsymbol{\mu}) \quad (7.53)$$

where $p(\boldsymbol{\mu})$ is the probability distribution that was used to sample $\boldsymbol{\mu}$ at training time.

Because this sum includes an exponential number of terms, it is intractable to evaluate except in cases where the structure of the model permits some form of simplification. So far, deep neural nets are not known to permit any tractable simplification. Instead, we can approximate the inference with sampling, by averaging together the output from many masks. Even 10-20 masks are often sufficient to obtain good performance.

However, there is an even better approach, that allows us to obtain a good approximation to the predictions of the entire ensemble, at the cost of only one forward propagation. To do so, we change to using the geometric mean rather than the arithmetic mean of the ensemble members’ predicted distributions. [Warde-Farley et al. \(2014\)](#) present arguments and empirical evidence that the geometric mean performs comparably to the arithmetic mean in this context.

The geometric mean of multiple probability distributions is not guaranteed to be a probability distribution. To guarantee that the result is a probability distribution, we impose the requirement that none of the sub-models assigns probability 0 to any event, and we renormalize the resulting distribution. The unnormalized probability distribution defined directly by the geometric mean is given by

$$\tilde{p}_{\text{ensemble}}(y | \mathbf{x}) = \sqrt[2^d]{\prod_{\boldsymbol{\mu}} p(y | \mathbf{x}, \boldsymbol{\mu})} \quad (7.54)$$

where d is the number of units that may be dropped. Here we use a uniform distribution over $\boldsymbol{\mu}$ to simplify the presentation, but non-uniform distributions are

also possible. To make predictions we must re-normalize the ensemble:

$$p_{\text{ensemble}}(y \mid \mathbf{x}) = \frac{\tilde{p}_{\text{ensemble}}(y \mid \mathbf{x})}{\sum_{y'} \tilde{p}_{\text{ensemble}}(y' \mid \mathbf{x})}. \quad (7.55)$$

A key insight ([Hinton et al., 2012c](#)) involved in dropout is that we can approximate p_{ensemble} by evaluating $p(y \mid \mathbf{x})$ in one model: the model with all units, but with the weights going out of unit i multiplied by the probability of including unit i . The motivation for this modification is to capture the right expected value of the output from that unit. We call this approach the **weight scaling inference rule**. There is not yet any theoretical argument for the accuracy of this approximate inference rule in deep nonlinear networks, but empirically it performs very well.

Because we usually use an inclusion probability of $\frac{1}{2}$, the weight scaling rule usually amounts to dividing the weights by 2 at the end of training, and then using the model as usual. Another way to achieve the same result is to multiply the states of the units by 2 during training. Either way, the goal is to make sure that the expected total input to a unit at test time is roughly the same as the expected total input to that unit at train time, even though half the units at train time are missing on average.

For many classes of models that do not have nonlinear hidden units, the weight scaling inference rule is exact. For a simple example, consider a softmax regression classifier with n input variables represented by the vector \mathbf{v} :

$$P(y = y \mid \mathbf{v}) = \text{softmax} \left(\mathbf{W}^\top \mathbf{v} + \mathbf{b} \right)_y. \quad (7.56)$$

We can index into the family of sub-models by element-wise multiplication of the input with a binary vector d :

$$P(y = y \mid \mathbf{v}; \mathbf{d}) = \text{softmax} \left(\mathbf{W}^\top (\mathbf{d} \odot \mathbf{v}) + \mathbf{b} \right)_y. \quad (7.57)$$

The ensemble predictor is defined by re-normalizing the geometric mean over all ensemble members' predictions:

$$P_{\text{ensemble}}(y = y \mid \mathbf{v}) = \frac{\tilde{P}_{\text{ensemble}}(y = y \mid \mathbf{v})}{\sum_{y'} \tilde{P}_{\text{ensemble}}(y = y' \mid \mathbf{v})} \quad (7.58)$$

where

$$\tilde{P}_{\text{ensemble}}(y = y \mid \mathbf{v}) = \sqrt[2^n]{\prod_{\mathbf{d} \in \{0,1\}^n} P(y = y \mid \mathbf{v}; \mathbf{d})}. \quad (7.59)$$

To see that the weight scaling rule is exact, we can simplify $\tilde{P}_{\text{ensemble}}$:

$$\tilde{P}_{\text{ensemble}}(y = y \mid \mathbf{v}) = \sqrt[2^n]{\prod_{\mathbf{d} \in \{0,1\}^n} P(y = y \mid \mathbf{v}; \mathbf{d})} \quad (7.60)$$

$$= \sqrt[2^n]{\prod_{\mathbf{d} \in \{0,1\}^n} \text{softmax}(\mathbf{W}^\top (\mathbf{d} \odot \mathbf{v}) + \mathbf{b})_y} \quad (7.61)$$

$$= \sqrt[2^n]{\prod_{\mathbf{d} \in \{0,1\}^n} \frac{\exp(\mathbf{W}_{y,:}^\top (\mathbf{d} \odot \mathbf{v}) + b_y)}{\sum_{y'} \exp(\mathbf{W}_{y',:}^\top (\mathbf{d} \odot \mathbf{v}) + b_{y'})}} \quad (7.62)$$

$$= \frac{\sqrt[2^n]{\prod_{\mathbf{d} \in \{0,1\}^n} \exp(\mathbf{W}_{y,:}^\top (\mathbf{d} \odot \mathbf{v}) + b_y)}}{\sqrt[2^n]{\prod_{\mathbf{d} \in \{0,1\}^n} \sum_{y'} \exp(\mathbf{W}_{y',:}^\top (\mathbf{d} \odot \mathbf{v}) + b_{y'})}} \quad (7.63)$$

Because \tilde{P} will be normalized, we can safely ignore multiplication by factors that are constant with respect to y :

$$\tilde{P}_{\text{ensemble}}(y = y \mid \mathbf{v}) \propto \sqrt[2^n]{\prod_{\mathbf{d} \in \{0,1\}^n} \exp(\mathbf{W}_{y,:}^\top (\mathbf{d} \odot \mathbf{v}) + b_y)} \quad (7.64)$$

$$= \exp\left(\frac{1}{2^n} \sum_{\mathbf{d} \in \{0,1\}^n} \mathbf{W}_{y,:}^\top (\mathbf{d} \odot \mathbf{v}) + b_y\right) \quad (7.65)$$

$$= \exp\left(\frac{1}{2} \mathbf{W}_{y,:}^\top \mathbf{v} + b_y\right). \quad (7.66)$$

Substituting this back into equation 7.58 we obtain a softmax classifier with weights $\frac{1}{2}\mathbf{W}$.

The weight scaling rule is also exact in other settings, including regression networks with conditionally normal outputs, and deep networks that have hidden layers without nonlinearities. However, the weight scaling rule is only an approximation for deep models that have nonlinearities. Though the approximation has not been theoretically characterized, it often works well, empirically. [Goodfellow et al. \(2013a\)](#) found experimentally that the weight scaling approximation can work better (in terms of classification accuracy) than Monte Carlo approximations to the ensemble predictor. This held true even when the Monte Carlo approximation was allowed to sample up to 1,000 sub-networks. [Gal and Ghahramani \(2015\)](#) found that some models obtain better classification accuracy using twenty samples and

the Monte Carlo approximation. It appears that the optimal choice of inference approximation is problem-dependent.

Srivastava *et al.* (2014) showed that dropout is more effective than other standard computationally inexpensive regularizers, such as weight decay, filter norm constraints and sparse activity regularization. Dropout may also be combined with other forms of regularization to yield a further improvement.

One advantage of dropout is that it is very computationally cheap. Using dropout during training requires only $O(n)$ computation per example per update, to generate n random binary numbers and multiply them by the state. Depending on the implementation, it may also require $O(n)$ memory to store these binary numbers until the back-propagation stage. Running inference in the trained model has the same cost per-example as if dropout were not used, though we must pay the cost of dividing the weights by 2 once before beginning to run inference on examples.

Another significant advantage of dropout is that it does not significantly limit the type of model or training procedure that can be used. It works well with nearly any model that uses a distributed representation and can be trained with stochastic gradient descent. This includes feedforward neural networks, probabilistic models such as restricted Boltzmann machines (Srivastava *et al.*, 2014), and recurrent neural networks (Bayer and Osendorfer, 2014; Pascanu *et al.*, 2014a). Many other regularization strategies of comparable power impose more severe restrictions on the architecture of the model.

Though the cost per-step of applying dropout to a specific model is negligible, the cost of using dropout in a complete system can be significant. Because dropout is a regularization technique, it reduces the effective capacity of a model. To offset this effect, we must increase the size of the model. Typically the optimal validation set error is much lower when using dropout, but this comes at the cost of a much larger model and many more iterations of the training algorithm. For very large datasets, regularization confers little reduction in generalization error. In these cases, the computational cost of using dropout and larger models may outweigh the benefit of regularization.

When extremely few labeled training examples are available, dropout is less effective. Bayesian neural networks (Neal, 1996) outperform dropout on the Alternative Splicing Dataset (Xiong *et al.*, 2011) where fewer than 5,000 examples are available (Srivastava *et al.*, 2014). When additional unlabeled data is available, unsupervised feature learning can gain an advantage over dropout.

Wager *et al.* (2013) showed that, when applied to linear regression, dropout is equivalent to L^2 weight decay, with a different weight decay coefficient for

each input feature. The magnitude of each feature’s weight decay coefficient is determined by its variance. Similar results hold for other linear models. For deep models, dropout is not equivalent to weight decay.

The stochasticity used while training with dropout is not necessary for the approach’s success. It is just a means of approximating the sum over all sub-models. [Wang and Manning \(2013\)](#) derived analytical approximations to this marginalization. Their approximation, known as **fast dropout** resulted in faster convergence time due to the reduced stochasticity in the computation of the gradient. This method can also be applied at test time, as a more principled (but also more computationally expensive) approximation to the average over all sub-networks than the weight scaling approximation. Fast dropout has been used to nearly match the performance of standard dropout on small neural network problems, but has not yet yielded a significant improvement or been applied to a large problem.

Just as stochasticity is not necessary to achieve the regularizing effect of dropout, it is also not sufficient. To demonstrate this, [Warde-Farley et al. \(2014\)](#) designed control experiments using a method called **dropout boosting** that they designed to use exactly the same mask noise as traditional dropout but lack its regularizing effect. Dropout boosting trains the entire ensemble to jointly maximize the log-likelihood on the training set. In the same sense that traditional dropout is analogous to bagging, this approach is analogous to boosting. As intended, experiments with dropout boosting show almost no regularization effect compared to training the entire network as a single model. This demonstrates that the interpretation of dropout as bagging has value beyond the interpretation of dropout as robustness to noise. The regularization effect of the bagged ensemble is only achieved when the stochastically sampled ensemble members are trained to perform well independently of each other.

Dropout has inspired other stochastic approaches to training exponentially large ensembles of models that share weights. DropConnect is a special case of dropout where each product between a single scalar weight and a single hidden unit state is considered a unit that can be dropped ([Wan et al., 2013](#)). Stochastic pooling is a form of randomized pooling (see section 9.3) for building ensembles of convolutional networks with each convolutional network attending to different spatial locations of each feature map. So far, dropout remains the most widely used implicit ensemble method.

One of the key insights of dropout is that training a network with stochastic behavior and making predictions by averaging over multiple stochastic decisions implements a form of bagging with parameter sharing. Earlier, we described

dropout as bagging an ensemble of models formed by including or excluding units. However, there is no need for this model averaging strategy to be based on inclusion and exclusion. In principle, any kind of random modification is admissible. In practice, we must choose modification families that neural networks are able to learn to resist. Ideally, we should also use model families that allow a fast approximate inference rule. We can think of any form of modification parametrized by a vector μ as training an ensemble consisting of $p(y | \mathbf{x}, \mu)$ for all possible values of μ . There is no requirement that μ have a finite number of values. For example, μ can be real-valued. Srivastava *et al.* (2014) showed that multiplying the weights by $\mu \sim \mathcal{N}(\mathbf{1}, I)$ can outperform dropout based on binary masks. Because $\mathbb{E}[\mu] = \mathbf{1}$ the standard network automatically implements approximate inference in the ensemble, without needing any weight scaling.

So far we have described dropout purely as a means of performing efficient, approximate bagging. However, there is another view of dropout that goes further than this. Dropout trains not just a bagged ensemble of models, but an ensemble of models that share hidden units. This means each hidden unit must be able to perform well regardless of which other hidden units are in the model. Hidden units must be prepared to be swapped and interchanged between models. Hinton *et al.* (2012c) were inspired by an idea from biology: sexual reproduction, which involves swapping genes between two different organisms, creates evolutionary pressure for genes to become not just good, but to become readily swapped between different organisms. Such genes and such features are very robust to changes in their environment because they are not able to incorrectly adapt to unusual features of any one organism or model. Dropout thus regularizes each hidden unit to be not merely a good feature but a feature that is good in many contexts. Warde-Farley *et al.* (2014) compared dropout training to training of large ensembles and concluded that dropout offers additional improvements to generalization error beyond those obtained by ensembles of independent models.

It is important to understand that a large portion of the power of dropout arises from the fact that the masking noise is applied to the hidden units. This can be seen as a form of highly intelligent, adaptive destruction of the information content of the input rather than destruction of the raw values of the input. For example, if the model learns a hidden unit h_i that detects a face by finding the nose, then dropping h_i corresponds to erasing the information that there is a nose in the image. The model must learn another h_i , either that redundantly encodes the presence of a nose, or that detects the face by another feature, such as the mouth. Traditional noise injection techniques that add unstructured noise at the input are not able to randomly erase the information about a nose from an image of a face unless the magnitude of the noise is so great that nearly all of the information in

the image is removed. Destroying extracted features rather than original values allows the destruction process to make use of all of the knowledge about the input distribution that the model has acquired so far.

Another important aspect of dropout is that the noise is multiplicative. If the noise were additive with fixed scale, then a rectified linear hidden unit h_i with added noise ϵ could simply learn to have h_i become very large in order to make the added noise ϵ insignificant by comparison. Multiplicative noise does not allow such a pathological solution to the noise robustness problem.

Another deep learning algorithm, batch normalization, reparametrizes the model in a way that introduces both additive and multiplicative noise on the hidden units at training time. The primary purpose of batch normalization is to improve optimization, but the noise can have a regularizing effect, and sometimes makes dropout unnecessary. Batch normalization is described further in section 8.7.1.

7.13 Adversarial Training

In many cases, neural networks have begun to reach human performance when evaluated on an i.i.d. test set. It is natural therefore to wonder whether these models have obtained a true human-level understanding of these tasks. In order to probe the level of understanding a network has of the underlying task, we can search for examples that the model misclassifies. [Szegedy et al. \(2014b\)](#) found that even neural networks that perform at human level accuracy have a nearly 100% error rate on examples that are intentionally constructed by using an optimization procedure to search for an input \mathbf{x}' near a data point \mathbf{x} such that the model output is very different at \mathbf{x}' . In many cases, \mathbf{x}' can be so similar to \mathbf{x} that a human observer cannot tell the difference between the original example and the **adversarial example**, but the network can make highly different predictions. See figure 7.8 for an example.

Adversarial examples have many implications, for example, in computer security, that are beyond the scope of this chapter. However, they are interesting in the context of regularization because one can reduce the error rate on the original i.i.d. test set via **adversarial training**—training on adversarially perturbed examples from the training set ([Szegedy et al., 2014b](#); [Goodfellow et al., 2014b](#)).

[Goodfellow et al. \(2014b\)](#) showed that one of the primary causes of these adversarial examples is excessive linearity. Neural networks are built out of primarily linear building blocks. In some experiments the overall function they implement proves to be highly linear as a result. These linear functions are easy

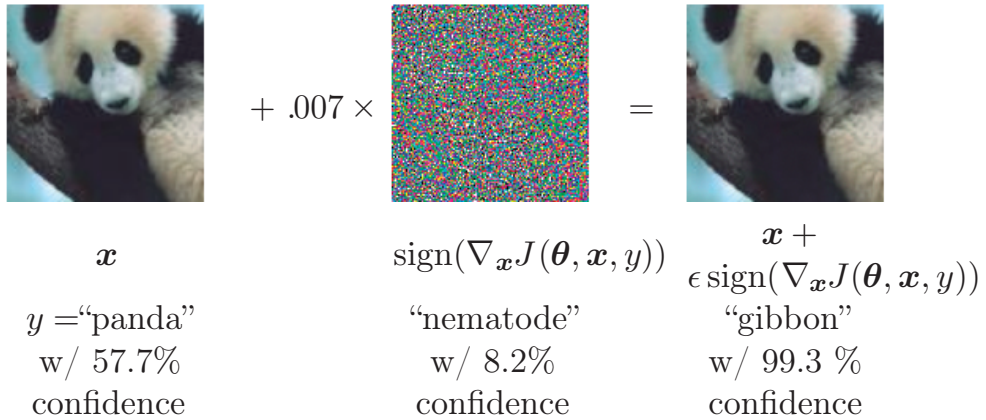


Figure 7.8: A demonstration of adversarial example generation applied to GoogLeNet ([Szegedy et al., 2014a](#)) on ImageNet. By adding an imperceptibly small vector whose elements are equal to the sign of the elements of the gradient of the cost function with respect to the input, we can change GoogLeNet’s classification of the image. Reproduced with permission from [Goodfellow et al. \(2014b\)](#).

to optimize. Unfortunately, the value of a linear function can change very rapidly if it has numerous inputs. If we change each input by ϵ , then a linear function with weights \mathbf{w} can change by as much as $\epsilon \|\mathbf{w}\|_1$, which can be a very large amount if \mathbf{w} is high-dimensional. Adversarial training discourages this highly sensitive locally linear behavior by encouraging the network to be locally constant in the neighborhood of the training data. This can be seen as a way of explicitly introducing a local constancy prior into supervised neural nets.

Adversarial training helps to illustrate the power of using a large function family in combination with aggressive regularization. Purely linear models, like logistic regression, are not able to resist adversarial examples because they are forced to be linear. Neural networks are able to represent functions that can range from nearly linear to nearly locally constant and thus have the flexibility to capture linear trends in the training data while still learning to resist local perturbation.

Adversarial examples also provide a means of accomplishing semi-supervised learning. At a point \mathbf{x} that is not associated with a label in the dataset, the model itself assigns some label \hat{y} . The model’s label \hat{y} may not be the true label, but if the model is high quality, then \hat{y} has a high probability of providing the true label. We can seek an adversarial example \mathbf{x}' that causes the classifier to output a label y' with $y' \neq \hat{y}$. Adversarial examples generated using not the true label but a label provided by a trained model are called **virtual adversarial examples** ([Miyato et al., 2015](#)). The classifier may then be trained to assign the same label to \mathbf{x} and \mathbf{x}' . This encourages the classifier to learn a function that is

robust to small changes anywhere along the manifold where the unlabeled data lies. The assumption motivating this approach is that different classes usually lie on disconnected manifolds, and a small perturbation should not be able to jump from one class manifold to another class manifold.

7.14 Tangent Distance, Tangent Prop, and Manifold Tangent Classifier

Many machine learning algorithms aim to overcome the curse of dimensionality by assuming that the data lies near a low-dimensional manifold, as described in section 5.11.3.

One of the early attempts to take advantage of the manifold hypothesis is the **tangent distance** algorithm (Simard *et al.*, 1993, 1998). It is a non-parametric nearest-neighbor algorithm in which the metric used is not the generic Euclidean distance but one that is derived from knowledge of the manifolds near which probability concentrates. It is assumed that we are trying to classify examples and that examples on the same manifold share the same category. Since the classifier should be invariant to the local factors of variation that correspond to movement on the manifold, it would make sense to use as nearest-neighbor distance between points \mathbf{x}_1 and \mathbf{x}_2 the distance between the manifolds M_1 and M_2 to which they respectively belong. Although that may be computationally difficult (it would require solving an optimization problem, to find the nearest pair of points on M_1 and M_2), a cheap alternative that makes sense locally is to approximate M_i by its tangent plane at \mathbf{x}_i and measure the distance between the two tangents, or between a tangent plane and a point. That can be achieved by solving a low-dimensional linear system (in the dimension of the manifolds). Of course, this algorithm requires one to specify the tangent vectors.

In a related spirit, the **tangent prop** algorithm (Simard *et al.*, 1992) (figure 7.9) trains a neural net classifier with an extra penalty to make each output $f(\mathbf{x})$ of the neural net locally invariant to known factors of variation. These factors of variation correspond to movement along the manifold near which examples of the same class concentrate. Local invariance is achieved by requiring $\nabla_{\mathbf{x}}f(\mathbf{x})$ to be orthogonal to the known manifold tangent vectors $\mathbf{v}^{(i)}$ at \mathbf{x} , or equivalently that the directional derivative of f at \mathbf{x} in the directions $\mathbf{v}^{(i)}$ be small by adding a regularization penalty Ω :

$$\Omega(f) = \sum_i \left((\nabla_{\mathbf{x}}f(\mathbf{x}))^\top \mathbf{v}^{(i)} \right)^2. \quad (7.67)$$

This regularizer can of course be scaled by an appropriate hyperparameter, and, for most neural networks, we would need to sum over many outputs rather than the lone output $f(\mathbf{x})$ described here for simplicity. As with the tangent distance algorithm, the tangent vectors are derived a priori, usually from the formal knowledge of the effect of transformations such as translation, rotation, and scaling in images. Tangent prop has been used not just for supervised learning (Simard *et al.*, 1992) but also in the context of reinforcement learning (Thrun, 1995).

Tangent propagation is closely related to dataset augmentation. In both cases, the user of the algorithm encodes his or her prior knowledge of the task by specifying a set of transformations that should not alter the output of the network. The difference is that in the case of dataset augmentation, the network is explicitly trained to correctly classify distinct inputs that were created by applying more than an infinitesimal amount of these transformations. Tangent propagation does not require explicitly visiting a new input point. Instead, it analytically regularizes the model to resist perturbation in the directions corresponding to the specified transformation. While this analytical approach is intellectually elegant, it has two major drawbacks. First, it only regularizes the model to resist infinitesimal perturbation. Explicit dataset augmentation confers resistance to larger perturbations. Second, the infinitesimal approach poses difficulties for models based on rectified linear units. These models can only shrink their derivatives by turning units off or shrinking their weights. They are not able to shrink their derivatives by saturating at a high value with large weights, as sigmoid or tanh units can. Dataset augmentation works well with rectified linear units because different subsets of rectified units can activate for different transformed versions of each original input.

Tangent propagation is also related to **double backprop** (Drucker and LeCun, 1992) and adversarial training (Szegedy *et al.*, 2014b; Goodfellow *et al.*, 2014b). Double backprop regularizes the Jacobian to be small, while adversarial training finds inputs near the original inputs and trains the model to produce the same output on these as on the original inputs. Tangent propagation and dataset augmentation using manually specified transformations both require that the model should be invariant to certain specified directions of change in the input. Double backprop and adversarial training both require that the model should be invariant to *all* directions of change in the input so long as the change is small. Just as dataset augmentation is the non-infinitesimal version of tangent propagation, adversarial training is the non-infinitesimal version of double backprop.

The manifold tangent classifier (Rifai *et al.*, 2011c), eliminates the need to know the tangent vectors a priori. As we will see in chapter 14, autoencoders can

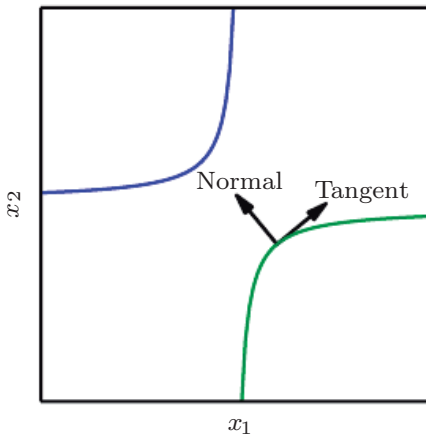


Figure 7.9: Illustration of the main idea of the tangent prop algorithm (Simard *et al.*, 1992) and manifold tangent classifier (Rifai *et al.*, 2011c), which both regularize the classifier output function $f(\mathbf{x})$. Each curve represents the manifold for a different class, illustrated here as a one-dimensional manifold embedded in a two-dimensional space. On one curve, we have chosen a single point and drawn a vector that is tangent to the class manifold (parallel to and touching the manifold) and a vector that is normal to the class manifold (orthogonal to the manifold). In multiple dimensions there may be many tangent directions and many normal directions. We expect the classification function to change rapidly as it moves in the direction normal to the manifold, and not to change as it moves along the class manifold. Both tangent propagation and the manifold tangent classifier regularize $f(\mathbf{x})$ to not change very much as \mathbf{x} moves along the manifold. Tangent propagation requires the user to manually specify functions that compute the tangent directions (such as specifying that small translations of images remain in the same class manifold) while the manifold tangent classifier estimates the manifold tangent directions by training an autoencoder to fit the training data. The use of autoencoders to estimate manifolds will be described in chapter 14.

estimate the manifold tangent vectors. The manifold tangent classifier makes use of this technique to avoid needing user-specified tangent vectors. As illustrated in figure 14.10, these estimated tangent vectors go beyond the classical invariants that arise out of the geometry of images (such as translation, rotation and scaling) and include factors that must be learned because they are object-specific (such as moving body parts). The algorithm proposed with the manifold tangent classifier is therefore simple: (1) use an autoencoder to learn the manifold structure by unsupervised learning, and (2) use these tangents to regularize a neural net classifier as in tangent prop (equation 7.67).

This chapter has described most of the general strategies used to regularize neural networks. Regularization is a central theme of machine learning and as such

will be revisited periodically by most of the remaining chapters. Another central theme of machine learning is optimization, described next.

Chapter 8

Optimization for Training Deep Models

Deep learning algorithms involve optimization in many contexts. For example, performing inference in models such as PCA involves solving an optimization problem. We often use analytical optimization to write proofs or design algorithms. Of all of the many optimization problems involved in deep learning, the most difficult is neural network training. It is quite common to invest days to months of time on hundreds of machines in order to solve even a single instance of the neural network training problem. Because this problem is so important and so expensive, a specialized set of optimization techniques have been developed for solving it. This chapter presents these optimization techniques for neural network training.

If you are unfamiliar with the basic principles of gradient-based optimization, we suggest reviewing chapter 4. That chapter includes a brief overview of numerical optimization in general.

This chapter focuses on one particular case of optimization: finding the parameters $\boldsymbol{\theta}$ of a neural network that significantly reduce a cost function $J(\boldsymbol{\theta})$, which typically includes a performance measure evaluated on the entire training set as well as additional regularization terms.

We begin with a description of how optimization used as a training algorithm for a machine learning task differs from pure optimization. Next, we present several of the concrete challenges that make optimization of neural networks difficult. We then define several practical algorithms, including both optimization algorithms themselves and strategies for initializing the parameters. More advanced algorithms adapt their learning rates during training or leverage information contained in

the second derivatives of the cost function. Finally, we conclude with a review of several optimization strategies that are formed by combining simple optimization algorithms into higher-level procedures.

8.1 How Learning Differs from Pure Optimization

Optimization algorithms used for training of deep models differ from traditional optimization algorithms in several ways. Machine learning usually acts indirectly. In most machine learning scenarios, we care about some performance measure P , that is defined with respect to the test set and may also be intractable. We therefore optimize P only indirectly. We reduce a different cost function $J(\boldsymbol{\theta})$ in the hope that doing so will improve P . This is in contrast to pure optimization, where minimizing J is a goal in and of itself. Optimization algorithms for training deep models also typically include some specialization on the specific structure of machine learning objective functions.

Typically, the cost function can be written as an average over the training set, such as

$$J(\boldsymbol{\theta}) = \mathbb{E}_{(\mathbf{x}, y) \sim \hat{p}_{\text{data}}} L(f(\mathbf{x}; \boldsymbol{\theta}), y), \quad (8.1)$$

where L is the per-example loss function, $f(\mathbf{x}; \boldsymbol{\theta})$ is the predicted output when the input is \mathbf{x} , \hat{p}_{data} is the empirical distribution. In the supervised learning case, y is the target output. Throughout this chapter, we develop the unregularized supervised case, where the arguments to L are $f(\mathbf{x}; \boldsymbol{\theta})$ and y . However, it is trivial to extend this development, for example, to include $\boldsymbol{\theta}$ or \mathbf{x} as arguments, or to exclude y as arguments, in order to develop various forms of regularization or unsupervised learning.

Equation 8.1 defines an objective function with respect to the training set. We would usually prefer to minimize the corresponding objective function where the expectation is taken across *the data generating distribution* p_{data} rather than just over the finite training set:

$$J^*(\boldsymbol{\theta}) = \mathbb{E}_{(\mathbf{x}, y) \sim p_{\text{data}}} L(f(\mathbf{x}; \boldsymbol{\theta}), y). \quad (8.2)$$

8.1.1 Empirical Risk Minimization

The goal of a machine learning algorithm is to reduce the expected generalization error given by equation 8.2. This quantity is known as the **risk**. We emphasize here that the expectation is taken over the true underlying distribution p_{data} . If we knew the true distribution $p_{\text{data}}(\mathbf{x}, y)$, risk minimization would be an optimization task

solvable by an optimization algorithm. However, when we do not know $p_{\text{data}}(\mathbf{x}, y)$ but only have a training set of samples, we have a machine learning problem.

The simplest way to convert a machine learning problem back into an optimization problem is to minimize the expected loss on the training set. This means replacing the true distribution $p(\mathbf{x}, y)$ with the empirical distribution $\hat{p}(\mathbf{x}, y)$ defined by the training set. We now minimize the **empirical risk**

$$\mathbb{E}_{\mathbf{x}, \mathbf{y} \sim \hat{p}_{\text{data}}(\mathbf{x}, \mathbf{y})}[L(f(\mathbf{x}; \boldsymbol{\theta}), y)] = \frac{1}{m} \sum_{i=1}^m L(f(\mathbf{x}^{(i)}; \boldsymbol{\theta}), y^{(i)}) \quad (8.3)$$

where m is the number of training examples.

The training process based on minimizing this average training error is known as **empirical risk minimization**. In this setting, machine learning is still very similar to straightforward optimization. Rather than optimizing the risk directly, we optimize the empirical risk, and hope that the risk decreases significantly as well. A variety of theoretical results establish conditions under which the true risk can be expected to decrease by various amounts.

However, empirical risk minimization is prone to overfitting. Models with high capacity can simply memorize the training set. In many cases, empirical risk minimization is not really feasible. The most effective modern optimization algorithms are based on gradient descent, but many useful loss functions, such as 0-1 loss, have no useful derivatives (the derivative is either zero or undefined everywhere). These two problems mean that, in the context of deep learning, we rarely use empirical risk minimization. Instead, we must use a slightly different approach, in which the quantity that we actually optimize is even more different from the quantity that we truly want to optimize.

8.1.2 Surrogate Loss Functions and Early Stopping

Sometimes, the loss function we actually care about (say classification error) is not one that can be optimized efficiently. For example, exactly minimizing expected 0-1 loss is typically intractable (exponential in the input dimension), even for a linear classifier (Marcotte and Savard, 1992). In such situations, one typically optimizes a **surrogate loss function** instead, which acts as a proxy but has advantages. For example, the negative log-likelihood of the correct class is typically used as a surrogate for the 0-1 loss. The negative log-likelihood allows the model to estimate the conditional probability of the classes, given the input, and if the model can do that well, then it can pick the classes that yield the least classification error in expectation.

In some cases, a surrogate loss function actually results in being able to learn more. For example, the test set 0-1 loss often continues to decrease for a long time after the training set 0-1 loss has reached zero, when training using the log-likelihood surrogate. This is because even when the expected 0-1 loss is zero, one can improve the robustness of the classifier by further pushing the classes apart from each other, obtaining a more confident and reliable classifier, thus extracting more information from the training data than would have been possible by simply minimizing the average 0-1 loss on the training set.

A very important difference between optimization in general and optimization as we use it for training algorithms is that training algorithms do not usually halt at a local minimum. Instead, a machine learning algorithm usually minimizes a surrogate loss function but halts when a convergence criterion based on early stopping (section 7.8) is satisfied. Typically the early stopping criterion is based on the true underlying loss function, such as 0-1 loss measured on a validation set, and is designed to cause the algorithm to halt whenever overfitting begins to occur. Training often halts while the surrogate loss function still has large derivatives, which is very different from the pure optimization setting, where an optimization algorithm is considered to have converged when the gradient becomes very small.

8.1.3 Batch and Minibatch Algorithms

One aspect of machine learning algorithms that separates them from general optimization algorithms is that the objective function usually decomposes as a sum over the training examples. Optimization algorithms for machine learning typically compute each update to the parameters based on an expected value of the cost function estimated using only a subset of the terms of the full cost function.

For example, maximum likelihood estimation problems, when viewed in log space, decompose into a sum over each example:

$$\boldsymbol{\theta}_{\text{ML}} = \arg \max_{\boldsymbol{\theta}} \sum_{i=1}^m \log p_{\text{model}}(\mathbf{x}^{(i)}, y^{(i)}; \boldsymbol{\theta}). \quad (8.4)$$

Maximizing this sum is equivalent to maximizing the expectation over the empirical distribution defined by the training set:

$$J(\boldsymbol{\theta}) = \mathbb{E}_{\mathbf{x}, y \sim \hat{p}_{\text{data}}} \log p_{\text{model}}(\mathbf{x}, y; \boldsymbol{\theta}). \quad (8.5)$$

Most of the properties of the objective function J used by most of our optimization algorithms are also expectations over the training set. For example, the

most commonly used property is the gradient:

$$\nabla_{\boldsymbol{\theta}} J(\boldsymbol{\theta}) = \mathbb{E}_{\mathbf{x}, y \sim \hat{p}_{\text{data}}} \nabla_{\boldsymbol{\theta}} \log p_{\text{model}}(\mathbf{x}, y; \boldsymbol{\theta}). \quad (8.6)$$

Computing this expectation exactly is very expensive because it requires evaluating the model on every example in the entire dataset. In practice, we can compute these expectations by randomly sampling a small number of examples from the dataset, then taking the average over only those examples.

Recall that the standard error of the mean (equation 5.46) estimated from n samples is given by σ / \sqrt{n} , where σ is the true standard deviation of the value of the samples. The denominator of \sqrt{n} shows that there are less than linear returns to using more examples to estimate the gradient. Compare two hypothetical estimates of the gradient, one based on 100 examples and another based on 10,000 examples. The latter requires 100 times more computation than the former, but reduces the standard error of the mean only by a factor of 10. Most optimization algorithms converge much faster (in terms of total computation, not in terms of number of updates) if they are allowed to rapidly compute approximate estimates of the gradient rather than slowly computing the exact gradient.

Another consideration motivating statistical estimation of the gradient from a small number of samples is redundancy in the training set. In the worst case, all m samples in the training set could be identical copies of each other. A sampling-based estimate of the gradient could compute the correct gradient with a single sample, using m times less computation than the naive approach. In practice, we are unlikely to truly encounter this worst-case situation, but we may find large numbers of examples that all make very similar contributions to the gradient.

Optimization algorithms that use the entire training set are called **batch** or **deterministic** gradient methods, because they process all of the training examples simultaneously in a large batch. This terminology can be somewhat confusing because the word “batch” is also often used to describe the minibatch used by minibatch stochastic gradient descent. Typically the term “batch gradient descent” implies the use of the full training set, while the use of the term “batch” to describe a group of examples does not. For example, it is very common to use the term “batch size” to describe the size of a minibatch.

Optimization algorithms that use only a single example at a time are sometimes called **stochastic** or sometimes **online** methods. The term **online** is usually reserved for the case where the examples are drawn from a stream of continually created examples rather than from a fixed-size training set over which several passes are made.

Most algorithms used for deep learning fall somewhere in between, using more

than one but less than all of the training examples. These were traditionally called **minibatch** or **minibatch stochastic** methods and it is now common to simply call them **stochastic** methods.

The canonical example of a stochastic method is stochastic gradient descent, presented in detail in section 8.3.1.

Minibatch sizes are generally driven by the following factors:

- Larger batches provide a more accurate estimate of the gradient, but with less than linear returns.
- Multicore architectures are usually underutilized by extremely small batches. This motivates using some absolute minimum batch size, below which there is no reduction in the time to process a minibatch.
- If all examples in the batch are to be processed in parallel (as is typically the case), then the amount of memory scales with the batch size. For many hardware setups this is the limiting factor in batch size.
- Some kinds of hardware achieve better runtime with specific sizes of arrays. Especially when using GPUs, it is common for power of 2 batch sizes to offer better runtime. Typical power of 2 batch sizes range from 32 to 256, with 16 sometimes being attempted for large models.
- Small batches can offer a regularizing effect (Wilson and Martinez, 2003), perhaps due to the noise they add to the learning process. Generalization error is often best for a batch size of 1. Training with such a small batch size might require a small learning rate to maintain stability due to the high variance in the estimate of the gradient. The total runtime can be very high due to the need to make more steps, both because of the reduced learning rate and because it takes more steps to observe the entire training set.

Different kinds of algorithms use different kinds of information from the mini-batch in different ways. Some algorithms are more sensitive to sampling error than others, either because they use information that is difficult to estimate accurately with few samples, or because they use information in ways that amplify sampling errors more. Methods that compute updates based only on the gradient \mathbf{g} are usually relatively robust and can handle smaller batch sizes like 100. Second-order methods, which use also the Hessian matrix \mathbf{H} and compute updates such as $\mathbf{H}^{-1}\mathbf{g}$, typically require much larger batch sizes like 10,000. These large batch sizes are required to minimize fluctuations in the estimates of $\mathbf{H}^{-1}\mathbf{g}$. Suppose that \mathbf{H} is estimated perfectly but has a poor condition number. Multiplication by

\mathbf{H} or its inverse amplifies pre-existing errors, in this case, estimation errors in \mathbf{g} . Very small changes in the estimate of \mathbf{g} can thus cause large changes in the update $\mathbf{H}^{-1}\mathbf{g}$, even if \mathbf{H} were estimated perfectly. Of course, \mathbf{H} will be estimated only approximately, so the update $\mathbf{H}^{-1}\mathbf{g}$ will contain even more error than we would predict from applying a poorly conditioned operation to the estimate of \mathbf{g} .

It is also crucial that the minibatches be selected randomly. Computing an unbiased estimate of the expected gradient from a set of samples requires that those samples be independent. We also wish for two subsequent gradient estimates to be independent from each other, so two subsequent minibatches of examples should also be independent from each other. Many datasets are most naturally arranged in a way where successive examples are highly correlated. For example, we might have a dataset of medical data with a long list of blood sample test results. This list might be arranged so that first we have five blood samples taken at different times from the first patient, then we have three blood samples taken from the second patient, then the blood samples from the third patient, and so on. If we were to draw examples in order from this list, then each of our minibatches would be extremely biased, because it would represent primarily one patient out of the many patients in the dataset. In cases such as these where the order of the dataset holds some significance, it is necessary to shuffle the examples before selecting minibatches. For very large datasets, for example datasets containing billions of examples in a data center, it can be impractical to sample examples truly uniformly at random every time we want to construct a minibatch. Fortunately, in practice it is usually sufficient to shuffle the order of the dataset once and then store it in shuffled fashion. This will impose a fixed set of possible minibatches of consecutive examples that all models trained thereafter will use, and each individual model will be forced to reuse this ordering every time it passes through the training data. However, this deviation from true random selection does not seem to have a significant detrimental effect. Failing to ever shuffle the examples in any way can seriously reduce the effectiveness of the algorithm.

Many optimization problems in machine learning decompose over examples well enough that we can compute entire separate updates over different examples in parallel. In other words, we can compute the update that minimizes $J(\mathbf{X})$ for one minibatch of examples \mathbf{X} at the same time that we compute the update for several other minibatches. Such asynchronous parallel distributed approaches are discussed further in section 12.1.3.

An interesting motivation for minibatch stochastic gradient descent is that it follows the gradient of the true *generalization error* (equation 8.2) so long as no examples are repeated. Most implementations of minibatch stochastic gradient

descent shuffle the dataset once and then pass through it multiple times. On the first pass, each minibatch is used to compute an unbiased estimate of the true generalization error. On the second pass, the estimate becomes biased because it is formed by re-sampling values that have already been used, rather than obtaining new fair samples from the data generating distribution.

The fact that stochastic gradient descent minimizes generalization error is easiest to see in the online learning case, where examples or minibatches are drawn from a **stream** of data. In other words, instead of receiving a fixed-size training set, the learner is similar to a living being who sees a new example at each instant, with every example (\mathbf{x}, y) coming from the data generating distribution $p_{\text{data}}(\mathbf{x}, y)$. In this scenario, examples are never repeated; every experience is a fair sample from p_{data} .

The equivalence is easiest to derive when both \mathbf{x} and y are discrete. In this case, the generalization error (equation 8.2) can be written as a sum

$$J^*(\boldsymbol{\theta}) = \sum_{\mathbf{x}} \sum_y p_{\text{data}}(\mathbf{x}, y) L(f(\mathbf{x}; \boldsymbol{\theta}), y), \quad (8.7)$$

with the exact gradient

$$\mathbf{g} = \nabla_{\boldsymbol{\theta}} J^*(\boldsymbol{\theta}) = \sum_{\mathbf{x}} \sum_y p_{\text{data}}(\mathbf{x}, y) \nabla_{\boldsymbol{\theta}} L(f(\mathbf{x}; \boldsymbol{\theta}), y). \quad (8.8)$$

We have already seen the same fact demonstrated for the log-likelihood in equation 8.5 and equation 8.6; we observe now that this holds for other functions L besides the likelihood. A similar result can be derived when \mathbf{x} and y are continuous, under mild assumptions regarding p_{data} and L .

Hence, we can obtain an unbiased estimator of the exact gradient of the generalization error by sampling a minibatch of examples $\{\mathbf{x}^{(1)}, \dots, \mathbf{x}^{(m)}\}$ with corresponding targets $y^{(i)}$ from the data generating distribution p_{data} , and computing the gradient of the loss with respect to the parameters for that minibatch:

$$\hat{\mathbf{g}} = \frac{1}{m} \nabla_{\boldsymbol{\theta}} \sum_i L(f(\mathbf{x}^{(i)}; \boldsymbol{\theta}), y^{(i)}). \quad (8.9)$$

Updating $\boldsymbol{\theta}$ in the direction of $\hat{\mathbf{g}}$ performs SGD on the generalization error.

Of course, this interpretation only applies when examples are not reused. Nonetheless, it is usually best to make several passes through the training set, unless the training set is extremely large. When multiple such epochs are used, only the first epoch follows the unbiased gradient of the generalization error, but

of course, the additional epochs usually provide enough benefit due to decreased training error to offset the harm they cause by increasing the gap between training error and test error.

With some datasets growing rapidly in size, faster than computing power, it is becoming more common for machine learning applications to use each training example only once or even to make an incomplete pass through the training set. When using an extremely large training set, overfitting is not an issue, so underfitting and computational efficiency become the predominant concerns. See also [Bottou and Bousquet \(2008\)](#) for a discussion of the effect of computational bottlenecks on generalization error, as the number of training examples grows.

8.2 Challenges in Neural Network Optimization

Optimization in general is an extremely difficult task. Traditionally, machine learning has avoided the difficulty of general optimization by carefully designing the objective function and constraints to ensure that the optimization problem is convex. When training neural networks, we must confront the general non-convex case. Even convex optimization is not without its complications. In this section, we summarize several of the most prominent challenges involved in optimization for training deep models.

8.2.1 Ill-Conditioning

Some challenges arise even when optimizing convex functions. Of these, the most prominent is ill-conditioning of the Hessian matrix \mathbf{H} . This is a very general problem in most numerical optimization, convex or otherwise, and is described in more detail in section [4.3.1](#).

The ill-conditioning problem is generally believed to be present in neural network training problems. Ill-conditioning can manifest by causing SGD to get “stuck” in the sense that even very small steps increase the cost function.

Recall from equation [4.9](#) that a second-order Taylor series expansion of the cost function predicts that a gradient descent step of $-\epsilon\mathbf{g}$ will add

$$\frac{1}{2}\epsilon^2\mathbf{g}^\top \mathbf{H}\mathbf{g} - \epsilon\mathbf{g}^\top \mathbf{g} \tag{8.10}$$

to the cost. Ill-conditioning of the gradient becomes a problem when $\frac{1}{2}\epsilon^2\mathbf{g}^\top \mathbf{H}\mathbf{g}$ exceeds $\epsilon\mathbf{g}^\top \mathbf{g}$. To determine whether ill-conditioning is detrimental to a neural network training task, one can monitor the squared gradient norm $\mathbf{g}^\top \mathbf{g}$ and

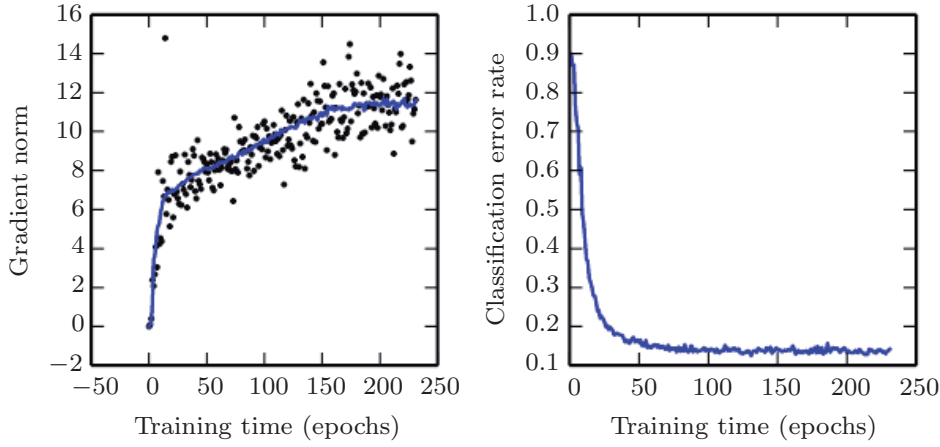


Figure 8.1: Gradient descent often does not arrive at a critical point of any kind. In this example, the gradient norm increases throughout training of a convolutional network used for object detection. (*Left*) A scatterplot showing how the norms of individual gradient evaluations are distributed over time. To improve legibility, only one gradient norm is plotted per epoch. The running average of all gradient norms is plotted as a solid curve. The gradient norm clearly increases over time, rather than decreasing as we would expect if the training process converged to a critical point. (*Right*) Despite the increasing gradient, the training process is reasonably successful. The validation set classification error decreases to a low level.

the $\mathbf{g}^\top \mathbf{H}\mathbf{g}$ term. In many cases, the gradient norm does not shrink significantly throughout learning, but the $\mathbf{g}^\top \mathbf{H}\mathbf{g}$ term grows by more than an order of magnitude. The result is that learning becomes very slow despite the presence of a strong gradient because the learning rate must be shrunk to compensate for even stronger curvature. Figure 8.1 shows an example of the gradient increasing significantly during the successful training of a neural network.

Though ill-conditioning is present in other settings besides neural network training, some of the techniques used to combat it in other contexts are less applicable to neural networks. For example, Newton's method is an excellent tool for minimizing convex functions with poorly conditioned Hessian matrices, but in the subsequent sections we will argue that Newton's method requires significant modification before it can be applied to neural networks.

8.2.2 Local Minima

One of the most prominent features of a convex optimization problem is that it can be reduced to the problem of finding a local minimum. Any local minimum is

guaranteed to be a global minimum. Some convex functions have a flat region at the bottom rather than a single global minimum point, but any point within such a flat region is an acceptable solution. When optimizing a convex function, we know that we have reached a good solution if we find a critical point of any kind.

With non-convex functions, such as neural nets, it is possible to have many local minima. Indeed, nearly any deep model is essentially guaranteed to have an extremely large number of local minima. However, as we will see, this is not necessarily a major problem.

Neural networks and any models with multiple equivalently parametrized latent variables all have multiple local minima because of the **model identifiability** problem. A model is said to be identifiable if a sufficiently large training set can rule out all but one setting of the model’s parameters. Models with latent variables are often not identifiable because we can obtain equivalent models by exchanging latent variables with each other. For example, we could take a neural network and modify layer 1 by swapping the incoming weight vector for unit i with the incoming weight vector for unit j , then doing the same for the outgoing weight vectors. If we have m layers with n units each, then there are $n!^m$ ways of arranging the hidden units. This kind of non-identifiability is known as **weight space symmetry**.

In addition to weight space symmetry, many kinds of neural networks have additional causes of non-identifiability. For example, in any rectified linear or maxout network, we can scale all of the incoming weights and biases of a unit by α if we also scale all of its outgoing weights by $\frac{1}{\alpha}$. This means that—if the cost function does not include terms such as weight decay that depend directly on the weights rather than the models’ outputs—every local minimum of a rectified linear or maxout network lies on an $(m \times n)$ -dimensional hyperbola of equivalent local minima.

These model identifiability issues mean that there can be an extremely large or even uncountably infinite amount of local minima in a neural network cost function. However, all of these local minima arising from non-identifiability are equivalent to each other in cost function value. As a result, these local minima are not a problematic form of non-convexity.

Local minima can be problematic if they have high cost in comparison to the global minimum. One can construct small neural networks, even without hidden units, that have local minima with higher cost than the global minimum (Sontag and Sussman, 1989; Brady *et al.*, 1989; Gori and Tesi, 1992). If local minima with high cost are common, this could pose a serious problem for gradient-based optimization algorithms.

It remains an open question whether there are many local minima of high cost

for networks of practical interest and whether optimization algorithms encounter them. For many years, most practitioners believed that local minima were a common problem plaguing neural network optimization. Today, that does not appear to be the case. The problem remains an active area of research, but experts now suspect that, for sufficiently large neural networks, most local minima have a low cost function value, and that it is not important to find a true global minimum rather than to find a point in parameter space that has low but not minimal cost ([Saxe *et al.*, 2013](#); [Dauphin *et al.*, 2014](#); [Goodfellow *et al.*, 2015](#); [Choromanska *et al.*, 2014](#)).

Many practitioners attribute nearly all difficulty with neural network optimization to local minima. We encourage practitioners to carefully test for specific problems. A test that can rule out local minima as the problem is to plot the norm of the gradient over time. If the norm of the gradient does not shrink to insignificant size, the problem is neither local minima nor any other kind of critical point. This kind of negative test can rule out local minima. In high dimensional spaces, it can be very difficult to positively establish that local minima are the problem. Many structures other than local minima also have small gradients.

8.2.3 Plateaus, Saddle Points and Other Flat Regions

For many high-dimensional non-convex functions, local minima (and maxima) are in fact rare compared to another kind of point with zero gradient: a saddle point. Some points around a saddle point have greater cost than the saddle point, while others have a lower cost. At a saddle point, the Hessian matrix has both positive and negative eigenvalues. Points lying along eigenvectors associated with positive eigenvalues have greater cost than the saddle point, while points lying along negative eigenvalues have lower value. We can think of a saddle point as being a local minimum along one cross-section of the cost function and a local maximum along another cross-section. See figure 4.5 for an illustration.

Many classes of random functions exhibit the following behavior: in low-dimensional spaces, local minima are common. In higher dimensional spaces, local minima are rare and saddle points are more common. For a function $f : \mathbb{R}^n \rightarrow \mathbb{R}$ of this type, the expected ratio of the number of saddle points to local minima grows exponentially with n . To understand the intuition behind this behavior, observe that the Hessian matrix at a local minimum has only positive eigenvalues. The Hessian matrix at a saddle point has a mixture of positive and negative eigenvalues. Imagine that the sign of each eigenvalue is generated by flipping a coin. In a single dimension, it is easy to obtain a local minimum by tossing a coin and getting heads once. In n -dimensional space, it is exponentially unlikely that all n coin tosses will

be heads. See [Dauphin et al. \(2014\)](#) for a review of the relevant theoretical work.

An amazing property of many random functions is that the eigenvalues of the Hessian become more likely to be positive as we reach regions of lower cost. In our coin tossing analogy, this means we are more likely to have our coin come up heads n times if we are at a critical point with low cost. This means that local minima are much more likely to have low cost than high cost. Critical points with high cost are far more likely to be saddle points. Critical points with extremely high cost are more likely to be local maxima.

This happens for many classes of random functions. Does it happen for neural networks? [Baldi and Hornik \(1989\)](#) showed theoretically that shallow autoencoders (feedforward networks trained to copy their input to their output, described in chapter 14) with no nonlinearities have global minima and saddle points but no local minima with higher cost than the global minimum. They observed without proof that these results extend to deeper networks without nonlinearities. The output of such networks is a linear function of their input, but they are useful to study as a model of nonlinear neural networks because their loss function is a non-convex function of their parameters. Such networks are essentially just multiple matrices composed together. [Saxe et al. \(2013\)](#) provided exact solutions to the complete learning dynamics in such networks and showed that learning in these models captures many of the qualitative features observed in the training of deep models with nonlinear activation functions. [Dauphin et al. \(2014\)](#) showed experimentally that real neural networks also have loss functions that contain very many high-cost saddle points. [Choromanska et al. \(2014\)](#) provided additional theoretical arguments, showing that another class of high-dimensional random functions related to neural networks does so as well.

What are the implications of the proliferation of saddle points for training algorithms? For first-order optimization algorithms that use only gradient information, the situation is unclear. The gradient can often become very small near a saddle point. On the other hand, gradient descent empirically seems to be able to escape saddle points in many cases. [Goodfellow et al. \(2015\)](#) provided visualizations of several learning trajectories of state-of-the-art neural networks, with an example given in figure 8.2. These visualizations show a flattening of the cost function near a prominent saddle point where the weights are all zero, but they also show the gradient descent trajectory rapidly escaping this region. [Goodfellow et al. \(2015\)](#) also argue that continuous-time gradient descent may be shown analytically to be repelled from, rather than attracted to, a nearby saddle point, but the situation may be different for more realistic uses of gradient descent.

For Newton's method, it is clear that saddle points constitute a problem.

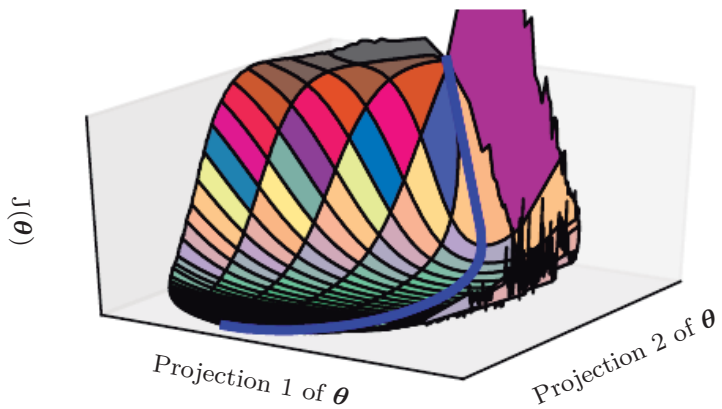


Figure 8.2: A visualization of the cost function of a neural network. Image adapted with permission from [Goodfellow et al. \(2015\)](#). These visualizations appear similar for feedforward neural networks, convolutional networks, and recurrent networks applied to real object recognition and natural language processing tasks. Surprisingly, these visualizations usually do not show many conspicuous obstacles. Prior to the success of stochastic gradient descent for training very large models beginning in roughly 2012, neural net cost function surfaces were generally believed to have much more non-convex structure than is revealed by these projections. The primary obstacle revealed by this projection is a saddle point of high cost near where the parameters are initialized, but, as indicated by the blue path, the SGD training trajectory escapes this saddle point readily. Most of training time is spent traversing the relatively flat valley of the cost function, which may be due to high noise in the gradient, poor conditioning of the Hessian matrix in this region, or simply the need to circumnavigate the tall “mountain” visible in the figure via an indirect arcing path.

Gradient descent is designed to move “downhill” and is not explicitly designed to seek a critical point. Newton’s method, however, is designed to solve for a point where the gradient is zero. Without appropriate modification, it can jump to a saddle point. The proliferation of saddle points in high dimensional spaces presumably explains why second-order methods have not succeeded in replacing gradient descent for neural network training. [Dauphin *et al.* \(2014\)](#) introduced a **saddle-free Newton method** for second-order optimization and showed that it improves significantly over the traditional version. Second-order methods remain difficult to scale to large neural networks, but this saddle-free approach holds promise if it could be scaled.

There are other kinds of points with zero gradient besides minima and saddle points. There are also maxima, which are much like saddle points from the perspective of optimization—many algorithms are not attracted to them, but unmodified Newton’s method is. Maxima of many classes of random functions become exponentially rare in high dimensional space, just like minima do.

There may also be wide, flat regions of constant value. In these locations, the gradient and also the Hessian are all zero. Such degenerate locations pose major problems for all numerical optimization algorithms. In a convex problem, a wide, flat region must consist entirely of global minima, but in a general optimization problem, such a region could correspond to a high value of the objective function.

8.2.4 Cliffs and Exploding Gradients

Neural networks with many layers often have extremely steep regions resembling cliffs, as illustrated in figure 8.3. These result from the multiplication of several large weights together. On the face of an extremely steep cliff structure, the gradient update step can move the parameters extremely far, usually jumping off of the cliff structure altogether.

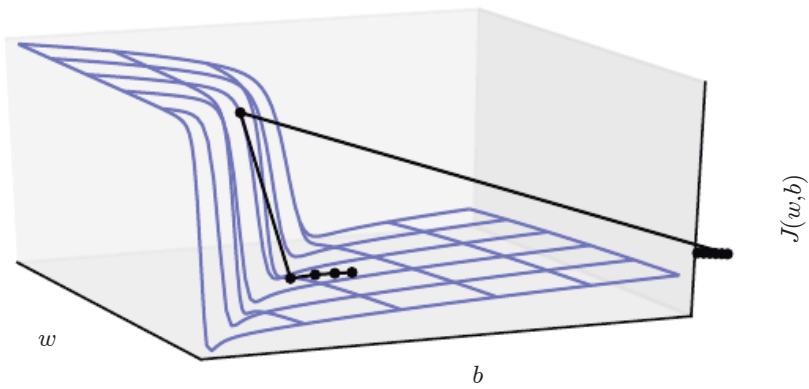


Figure 8.3: The objective function for highly nonlinear deep neural networks or for recurrent neural networks often contains sharp nonlinearities in parameter space resulting from the multiplication of several parameters. These nonlinearities give rise to very high derivatives in some places. When the parameters get close to such a cliff region, a gradient descent update can catapult the parameters very far, possibly losing most of the optimization work that had been done. Figure adapted with permission from [Pascanu et al. \(2013\)](#).

The cliff can be dangerous whether we approach it from above or from below, but fortunately its most serious consequences can be avoided using the **gradient clipping** heuristic described in section 10.11.1. The basic idea is to recall that the gradient does not specify the optimal step size, but only the optimal direction within an infinitesimal region. When the traditional gradient descent algorithm proposes to make a very large step, the gradient clipping heuristic intervenes to reduce the step size to be small enough that it is less likely to go outside the region where the gradient indicates the direction of approximately steepest descent. Cliff structures are most common in the cost functions for recurrent neural networks, because such models involve a multiplication of many factors, with one factor for each time step. Long temporal sequences thus incur an extreme amount of multiplication.

8.2.5 Long-Term Dependencies

Another difficulty that neural network optimization algorithms must overcome arises when the computational graph becomes extremely deep. Feedforward networks with many layers have such deep computational graphs. So do recurrent networks, described in chapter 10, which construct very deep computational graphs

by repeatedly applying the same operation at each time step of a long temporal sequence. Repeated application of the same parameters gives rise to especially pronounced difficulties.

For example, suppose that a computational graph contains a path that consists of repeatedly multiplying by a matrix \mathbf{W} . After t steps, this is equivalent to multiplying by \mathbf{W}^t . Suppose that \mathbf{W} has an eigendecomposition $\mathbf{W} = \mathbf{V}\text{diag}(\boldsymbol{\lambda})\mathbf{V}^{-1}$. In this simple case, it is straightforward to see that

$$\mathbf{W}^t = (\mathbf{V}\text{diag}(\boldsymbol{\lambda})\mathbf{V}^{-1})^t = \mathbf{V}\text{diag}(\boldsymbol{\lambda})^t\mathbf{V}^{-1}. \quad (8.11)$$

Any eigenvalues λ_i that are not near an absolute value of 1 will either explode if they are greater than 1 in magnitude or vanish if they are less than 1 in magnitude. The **vanishing and exploding gradient problem** refers to the fact that gradients through such a graph are also scaled according to $\text{diag}(\boldsymbol{\lambda})^t$. Vanishing gradients make it difficult to know which direction the parameters should move to improve the cost function, while exploding gradients can make learning unstable. The cliff structures described earlier that motivate gradient clipping are an example of the exploding gradient phenomenon.

The repeated multiplication by \mathbf{W} at each time step described here is very similar to the **power method** algorithm used to find the largest eigenvalue of a matrix \mathbf{W} and the corresponding eigenvector. From this point of view it is not surprising that $\mathbf{x}^\top \mathbf{W}^t$ will eventually discard all components of \mathbf{x} that are orthogonal to the principal eigenvector of \mathbf{W} .

Recurrent networks use the same matrix \mathbf{W} at each time step, but feedforward networks do not, so even very deep feedforward networks can largely avoid the vanishing and exploding gradient problem ([Sussillo, 2014](#)).

We defer a further discussion of the challenges of training recurrent networks until section [10.7](#), after recurrent networks have been described in more detail.

8.2.6 Inexact Gradients

Most optimization algorithms are designed with the assumption that we have access to the exact gradient or Hessian matrix. In practice, we usually only have a noisy or even biased estimate of these quantities. Nearly every deep learning algorithm relies on sampling-based estimates at least insofar as using a minibatch of training examples to compute the gradient.

In other cases, the objective function we want to minimize is actually intractable. When the objective function is intractable, typically its gradient is intractable as well. In such cases we can only approximate the gradient. These issues mostly arise

with the more advanced models in part III. For example, contrastive divergence gives a technique for approximating the gradient of the intractable log-likelihood of a Boltzmann machine.

Various neural network optimization algorithms are designed to account for imperfections in the gradient estimate. One can also avoid the problem by choosing a surrogate loss function that is easier to approximate than the true loss.

8.2.7 Poor Correspondence between Local and Global Structure

Many of the problems we have discussed so far correspond to properties of the loss function at a single point—it can be difficult to make a single step if $J(\boldsymbol{\theta})$ is poorly conditioned at the current point $\boldsymbol{\theta}$, or if $\boldsymbol{\theta}$ lies on a cliff, or if $\boldsymbol{\theta}$ is a saddle point hiding the opportunity to make progress downhill from the gradient.

It is possible to overcome all of these problems at a single point and still perform poorly if the direction that results in the most improvement locally does not point toward distant regions of much lower cost.

Goodfellow *et al.* (2015) argue that much of the runtime of training is due to the length of the trajectory needed to arrive at the solution. Figure 8.2 shows that the learning trajectory spends most of its time tracing out a wide arc around a mountain-shaped structure.

Much of research into the difficulties of optimization has focused on whether training arrives at a global minimum, a local minimum, or a saddle point, but in practice neural networks do not arrive at a critical point of any kind. Figure 8.1 shows that neural networks often do not arrive at a region of small gradient. Indeed, such critical points do not even necessarily exist. For example, the loss function $-\log p(y | \mathbf{x}; \boldsymbol{\theta})$ can lack a global minimum point and instead asymptotically approach some value as the model becomes more confident. For a classifier with discrete y and $p(y | \mathbf{x})$ provided by a softmax, the negative log-likelihood can become arbitrarily close to zero if the model is able to correctly classify every example in the training set, but it is impossible to actually reach the value of zero. Likewise, a model of real values $p(y | \mathbf{x}) = \mathcal{N}(y; f(\boldsymbol{\theta}), \beta^{-1})$ can have negative log-likelihood that asymptotes to negative infinity—if $f(\boldsymbol{\theta})$ is able to correctly predict the value of all training set y targets, the learning algorithm will increase β without bound. See figure 8.4 for an example of a failure of local optimization to find a good cost function value even in the absence of any local minima or saddle points.

Future research will need to develop further understanding of the factors that influence the length of the learning trajectory and better characterize the outcome

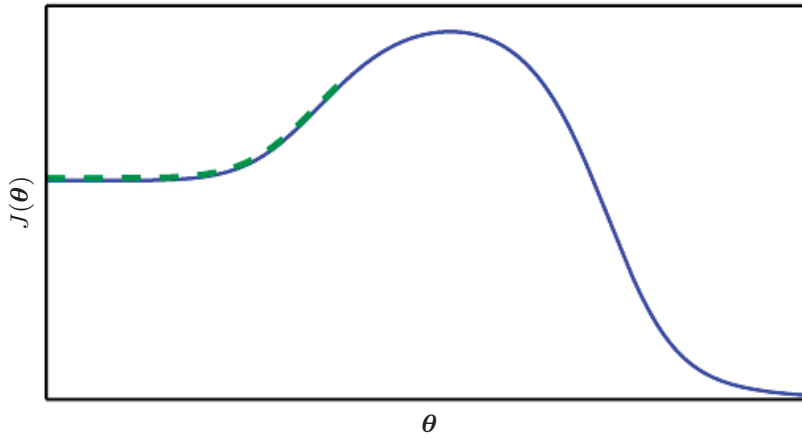


Figure 8.4: Optimization based on local downhill moves can fail if the local surface does not point toward the global solution. Here we provide an example of how this can occur, even if there are no saddle points and no local minima. This example cost function contains only asymptotes toward low values, not minima. The main cause of difficulty in this case is being initialized on the wrong side of the “mountain” and not being able to traverse it. In higher dimensional space, learning algorithms can often circumnavigate such mountains but the trajectory associated with doing so may be long and result in excessive training time, as illustrated in figure 8.2.

of the process.

Many existing research directions are aimed at finding good initial points for problems that have difficult global structure, rather than developing algorithms that use non-local moves.

Gradient descent and essentially all learning algorithms that are effective for training neural networks are based on making small, local moves. The previous sections have primarily focused on how the correct direction of these local moves can be difficult to compute. We may be able to compute some properties of the objective function, such as its gradient, only approximately, with bias or variance in our estimate of the correct direction. In these cases, local descent may or may not define a reasonably short path to a valid solution, but we are not actually able to follow the local descent path. The objective function may have issues such as poor conditioning or discontinuous gradients, causing the region where the gradient provides a good model of the objective function to be very small. In these cases, local descent with steps of size ϵ may define a reasonably short path to the solution, but we are only able to compute the local descent direction with steps of size $\delta \ll \epsilon$. In these cases, local descent may or may not define a path to the solution, but the path contains many steps, so following the path incurs a

high computational cost. Sometimes local information provides us no guide, when the function has a wide flat region, or if we manage to land exactly on a critical point (usually this latter scenario only happens to methods that solve explicitly for critical points, such as Newton’s method). In these cases, local descent does not define a path to a solution at all. In other cases, local moves can be too greedy and lead us along a path that moves downhill but away from any solution, as in figure 8.4, or along an unnecessarily long trajectory to the solution, as in figure 8.2. Currently, we do not understand which of these problems are most relevant to making neural network optimization difficult, and this is an active area of research.

Regardless of which of these problems are most significant, all of them might be avoided if there exists a region of space connected reasonably directly to a solution by a path that local descent can follow, and if we are able to initialize learning within that well-behaved region. This last view suggests research into choosing good initial points for traditional optimization algorithms to use.

8.2.8 Theoretical Limits of Optimization

Several theoretical results show that there are limits on the performance of any optimization algorithm we might design for neural networks (Blum and Rivest, 1992; Judd, 1989; Wolpert and MacReady, 1997). Typically these results have little bearing on the use of neural networks in practice.

Some theoretical results apply only to the case where the units of a neural network output discrete values. However, most neural network units output smoothly increasing values that make optimization via local search feasible. Some theoretical results show that there exist problem classes that are intractable, but it can be difficult to tell whether a particular problem falls into that class. Other results show that finding a solution for a network of a given size is intractable, but in practice we can find a solution easily by using a larger network for which many more parameter settings correspond to an acceptable solution. Moreover, in the context of neural network training, we usually do not care about finding the exact minimum of a function, but seek only to reduce its value sufficiently to obtain good generalization error. Theoretical analysis of whether an optimization algorithm can accomplish this goal is extremely difficult. Developing more realistic bounds on the performance of optimization algorithms therefore remains an important goal for machine learning research.

8.3 Basic Algorithms

We have previously introduced the gradient descent (section 4.3) algorithm that follows the gradient of an entire training set downhill. This may be accelerated considerably by using stochastic gradient descent to follow the gradient of randomly selected minibatches downhill, as discussed in section 5.9 and section 8.1.3.

8.3.1 Stochastic Gradient Descent

Stochastic gradient descent (SGD) and its variants are probably the most used optimization algorithms for machine learning in general and for deep learning in particular. As discussed in section 8.1.3, it is possible to obtain an unbiased estimate of the gradient by taking the average gradient on a minibatch of m examples drawn i.i.d from the data generating distribution.

Algorithm 8.1 shows how to follow this estimate of the gradient downhill.

Algorithm 8.1 Stochastic gradient descent (SGD) update at training iteration k

Require: Learning rate ϵ_k .

Require: Initial parameter θ

while stopping criterion not met **do**

 Sample a minibatch of m examples from the training set $\{\mathbf{x}^{(1)}, \dots, \mathbf{x}^{(m)}\}$ with corresponding targets $\mathbf{y}^{(i)}$.

 Compute gradient estimate: $\hat{\mathbf{g}} \leftarrow +\frac{1}{m} \nabla_{\theta} \sum_i L(f(\mathbf{x}^{(i)}; \theta), \mathbf{y}^{(i)})$

 Apply update: $\theta \leftarrow \theta - \epsilon \hat{\mathbf{g}}$

end while

A crucial parameter for the SGD algorithm is the learning rate. Previously, we have described SGD as using a fixed learning rate ϵ . In practice, it is necessary to gradually decrease the learning rate over time, so we now denote the learning rate at iteration k as ϵ_k .

This is because the SGD gradient estimator introduces a source of noise (the random sampling of m training examples) that does not vanish even when we arrive at a minimum. By comparison, the true gradient of the total cost function becomes small and then $\mathbf{0}$ when we approach and reach a minimum using batch gradient descent, so batch gradient descent can use a fixed learning rate. A sufficient condition to guarantee convergence of SGD is that

$$\sum_{k=1}^{\infty} \epsilon_k = \infty, \quad \text{and} \tag{8.12}$$

$$\sum_{k=1}^{\infty} \epsilon_k^2 < \infty. \quad (8.13)$$

In practice, it is common to decay the learning rate linearly until iteration τ :

$$\epsilon_k = (1 - \alpha)\epsilon_0 + \alpha\epsilon_\tau \quad (8.14)$$

with $\alpha = \frac{k}{\tau}$. After iteration τ , it is common to leave ϵ constant.

The learning rate may be chosen by trial and error, but it is usually best to choose it by monitoring learning curves that plot the objective function as a function of time. This is more of an art than a science, and most guidance on this subject should be regarded with some skepticism. When using the linear schedule, the parameters to choose are ϵ_0 , ϵ_τ , and τ . Usually τ may be set to the number of iterations required to make a few hundred passes through the training set. Usually ϵ_τ should be set to roughly 1% the value of ϵ_0 . The main question is how to set ϵ_0 . If it is too large, the learning curve will show violent oscillations, with the cost function often increasing significantly. Gentle oscillations are fine, especially if training with a stochastic cost function such as the cost function arising from the use of dropout. If the learning rate is too low, learning proceeds slowly, and if the initial learning rate is too low, learning may become stuck with a high cost value. Typically, the optimal initial learning rate, in terms of total training time and the final cost value, is higher than the learning rate that yields the best performance after the first 100 iterations or so. Therefore, it is usually best to monitor the first several iterations and use a learning rate that is higher than the best-performing learning rate at this time, but not so high that it causes severe instability.

The most important property of SGD and related minibatch or online gradient-based optimization is that computation time per update does not grow with the number of training examples. This allows convergence even when the number of training examples becomes very large. For a large enough dataset, SGD may converge to within some fixed tolerance of its final test set error before it has processed the entire training set.

To study the convergence rate of an optimization algorithm it is common to measure the **excess error** $J(\boldsymbol{\theta}) - \min_{\boldsymbol{\theta}} J(\boldsymbol{\theta})$, which is the amount that the current cost function exceeds the minimum possible cost. When SGD is applied to a convex problem, the excess error is $O(\frac{1}{\sqrt{k}})$ after k iterations, while in the strongly convex case it is $O(\frac{1}{k})$. These bounds cannot be improved unless extra conditions are assumed. Batch gradient descent enjoys better convergence rates than stochastic gradient descent in theory. However, the Cramér-Rao bound (Cramér, 1946; Rao, 1945) states that generalization error cannot decrease faster than $O(\frac{1}{k})$. Bottou

and Bousquet (2008) argue that it therefore may not be worthwhile to pursue an optimization algorithm that converges faster than $O(\frac{1}{k})$ for machine learning tasks—faster convergence presumably corresponds to overfitting. Moreover, the asymptotic analysis obscures many advantages that stochastic gradient descent has after a small number of steps. With large datasets, the ability of SGD to make rapid initial progress while evaluating the gradient for only very few examples outweighs its slow asymptotic convergence. Most of the algorithms described in the remainder of this chapter achieve benefits that matter in practice but are lost in the constant factors obscured by the $O(\frac{1}{k})$ asymptotic analysis. One can also trade off the benefits of both batch and stochastic gradient descent by gradually increasing the minibatch size during the course of learning.

For more information on SGD, see Bottou (1998).

8.3.2 Momentum

While stochastic gradient descent remains a very popular optimization strategy, learning with it can sometimes be slow. The method of momentum (Polyak, 1964) is designed to accelerate learning, especially in the face of high curvature, small but consistent gradients, or noisy gradients. The momentum algorithm accumulates an exponentially decaying moving average of past gradients and continues to move in their direction. The effect of momentum is illustrated in figure 8.5.

Formally, the momentum algorithm introduces a variable \mathbf{v} that plays the role of velocity—it is the direction and speed at which the parameters move through parameter space. The velocity is set to an exponentially decaying average of the negative gradient. The name **momentum** derives from a physical analogy, in which the negative gradient is a force moving a particle through parameter space, according to Newton’s laws of motion. Momentum in physics is mass times velocity. In the momentum learning algorithm, we assume unit mass, so the velocity vector \mathbf{v} may also be regarded as the momentum of the particle. A hyperparameter $\alpha \in [0, 1)$ determines how quickly the contributions of previous gradients exponentially decay. The update rule is given by:

$$\mathbf{v} \leftarrow \alpha \mathbf{v} - \epsilon \nabla_{\boldsymbol{\theta}} \left(\frac{1}{m} \sum_{i=1}^m L(\mathbf{f}(\mathbf{x}^{(i)}; \boldsymbol{\theta}), \mathbf{y}^{(i)}) \right), \quad (8.15)$$

$$\boldsymbol{\theta} \leftarrow \boldsymbol{\theta} + \mathbf{v}. \quad (8.16)$$

The velocity \mathbf{v} accumulates the gradient elements $\nabla_{\boldsymbol{\theta}} \left(\frac{1}{m} \sum_{i=1}^m L(\mathbf{f}(\mathbf{x}^{(i)}; \boldsymbol{\theta}), \mathbf{y}^{(i)}) \right)$. The larger α is relative to ϵ , the more previous gradients affect the current direction. The SGD algorithm with momentum is given in algorithm 8.2.

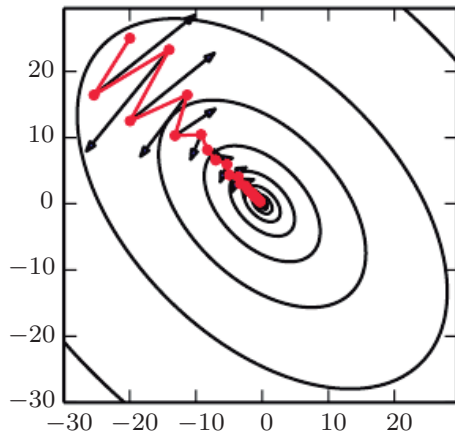


Figure 8.5: Momentum aims primarily to solve two problems: poor conditioning of the Hessian matrix and variance in the stochastic gradient. Here, we illustrate how momentum overcomes the first of these two problems. The contour lines depict a quadratic loss function with a poorly conditioned Hessian matrix. The red path cutting across the contours indicates the path followed by the momentum learning rule as it minimizes this function. At each step along the way, we draw an arrow indicating the step that gradient descent would take at that point. We can see that a poorly conditioned quadratic objective looks like a long, narrow valley or canyon with steep sides. Momentum correctly traverses the canyon lengthwise, while gradient steps waste time moving back and forth across the narrow axis of the canyon. Compare also figure 4.6, which shows the behavior of gradient descent without momentum.

Previously, the size of the step was simply the norm of the gradient multiplied by the learning rate. Now, the size of the step depends on how large and how aligned a *sequence* of gradients are. The step size is largest when many successive gradients point in exactly the same direction. If the momentum algorithm always observes gradient \mathbf{g} , then it will accelerate in the direction of $-\mathbf{g}$, until reaching a terminal velocity where the size of each step is

$$\frac{\epsilon \|\mathbf{g}\|}{1 - \alpha}. \quad (8.17)$$

It is thus helpful to think of the momentum hyperparameter in terms of $\frac{1}{1-\alpha}$. For example, $\alpha = .9$ corresponds to multiplying the maximum speed by 10 relative to the gradient descent algorithm.

Common values of α used in practice include .5, .9, and .99. Like the learning rate, α may also be adapted over time. Typically it begins with a small value and is later raised. It is less important to adapt α over time than to shrink ϵ over time.

Algorithm 8.2 Stochastic gradient descent (SGD) with momentum

Require: Learning rate ϵ , momentum parameter α .

Require: Initial parameter $\boldsymbol{\theta}$, initial velocity \mathbf{v} .

while stopping criterion not met **do**

 Sample a minibatch of m examples from the training set $\{\mathbf{x}^{(1)}, \dots, \mathbf{x}^{(m)}\}$ with corresponding targets $\mathbf{y}^{(i)}$.

 Compute gradient estimate: $\mathbf{g} \leftarrow \frac{1}{m} \nabla_{\boldsymbol{\theta}} \sum_i L(f(\mathbf{x}^{(i)}; \boldsymbol{\theta}), \mathbf{y}^{(i)})$

 Compute velocity update: $\mathbf{v} \leftarrow \alpha \mathbf{v} - \epsilon \mathbf{g}$

 Apply update: $\boldsymbol{\theta} \leftarrow \boldsymbol{\theta} + \mathbf{v}$

end while

We can view the momentum algorithm as simulating a particle subject to continuous-time Newtonian dynamics. The physical analogy can help to build intuition for how the momentum and gradient descent algorithms behave.

The position of the particle at any point in time is given by $\boldsymbol{\theta}(t)$. The particle experiences net force $\mathbf{f}(t)$. This force causes the particle to accelerate:

$$\mathbf{f}(t) = \frac{\partial^2}{\partial t^2} \boldsymbol{\theta}(t). \quad (8.18)$$

Rather than viewing this as a second-order differential equation of the position, we can introduce the variable $\mathbf{v}(t)$ representing the velocity of the particle at time t and rewrite the Newtonian dynamics as a first-order differential equation:

$$\mathbf{v}(t) = \frac{\partial}{\partial t} \boldsymbol{\theta}(t), \quad (8.19)$$

$$\mathbf{f}(t) = \frac{\partial}{\partial t} \mathbf{v}(t). \quad (8.20)$$

The momentum algorithm then consists of solving the differential equations via numerical simulation. A simple numerical method for solving differential equations is Euler's method, which simply consists of simulating the dynamics defined by the equation by taking small, finite steps in the direction of each gradient.

This explains the basic form of the momentum update, but what specifically are the forces? One force is proportional to the negative gradient of the cost function: $-\nabla_{\theta} J(\theta)$. This force pushes the particle downhill along the cost function surface. The gradient descent algorithm would simply take a single step based on each gradient, but the Newtonian scenario used by the momentum algorithm instead uses this force to alter the velocity of the particle. We can think of the particle as being like a hockey puck sliding down an icy surface. Whenever it descends a steep part of the surface, it gathers speed and continues sliding in that direction until it begins to go uphill again.

One other force is necessary. If the only force is the gradient of the cost function, then the particle might never come to rest. Imagine a hockey puck sliding down one side of a valley and straight up the other side, oscillating back and forth forever, assuming the ice is perfectly frictionless. To resolve this problem, we add one other force, proportional to $-\mathbf{v}(t)$. In physics terminology, this force corresponds to viscous drag, as if the particle must push through a resistant medium such as syrup. This causes the particle to gradually lose energy over time and eventually converge to a local minimum.

Why do we use $-\mathbf{v}(t)$ and viscous drag in particular? Part of the reason to use $-\mathbf{v}(t)$ is mathematical convenience—an integer power of the velocity is easy to work with. However, other physical systems have other kinds of drag based on other integer powers of the velocity. For example, a particle traveling through the air experiences turbulent drag, with force proportional to the square of the velocity, while a particle moving along the ground experiences dry friction, with a force of constant magnitude. We can reject each of these options. Turbulent drag, proportional to the square of the velocity, becomes very weak when the velocity is small. It is not powerful enough to force the particle to come to rest. A particle with a non-zero initial velocity that experiences only the force of turbulent drag will move away from its initial position forever, with the distance from the starting point growing like $O(\log t)$. We must therefore use a lower power of the velocity. If we use a power of zero, representing dry friction, then the force is too strong. When the force due to the gradient of the cost function is small but non-zero, the constant force due to friction can cause the particle to come to rest before reaching a local minimum. Viscous drag avoids both of these problems—it is weak enough

that the gradient can continue to cause motion until a minimum is reached, but strong enough to prevent motion if the gradient does not justify moving.

8.3.3 Nesterov Momentum

Sutskever *et al.* (2013) introduced a variant of the momentum algorithm that was inspired by Nesterov's accelerated gradient method (Nesterov, 1983, 2004). The update rules in this case are given by:

$$\mathbf{v} \leftarrow \alpha \mathbf{v} - \epsilon \nabla_{\boldsymbol{\theta}} \left[\frac{1}{m} \sum_{i=1}^m L(\mathbf{f}(\mathbf{x}^{(i)}; \boldsymbol{\theta} + \alpha \mathbf{v}), \mathbf{y}^{(i)}) \right], \quad (8.21)$$

$$\boldsymbol{\theta} \leftarrow \boldsymbol{\theta} + \mathbf{v}, \quad (8.22)$$

where the parameters α and ϵ play a similar role as in the standard momentum method. The difference between Nesterov momentum and standard momentum is where the gradient is evaluated. With Nesterov momentum the gradient is evaluated after the current velocity is applied. Thus one can interpret Nesterov momentum as attempting to add a *correction factor* to the standard method of momentum. The complete Nesterov momentum algorithm is presented in algorithm 8.3.

In the convex batch gradient case, Nesterov momentum brings the rate of convergence of the excess error from $O(1/k)$ (after k steps) to $O(1/k^2)$ as shown by Nesterov (1983). Unfortunately, in the stochastic gradient case, Nesterov momentum does not improve the rate of convergence.

Algorithm 8.3 Stochastic gradient descent (SGD) with Nesterov momentum

Require: Learning rate ϵ , momentum parameter α .

Require: Initial parameter $\boldsymbol{\theta}$, initial velocity \mathbf{v} .

while stopping criterion not met **do**

 Sample a minibatch of m examples from the training set $\{\mathbf{x}^{(1)}, \dots, \mathbf{x}^{(m)}\}$ with corresponding labels $\mathbf{y}^{(i)}$.

 Apply interim update: $\tilde{\boldsymbol{\theta}} \leftarrow \boldsymbol{\theta} + \alpha \mathbf{v}$

 Compute gradient (at interim point): $\mathbf{g} \leftarrow \frac{1}{m} \nabla_{\tilde{\boldsymbol{\theta}}} \sum_i L(\mathbf{f}(\mathbf{x}^{(i)}; \tilde{\boldsymbol{\theta}}), \mathbf{y}^{(i)})$

 Compute velocity update: $\mathbf{v} \leftarrow \alpha \mathbf{v} - \epsilon \mathbf{g}$

 Apply update: $\boldsymbol{\theta} \leftarrow \boldsymbol{\theta} + \mathbf{v}$

end while

8.4 Parameter Initialization Strategies

Some optimization algorithms are not iterative by nature and simply solve for a solution point. Other optimization algorithms are iterative by nature but, when applied to the right class of optimization problems, converge to acceptable solutions in an acceptable amount of time regardless of initialization. Deep learning training algorithms usually do not have either of these luxuries. Training algorithms for deep learning models are usually iterative in nature and thus require the user to specify some initial point from which to begin the iterations. Moreover, training deep models is a sufficiently difficult task that most algorithms are strongly affected by the choice of initialization. The initial point can determine whether the algorithm converges at all, with some initial points being so unstable that the algorithm encounters numerical difficulties and fails altogether. When learning does converge, the initial point can determine how quickly learning converges and whether it converges to a point with high or low cost. Also, points of comparable cost can have wildly varying generalization error, and the initial point can affect the generalization as well.

Modern initialization strategies are simple and heuristic. Designing improved initialization strategies is a difficult task because neural network optimization is not yet well understood. Most initialization strategies are based on achieving some nice properties when the network is initialized. However, we do not have a good understanding of which of these properties are preserved under which circumstances after learning begins to proceed. A further difficulty is that some initial points may be beneficial from the viewpoint of optimization but detrimental from the viewpoint of generalization. Our understanding of how the initial point affects generalization is especially primitive, offering little to no guidance for how to select the initial point.

Perhaps the only property known with complete certainty is that the initial parameters need to “break symmetry” between different units. If two hidden units with the same activation function are connected to the same inputs, then these units must have different initial parameters. If they have the same initial parameters, then a deterministic learning algorithm applied to a deterministic cost and model will constantly update both of these units in the same way. Even if the model or training algorithm is capable of using stochasticity to compute different updates for different units (for example, if one trains with dropout), it is usually best to initialize each unit to compute a different function from all of the other units. This may help to make sure that no input patterns are lost in the null space of forward propagation and no gradient patterns are lost in the null space of back-propagation. The goal of having each unit compute a different function

motivates random initialization of the parameters. We could explicitly search for a large set of basis functions that are all mutually different from each other, but this often incurs a noticeable computational cost. For example, if we have at most as many outputs as inputs, we could use Gram-Schmidt orthogonalization on an initial weight matrix, and be guaranteed that each unit computes a very different function from each other unit. Random initialization from a high-entropy distribution over a high-dimensional space is computationally cheaper and unlikely to assign any units to compute the same function as each other.

Typically, we set the biases for each unit to heuristically chosen constants, and initialize only the weights randomly. Extra parameters, for example, parameters encoding the conditional variance of a prediction, are usually set to heuristically chosen constants much like the biases are.

We almost always initialize all the weights in the model to values drawn randomly from a Gaussian or uniform distribution. The choice of Gaussian or uniform distribution does not seem to matter very much, but has not been exhaustively studied. The scale of the initial distribution, however, does have a large effect on both the outcome of the optimization procedure and on the ability of the network to generalize.

Larger initial weights will yield a stronger symmetry breaking effect, helping to avoid redundant units. They also help to avoid losing signal during forward or back-propagation through the linear component of each layer—larger values in the matrix result in larger outputs of matrix multiplication. Initial weights that are too large may, however, result in exploding values during forward propagation or back-propagation. In recurrent networks, large weights can also result in **chaos** (such extreme sensitivity to small perturbations of the input that the behavior of the deterministic forward propagation procedure appears random). To some extent, the exploding gradient problem can be mitigated by gradient clipping (thresholding the values of the gradients before performing a gradient descent step). Large weights may also result in extreme values that cause the activation function to saturate, causing complete loss of gradient through saturated units. These competing factors determine the ideal initial scale of the weights.

The perspectives of regularization and optimization can give very different insights into how we should initialize a network. The optimization perspective suggests that the weights should be large enough to propagate information successfully, but some regularization concerns encourage making them smaller. The use of an optimization algorithm such as stochastic gradient descent that makes small incremental changes to the weights and tends to halt in areas that are nearer to the initial parameters (whether due to getting stuck in a region of low gradient, or

due to triggering some early stopping criterion based on overfitting) expresses a prior that the final parameters should be close to the initial parameters. Recall from section 7.8 that gradient descent with early stopping is equivalent to weight decay for some models. In the general case, gradient descent with early stopping is not the same as weight decay, but does provide a loose analogy for thinking about the effect of initialization. We can think of initializing the parameters θ to θ_0 as being similar to imposing a Gaussian prior $p(\theta)$ with mean θ_0 . From this point of view, it makes sense to choose θ_0 to be near 0. This prior says that it is more likely that units do not interact with each other than that they do interact. Units interact only if the likelihood term of the objective function expresses a strong preference for them to interact. On the other hand, if we initialize θ_0 to large values, then our prior specifies which units should interact with each other, and how they should interact.

Some heuristics are available for choosing the initial scale of the weights. One heuristic is to initialize the weights of a fully connected layer with m inputs and n outputs by sampling each weight from $U(-\frac{1}{\sqrt{m}}, \frac{1}{\sqrt{m}})$, while [Glorot and Bengio \(2010\)](#) suggest using the **normalized initialization**

$$W_{i,j} \sim U\left(-\sqrt{\frac{6}{m+n}}, \sqrt{\frac{6}{m+n}}\right). \quad (8.23)$$

This latter heuristic is designed to compromise between the goal of initializing all layers to have the same activation variance and the goal of initializing all layers to have the same gradient variance. The formula is derived using the assumption that the network consists only of a chain of matrix multiplications, with no nonlinearities. Real neural networks obviously violate this assumption, but many strategies designed for the linear model perform reasonably well on its nonlinear counterparts.

[Saxe et al. \(2013\)](#) recommend initializing to random orthogonal matrices, with a carefully chosen scaling or **gain** factor g that accounts for the nonlinearity applied at each layer. They derive specific values of the scaling factor for different types of nonlinear activation functions. This initialization scheme is also motivated by a model of a deep network as a sequence of matrix multiplies without nonlinearities. Under such a model, this initialization scheme guarantees that the total number of training iterations required to reach convergence is independent of depth.

Increasing the scaling factor g pushes the network toward the regime where activations increase in norm as they propagate forward through the network and gradients increase in norm as they propagate backward. [Sussillo \(2014\)](#) showed that setting the gain factor correctly is sufficient to train networks as deep as

1,000 layers, without needing to use orthogonal initializations. A key insight of this approach is that in feedforward networks, activations and gradients can grow or shrink on each step of forward or back-propagation, following a random walk behavior. This is because feedforward networks use a different weight matrix at each layer. If this random walk is tuned to preserve norms, then feedforward networks can mostly avoid the vanishing and exploding gradients problem that arises when the same weight matrix is used at each step, described in section 8.2.5.

Unfortunately, these optimal criteria for initial weights often do not lead to optimal performance. This may be for three different reasons. First, we may be using the wrong criteria—it may not actually be beneficial to preserve the norm of a signal throughout the entire network. Second, the properties imposed at initialization may not persist after learning has begun to proceed. Third, the criteria might succeed at improving the speed of optimization but inadvertently increase generalization error. In practice, we usually need to treat the scale of the weights as a hyperparameter whose optimal value lies somewhere roughly near but not exactly equal to the theoretical predictions.

One drawback to scaling rules that set all of the initial weights to have the same standard deviation, such as $\frac{1}{\sqrt{m}}$, is that every individual weight becomes extremely small when the layers become large. Martens (2010) introduced an alternative initialization scheme called **sparse initialization** in which each unit is initialized to have exactly k non-zero weights. The idea is to keep the total amount of input to the unit independent from the number of inputs m without making the magnitude of individual weight elements shrink with m . Sparse initialization helps to achieve more diversity among the units at initialization time. However, it also imposes a very strong prior on the weights that are chosen to have large Gaussian values. Because it takes a long time for gradient descent to shrink “incorrect” large values, this initialization scheme can cause problems for units such as maxout units that have several filters that must be carefully coordinated with each other.

When computational resources allow it, it is usually a good idea to treat the initial scale of the weights for each layer as a hyperparameter, and to choose these scales using a hyperparameter search algorithm described in section 11.4.2, such as random search. The choice of whether to use dense or sparse initialization can also be made a hyperparameter. Alternately, one can manually search for the best initial scales. A good rule of thumb for choosing the initial scales is to look at the range or standard deviation of activations or gradients on a single minibatch of data. If the weights are too small, the range of activations across the minibatch will shrink as the activations propagate forward through the network. By repeatedly identifying the first layer with unacceptably small activations and

increasing its weights, it is possible to eventually obtain a network with reasonable initial activations throughout. If learning is still too slow at this point, it can be useful to look at the range or standard deviation of the gradients as well as the activations. This procedure can in principle be automated and is generally less computationally costly than hyperparameter optimization based on validation set error because it is based on feedback from the behavior of the initial model on a single batch of data, rather than on feedback from a trained model on the validation set. While long used heuristically, this protocol has recently been specified more formally and studied by [Mishkin and Matas \(2015\)](#).

So far we have focused on the initialization of the weights. Fortunately, initialization of other parameters is typically easier.

The approach for setting the biases must be coordinated with the approach for settings the weights. Setting the biases to zero is compatible with most weight initialization schemes. There are a few situations where we may set some biases to non-zero values:

- If a bias is for an output unit, then it is often beneficial to initialize the bias to obtain the right marginal statistics of the output. To do this, we assume that the initial weights are small enough that the output of the unit is determined only by the bias. This justifies setting the bias to the inverse of the activation function applied to the marginal statistics of the output in the training set. For example, if the output is a distribution over classes and this distribution is a highly skewed distribution with the marginal probability of class i given by element c_i of some vector \mathbf{c} , then we can set the bias vector \mathbf{b} by solving the equation $\text{softmax}(\mathbf{b}) = \mathbf{c}$. This applies not only to classifiers but also to models we will encounter in Part III, such as autoencoders and Boltzmann machines. These models have layers whose output should resemble the input data \mathbf{x} , and it can be very helpful to initialize the biases of such layers to match the marginal distribution over \mathbf{x} .
- Sometimes we may want to choose the bias to avoid causing too much saturation at initialization. For example, we may set the bias of a ReLU hidden unit to 0.1 rather than 0 to avoid saturating the ReLU at initialization. This approach is not compatible with weight initialization schemes that do not expect strong input from the biases though. For example, it is not recommended for use with random walk initialization ([Sussillo, 2014](#)).
- Sometimes a unit controls whether other units are able to participate in a function. In such situations, we have a unit with output u and another unit $h \in [0, 1]$, and they are multiplied together to produce an output uh . We

can view h as a gate that determines whether $uh \approx u$ or $uh \approx 0$. In these situations, we want to set the bias for h so that $h \approx 1$ most of the time at initialization. Otherwise u does not have a chance to learn. For example, [Jozefowicz et al. \(2015\)](#) advocate setting the bias to 1 for the forget gate of the LSTM model, described in section [10.10](#).

Another common type of parameter is a variance or precision parameter. For example, we can perform linear regression with a conditional variance estimate using the model

$$p(y | \mathbf{x}) = \mathcal{N}(y | \mathbf{w}^T \mathbf{x} + b, 1/\beta) \quad (8.24)$$

where β is a precision parameter. We can usually initialize variance or precision parameters to 1 safely. Another approach is to assume the initial weights are close enough to zero that the biases may be set while ignoring the effect of the weights, then set the biases to produce the correct marginal mean of the output, and set the variance parameters to the marginal variance of the output in the training set.

Besides these simple constant or random methods of initializing model parameters, it is possible to initialize model parameters using machine learning. A common strategy discussed in part [III](#) of this book is to initialize a supervised model with the parameters learned by an unsupervised model trained on the same inputs. One can also perform supervised training on a related task. Even performing supervised training on an unrelated task can sometimes yield an initialization that offers faster convergence than a random initialization. Some of these initialization strategies may yield faster convergence and better generalization because they encode information about the distribution in the initial parameters of the model. Others apparently perform well primarily because they set the parameters to have the right scale or set different units to compute different functions from each other.

8.5 Algorithms with Adaptive Learning Rates

Neural network researchers have long realized that the learning rate was reliably one of the hyperparameters that is the most difficult to set because it has a significant impact on model performance. As we have discussed in sections [4.3](#) and [8.2](#), the cost is often highly sensitive to some directions in parameter space and insensitive to others. The momentum algorithm can mitigate these issues somewhat, but does so at the expense of introducing another hyperparameter. In the face of this, it is natural to ask if there is another way. If we believe that the directions of sensitivity are somewhat axis-aligned, it can make sense to use a separate learning

rate for each parameter, and automatically adapt these learning rates throughout the course of learning.

The **delta-bar-delta** algorithm (Jacobs, 1988) is an early heuristic approach to adapting individual learning rates for model parameters during training. The approach is based on a simple idea: if the partial derivative of the loss, with respect to a given model parameter, remains the same sign, then the learning rate should increase. If the partial derivative with respect to that parameter changes sign, then the learning rate should decrease. Of course, this kind of rule can only be applied to full batch optimization.

More recently, a number of incremental (or mini-batch-based) methods have been introduced that adapt the learning rates of model parameters. This section will briefly review a few of these algorithms.

8.5.1 AdaGrad

The **AdaGrad** algorithm, shown in algorithm 8.4, individually adapts the learning rates of all model parameters by scaling them inversely proportional to the square root of the sum of all of their historical squared values (Duchi *et al.*, 2011). The parameters with the largest partial derivative of the loss have a correspondingly rapid decrease in their learning rate, while parameters with small partial derivatives have a relatively small decrease in their learning rate. The net effect is greater progress in the more gently sloped directions of parameter space.

In the context of convex optimization, the AdaGrad algorithm enjoys some desirable theoretical properties. However, empirically it has been found that—for training deep neural network models—the accumulation of squared gradients *from the beginning of training* can result in a premature and excessive decrease in the effective learning rate. AdaGrad performs well for some but not all deep learning models.

8.5.2 RMSProp

The **RMSProp** algorithm (Hinton, 2012) modifies AdaGrad to perform better in the non-convex setting by changing the gradient accumulation into an exponentially weighted moving average. AdaGrad is designed to converge rapidly when applied to a convex function. When applied to a non-convex function to train a neural network, the learning trajectory may pass through many different structures and eventually arrive at a region that is a locally convex bowl. AdaGrad shrinks the learning rate according to the entire history of the squared gradient and may

Algorithm 8.4 The AdaGrad algorithm

Require: Global learning rate ϵ
Require: Initial parameter θ
Require: Small constant δ , perhaps 10^{-7} , for numerical stability
 Initialize gradient accumulation variable $r = \mathbf{0}$
 while stopping criterion not met **do**
 Sample a minibatch of m examples from the training set $\{\mathbf{x}^{(1)}, \dots, \mathbf{x}^{(m)}\}$ with corresponding targets $\mathbf{y}^{(i)}$.
 Compute gradient: $\mathbf{g} \leftarrow \frac{1}{m} \nabla_{\theta} \sum_i L(f(\mathbf{x}^{(i)}; \theta), \mathbf{y}^{(i)})$
 Accumulate squared gradient: $\mathbf{r} \leftarrow \mathbf{r} + \mathbf{g} \odot \mathbf{g}$
 Compute update: $\Delta\theta \leftarrow -\frac{\epsilon}{\delta + \sqrt{\mathbf{r}}} \odot \mathbf{g}$. (Division and square root applied element-wise)
 Apply update: $\theta \leftarrow \theta + \Delta\theta$
 end while

have made the learning rate too small before arriving at such a convex structure. RMSProp uses an exponentially decaying average to discard history from the extreme past so that it can converge rapidly after finding a convex bowl, as if it were an instance of the AdaGrad algorithm initialized within that bowl.

RMSProp is shown in its standard form in algorithm 8.5 and combined with Nesterov momentum in algorithm 8.6. Compared to AdaGrad, the use of the moving average introduces a new hyperparameter, ρ , that controls the length scale of the moving average.

Empirically, RMSProp has been shown to be an effective and practical optimization algorithm for deep neural networks. It is currently one of the go-to optimization methods being employed routinely by deep learning practitioners.

8.5.3 Adam

Adam (Kingma and Ba, 2014) is yet another adaptive learning rate optimization algorithm and is presented in algorithm 8.7. The name “Adam” derives from the phrase “adaptive moments.” In the context of the earlier algorithms, it is perhaps best seen as a variant on the combination of RMSProp and momentum with a few important distinctions. First, in Adam, momentum is incorporated directly as an estimate of the first order moment (with exponential weighting) of the gradient. The most straightforward way to add momentum to RMSProp is to apply momentum to the rescaled gradients. The use of momentum in combination with rescaling does not have a clear theoretical motivation. Second, Adam includes

Algorithm 8.5 The RMSProp algorithm

Require: Global learning rate ϵ , decay rate ρ .
Require: Initial parameter θ
Require: Small constant δ , usually 10^{-6} , used to stabilize division by small numbers.
Initialize accumulation variables $r = 0$
while stopping criterion not met **do**
 Sample a minibatch of m examples from the training set $\{\mathbf{x}^{(1)}, \dots, \mathbf{x}^{(m)}\}$ with corresponding targets $\mathbf{y}^{(i)}$.
 Compute gradient: $\mathbf{g} \leftarrow \frac{1}{m} \nabla_{\theta} \sum_i L(f(\mathbf{x}^{(i)}; \theta), \mathbf{y}^{(i)})$
 Accumulate squared gradient: $\mathbf{r} \leftarrow \rho \mathbf{r} + (1 - \rho) \mathbf{g} \odot \mathbf{g}$
 Compute parameter update: $\Delta \theta = -\frac{\epsilon}{\sqrt{\delta + \mathbf{r}}} \odot \mathbf{g}$. ($\frac{1}{\sqrt{\delta + \mathbf{r}}}$ applied element-wise)
 Apply update: $\theta \leftarrow \theta + \Delta \theta$
end while

bias corrections to the estimates of both the first-order moments (the momentum term) and the (uncentered) second-order moments to account for their initialization at the origin (see algorithm 8.7). RMSProp also incorporates an estimate of the (uncentered) second-order moment, however it lacks the correction factor. Thus, unlike in Adam, the RMSProp second-order moment estimate may have high bias early in training. Adam is generally regarded as being fairly robust to the choice of hyperparameters, though the learning rate sometimes needs to be changed from the suggested default.

8.5.4 Choosing the Right Optimization Algorithm

In this section, we discussed a series of related algorithms that each seek to address the challenge of optimizing deep models by adapting the learning rate for each model parameter. At this point, a natural question is: which algorithm should one choose?

Unfortunately, there is currently no consensus on this point. Schaul *et al.* (2014) presented a valuable comparison of a large number of optimization algorithms across a wide range of learning tasks. While the results suggest that the family of algorithms with adaptive learning rates (represented by RMSProp and AdaDelta) performed fairly robustly, no single best algorithm has emerged.

Currently, the most popular optimization algorithms actively in use include SGD, SGD with momentum, RMSProp, RMSProp with momentum, AdaDelta and Adam. The choice of which algorithm to use, at this point, seems to depend

Algorithm 8.6 RMSProp algorithm with Nesterov momentum

Require: Global learning rate ϵ , decay rate ρ , momentum coefficient α .

Require: Initial parameter $\boldsymbol{\theta}$, initial velocity \mathbf{v} .

Initialize accumulation variable $\mathbf{r} = \mathbf{0}$

while stopping criterion not met **do**

 Sample a minibatch of m examples from the training set $\{\mathbf{x}^{(1)}, \dots, \mathbf{x}^{(m)}\}$ with corresponding targets $\mathbf{y}^{(i)}$.

 Compute interim update: $\tilde{\boldsymbol{\theta}} \leftarrow \boldsymbol{\theta} + \alpha \mathbf{v}$

 Compute gradient: $\mathbf{g} \leftarrow \frac{1}{m} \nabla_{\tilde{\boldsymbol{\theta}}} \sum_i L(f(\mathbf{x}^{(i)}; \tilde{\boldsymbol{\theta}}), \mathbf{y}^{(i)})$

 Accumulate gradient: $\mathbf{r} \leftarrow \rho \mathbf{r} + (1 - \rho) \mathbf{g} \odot \mathbf{g}$

 Compute velocity update: $\mathbf{v} \leftarrow \alpha \mathbf{v} - \frac{\epsilon}{\sqrt{\mathbf{r}}} \odot \mathbf{g}$. ($\frac{1}{\sqrt{\mathbf{r}}}$ applied element-wise)

 Apply update: $\boldsymbol{\theta} \leftarrow \boldsymbol{\theta} + \mathbf{v}$

end while

largely on the user’s familiarity with the algorithm (for ease of hyperparameter tuning).

8.6 Approximate Second-Order Methods

In this section we discuss the application of second-order methods to the training of deep networks. See [LeCun *et al.* \(1998a\)](#) for an earlier treatment of this subject. For simplicity of exposition, the only objective function we examine is the empirical risk:

$$J(\boldsymbol{\theta}) = \mathbb{E}_{\mathbf{x}, y \sim \hat{p}_{\text{data}}(\mathbf{x}, y)} [L(f(\mathbf{x}; \boldsymbol{\theta}), y)] = \frac{1}{m} \sum_{i=1}^m L(f(\mathbf{x}^{(i)}; \boldsymbol{\theta}), y^{(i)}). \quad (8.25)$$

However the methods we discuss here extend readily to more general objective functions that, for instance, include parameter regularization terms such as those discussed in chapter 7.

8.6.1 Newton’s Method

In section 4.3, we introduced second-order gradient methods. In contrast to first-order methods, second-order methods make use of second derivatives to improve optimization. The most widely used second-order method is Newton’s method. We now describe Newton’s method in more detail, with emphasis on its application to neural network training.

Algorithm 8.7 The Adam algorithm

Require: Step size ϵ (Suggested default: 0.001)

Require: Exponential decay rates for moment estimates, ρ_1 and ρ_2 in $[0, 1]$.
(Suggested defaults: 0.9 and 0.999 respectively)

Require: Small constant δ used for numerical stabilization. (Suggested default:
 10^{-8})

Require: Initial parameters θ

Initialize 1st and 2nd moment variables $s = \mathbf{0}$, $r = \mathbf{0}$

Initialize time step $t = 0$

while stopping criterion not met **do**

- Sample a minibatch of m examples from the training set $\{\mathbf{x}^{(1)}, \dots, \mathbf{x}^{(m)}\}$ with corresponding targets $\mathbf{y}^{(i)}$.
- Compute gradient: $\mathbf{g} \leftarrow \frac{1}{m} \nabla_{\theta} \sum_i L(f(\mathbf{x}^{(i)}; \theta), \mathbf{y}^{(i)})$
- $t \leftarrow t + 1$
- Update biased first moment estimate: $\mathbf{s} \leftarrow \rho_1 \mathbf{s} + (1 - \rho_1) \mathbf{g}$
- Update biased second moment estimate: $\mathbf{r} \leftarrow \rho_2 \mathbf{r} + (1 - \rho_2) \mathbf{g} \odot \mathbf{g}$
- Correct bias in first moment: $\hat{\mathbf{s}} \leftarrow \frac{\mathbf{s}}{1 - \rho_1^t}$
- Correct bias in second moment: $\hat{\mathbf{r}} \leftarrow \frac{\mathbf{r}}{1 - \rho_2^t}$
- Compute update: $\Delta\theta = -\epsilon \frac{\hat{\mathbf{s}}}{\sqrt{\hat{\mathbf{r}}} + \delta}$ (operations applied element-wise)
- Apply update: $\theta \leftarrow \theta + \Delta\theta$

end while

Newton's method is an optimization scheme based on using a second-order Taylor series expansion to approximate $J(\theta)$ near some point θ_0 , ignoring derivatives of higher order:

$$J(\theta) \approx J(\theta_0) + (\theta - \theta_0)^T \nabla_{\theta} J(\theta_0) + \frac{1}{2} (\theta - \theta_0)^T \mathbf{H} (\theta - \theta_0), \quad (8.26)$$

where \mathbf{H} is the Hessian of J with respect to θ evaluated at θ_0 . If we then solve for the critical point of this function, we obtain the Newton parameter update rule:

$$\theta^* = \theta_0 - \mathbf{H}^{-1} \nabla_{\theta} J(\theta_0) \quad (8.27)$$

Thus for a locally quadratic function (with positive definite \mathbf{H}), by rescaling the gradient by \mathbf{H}^{-1} , Newton's method jumps directly to the minimum. If the objective function is convex but not quadratic (there are higher-order terms), this update can be iterated, yielding the training algorithm associated with Newton's method, given in algorithm 8.8.

Algorithm 8.8 Newton’s method with objective $J(\boldsymbol{\theta}) = \frac{1}{m} \sum_{i=1}^m L(f(\mathbf{x}^{(i)}; \boldsymbol{\theta}), y^{(i)})$.

Require: Initial parameter $\boldsymbol{\theta}_0$

Require: Training set of m examples

while stopping criterion not met **do**

 Compute gradient: $\mathbf{g} \leftarrow \frac{1}{m} \nabla_{\boldsymbol{\theta}} \sum_i L(f(\mathbf{x}^{(i)}; \boldsymbol{\theta}), y^{(i)})$

 Compute Hessian: $\mathbf{H} \leftarrow \frac{1}{m} \nabla_{\boldsymbol{\theta}}^2 \sum_i L(f(\mathbf{x}^{(i)}; \boldsymbol{\theta}), y^{(i)})$

 Compute Hessian inverse: \mathbf{H}^{-1}

 Compute update: $\Delta \boldsymbol{\theta} = -\mathbf{H}^{-1} \mathbf{g}$

 Apply update: $\boldsymbol{\theta} = \boldsymbol{\theta} + \Delta \boldsymbol{\theta}$

end while

For surfaces that are not quadratic, as long as the Hessian remains positive definite, Newton’s method can be applied iteratively. This implies a two-step iterative procedure. First, update or compute the inverse Hessian (i.e. by updating the quadratic approximation). Second, update the parameters according to equation 8.27.

In section 8.2.3, we discussed how Newton’s method is appropriate only when the Hessian is positive definite. In deep learning, the surface of the objective function is typically non-convex with many features, such as saddle points, that are problematic for Newton’s method. If the eigenvalues of the Hessian are not all positive, for example, near a saddle point, then Newton’s method can actually cause updates to move in the wrong direction. This situation can be avoided by regularizing the Hessian. Common regularization strategies include adding a constant, α , along the diagonal of the Hessian. The regularized update becomes

$$\boldsymbol{\theta}^* = \boldsymbol{\theta}_0 - [\mathbf{H}(f(\boldsymbol{\theta}_0)) + \alpha \mathbf{I}]^{-1} \nabla_{\boldsymbol{\theta}} f(\boldsymbol{\theta}_0). \quad (8.28)$$

This regularization strategy is used in approximations to Newton’s method, such as the Levenberg–Marquardt algorithm (Levenberg, 1944; Marquardt, 1963), and works fairly well as long as the negative eigenvalues of the Hessian are still relatively close to zero. In cases where there are more extreme directions of curvature, the value of α would have to be sufficiently large to offset the negative eigenvalues. However, as α increases in size, the Hessian becomes dominated by the $\alpha \mathbf{I}$ diagonal and the direction chosen by Newton’s method converges to the standard gradient divided by α . When strong negative curvature is present, α may need to be so large that Newton’s method would make smaller steps than gradient descent with a properly chosen learning rate.

Beyond the challenges created by certain features of the objective function,

such as saddle points, the application of Newton’s method for training large neural networks is limited by the significant computational burden it imposes. The number of elements in the Hessian is squared in the number of parameters, so with k parameters (and for even very small neural networks the number of parameters k can be in the millions), Newton’s method would require the inversion of a $k \times k$ matrix—with computational complexity of $O(k^3)$. Also, since the parameters will change with every update, the inverse Hessian has to be computed *at every training iteration*. As a consequence, only networks with a very small number of parameters can be practically trained via Newton’s method. In the remainder of this section, we will discuss alternatives that attempt to gain some of the advantages of Newton’s method while side-stepping the computational hurdles.

8.6.2 Conjugate Gradients

Conjugate gradients is a method to efficiently avoid the calculation of the inverse Hessian by iteratively descending **conjugate directions**. The inspiration for this approach follows from a careful study of the weakness of the method of steepest descent (see section 4.3 for details), where line searches are applied iteratively in the direction associated with the gradient. Figure 8.6 illustrates how the method of steepest descent, when applied in a quadratic bowl, progresses in a rather ineffective back-and-forth, zig-zag pattern. This happens because each line search direction, when given by the gradient, is guaranteed to be orthogonal to the previous line search direction.

Let the previous search direction be \mathbf{d}_{t-1} . At the minimum, where the line search terminates, the directional derivative is zero in direction \mathbf{d}_{t-1} : $\nabla_{\boldsymbol{\theta}} J(\boldsymbol{\theta}) \cdot \mathbf{d}_{t-1} = 0$. Since the gradient at this point defines the current search direction, $\mathbf{d}_t = \nabla_{\boldsymbol{\theta}} J(\boldsymbol{\theta})$ will have no contribution in the direction \mathbf{d}_{t-1} . Thus \mathbf{d}_t is orthogonal to \mathbf{d}_{t-1} . This relationship between \mathbf{d}_{t-1} and \mathbf{d}_t is illustrated in figure 8.6 for multiple iterations of steepest descent. As demonstrated in the figure, the choice of orthogonal directions of descent do not preserve the minimum along the previous search directions. This gives rise to the zig-zag pattern of progress, where by descending to the minimum in the current gradient direction, we must re-minimize the objective in the previous gradient direction. Thus, by following the gradient at the end of each line search we are, in a sense, undoing progress we have already made in the direction of the previous line search. The method of conjugate gradients seeks to address this problem.

In the method of conjugate gradients, we seek to find a search direction that is **conjugate** to the previous line search direction, i.e. it will not undo progress made in that direction. At training iteration t , the next search direction \mathbf{d}_t takes

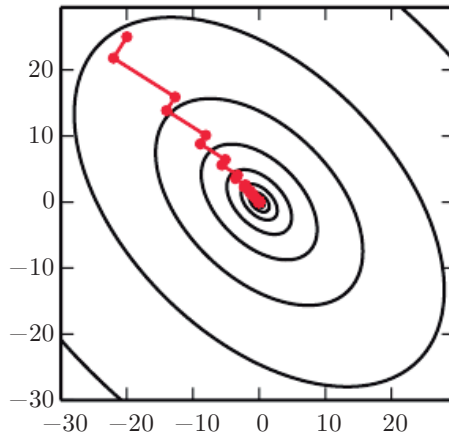


Figure 8.6: The method of steepest descent applied to a quadratic cost surface. The method of steepest descent involves jumping to the point of lowest cost along the line defined by the gradient at the initial point on each step. This resolves some of the problems seen with using a fixed learning rate in figure 4.6, but even with the optimal step size the algorithm still makes back-and-forth progress toward the optimum. By definition, at the minimum of the objective along a given direction, the gradient at the final point is orthogonal to that direction.

the form:

$$\mathbf{d}_t = \nabla_{\boldsymbol{\theta}} J(\boldsymbol{\theta}) + \beta_t \mathbf{d}_{t-1} \quad (8.29)$$

where β_t is a coefficient whose magnitude controls how much of the direction, \mathbf{d}_{t-1} , we should add back to the current search direction.

Two directions, \mathbf{d}_t and \mathbf{d}_{t-1} , are defined as conjugate if $\mathbf{d}_t^\top \mathbf{H} \mathbf{d}_{t-1} = 0$, where \mathbf{H} is the Hessian matrix.

The straightforward way to impose conjugacy would involve calculation of the eigenvectors of \mathbf{H} to choose β_t , which would not satisfy our goal of developing a method that is more computationally viable than Newton's method for large problems. Can we calculate the conjugate directions without resorting to these calculations? Fortunately the answer to that is yes.

Two popular methods for computing the β_t are:

1. Fletcher-Reeves:

$$\beta_t = \frac{\nabla_{\boldsymbol{\theta}} J(\boldsymbol{\theta}_t)^\top \nabla_{\boldsymbol{\theta}} J(\boldsymbol{\theta}_t)}{\nabla_{\boldsymbol{\theta}} J(\boldsymbol{\theta}_{t-1})^\top \nabla_{\boldsymbol{\theta}} J(\boldsymbol{\theta}_{t-1})} \quad (8.30)$$

2. Polak-Ribière:

$$\beta_t = \frac{(\nabla_{\theta} J(\theta_t) - \nabla_{\theta} J(\theta_{t-1}))^\top \nabla_{\theta} J(\theta_t)}{\nabla_{\theta} J(\theta_{t-1})^\top \nabla_{\theta} J(\theta_{t-1})} \quad (8.31)$$

For a quadratic surface, the conjugate directions ensure that the gradient along the previous direction does not increase in magnitude. We therefore stay at the minimum along the previous directions. As a consequence, in a k -dimensional parameter space, the conjugate gradient method requires at most k line searches to achieve the minimum. The conjugate gradient algorithm is given in algorithm 8.9.

Algorithm 8.9 The conjugate gradient method

Require: Initial parameters θ_0

Require: Training set of m examples

Initialize $\rho_0 = \mathbf{0}$

Initialize $g_0 = 0$

Initialize $t = 1$

while stopping criterion not met **do**

 Initialize the gradient $g_t = \mathbf{0}$

 Compute gradient: $g_t \leftarrow \frac{1}{m} \nabla_{\theta} \sum_i L(f(\mathbf{x}^{(i)}; \theta), \mathbf{y}^{(i)})$

 Compute $\beta_t = \frac{(g_t - g_{t-1})^\top g_t}{g_{t-1}^\top g_{t-1}}$ (Polak-Ribière)

 (Nonlinear conjugate gradient: optionally reset β_t to zero, for example if t is a multiple of some constant k , such as $k = 5$)

 Compute search direction: $\rho_t = -g_t + \beta_t \rho_{t-1}$

 Perform line search to find: $\epsilon^* = \operatorname{argmin}_{\epsilon} \frac{1}{m} \sum_{i=1}^m L(f(\mathbf{x}^{(i)}; \theta_t + \epsilon \rho_t), \mathbf{y}^{(i)})$

 (On a truly quadratic cost function, analytically solve for ϵ^* rather than explicitly searching for it)

 Apply update: $\theta_{t+1} = \theta_t + \epsilon^* \rho_t$

$t \leftarrow t + 1$

end while

Nonlinear Conjugate Gradients: So far we have discussed the method of conjugate gradients as it is applied to quadratic objective functions. Of course, our primary interest in this chapter is to explore optimization methods for training neural networks and other related deep learning models where the corresponding objective function is far from quadratic. Perhaps surprisingly, the method of conjugate gradients is still applicable in this setting, though with some modification. Without any assurance that the objective is quadratic, the conjugate directions

are no longer assured to remain at the minimum of the objective for previous directions. As a result, the **nonlinear conjugate gradients** algorithm includes occasional resets where the method of conjugate gradients is restarted with line search along the unaltered gradient.

Practitioners report reasonable results in applications of the nonlinear conjugate gradients algorithm to training neural networks, though it is often beneficial to initialize the optimization with a few iterations of stochastic gradient descent before commencing nonlinear conjugate gradients. Also, while the (nonlinear) conjugate gradients algorithm has traditionally been cast as a batch method, minibatch versions have been used successfully for the training of neural networks (Le *et al.*, 2011). Adaptations of conjugate gradients specifically for neural networks have been proposed earlier, such as the scaled conjugate gradients algorithm (Moller, 1993).

8.6.3 BFGS

The **Broyden–Fletcher–Goldfarb–Shanno (BFGS) algorithm** attempts to bring some of the advantages of Newton’s method without the computational burden. In that respect, BFGS is similar to the conjugate gradient method. However, BFGS takes a more direct approach to the approximation of Newton’s update. Recall that Newton’s update is given by

$$\boldsymbol{\theta}^* = \boldsymbol{\theta}_0 - \mathbf{H}^{-1} \nabla_{\boldsymbol{\theta}} J(\boldsymbol{\theta}_0), \quad (8.32)$$

where \mathbf{H} is the Hessian of J with respect to $\boldsymbol{\theta}$ evaluated at $\boldsymbol{\theta}_0$. The primary computational difficulty in applying Newton’s update is the calculation of the inverse Hessian \mathbf{H}^{-1} . The approach adopted by quasi-Newton methods (of which the BFGS algorithm is the most prominent) is to approximate the inverse with a matrix \mathbf{M}_t that is iteratively refined by low rank updates to become a better approximation of \mathbf{H}^{-1} .

The specification and derivation of the BFGS approximation is given in many textbooks on optimization, including Luenberger (1984).

Once the inverse Hessian approximation \mathbf{M}_t is updated, the direction of descent $\boldsymbol{\rho}_t$ is determined by $\boldsymbol{\rho}_t = \mathbf{M}_t \mathbf{g}_t$. A line search is performed in this direction to determine the size of the step, ϵ^* , taken in this direction. The final update to the parameters is given by:

$$\boldsymbol{\theta}_{t+1} = \boldsymbol{\theta}_t + \epsilon^* \boldsymbol{\rho}_t. \quad (8.33)$$

Like the method of conjugate gradients, the BFGS algorithm iterates a series of line searches with the direction incorporating second-order information. However

unlike conjugate gradients, the success of the approach is not heavily dependent on the line search finding a point very close to the true minimum along the line. Thus, relative to conjugate gradients, BFGS has the advantage that it can spend less time refining each line search. On the other hand, the BFGS algorithm must store the inverse Hessian matrix, \mathbf{M} , that requires $O(n^2)$ memory, making BFGS impractical for most modern deep learning models that typically have millions of parameters.

Limited Memory BFGS (or L-BFGS) The memory costs of the BFGS algorithm can be significantly decreased by avoiding storing the complete inverse Hessian approximation \mathbf{M} . The L-BFGS algorithm computes the approximation \mathbf{M} using the same method as the BFGS algorithm, but beginning with the assumption that $\mathbf{M}^{(t-1)}$ is the identity matrix, rather than storing the approximation from one step to the next. If used with exact line searches, the directions defined by L-BFGS are mutually conjugate. However, unlike the method of conjugate gradients, this procedure remains well behaved when the minimum of the line search is reached only approximately. The L-BFGS strategy with no storage described here can be generalized to include more information about the Hessian by storing some of the vectors used to update \mathbf{M} at each time step, which costs only $O(n)$ per step.

8.7 Optimization Strategies and Meta-Algorithms

Many optimization techniques are not exactly algorithms, but rather general templates that can be specialized to yield algorithms, or subroutines that can be incorporated into many different algorithms.

8.7.1 Batch Normalization

Batch normalization ([Ioffe and Szegedy, 2015](#)) is one of the most exciting recent innovations in optimizing deep neural networks and it is actually not an optimization algorithm at all. Instead, it is a method of adaptive reparametrization, motivated by the difficulty of training very deep models.

Very deep models involve the composition of several functions or layers. The gradient tells how to update each parameter, under the assumption that the other layers do not change. In practice, we update all of the layers simultaneously. When we make the update, unexpected results can happen because many functions composed together are changed simultaneously, using updates that were computed under the assumption that the other functions remain constant. As a simple

example, suppose we have a deep neural network that has only one unit per layer and does not use an activation function at each hidden layer: $\hat{y} = xw_1 w_2 w_3 \dots w_l$. Here, w_i provides the weight used by layer i . The output of layer i is $h_i = h_{i-1} w_i$. The output \hat{y} is a linear function of the input x , but a nonlinear function of the weights w_i . Suppose our cost function has put a gradient of 1 on \hat{y} , so we wish to decrease \hat{y} slightly. The back-propagation algorithm can then compute a gradient $\mathbf{g} = \nabla_{\mathbf{w}} \hat{y}$. Consider what happens when we make an update $\mathbf{w} \leftarrow \mathbf{w} - \epsilon \mathbf{g}$. The first-order Taylor series approximation of \hat{y} predicts that the value of \hat{y} will decrease by $\epsilon \mathbf{g}^\top \mathbf{g}$. If we wanted to decrease \hat{y} by .1, this first-order information available in the gradient suggests we could set the learning rate ϵ to $\frac{.1}{\mathbf{g}^\top \mathbf{g}}$. However, the actual update will include second-order and third-order effects, on up to effects of order l . The new value of \hat{y} is given by

$$x(w_1 - \epsilon g_1)(w_2 - \epsilon g_2) \dots (w_l - \epsilon g_l). \quad (8.34)$$

An example of one second-order term arising from this update is $\epsilon^2 g_1 g_2 \prod_{i=3}^l w_i$. This term might be negligible if $\prod_{i=3}^l w_i$ is small, or might be exponentially large if the weights on layers 3 through l are greater than 1. This makes it very hard to choose an appropriate learning rate, because the effects of an update to the parameters for one layer depends so strongly on all of the other layers. Second-order optimization algorithms address this issue by computing an update that takes these second-order interactions into account, but we can see that in very deep networks, even higher-order interactions can be significant. Even second-order optimization algorithms are expensive and usually require numerous approximations that prevent them from truly accounting for all significant second-order interactions. Building an n -th order optimization algorithm for $n > 2$ thus seems hopeless. What can we do instead?

Batch normalization provides an elegant way of reparametrizing almost any deep network. The reparametrization significantly reduces the problem of coordinating updates across many layers. Batch normalization can be applied to any input or hidden layer in a network. Let \mathbf{H} be a minibatch of activations of the layer to normalize, arranged as a design matrix, with the activations for each example appearing in a row of the matrix. To normalize \mathbf{H} , we replace it with

$$\mathbf{H}' = \frac{\mathbf{H} - \boldsymbol{\mu}}{\boldsymbol{\sigma}}, \quad (8.35)$$

where $\boldsymbol{\mu}$ is a vector containing the mean of each unit and $\boldsymbol{\sigma}$ is a vector containing the standard deviation of each unit. The arithmetic here is based on broadcasting the vector $\boldsymbol{\mu}$ and the vector $\boldsymbol{\sigma}$ to be applied to every row of the matrix \mathbf{H} . Within each row, the arithmetic is element-wise, so $H_{i,j}$ is normalized by subtracting μ_j

and dividing by σ_j . The rest of the network then operates on \mathbf{H}' in exactly the same way that the original network operated on \mathbf{H} .

At training time,

$$\boldsymbol{\mu} = \frac{1}{m} \sum_i \mathbf{H}_{i,:} \quad (8.36)$$

and

$$\sigma = \sqrt{\delta + \frac{1}{m} \sum_i (\mathbf{H} - \boldsymbol{\mu})_i^2}, \quad (8.37)$$

where δ is a small positive value such as 10^{-8} imposed to avoid encountering the undefined gradient of \sqrt{z} at $z = 0$. Crucially, we *back-propagate through these operations* for computing the mean and the standard deviation, and for applying them to normalize \mathbf{H} . This means that the gradient will never propose an operation that acts simply to increase the standard deviation or mean of h_i ; the normalization operations remove the effect of such an action and zero out its component in the gradient. This was a major innovation of the batch normalization approach. Previous approaches had involved adding penalties to the cost function to encourage units to have normalized activation statistics or involved intervening to renormalize unit statistics after each gradient descent step. The former approach usually resulted in imperfect normalization and the latter usually resulted in significant wasted time as the learning algorithm repeatedly proposed changing the mean and variance and the normalization step repeatedly undid this change. Batch normalization reparametrizes the model to make some units always be standardized by definition, deftly sidestepping both problems.

At test time, $\boldsymbol{\mu}$ and σ may be replaced by running averages that were collected during training time. This allows the model to be evaluated on a single example, without needing to use definitions of $\boldsymbol{\mu}$ and σ that depend on an entire minibatch.

Revisiting the $\hat{y} = xw_1w_2 \dots w_l$ example, we see that we can mostly resolve the difficulties in learning this model by normalizing h_{l-1} . Suppose that x is drawn from a unit Gaussian. Then h_{l-1} will also come from a Gaussian, because the transformation from x to h_l is linear. However, h_{l-1} will no longer have zero mean and unit variance. After applying batch normalization, we obtain the normalized \hat{h}_{l-1} that restores the zero mean and unit variance properties. For almost any update to the lower layers, \hat{h}_{l-1} will remain a unit Gaussian. The output \hat{y} may then be learned as a simple linear function $\hat{y} = w_l \hat{h}_{l-1}$. Learning in this model is now very simple because the parameters at the lower layers simply do not have an effect in most cases; their output is always renormalized to a unit Gaussian. In some corner cases, the lower layers can have an effect. Changing one of the lower layer weights to 0 can make the output become degenerate, and changing the sign

of one of the lower weights can flip the relationship between \hat{h}_{l-1} and y . These situations are very rare. Without normalization, nearly every update would have an extreme effect on the statistics of h_{l-1} . Batch normalization has thus made this model significantly easier to learn. In this example, the ease of learning of course came at the cost of making the lower layers useless. In our linear example, the lower layers no longer have any harmful effect, but they also no longer have any beneficial effect. This is because we have normalized out the first and second order statistics, which is all that a linear network can influence. In a deep neural network with nonlinear activation functions, the lower layers can perform nonlinear transformations of the data, so they remain useful. Batch normalization acts to standardize only the mean and variance of each unit in order to stabilize learning, but allows the relationships between units and the nonlinear statistics of a single unit to change.

Because the final layer of the network is able to learn a linear transformation, we may actually wish to remove all linear relationships between units within a layer. Indeed, this is the approach taken by Desjardins *et al.* (2015), who provided the inspiration for batch normalization. Unfortunately, eliminating all linear interactions is much more expensive than standardizing the mean and standard deviation of each individual unit, and so far batch normalization remains the most practical approach.

Normalizing the mean and standard deviation of a unit can reduce the expressive power of the neural network containing that unit. In order to maintain the expressive power of the network, it is common to replace the batch of hidden unit activations \mathbf{H} with $\gamma\mathbf{H}' + \beta$ rather than simply the normalized \mathbf{H}' . The variables γ and β are learned parameters that allow the new variable to have any mean and standard deviation. At first glance, this may seem useless—why did we set the mean to $\mathbf{0}$, and then introduce a parameter that allows it to be set back to any arbitrary value β ? The answer is that the new parametrization can represent the same family of functions of the input as the old parametrization, but the new parametrization has different learning dynamics. In the old parametrization, the mean of \mathbf{H} was determined by a complicated interaction between the parameters in the layers below \mathbf{H} . In the new parametrization, the mean of $\gamma\mathbf{H}' + \beta$ is determined solely by β . The new parametrization is much easier to learn with gradient descent.

Most neural network layers take the form of $\phi(\mathbf{XW} + \mathbf{b})$ where ϕ is some fixed nonlinear activation function such as the rectified linear transformation. It is natural to wonder whether we should apply batch normalization to the input \mathbf{X} , or to the transformed value $\mathbf{XW} + \mathbf{b}$. Ioffe and Szegedy (2015) recommend

the latter. More specifically, $\mathbf{X}\mathbf{W} + \mathbf{b}$ should be replaced by a normalized version of $\mathbf{X}\mathbf{W}$. The bias term should be omitted because it becomes redundant with the β parameter applied by the batch normalization reparametrization. The input to a layer is usually the output of a nonlinear activation function such as the rectified linear function in a previous layer. The statistics of the input are thus more non-Gaussian and less amenable to standardization by linear operations.

In convolutional networks, described in chapter 9, it is important to apply the same normalizing μ and σ at every spatial location within a feature map, so that the statistics of the feature map remain the same regardless of spatial location.

8.7.2 Coordinate Descent

In some cases, it may be possible to solve an optimization problem quickly by breaking it into separate pieces. If we minimize $f(\mathbf{x})$ with respect to a single variable x_i , then minimize it with respect to another variable x_j and so on, repeatedly cycling through all variables, we are guaranteed to arrive at a (local) minimum. This practice is known as **coordinate descent**, because we optimize one coordinate at a time. More generally, **block coordinate descent** refers to minimizing with respect to a subset of the variables simultaneously. The term “coordinate descent” is often used to refer to block coordinate descent as well as the strictly individual coordinate descent.

Coordinate descent makes the most sense when the different variables in the optimization problem can be clearly separated into groups that play relatively isolated roles, or when optimization with respect to one group of variables is significantly more efficient than optimization with respect to all of the variables. For example, consider the cost function

$$J(\mathbf{H}, \mathbf{W}) = \sum_{i,j} |H_{i,j}| + \sum_{i,j} (\mathbf{X} - \mathbf{W}^\top \mathbf{H})_{i,j}^2. \quad (8.38)$$

This function describes a learning problem called sparse coding, where the goal is to find a weight matrix \mathbf{W} that can linearly decode a matrix of activation values \mathbf{H} to reconstruct the training set \mathbf{X} . Most applications of sparse coding also involve weight decay or a constraint on the norms of the columns of \mathbf{W} , in order to prevent the pathological solution with extremely small \mathbf{H} and large \mathbf{W} .

The function J is not convex. However, we can divide the inputs to the training algorithm into two sets: the dictionary parameters \mathbf{W} and the code representations \mathbf{H} . Minimizing the objective function with respect to either one of these sets of variables is a convex problem. Block coordinate descent thus gives

us an optimization strategy that allows us to use efficient convex optimization algorithms, by alternating between optimizing \mathbf{W} with \mathbf{H} fixed, then optimizing \mathbf{H} with \mathbf{W} fixed.

Coordinate descent is not a very good strategy when the value of one variable strongly influences the optimal value of another variable, as in the function $f(\mathbf{x}) = (x_1 - x_2)^2 + \alpha(x_1^2 + x_2^2)$ where α is a positive constant. The first term encourages the two variables to have similar value, while the second term encourages them to be near zero. The solution is to set both to zero. Newton's method can solve the problem in a single step because it is a positive definite quadratic problem. However, for small α , coordinate descent will make very slow progress because the first term does not allow a single variable to be changed to a value that differs significantly from the current value of the other variable.

8.7.3 Polyak Averaging

Polyak averaging (Polyak and Juditsky, 1992) consists of averaging together several points in the trajectory through parameter space visited by an optimization algorithm. If t iterations of gradient descent visit points $\boldsymbol{\theta}^{(1)}, \dots, \boldsymbol{\theta}^{(t)}$, then the output of the Polyak averaging algorithm is $\hat{\boldsymbol{\theta}}^{(t)} = \frac{1}{t} \sum_i \boldsymbol{\theta}^{(i)}$. On some problem classes, such as gradient descent applied to convex problems, this approach has strong convergence guarantees. When applied to neural networks, its justification is more heuristic, but it performs well in practice. The basic idea is that the optimization algorithm may leap back and forth across a valley several times without ever visiting a point near the bottom of the valley. The average of all of the locations on either side should be close to the bottom of the valley though.

In non-convex problems, the path taken by the optimization trajectory can be very complicated and visit many different regions. Including points in parameter space from the distant past that may be separated from the current point by large barriers in the cost function does not seem like a useful behavior. As a result, when applying Polyak averaging to non-convex problems, it is typical to use an exponentially decaying running average:

$$\hat{\boldsymbol{\theta}}^{(t)} = \alpha \hat{\boldsymbol{\theta}}^{(t-1)} + (1 - \alpha) \boldsymbol{\theta}^{(t)}. \quad (8.39)$$

The running average approach is used in numerous applications. See Szegedy *et al.* (2015) for a recent example.

8.7.4 Supervised Pretraining

Sometimes, directly training a model to solve a specific task can be too ambitious if the model is complex and hard to optimize or if the task is very difficult. It is sometimes more effective to train a simpler model to solve the task, then make the model more complex. It can also be more effective to train the model to solve a simpler task, then move on to confront the final task. These strategies that involve training simple models on simple tasks before confronting the challenge of training the desired model to perform the desired task are collectively known as **pretraining**.

Greedy algorithms break a problem into many components, then solve for the optimal version of each component in isolation. Unfortunately, combining the individually optimal components is not guaranteed to yield an optimal complete solution. However, greedy algorithms can be computationally much cheaper than algorithms that solve for the best joint solution, and the quality of a greedy solution is often acceptable if not optimal. Greedy algorithms may also be followed by a **fine-tuning** stage in which a joint optimization algorithm searches for an optimal solution to the full problem. Initializing the joint optimization algorithm with a greedy solution can greatly speed it up and improve the quality of the solution it finds.

Pretraining, and especially greedy pretraining, algorithms are ubiquitous in deep learning. In this section, we describe specifically those pretraining algorithms that break supervised learning problems into other simpler supervised learning problems. This approach is known as **greedy supervised pretraining**.

In the original (Bengio *et al.*, 2007) version of greedy supervised pretraining, each stage consists of a supervised learning training task involving only a subset of the layers in the final neural network. An example of greedy supervised pretraining is illustrated in figure 8.7, in which each added hidden layer is pretrained as part of a shallow supervised MLP, taking as input the output of the previously trained hidden layer. Instead of pretraining one layer at a time, Simonyan and Zisserman (2015) pretrain a deep convolutional network (eleven weight layers) and then use the first four and last three layers from this network to initialize even deeper networks (with up to nineteen layers of weights). The middle layers of the new, very deep network are initialized randomly. The new network is then jointly trained. Another option, explored by Yu *et al.* (2010) is to use the *outputs* of the previously trained MLPs, as well as the raw input, as inputs for each added stage.

Why would greedy supervised pretraining help? The hypothesis initially discussed by Bengio *et al.* (2007) is that it helps to provide better guidance to the

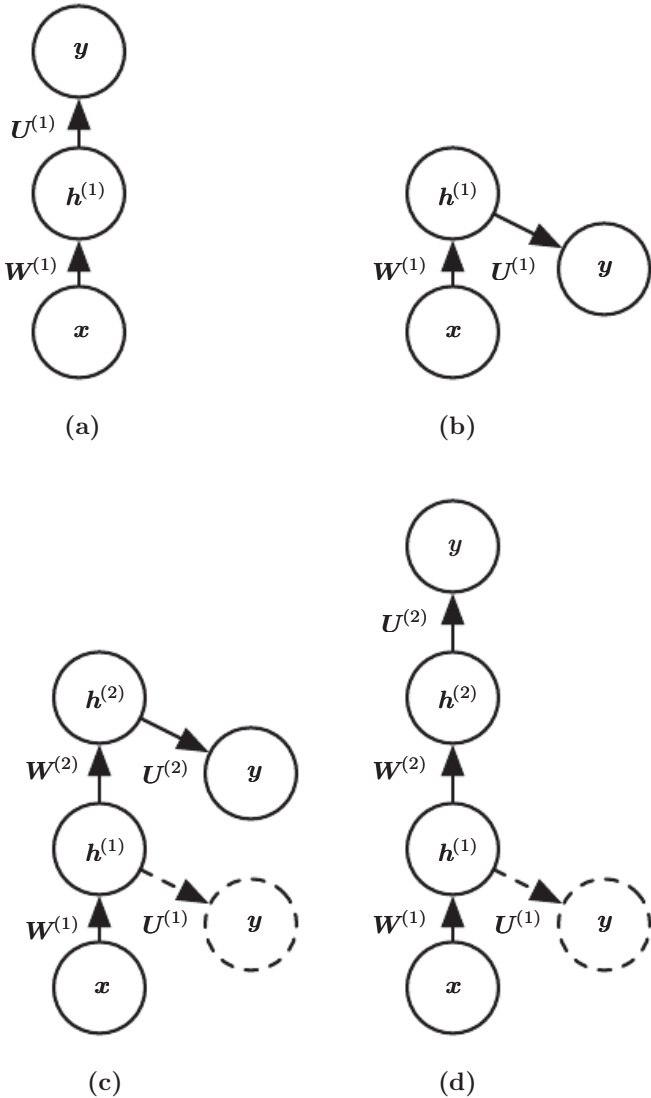


Figure 8.7: Illustration of one form of greedy supervised pretraining (Bengio *et al.*, 2007). (a) We start by training a sufficiently shallow architecture. (b) Another drawing of the same architecture. (c) We keep only the input-to-hidden layer of the original network and discard the hidden-to-output layer. We send the output of the first hidden layer as input to another supervised single hidden layer MLP that is trained with the same objective as the first network was, thus adding a second hidden layer. This can be repeated for as many layers as desired. (d) Another drawing of the result, viewed as a feedforward network. To further improve the optimization, we can jointly fine-tune all the layers, either only at the end or at each stage of this process.

intermediate levels of a deep hierarchy. In general, pretraining may help both in terms of optimization and in terms of generalization.

An approach related to supervised pretraining extends the idea to the context of transfer learning: [Yosinski *et al.* \(2014\)](#) pretrain a deep convolutional net with 8 layers of weights on a set of tasks (a subset of the 1000 ImageNet object categories) and then initialize a same-size network with the first k layers of the first net. All the layers of the second network (with the upper layers initialized randomly) are then jointly trained to perform a different set of tasks (another subset of the 1000 ImageNet object categories), with fewer training examples than for the first set of tasks. Other approaches to transfer learning with neural networks are discussed in section [15.2](#).

Another related line of work is the **FitNets** ([Romero *et al.*, 2015](#)) approach. This approach begins by training a network that has low enough depth and great enough width (number of units per layer) to be easy to train. This network then becomes a **teacher** for a second network, designated the **student**. The student network is much deeper and thinner (eleven to nineteen layers) and would be difficult to train with SGD under normal circumstances. The training of the student network is made easier by training the student network not only to predict the output for the original task, but also to predict the value of the middle layer of the teacher network. This extra task provides a set of hints about how the hidden layers should be used and can simplify the optimization problem. Additional parameters are introduced to regress the middle layer of the 5-layer teacher network from the middle layer of the deeper student network. However, instead of predicting the final classification target, the objective is to predict the middle hidden layer of the teacher network. The lower layers of the student networks thus have two objectives: to help the outputs of the student network accomplish their task, as well as to predict the intermediate layer of the teacher network. Although a thin and deep network appears to be more difficult to train than a wide and shallow network, the thin and deep network may generalize better and certainly has lower computational cost if it is thin enough to have far fewer parameters. Without the hints on the hidden layer, the student network performs very poorly in the experiments, both on the training and test set. Hints on middle layers may thus be one of the tools to help train neural networks that otherwise seem difficult to train, but other optimization techniques or changes in the architecture may also solve the problem.

8.7.5 Designing Models to Aid Optimization

To improve optimization, the best strategy is not always to improve the optimization algorithm. Instead, many improvements in the optimization of deep models have come from designing the models to be easier to optimize.

In principle, we could use activation functions that increase and decrease in jagged non-monotonic patterns. However, this would make optimization extremely difficult. In practice, *it is more important to choose a model family that is easy to optimize than to use a powerful optimization algorithm*. Most of the advances in neural network learning over the past 30 years have been obtained by changing the model family rather than changing the optimization procedure. Stochastic gradient descent with momentum, which was used to train neural networks in the 1980s, remains in use in modern state of the art neural network applications.

Specifically, modern neural networks reflect a *design choice* to use linear transformations between layers and activation functions that are differentiable almost everywhere and have significant slope in large portions of their domain. In particular, model innovations like the LSTM, rectified linear units and maxout units have all moved toward using more linear functions than previous models like deep networks based on sigmoidal units. These models have nice properties that make optimization easier. The gradient flows through many layers provided that the Jacobian of the linear transformation has reasonable singular values. Moreover, linear functions consistently increase in a single direction, so even if the model’s output is very far from correct, it is clear simply from computing the gradient which direction its output should move to reduce the loss function. In other words, modern neural nets have been designed so that their *local* gradient information corresponds reasonably well to moving toward a distant solution.

Other model design strategies can help to make optimization easier. For example, linear paths or skip connections between layers reduce the length of the shortest path from the lower layer’s parameters to the output, and thus mitigate the vanishing gradient problem (Srivastava *et al.*, 2015). A related idea to skip connections is adding extra copies of the output that are attached to the intermediate hidden layers of the network, as in GoogLeNet (Szegedy *et al.*, 2014a) and deeply-supervised nets (Lee *et al.*, 2014). These “auxiliary heads” are trained to perform the same task as the primary output at the top of the network in order to ensure that the lower layers receive a large gradient. When training is complete the auxiliary heads may be discarded. This is an alternative to the pretraining strategies, which were introduced in the previous section. In this way, one can train jointly all the layers in a single phase but change the architecture, so that intermediate layers (especially the lower ones) can get some hints about what they

should do, via a shorter path. These hints provide an error signal to lower layers.

8.7.6 Continuation Methods and Curriculum Learning

As argued in section 8.2.7, many of the challenges in optimization arise from the global structure of the cost function and cannot be resolved merely by making better estimates of local update directions. The predominant strategy for overcoming this problem is to attempt to initialize the parameters in a region that is connected to the solution by a short path through parameter space that local descent can discover.

Continuation methods are a family of strategies that can make optimization easier by choosing initial points to ensure that local optimization spends most of its time in well-behaved regions of space. The idea behind continuation methods is to construct a series of objective functions over the same parameters. In order to minimize a cost function $J(\boldsymbol{\theta})$, we will construct new cost functions $\{J^{(0)}, \dots, J^{(n)}\}$. These cost functions are designed to be increasingly difficult, with $J^{(0)}$ being fairly easy to minimize, and $J^{(n)}$, the most difficult, being $J(\boldsymbol{\theta})$, the true cost function motivating the entire process. When we say that $J^{(i)}$ is easier than $J^{(i+1)}$, we mean that it is well behaved over more of $\boldsymbol{\theta}$ space. A random initialization is more likely to land in the region where local descent can minimize the cost function successfully because this region is larger. The series of cost functions are designed so that a solution to one is a good initial point of the next. We thus begin by solving an easy problem then refine the solution to solve incrementally harder problems until we arrive at a solution to the true underlying problem.

Traditional continuation methods (predating the use of continuation methods for neural network training) are usually based on smoothing the objective function. See [Wu \(1997\)](#) for an example of such a method and a review of some related methods. Continuation methods are also closely related to simulated annealing, which adds noise to the parameters ([Kirkpatrick *et al.*, 1983](#)). Continuation methods have been extremely successful in recent years. See [Mobahi and Fisher \(2015\)](#) for an overview of recent literature, especially for AI applications.

Continuation methods traditionally were mostly designed with the goal of overcoming the challenge of local minima. Specifically, they were designed to reach a global minimum despite the presence of many local minima. To do so, these continuation methods would construct easier cost functions by “blurring” the original cost function. This blurring operation can be done by approximating

$$J^{(i)}(\boldsymbol{\theta}) = \mathbb{E}_{\boldsymbol{\theta}' \sim \mathcal{N}(\boldsymbol{\theta}'; \boldsymbol{\theta}, \sigma^{(i)2})} J(\boldsymbol{\theta}') \quad (8.40)$$

via sampling. The intuition for this approach is that some non-convex functions

become approximately convex when blurred. In many cases, this blurring preserves enough information about the location of a global minimum that we can find the global minimum by solving progressively less blurred versions of the problem. This approach can break down in three different ways. First, it might successfully define a series of cost functions where the first is convex and the optimum tracks from one function to the next arriving at the global minimum, but it might require so many incremental cost functions that the cost of the entire procedure remains high. NP-hard optimization problems remain NP-hard, even when continuation methods are applicable. The other two ways that continuation methods fail both correspond to the method not being applicable. First, the function might not become convex, no matter how much it is blurred. Consider for example the function $J(\theta) = -\theta^\top \theta$. Second, the function may become convex as a result of blurring, but the minimum of this blurred function may track to a local rather than a global minimum of the original cost function.

Though continuation methods were mostly originally designed to deal with the problem of local minima, local minima are no longer believed to be the primary problem for neural network optimization. Fortunately, continuation methods can still help. The easier objective functions introduced by the continuation method can eliminate flat regions, decrease variance in gradient estimates, improve conditioning of the Hessian matrix, or do anything else that will either make local updates easier to compute or improve the correspondence between local update directions and progress toward a global solution.

[Bengio et al. \(2009\)](#) observed that an approach called **curriculum learning** or **shaping** can be interpreted as a continuation method. Curriculum learning is based on the idea of planning a learning process to begin by learning simple concepts and progress to learning more complex concepts that depend on these simpler concepts. This basic strategy was previously known to accelerate progress in animal training ([Skinner, 1958](#); [Peterson, 2004](#); [Krueger and Dayan, 2009](#)) and machine learning ([Solomonoff, 1989](#); [Elman, 1993](#); [Sanger, 1994](#)). [Bengio et al. \(2009\)](#) justified this strategy as a continuation method, where earlier $J^{(i)}$ are made easier by increasing the influence of simpler examples (either by assigning their contributions to the cost function larger coefficients, or by sampling them more frequently), and experimentally demonstrated that better results could be obtained by following a curriculum on a large-scale neural language modeling task. Curriculum learning has been successful on a wide range of natural language ([Spitkovsky et al., 2010](#); [Collobert et al., 2011a](#); [Mikolov et al., 2011b](#); [Tu and Honavar, 2011](#)) and computer vision ([Kumar et al., 2010](#); [Lee and Grauman, 2011](#); [Supancic and Ramanan, 2013](#)) tasks. Curriculum learning was also verified as being consistent with the way in which humans *teach* ([Khan et al., 2011](#)): teachers start by showing easier and

more prototypical examples and then help the learner refine the decision surface with the less obvious cases. Curriculum-based strategies are *more effective* for teaching humans than strategies based on uniform sampling of examples, and can also increase the effectiveness of other teaching strategies ([Basu and Christensen, 2013](#)).

Another important contribution to research on curriculum learning arose in the context of training recurrent neural networks to capture long-term dependencies: [Zaremba and Sutskever \(2014\)](#) found that much better results were obtained with a *stochastic curriculum*, in which a random mix of easy and difficult examples is always presented to the learner, but where the average proportion of the more difficult examples (here, those with longer-term dependencies) is gradually increased. With a deterministic curriculum, no improvement over the baseline (ordinary training from the full training set) was observed.

We have now described the basic family of neural network models and how to regularize and optimize them. In the chapters ahead, we turn to specializations of the neural network family, that allow neural networks to scale to very large sizes and process input data that has special structure. The optimization methods discussed in this chapter are often directly applicable to these specialized architectures with little or no modification.

Chapter 9

Convolutional Networks

Convolutional networks (LeCun, 1989), also known as **convolutional neural networks** or CNNs, are a specialized kind of neural network for processing data that has a known, grid-like topology. Examples include time-series data, which can be thought of as a 1D grid taking samples at regular time intervals, and image data, which can be thought of as a 2D grid of pixels. Convolutional networks have been tremendously successful in practical applications. The name “convolutional neural network” indicates that the network employs a mathematical operation called **convolution**. Convolution is a specialized kind of linear operation. *Convolutional networks are simply neural networks that use convolution in place of general matrix multiplication in at least one of their layers.*

In this chapter, we will first describe what convolution is. Next, we will explain the motivation behind using convolution in a neural network. We will then describe an operation called **pooling**, which almost all convolutional networks employ. Usually, the operation used in a convolutional neural network does not correspond precisely to the definition of convolution as used in other fields such as engineering or pure mathematics. We will describe several variants on the convolution function that are widely used in practice for neural networks. We will also show how convolution may be applied to many kinds of data, with different numbers of dimensions. We then discuss means of making convolution more efficient. Convolutional networks stand out as an example of neuroscientific principles influencing deep learning. We will discuss these neuroscientific principles, then conclude with comments about the role convolutional networks have played in the history of deep learning. One topic this chapter does not address is how to choose the architecture of your convolutional network. The goal of this chapter is to describe the kinds of tools that convolutional networks provide, while chapter 11

describes general guidelines for choosing which tools to use in which circumstances. Research into convolutional network architectures proceeds so rapidly that a new best architecture for a given benchmark is announced every few weeks to months, rendering it impractical to describe the best architecture in print. However, the best architectures have consistently been composed of the building blocks described here.

9.1 The Convolution Operation

In its most general form, convolution is an operation on two functions of a real-valued argument. To motivate the definition of convolution, we start with examples of two functions we might use.

Suppose we are tracking the location of a spaceship with a laser sensor. Our laser sensor provides a single output $x(t)$, the position of the spaceship at time t . Both x and t are real-valued, i.e., we can get a different reading from the laser sensor at any instant in time.

Now suppose that our laser sensor is somewhat noisy. To obtain a less noisy estimate of the spaceship's position, we would like to average together several measurements. Of course, more recent measurements are more relevant, so we will want this to be a weighted average that gives more weight to recent measurements. We can do this with a weighting function $w(a)$, where a is the age of a measurement. If we apply such a weighted average operation at every moment, we obtain a new function s providing a smoothed estimate of the position of the spaceship:

$$s(t) = \int x(a)w(t-a)da \tag{9.1}$$

This operation is called **convolution**. The convolution operation is typically denoted with an asterisk:

$$s(t) = (x * w)(t) \tag{9.2}$$

In our example, w needs to be a valid probability density function, or the output is not a weighted average. Also, w needs to be 0 for all negative arguments, or it will look into the future, which is presumably beyond our capabilities. These limitations are particular to our example though. In general, convolution is defined for any functions for which the above integral is defined, and may be used for other purposes besides taking weighted averages.

In convolutional network terminology, the first argument (in this example, the function x) to the convolution is often referred to as the **input** and the second

argument (in this example, the function w) as the **kernel**. The output is sometimes referred to as the **feature map**.

In our example, the idea of a laser sensor that can provide measurements at every instant in time is not realistic. Usually, when we work with data on a computer, time will be discretized, and our sensor will provide data at regular intervals. In our example, it might be more realistic to assume that our laser provides a measurement once per second. The time index t can then take on only integer values. If we now assume that x and w are defined only on integer t , we can define the discrete convolution:

$$s(t) = (x * w)(t) = \sum_{a=-\infty}^{\infty} x(a)w(t-a) \quad (9.3)$$

In machine learning applications, the input is usually a multidimensional array of data and the kernel is usually a multidimensional array of parameters that are adapted by the learning algorithm. We will refer to these multidimensional arrays as tensors. Because each element of the input and kernel must be explicitly stored separately, we usually assume that these functions are zero everywhere but the finite set of points for which we store the values. This means that in practice we can implement the infinite summation as a summation over a finite number of array elements.

Finally, we often use convolutions over more than one axis at a time. For example, if we use a two-dimensional image I as our input, we probably also want to use a two-dimensional kernel K :

$$S(i, j) = (I * K)(i, j) = \sum_m \sum_n I(m, n)K(i - m, j - n). \quad (9.4)$$

Convolution is commutative, meaning we can equivalently write:

$$S(i, j) = (K * I)(i, j) = \sum_m \sum_n I(i - m, j - n)K(m, n). \quad (9.5)$$

Usually the latter formula is more straightforward to implement in a machine learning library, because there is less variation in the range of valid values of m and n .

The commutative property of convolution arises because we have **flipped** the kernel relative to the input, in the sense that as m increases, the index into the input increases, but the index into the kernel decreases. The only reason to flip the kernel is to obtain the commutative property. While the commutative property

is useful for writing proofs, it is not usually an important property of a neural network implementation. Instead, many neural network libraries implement a related function called the **cross-correlation**, which is the same as convolution but without flipping the kernel:

$$S(i, j) = (I * K)(i, j) = \sum_m \sum_n I(i + m, j + n)K(m, n). \quad (9.6)$$

Many machine learning libraries implement cross-correlation but call it convolution. In this text we will follow this convention of calling both operations convolution, and specify whether we mean to flip the kernel or not in contexts where kernel flipping is relevant. In the context of machine learning, the learning algorithm will learn the appropriate values of the kernel in the appropriate place, so an algorithm based on convolution with kernel flipping will learn a kernel that is flipped relative to the kernel learned by an algorithm without the flipping. It is also rare for convolution to be used alone in machine learning; instead convolution is used simultaneously with other functions, and the combination of these functions does not commute regardless of whether the convolution operation flips its kernel or not.

See figure 9.1 for an example of convolution (without kernel flipping) applied to a 2-D tensor.

Discrete convolution can be viewed as multiplication by a matrix. However, the matrix has several entries constrained to be equal to other entries. For example, for univariate discrete convolution, each row of the matrix is constrained to be equal to the row above shifted by one element. This is known as a **Toeplitz matrix**. In two dimensions, a **doubly block circulant matrix** corresponds to convolution. In addition to these constraints that several elements be equal to each other, convolution usually corresponds to a very sparse matrix (a matrix whose entries are mostly equal to zero). This is because the kernel is usually much smaller than the input image. Any neural network algorithm that works with matrix multiplication and does not depend on specific properties of the matrix structure should work with convolution, without requiring any further changes to the neural network. Typical convolutional neural networks do make use of further specializations in order to deal with large inputs efficiently, but these are not strictly necessary from a theoretical perspective.

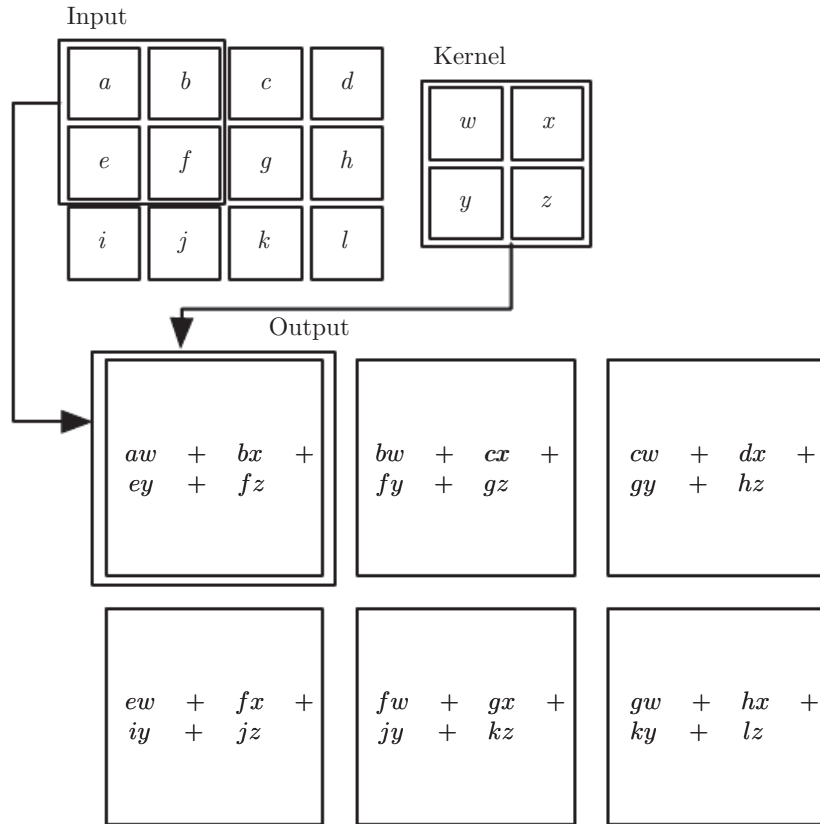


Figure 9.1: An example of 2-D convolution without kernel-flipping. In this case we restrict the output to only positions where the kernel lies entirely within the image, called “valid” convolution in some contexts. We draw boxes with arrows to indicate how the upper-left element of the output tensor is formed by applying the kernel to the corresponding upper-left region of the input tensor.

9.2 Motivation

Convolution leverages three important ideas that can help improve a machine learning system: **sparse interactions**, **parameter sharing** and **equivariant representations**. Moreover, convolution provides a means for working with inputs of variable size. We now describe each of these ideas in turn.

Traditional neural network layers use matrix multiplication by a matrix of parameters with a separate parameter describing the interaction between each input unit and each output unit. This means every output unit interacts with every input unit. Convolutional networks, however, typically have **sparse interactions** (also referred to as **sparse connectivity** or **sparse weights**). This is accomplished by making the kernel smaller than the input. For example, when processing an image, the input image might have thousands or millions of pixels, but we can detect small, meaningful features such as edges with kernels that occupy only tens or hundreds of pixels. This means that we need to store fewer parameters, which both reduces the memory requirements of the model and improves its statistical efficiency. It also means that computing the output requires fewer operations. These improvements in efficiency are usually quite large. If there are m inputs and n outputs, then matrix multiplication requires $m \times n$ parameters and the algorithms used in practice have $O(m \times n)$ runtime (per example). If we limit the number of connections each output may have to k , then the sparsely connected approach requires only $k \times n$ parameters and $O(k \times n)$ runtime. For many practical applications, it is possible to obtain good performance on the machine learning task while keeping k several orders of magnitude smaller than m . For graphical demonstrations of sparse connectivity, see figure 9.2 and figure 9.3. In a deep convolutional network, units in the deeper layers may *indirectly* interact with a larger portion of the input, as shown in figure 9.4. This allows the network to efficiently describe complicated interactions between many variables by constructing such interactions from simple building blocks that each describe only sparse interactions.

Parameter sharing refers to using the same parameter for more than one function in a model. In a traditional neural net, each element of the weight matrix is used exactly once when computing the output of a layer. It is multiplied by one element of the input and then never revisited. As a synonym for parameter sharing, one can say that a network has **tied weights**, because the value of the weight applied to one input is tied to the value of a weight applied elsewhere. In a convolutional neural net, each member of the kernel is used at every position of the input (except perhaps some of the boundary pixels, depending on the design decisions regarding the boundary). The parameter sharing used by the convolution operation means that rather than learning a separate set of parameters

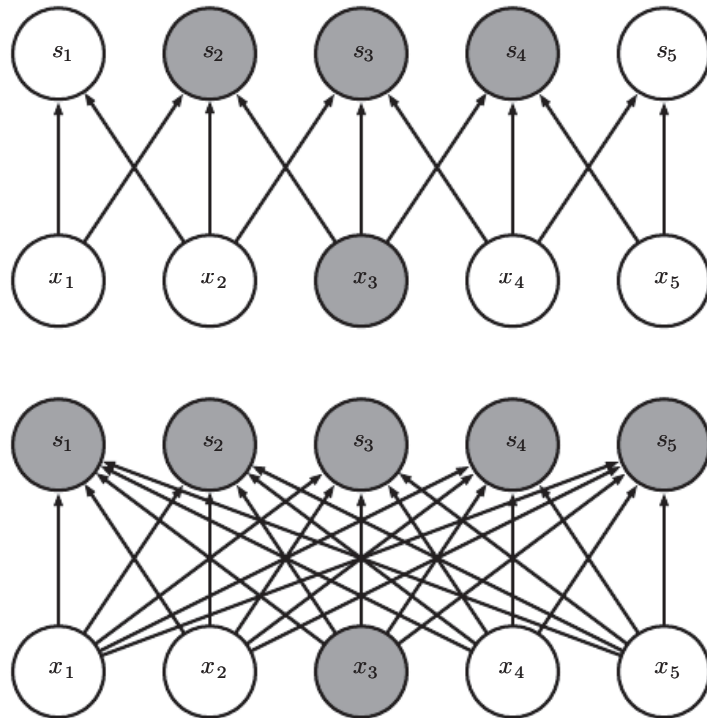


Figure 9.2: *Sparse connectivity, viewed from below:* We highlight one input unit, x_3 , and also highlight the output units in \mathbf{s} that are affected by this unit. (Top) When \mathbf{s} is formed by convolution with a kernel of width 3, only three outputs are affected by \mathbf{x} . (Bottom) When \mathbf{s} is formed by matrix multiplication, connectivity is no longer sparse, so all of the outputs are affected by x_3 .

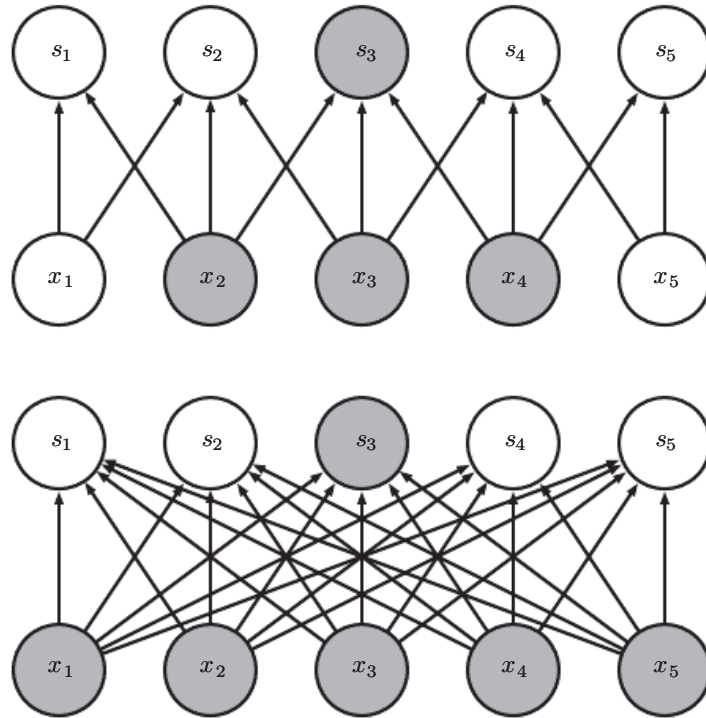


Figure 9.3: *Sparse connectivity, viewed from above:* We highlight one output unit, s_3 , and also highlight the input units in \mathbf{x} that affect this unit. These units are known as the **receptive field** of s_3 . (Top) When \mathbf{s} is formed by convolution with a kernel of width 3, only three inputs affect s_3 . (Bottom) When \mathbf{s} is formed by matrix multiplication, connectivity is no longer sparse, so all of the inputs affect s_3 .

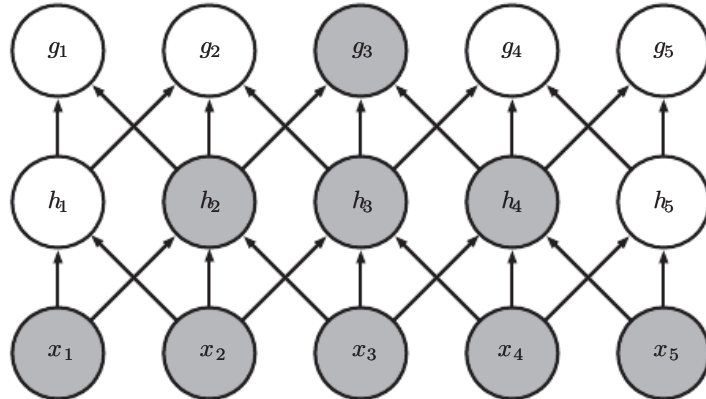


Figure 9.4: The receptive field of the units in the deeper layers of a convolutional network is larger than the receptive field of the units in the shallow layers. This effect increases if the network includes architectural features like strided convolution (figure 9.12) or pooling (section 9.3). This means that even though *direct* connections in a convolutional net are very sparse, units in the deeper layers can be *indirectly* connected to all or most of the input image.

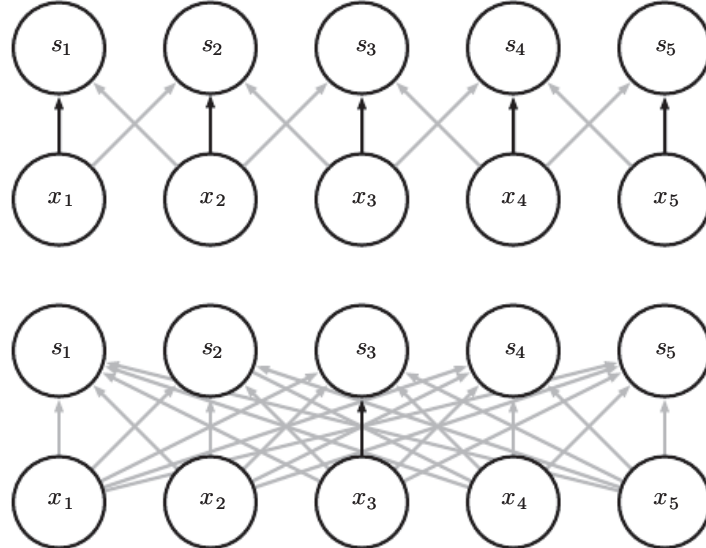


Figure 9.5: Parameter sharing: Black arrows indicate the connections that use a particular parameter in two different models. (*Top*)The black arrows indicate uses of the central element of a 3-element kernel in a convolutional model. Due to parameter sharing, this single parameter is used at all input locations. (*Bottom*)The single black arrow indicates the use of the central element of the weight matrix in a fully connected model. This model has no parameter sharing so the parameter is used only once.

for every location, we learn only one set. This does not affect the runtime of forward propagation—it is still $O(k \times n)$ —but it does further reduce the storage requirements of the model to k parameters. Recall that k is usually several orders of magnitude less than m . Since m and n are usually roughly the same size, k is practically insignificant compared to $m \times n$. Convolution is thus dramatically more efficient than dense matrix multiplication in terms of the memory requirements and statistical efficiency. For a graphical depiction of how parameter sharing works, see figure 9.5.

As an example of both of these first two principles in action, figure 9.6 shows how sparse connectivity and parameter sharing can dramatically improve the efficiency of a linear function for detecting edges in an image.

In the case of convolution, the particular form of parameter sharing causes the layer to have a property called **equivariance** to translation. To say a function is equivariant means that if the input changes, the output changes in the same way. Specifically, a function $f(x)$ is equivariant to a function g if $f(g(x)) = g(f(x))$. In the case of convolution, if we let g be any function that translates the input, i.e., shifts it, then the convolution function is equivariant to g . For example, let I be a function giving image brightness at integer coordinates. Let g be a function

mapping one image function to another image function, such that $I' = g(I)$ is the image function with $I'(x, y) = I(x - 1, y)$. This shifts every pixel of I one unit to the right. If we apply this transformation to I , then apply convolution, the result will be the same as if we applied convolution to I' , then applied the transformation g to the output. When processing time series data, this means that convolution produces a sort of timeline that shows when different features appear in the input. If we move an event later in time in the input, the exact same representation of it will appear in the output, just later in time. Similarly with images, convolution creates a 2-D map of where certain features appear in the input. If we move the object in the input, its representation will move the same amount in the output. This is useful for when we know that some function of a small number of neighboring pixels is useful when applied to multiple input locations. For example, when processing images, it is useful to detect edges in the first layer of a convolutional network. The same edges appear more or less everywhere in the image, so it is practical to share parameters across the entire image. In some cases, we may not wish to share parameters across the entire image. For example, if we are processing images that are cropped to be centered on an individual's face, we probably want to extract different features at different locations—the part of the network processing the top of the face needs to look for eyebrows, while the part of the network processing the bottom of the face needs to look for a chin.

Convolution is not naturally equivariant to some other transformations, such as changes in the scale or rotation of an image. Other mechanisms are necessary for handling these kinds of transformations.

Finally, some kinds of data cannot be processed by neural networks defined by matrix multiplication with a fixed-shape matrix. Convolution enables processing of some of these kinds of data. We discuss this further in section 9.7.

9.3 Pooling

A typical layer of a convolutional network consists of three stages (see figure 9.7). In the first stage, the layer performs several convolutions in parallel to produce a set of linear activations. In the second stage, each linear activation is run through a nonlinear activation function, such as the rectified linear activation function. This stage is sometimes called the **detector** stage. In the third stage, we use a **pooling function** to modify the output of the layer further.

A pooling function replaces the output of the net at a certain location with a summary statistic of the nearby outputs. For example, the **max pooling** (Zhou

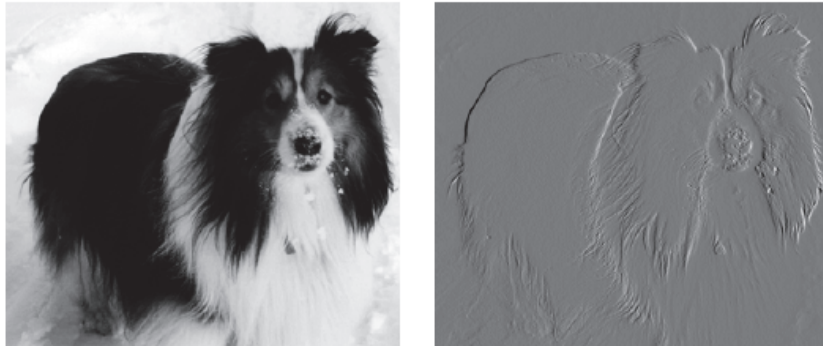


Figure 9.6: *Efficiency of edge detection.* The image on the right was formed by taking each pixel in the original image and subtracting the value of its neighboring pixel on the left. This shows the strength of all of the vertically oriented edges in the input image, which can be a useful operation for object detection. Both images are 280 pixels tall. The input image is 320 pixels wide while the output image is 319 pixels wide. This transformation can be described by a convolution kernel containing two elements, and requires $319 \times 280 \times 3 = 267,960$ floating point operations (two multiplications and one addition per output pixel) to compute using convolution. To describe the same transformation with a matrix multiplication would take $320 \times 280 \times 319 \times 280$, or over eight billion, entries in the matrix, making convolution four billion times more efficient for representing this transformation. The straightforward matrix multiplication algorithm performs over sixteen billion floating point operations, making convolution roughly 60,000 times more efficient computationally. Of course, most of the entries of the matrix would be zero. If we stored only the nonzero entries of the matrix, then both matrix multiplication and convolution would require the same number of floating point operations to compute. The matrix would still need to contain $2 \times 319 \times 280 = 178,640$ entries. Convolution is an extremely efficient way of describing transformations that apply the same linear transformation of a small, local region across the entire input. (Photo credit: Paula Goodfellow)

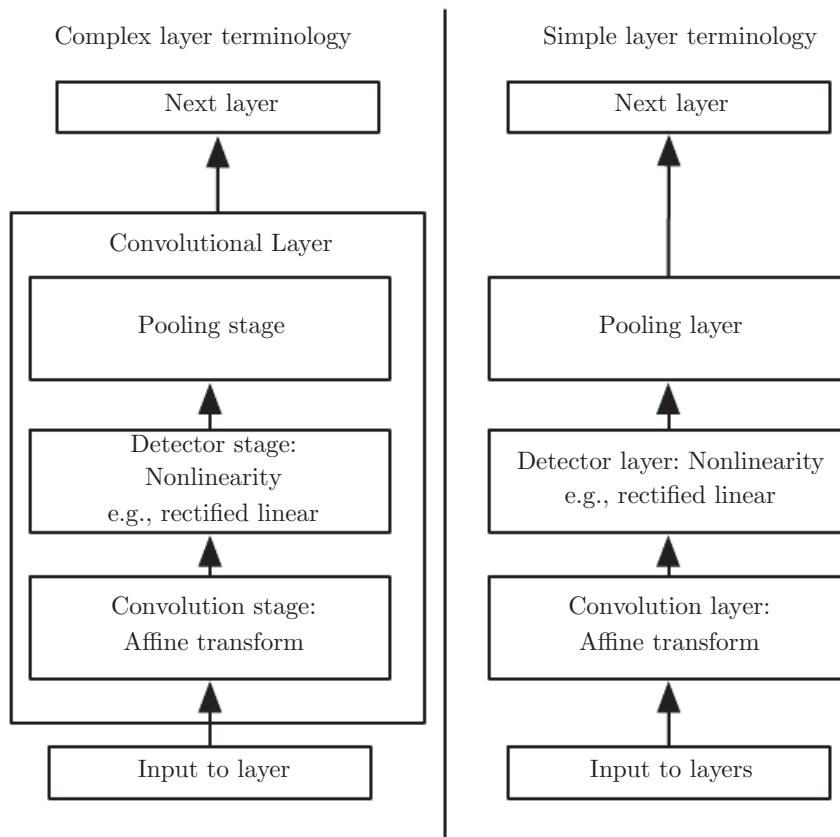


Figure 9.7: The components of a typical convolutional neural network layer. There are two commonly used sets of terminology for describing these layers. (*Left*) In this terminology, the convolutional net is viewed as a small number of relatively complex layers, with each layer having many “stages.” In this terminology, there is a one-to-one mapping between kernel tensors and network layers. In this book we generally use this terminology. (*Right*) In this terminology, the convolutional net is viewed as a larger number of simple layers; every step of processing is regarded as a layer in its own right. This means that not every “layer” has parameters.

and Chellappa, 1988) operation reports the maximum output within a rectangular neighborhood. Other popular pooling functions include the average of a rectangular neighborhood, the L^2 norm of a rectangular neighborhood, or a weighted average based on the distance from the central pixel.

In all cases, pooling helps to make the representation become approximately **invariant** to small translations of the input. Invariance to translation means that if we translate the input by a small amount, the values of most of the pooled outputs do not change. See figure 9.8 for an example of how this works. *Invariance to local translation can be a very useful property if we care more about whether some feature is present than exactly where it is.* For example, when determining whether an image contains a face, we need not know the location of the eyes with pixel-perfect accuracy, we just need to know that there is an eye on the left side of the face and an eye on the right side of the face. In other contexts, it is more important to preserve the location of a feature. For example, if we want to find a corner defined by two edges meeting at a specific orientation, we need to preserve the location of the edges well enough to test whether they meet.

The use of pooling can be viewed as adding an infinitely strong prior that the function the layer learns must be invariant to small translations. When this assumption is correct, it can greatly improve the statistical efficiency of the network.

Pooling over spatial regions produces invariance to translation, but if we pool over the outputs of separately parametrized convolutions, the features can learn which transformations to become invariant to (see figure 9.9).

Because pooling summarizes the responses over a whole neighborhood, it is possible to use fewer pooling units than detector units, by reporting summary statistics for pooling regions spaced k pixels apart rather than 1 pixel apart. See figure 9.10 for an example. This improves the computational efficiency of the network because the next layer has roughly k times fewer inputs to process. When the number of parameters in the next layer is a function of its input size (such as when the next layer is fully connected and based on matrix multiplication) this reduction in the input size can also result in improved statistical efficiency and reduced memory requirements for storing the parameters.

For many tasks, pooling is essential for handling inputs of varying size. For example, if we want to classify images of variable size, the input to the classification layer must have a fixed size. This is usually accomplished by varying the size of an offset between pooling regions so that the classification layer always receives the same number of summary statistics regardless of the input size. For example, the final pooling layer of the network may be defined to output four sets of summary statistics, one for each quadrant of an image, regardless of the image size.

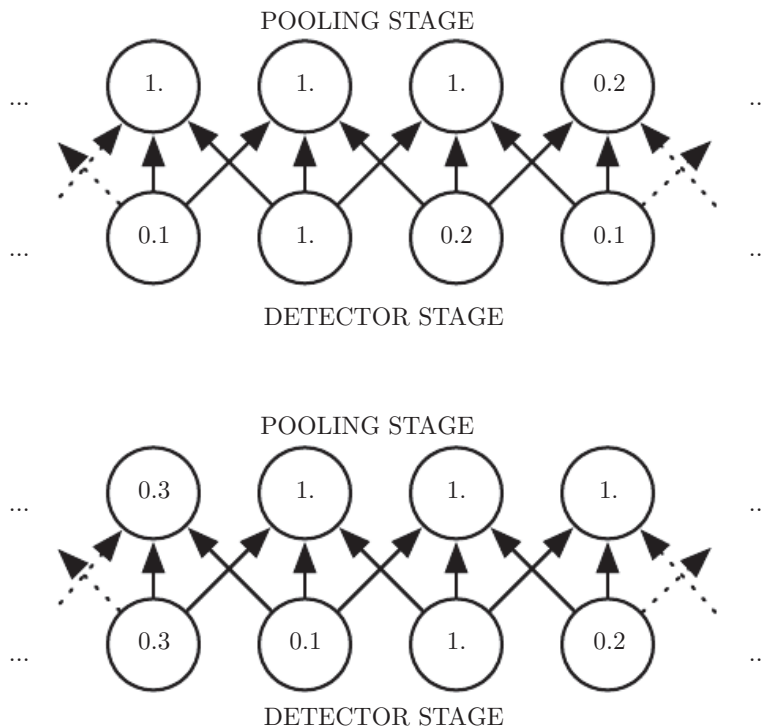


Figure 9.8: Max pooling introduces invariance. (*Top*) A view of the middle of the output of a convolutional layer. The bottom row shows outputs of the nonlinearity. The top row shows the outputs of max pooling, with a stride of one pixel between pooling regions and a pooling region width of three pixels. (*Bottom*) A view of the same network, after the input has been shifted to the right by one pixel. Every value in the bottom row has changed, but only half of the values in the top row have changed, because the max pooling units are only sensitive to the maximum value in the neighborhood, not its exact location.

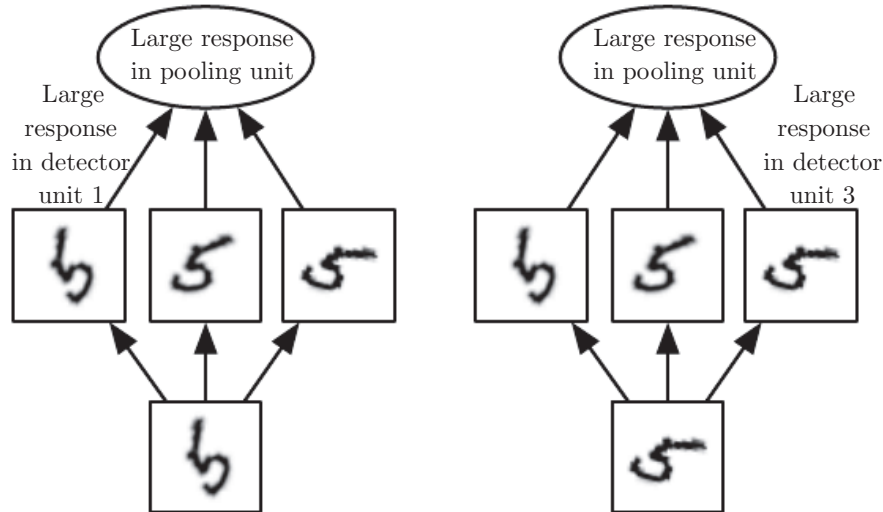


Figure 9.9: *Example of learned invariances*: A pooling unit that pools over multiple features that are learned with separate parameters can learn to be invariant to transformations of the input. Here we show how a set of three learned filters and a max pooling unit can learn to become invariant to rotation. All three filters are intended to detect a hand-written 5. Each filter attempts to match a slightly different orientation of the 5. When a 5 appears in the input, the corresponding filter will match it and cause a large activation in a detector unit. The max pooling unit then has a large activation regardless of which detector unit was activated. We show here how the network processes two different inputs, resulting in two different detector units being activated. The effect on the pooling unit is roughly the same either way. This principle is leveraged by maxout networks (Goodfellow *et al.*, 2013a) and other convolutional networks. Max pooling over spatial positions is naturally invariant to translation; this multi-channel approach is only necessary for learning other transformations.

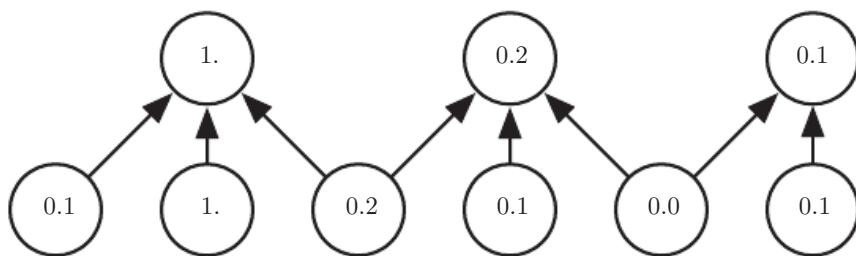


Figure 9.10: *Pooling with downsampling*. Here we use max-pooling with a pool width of three and a stride between pools of two. This reduces the representation size by a factor of two, which reduces the computational and statistical burden on the next layer. Note that the rightmost pooling region has a smaller size, but must be included if we do not want to ignore some of the detector units.

Some theoretical work gives guidance as to which kinds of pooling one should use in various situations (Boureau *et al.*, 2010). It is also possible to dynamically pool features together, for example, by running a clustering algorithm on the locations of interesting features (Boureau *et al.*, 2011). This approach yields a different set of pooling regions for each image. Another approach is to *learn* a single pooling structure that is then applied to all images (Jia *et al.*, 2012).

Pooling can complicate some kinds of neural network architectures that use top-down information, such as Boltzmann machines and autoencoders. These issues will be discussed further when we present these types of networks in part III. Pooling in convolutional Boltzmann machines is presented in section 20.6. The inverse-like operations on pooling units needed in some differentiable networks will be covered in section 20.10.6.

Some examples of complete convolutional network architectures for classification using convolution and pooling are shown in figure 9.11.

9.4 Convolution and Pooling as an Infinitely Strong Prior

Recall the concept of a **prior probability distribution** from section 5.2. This is a probability distribution over the parameters of a model that encodes our beliefs about what models are reasonable, before we have seen any data.

Priors can be considered weak or strong depending on how concentrated the probability density in the prior is. A weak prior is a prior distribution with high entropy, such as a Gaussian distribution with high variance. Such a prior allows the data to move the parameters more or less freely. A strong prior has very low entropy, such as a Gaussian distribution with low variance. Such a prior plays a more active role in determining where the parameters end up.

An infinitely strong prior places zero probability on some parameters and says that these parameter values are completely forbidden, regardless of how much support the data gives to those values.

We can imagine a convolutional net as being similar to a fully connected net, but with an infinitely strong prior over its weights. This infinitely strong prior says that the weights for one hidden unit must be identical to the weights of its neighbor, but shifted in space. The prior also says that the weights must be zero, except for in the small, spatially contiguous receptive field assigned to that hidden unit. Overall, we can think of the use of convolution as introducing an infinitely strong prior probability distribution over the parameters of a layer. This prior

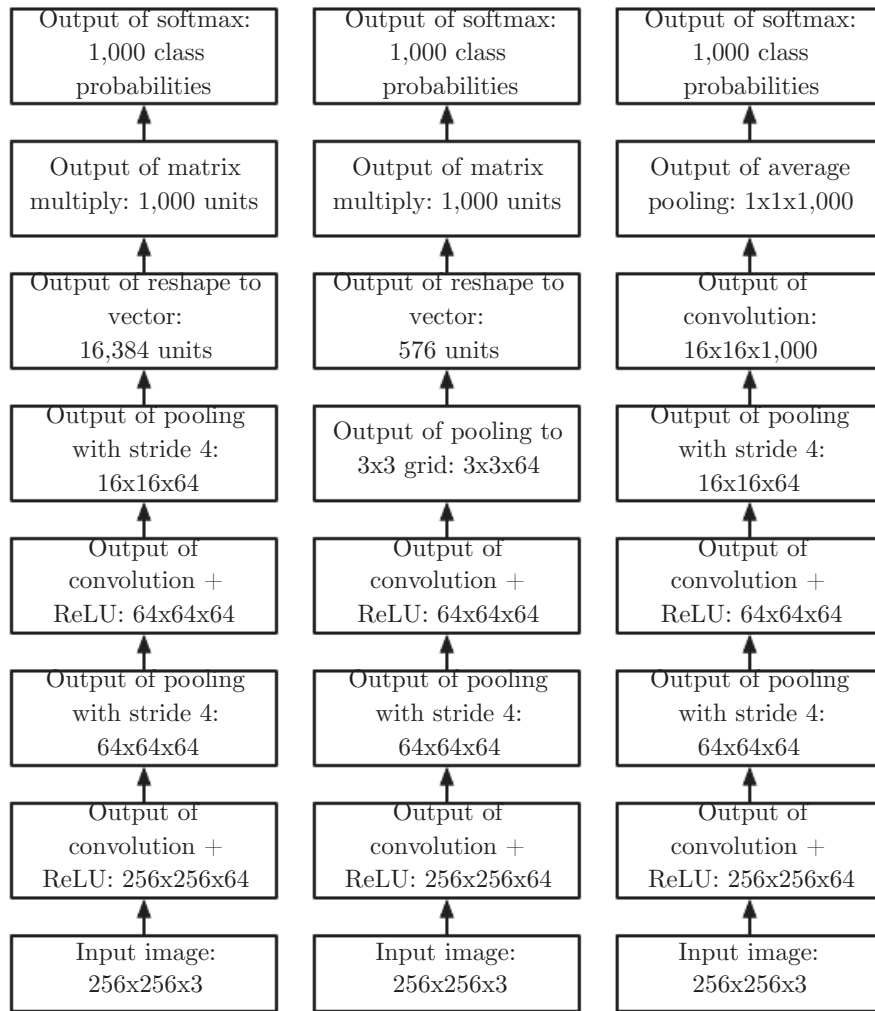


Figure 9.11: Examples of architectures for classification with convolutional networks. The specific strides and depths used in this figure are not advisable for real use; they are designed to be very shallow in order to fit onto the page. Real convolutional networks also often involve significant amounts of branching, unlike the chain structures used here for simplicity. *(Left)*A convolutional network that processes a fixed image size. After alternating between convolution and pooling for a few layers, the tensor for the convolutional feature map is reshaped to flatten out the spatial dimensions. The rest of the network is an ordinary feedforward network classifier, as described in chapter 6. *(Center)*A convolutional network that processes a variable-sized image, but still maintains a fully connected section. This network uses a pooling operation with variably-sized pools but a fixed number of pools, in order to provide a fixed-size vector of 576 units to the fully connected portion of the network. *(Right)*A convolutional network that does not have any fully connected weight layer. Instead, the last convolutional layer outputs one feature map per class. The model presumably learns a map of how likely each class is to occur at each spatial location. Averaging a feature map down to a single value provides the argument to the softmax classifier at the top.

says that the function the layer should learn contains only local interactions and is equivariant to translation. Likewise, the use of pooling is an infinitely strong prior that each unit should be invariant to small translations.

Of course, implementing a convolutional net as a fully connected net with an infinitely strong prior would be extremely computationally wasteful. But thinking of a convolutional net as a fully connected net with an infinitely strong prior can give us some insights into how convolutional nets work.

One key insight is that convolution and pooling can cause underfitting. Like any prior, convolution and pooling are only useful when the assumptions made by the prior are reasonably accurate. If a task relies on preserving precise spatial information, then using pooling on all features can increase the training error. Some convolutional network architectures ([Szegedy et al., 2014a](#)) are designed to use pooling on some channels but not on other channels, in order to get both highly invariant features and features that will not underfit when the translation invariance prior is incorrect. When a task involves incorporating information from very distant locations in the input, then the prior imposed by convolution may be inappropriate.

Another key insight from this view is that we should only compare convolutional models to other convolutional models in benchmarks of statistical learning performance. Models that do not use convolution would be able to learn even if we permuted all of the pixels in the image. For many image datasets, there are separate benchmarks for models that are **permutation invariant** and must discover the concept of topology via learning, and models that have the knowledge of spatial relationships hard-coded into them by their designer.

9.5 Variants of the Basic Convolution Function

When discussing convolution in the context of neural networks, we usually do not refer exactly to the standard discrete convolution operation as it is usually understood in the mathematical literature. The functions used in practice differ slightly. Here we describe these differences in detail, and highlight some useful properties of the functions used in neural networks.

First, when we refer to convolution in the context of neural networks, we usually actually mean an operation that consists of many applications of convolution in parallel. This is because convolution with a single kernel can only extract one kind of feature, albeit at many spatial locations. Usually we want each layer of our network to extract many kinds of features, at many locations.

Additionally, the input is usually not just a grid of real values. Rather, it is a grid of vector-valued observations. For example, a color image has a red, green and blue intensity at each pixel. In a multilayer convolutional network, the input to the second layer is the output of the first layer, which usually has the output of many different convolutions at each position. When working with images, we usually think of the input and output of the convolution as being 3-D tensors, with one index into the different channels and two indices into the spatial coordinates of each channel. Software implementations usually work in batch mode, so they will actually use 4-D tensors, with the fourth axis indexing different examples in the batch, but we will omit the batch axis in our description here for simplicity.

Because convolutional networks usually use multi-channel convolution, the linear operations they are based on are not guaranteed to be commutative, even if kernel-flipping is used. These multi-channel operations are only commutative if each operation has the same number of output channels as input channels.

Assume we have a 4-D kernel tensor \mathbf{K} with element $K_{i,j,k,l}$ giving the connection strength between a unit in channel i of the output and a unit in channel j of the input, with an offset of k rows and l columns between the output unit and the input unit. Assume our input consists of observed data \mathbf{V} with element $V_{i,j,k}$ giving the value of the input unit within channel i at row j and column k . Assume our output consists of \mathbf{Z} with the same format as \mathbf{V} . If \mathbf{Z} is produced by convolving \mathbf{K} across \mathbf{V} without flipping \mathbf{K} , then

$$Z_{i,j,k} = \sum_{l,m,n} V_{l,j+m-1,k+n-1} K_{i,l,m,n} \quad (9.7)$$

where the summation over l , m and n is over all values for which the tensor indexing operations inside the summation is valid. In linear algebra notation, we index into arrays using a 1 for the first entry. This necessitates the -1 in the above formula. Programming languages such as C and Python index starting from 0, rendering the above expression even simpler.

We may want to skip over some positions of the kernel in order to reduce the computational cost (at the expense of not extracting our features as finely). We can think of this as downsampling the output of the full convolution function. If we want to sample only every s pixels in each direction in the output, then we can define a downsampled convolution function c such that

$$Z_{i,j,k} = c(\mathbf{K}, \mathbf{V}, s)_{i,j,k} = \sum_{l,m,n} [V_{l,(j-1)\times s+m, (k-1)\times s+n} K_{i,l,m,n}] . \quad (9.8)$$

We refer to s as the **stride** of this downsampled convolution. It is also possible

to define a separate stride for each direction of motion. See figure 9.12 for an illustration.

One essential feature of any convolutional network implementation is the ability to implicitly zero-pad the input \mathbf{V} in order to make it wider. Without this feature, the width of the representation shrinks by one pixel less than the kernel width at each layer. Zero padding the input allows us to control the kernel width and the size of the output independently. Without zero padding, we are forced to choose between shrinking the spatial extent of the network rapidly and using small kernels—both scenarios that significantly limit the expressive power of the network. See figure 9.13 for an example.

Three special cases of the zero-padding setting are worth mentioning. One is the extreme case in which no zero-padding is used whatsoever, and the convolution kernel is only allowed to visit positions where the entire kernel is contained entirely within the image. In MATLAB terminology, this is called **valid** convolution. In this case, all pixels in the output are a function of the same number of pixels in the input, so the behavior of an output pixel is somewhat more regular. However, the size of the output shrinks at each layer. If the input image has width m and the kernel has width k , the output will be of width $m - k + 1$. The rate of this shrinkage can be dramatic if the kernels used are large. Since the shrinkage is greater than 0, it limits the number of convolutional layers that can be included in the network. As layers are added, the spatial dimension of the network will eventually drop to 1×1 , at which point additional layers cannot meaningfully be considered convolutional. Another special case of the zero-padding setting is when just enough zero-padding is added to keep the size of the output equal to the size of the input. MATLAB calls this **same** convolution. In this case, the network can contain as many convolutional layers as the available hardware can support, since the operation of convolution does not modify the architectural possibilities available to the next layer. However, the input pixels near the border influence fewer output pixels than the input pixels near the center. This can make the border pixels somewhat underrepresented in the model. This motivates the other extreme case, which MATLAB refers to as **full** convolution, in which enough zeroes are added for every pixel to be visited k times in each direction, resulting in an output image of width $m + k - 1$. In this case, the output pixels near the border are a function of fewer pixels than the output pixels near the center. This can make it difficult to learn a single kernel that performs well at all positions in the convolutional feature map. Usually the optimal amount of zero padding (in terms of test set classification accuracy) lies somewhere between “valid” and “same” convolution.

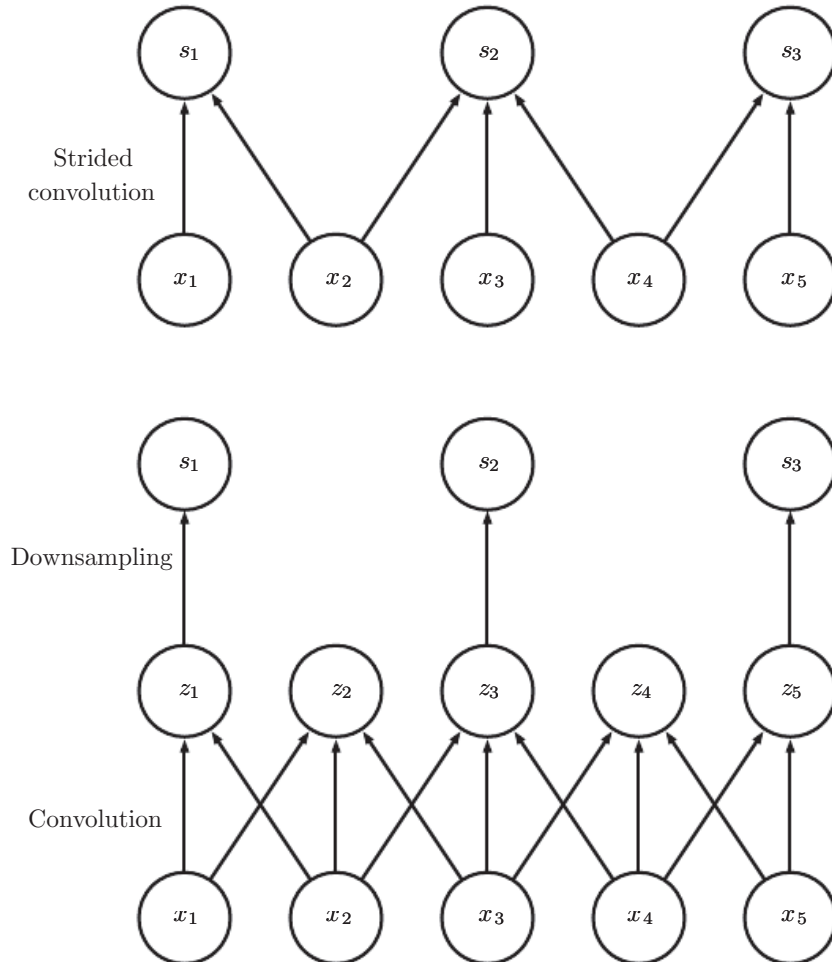


Figure 9.12: Convolution with a stride. In this example, we use a stride of two. (*Top*) Convolution with a stride length of two implemented in a single operation. (*Bottom*) Convolution with a stride greater than one pixel is mathematically equivalent to convolution with unit stride followed by downsampling. Obviously, the two-step approach involving downsampling is computationally wasteful, because it computes many values that are then discarded.

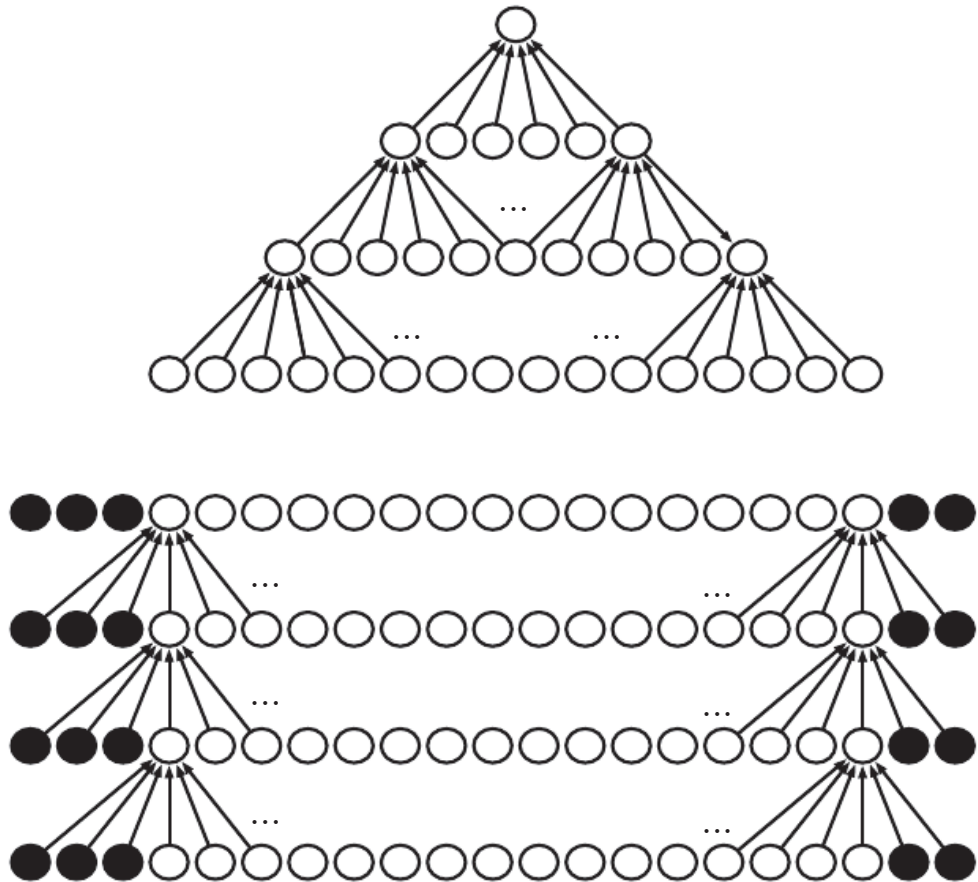


Figure 9.13: *The effect of zero padding on network size*: Consider a convolutional network with a kernel of width six at every layer. In this example, we do not use any pooling, so only the convolution operation itself shrinks the network size. (*Top*) In this convolutional network, we do not use any implicit zero padding. This causes the representation to shrink by five pixels at each layer. Starting from an input of sixteen pixels, we are only able to have three convolutional layers, and the last layer does not ever move the kernel, so arguably only two of the layers are truly convolutional. The rate of shrinking can be mitigated by using smaller kernels, but smaller kernels are less expressive and some shrinking is inevitable in this kind of architecture. (*Bottom*) By adding five implicit zeroes to each layer, we prevent the representation from shrinking with depth. This allows us to make an arbitrarily deep convolutional network.

In some cases, we do not actually want to use convolution, but rather locally connected layers (LeCun, 1986, 1989). In this case, the adjacency matrix in the graph of our MLP is the same, but every connection has its own weight, specified by a 6-D tensor \mathbf{W} . The indices into \mathbf{W} are respectively: i , the output channel, j , the output row, k , the output column, l , the input channel, m , the row offset within the input, and n , the column offset within the input. The linear part of a locally connected layer is then given by

$$Z_{i,j,k} = \sum_{l,m,n} [V_{l,j+m-1,k+n-1} w_{i,j,k,l,m,n}]. \quad (9.9)$$

This is sometimes also called **unshared convolution**, because it is a similar operation to discrete convolution with a small kernel, but without sharing parameters across locations. Figure 9.14 compares local connections, convolution, and full connections.

Locally connected layers are useful when we know that each feature should be a function of a small part of space, but there is no reason to think that the same feature should occur across all of space. For example, if we want to tell if an image is a picture of a face, we only need to look for the mouth in the bottom half of the image.

It can also be useful to make versions of convolution or locally connected layers in which the connectivity is further restricted, for example to constrain each output channel i to be a function of only a subset of the input channels l . A common way to do this is to make the first m output channels connect to only the first n input channels, the second m output channels connect to only the second n input channels, and so on. See figure 9.15 for an example. Modeling interactions between few channels allows the network to have fewer parameters in order to reduce memory consumption and increase statistical efficiency, and also reduces the amount of computation needed to perform forward and back-propagation. It accomplishes these goals without reducing the number of hidden units.

Tiled convolution (Gregor and LeCun, 2010a; Le *et al.*, 2010) offers a compromise between a convolutional layer and a locally connected layer. Rather than learning a separate set of weights at *every* spatial location, we learn a set of kernels that we rotate through as we move through space. This means that immediately neighboring locations will have different filters, like in a locally connected layer, but the memory requirements for storing the parameters will increase only by a factor of the size of this set of kernels, rather than the size of the entire output feature map. See figure 9.16 for a comparison of locally connected layers, tiled convolution, and standard convolution.

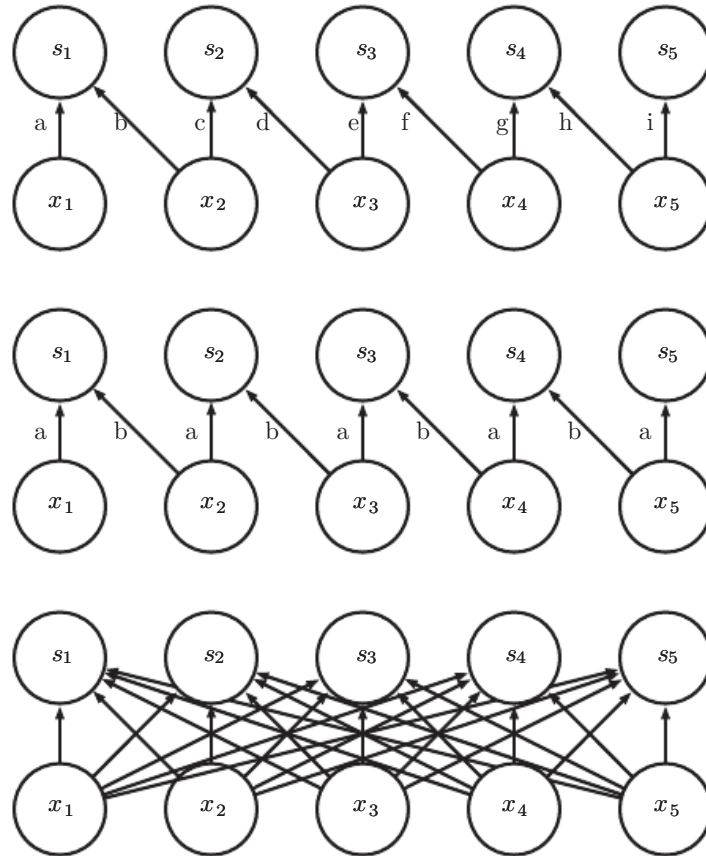


Figure 9.14: Comparison of local connections, convolution, and full connections.

(Top) A locally connected layer with a patch size of two pixels. Each edge is labeled with a unique letter to show that each edge is associated with its own weight parameter.

(Center) A convolutional layer with a kernel width of two pixels. This model has exactly the same connectivity as the locally connected layer. The difference lies not in which units interact with each other, but in how the parameters are shared. The locally connected layer has no parameter sharing. The convolutional layer uses the same two weights repeatedly across the entire input, as indicated by the repetition of the letters labeling each edge.

(Bottom) A fully connected layer resembles a locally connected layer in the sense that each edge has its own parameter (there are too many to label explicitly with letters in this diagram). However, it does not have the restricted connectivity of the locally connected layer.

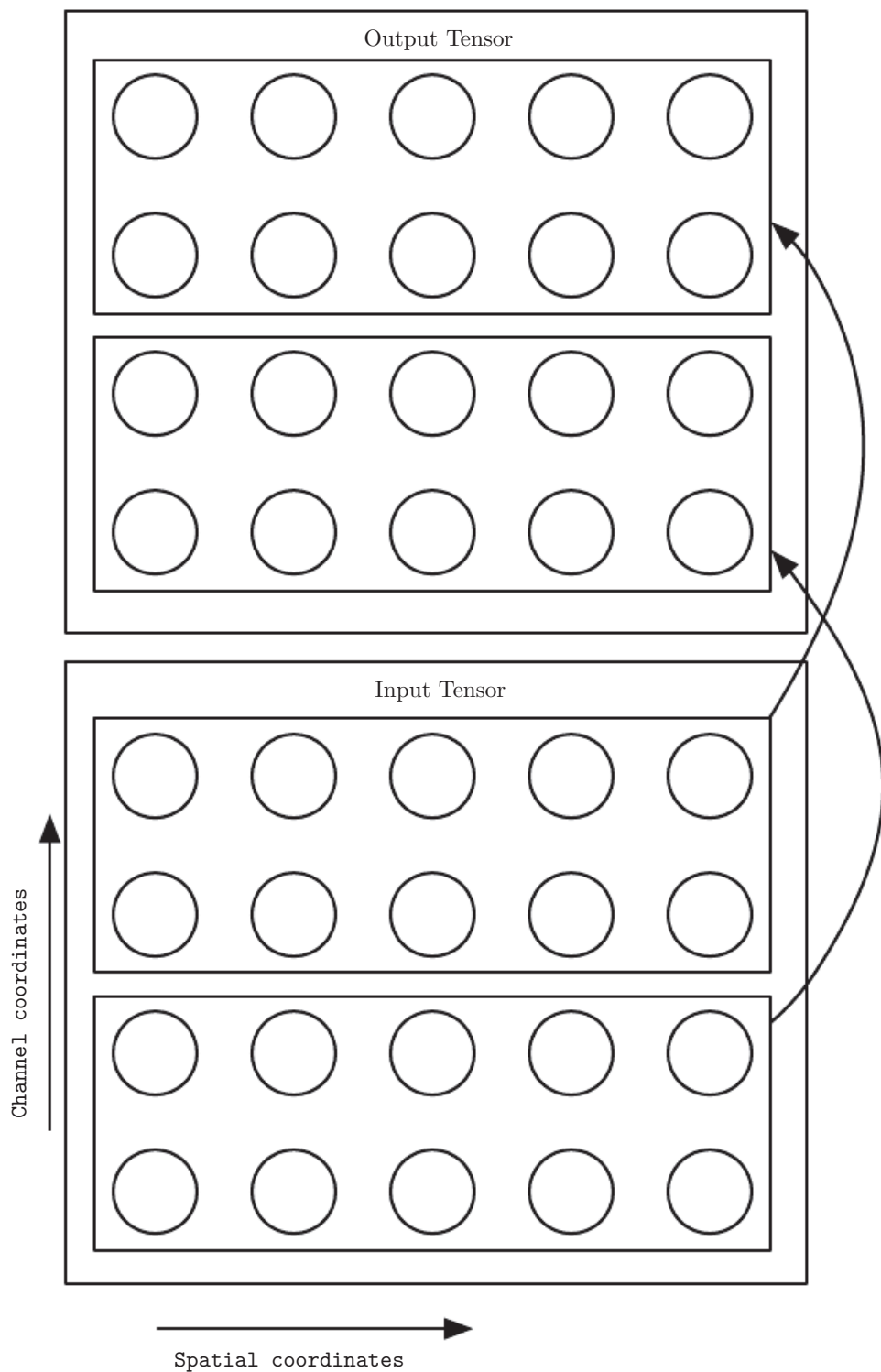


Figure 9.15: A convolutional network with the first two output channels connected to only the first two input channels, and the second two output channels connected to only the second two input channels.

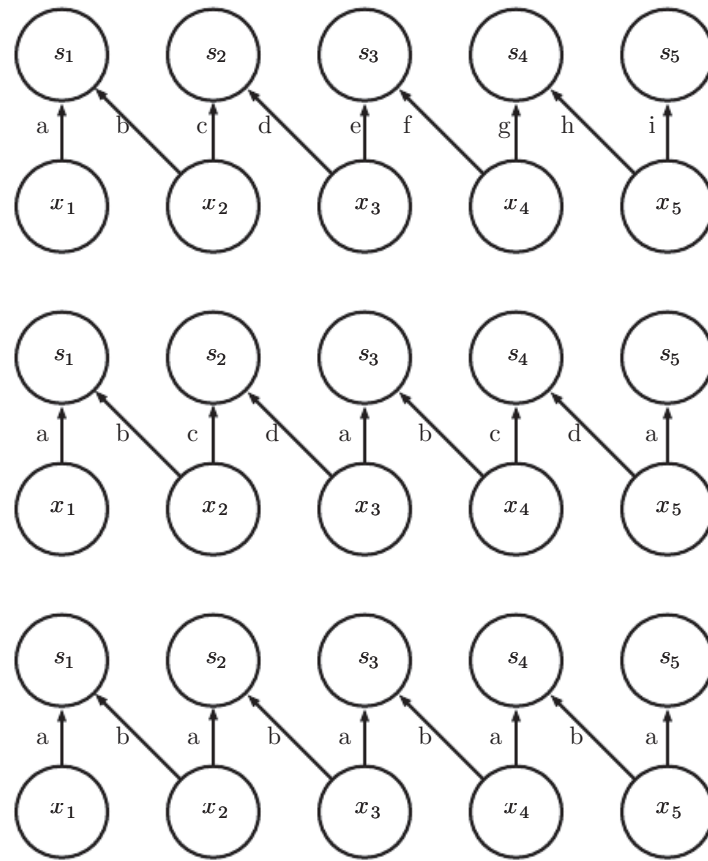


Figure 9.16: A comparison of locally connected layers, tiled convolution, and standard convolution. All three have the same sets of connections between units, when the same size of kernel is used. This diagram illustrates the use of a kernel that is two pixels wide. The differences between the methods lies in how they share parameters. *(Top)*A locally connected layer has no sharing at all. We indicate that each connection has its own weight by labeling each connection with a unique letter. *(Center)*Tiled convolution has a set of t different kernels. Here we illustrate the case of $t = 2$. One of these kernels has edges labeled “a” and “b,” while the other has edges labeled “c” and “d.” Each time we move one pixel to the right in the output, we move on to using a different kernel. This means that, like the locally connected layer, neighboring units in the output have different parameters. Unlike the locally connected layer, after we have gone through all t available kernels, we cycle back to the first kernel. If two output units are separated by a multiple of t steps, then they share parameters. *(Bottom)*Traditional convolution is equivalent to tiled convolution with $t = 1$. There is only one kernel and it is applied everywhere, as indicated in the diagram by using the kernel with weights labeled “a” and “b” everywhere.

To define tiled convolution algebraically, let k be a 6-D tensor, where two of the dimensions correspond to different locations in the output map. Rather than having a separate index for each location in the output map, output locations cycle through a set of t different choices of kernel stack in each direction. If t is equal to the output width, this is the same as a locally connected layer.

$$Z_{i,j,k} = \sum_{l,m,n} V_{l,j+m-1,k+n-1} K_{i,l,m,n,j \% t+1,k \% t+1}, \quad (9.10)$$

where $\%$ is the modulo operation, with $t \% t = 0$, $(t + 1) \% t = 1$, etc. It is straightforward to generalize this equation to use a different tiling range for each dimension.

Both locally connected layers and tiled convolutional layers have an interesting interaction with max-pooling: the detector units of these layers are driven by different filters. If these filters learn to detect different transformed versions of the same underlying features, then the max-pooled units become invariant to the learned transformation (see figure 9.9). Convolutional layers are hard-coded to be invariant specifically to translation.

Other operations besides convolution are usually necessary to implement a convolutional network. To perform learning, one must be able to compute the gradient with respect to the kernel, given the gradient with respect to the outputs. In some simple cases, this operation can be performed using the convolution operation, but many cases of interest, including the case of stride greater than 1, do not have this property.

Recall that convolution is a linear operation and can thus be described as a matrix multiplication (if we first reshape the input tensor into a flat vector). The matrix involved is a function of the convolution kernel. The matrix is sparse and each element of the kernel is copied to several elements of the matrix. This view helps us to derive some of the other operations needed to implement a convolutional network.

Multiplication by the transpose of the matrix defined by convolution is one such operation. This is the operation needed to back-propagate error derivatives through a convolutional layer, so it is needed to train convolutional networks that have more than one hidden layer. This same operation is also needed if we wish to reconstruct the visible units from the hidden units (Simard *et al.*, 1992). Reconstructing the visible units is an operation commonly used in the models described in part III of this book, such as autoencoders, RBMs, and sparse coding.

Transpose convolution is necessary to construct convolutional versions of those models. Like the kernel gradient operation, this input gradient operation can be

implemented using a convolution in some cases, but in the general case requires a third operation to be implemented. Care must be taken to coordinate this transpose operation with the forward propagation. The size of the output that the transpose operation should return depends on the zero padding policy and stride of the forward propagation operation, as well as the size of the forward propagation's output map. In some cases, multiple sizes of input to forward propagation can result in the same size of output map, so the transpose operation must be explicitly told what the size of the original input was.

These three operations—convolution, backprop from output to weights, and backprop from output to inputs—are sufficient to compute all of the gradients needed to train any depth of feedforward convolutional network, as well as to train convolutional networks with reconstruction functions based on the transpose of convolution. See [Goodfellow \(2010\)](#) for a full derivation of the equations in the fully general multi-dimensional, multi-example case. To give a sense of how these equations work, we present the two dimensional, single example version here.

Suppose we want to train a convolutional network that incorporates strided convolution of kernel stack \mathbf{K} applied to multi-channel image \mathbf{V} with stride s as defined by $c(\mathbf{K}, \mathbf{V}, s)$ as in equation 9.8. Suppose we want to minimize some loss function $J(\mathbf{V}, \mathbf{K})$. During forward propagation, we will need to use c itself to output \mathbf{Z} , which is then propagated through the rest of the network and used to compute the cost function J . During back-propagation, we will receive a tensor \mathbf{G} such that $G_{i,j,k} = \frac{\partial}{\partial Z_{i,j,k}} J(\mathbf{V}, \mathbf{K})$.

To train the network, we need to compute the derivatives with respect to the weights in the kernel. To do so, we can use a function

$$g(\mathbf{G}, \mathbf{V}, s)_{i,j,k,l} = \frac{\partial}{\partial K_{i,j,k,l}} J(\mathbf{V}, \mathbf{K}) = \sum_{m,n} G_{i,m,n} V_{j,(m-1)\times s+k, (n-1)\times s+l}. \quad (9.11)$$

If this layer is not the bottom layer of the network, we will need to compute the gradient with respect to \mathbf{V} in order to back-propagate the error farther down. To do so, we can use a function

$$h(\mathbf{K}, \mathbf{G}, s)_{i,j,k} = \frac{\partial}{\partial V_{i,j,k}} J(\mathbf{V}, \mathbf{K}) \quad (9.12)$$

$$= \sum_{\substack{l,m \\ \text{s.t.} \\ (l-1)\times s+m=j}} \sum_{\substack{n,p \\ \text{s.t.} \\ (n-1)\times s+p=k}} \sum_q K_{q,i,m,p} G_{q,l,n}. \quad (9.13)$$

Autoencoder networks, described in chapter 14, are feedforward networks trained to copy their input to their output. A simple example is the PCA algorithm,

that copies its input \mathbf{x} to an approximate reconstruction \mathbf{r} using the function $\mathbf{W}^\top \mathbf{W}\mathbf{x}$. It is common for more general autoencoders to use multiplication by the transpose of the weight matrix just as PCA does. To make such models convolutional, we can use the function h to perform the transpose of the convolution operation. Suppose we have hidden units \mathbf{H} in the same format as \mathbf{Z} and we define a reconstruction

$$\mathbf{R} = h(\mathbf{K}, \mathbf{H}, s). \quad (9.14)$$

In order to train the autoencoder, we will receive the gradient with respect to \mathbf{R} as a tensor \mathbf{E} . To train the decoder, we need to obtain the gradient with respect to \mathbf{K} . This is given by $g(\mathbf{H}, \mathbf{E}, s)$. To train the encoder, we need to obtain the gradient with respect to \mathbf{H} . This is given by $c(\mathbf{K}, \mathbf{E}, s)$. It is also possible to differentiate through g using c and h , but these operations are not needed for the back-propagation algorithm on any standard network architectures.

Generally, we do not use only a linear operation in order to transform from the inputs to the outputs in a convolutional layer. We generally also add some bias term to each output before applying the nonlinearity. This raises the question of how to share parameters among the biases. For locally connected layers it is natural to give each unit its own bias, and for tiled convolution, it is natural to share the biases with the same tiling pattern as the kernels. For convolutional layers, it is typical to have one bias per channel of the output and share it across all locations within each convolution map. However, if the input is of known, fixed size, it is also possible to learn a separate bias at each location of the output map. Separating the biases may slightly reduce the statistical efficiency of the model, but also allows the model to correct for differences in the image statistics at different locations. For example, when using implicit zero padding, detector units at the edge of the image receive less total input and may need larger biases.

9.6 Structured Outputs

Convolutional networks can be used to output a high-dimensional, structured object, rather than just predicting a class label for a classification task or a real value for a regression task. Typically this object is just a tensor, emitted by a standard convolutional layer. For example, the model might emit a tensor \mathbf{S} , where $S_{i,j,k}$ is the probability that pixel (j, k) of the input to the network belongs to class i . This allows the model to label every pixel in an image and draw precise masks that follow the outlines of individual objects.

One issue that often comes up is that the output plane can be smaller than the

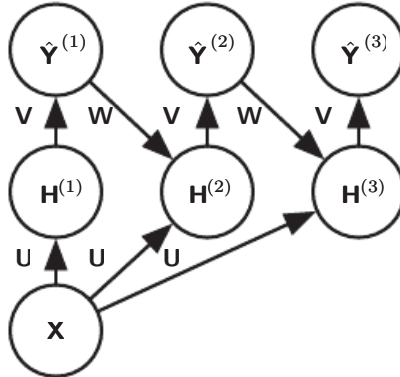


Figure 9.17: An example of a recurrent convolutional network for pixel labeling. The input is an image tensor \mathbf{X} , with axes corresponding to image rows, image columns, and channels (red, green, blue). The goal is to output a tensor of labels $\hat{\mathbf{Y}}$, with a probability distribution over labels for each pixel. This tensor has axes corresponding to image rows, image columns, and the different classes. Rather than outputting $\hat{\mathbf{Y}}$ in a single shot, the recurrent network iteratively refines its estimate $\hat{\mathbf{Y}}$ by using a previous estimate of $\hat{\mathbf{Y}}$ as input for creating a new estimate. The same parameters are used for each updated estimate, and the estimate can be refined as many times as we wish. The tensor of convolution kernels \mathbf{U} is used on each step to compute the hidden representation given the input image. The kernel tensor \mathbf{V} is used to produce an estimate of the labels given the hidden values. On all but the first step, the kernels \mathbf{W} are convolved over $\hat{\mathbf{Y}}$ to provide input to the hidden layer. On the first time step, this term is replaced by zero. Because the same parameters are used on each step, this is an example of a recurrent network, as described in chapter 10.

input plane, as shown in figure 9.13. In the kinds of architectures typically used for classification of a single object in an image, the greatest reduction in the spatial dimensions of the network comes from using pooling layers with large stride. In order to produce an output map of similar size as the input, one can avoid pooling altogether (Jain *et al.*, 2007). Another strategy is to simply emit a lower-resolution grid of labels (Pinheiro and Collobert, 2014, 2015). Finally, in principle, one could use a pooling operator with unit stride.

One strategy for pixel-wise labeling of images is to produce an initial guess of the image labels, then refine this initial guess using the interactions between neighboring pixels. Repeating this refinement step several times corresponds to using the same convolutions at each stage, sharing weights between the last layers of the deep net (Jain *et al.*, 2007). This makes the sequence of computations performed by the successive convolutional layers with weights shared across layers a particular kind of recurrent network (Pinheiro and Collobert, 2014, 2015). Figure 9.17 shows the architecture of such a recurrent convolutional network.

Once a prediction for each pixel is made, various methods can be used to further process these predictions in order to obtain a segmentation of the image into regions (Briggman *et al.*, 2009; Turaga *et al.*, 2010; Farabet *et al.*, 2013). The general idea is to assume that large groups of contiguous pixels tend to be associated with the same label. Graphical models can describe the probabilistic relationships between neighboring pixels. Alternatively, the convolutional network can be trained to maximize an approximation of the graphical model training objective (Ning *et al.*, 2005; Thompson *et al.*, 2014).

9.7 Data Types

The data used with a convolutional network usually consists of several channels, each channel being the observation of a different quantity at some point in space or time. See table 9.1 for examples of data types with different dimensionalities and number of channels.

For an example of convolutional networks applied to video, see Chen *et al.* (2010).

So far we have discussed only the case where every example in the train and test data has the same spatial dimensions. One advantage to convolutional networks is that they can also process inputs with varying spatial extents. These kinds of input simply cannot be represented by traditional, matrix multiplication-based neural networks. This provides a compelling reason to use convolutional networks even when computational cost and overfitting are not significant issues.

For example, consider a collection of images, where each image has a different width and height. It is unclear how to model such inputs with a weight matrix of fixed size. Convolution is straightforward to apply; the kernel is simply applied a different number of times depending on the size of the input, and the output of the convolution operation scales accordingly. Convolution may be viewed as matrix multiplication; the same convolution kernel induces a different size of doubly block circulant matrix for each size of input. Sometimes the output of the network is allowed to have variable size as well as the input, for example if we want to assign a class label to each pixel of the input. In this case, no further design work is necessary. In other cases, the network must produce some fixed-size output, for example if we want to assign a single class label to the entire image. In this case we must make some additional design steps, like inserting a pooling layer whose pooling regions scale in size proportional to the size of the input, in order to maintain a fixed number of pooled outputs. Some examples of this kind of strategy are shown in figure 9.11.

	Single channel	Multi-channel
1-D	Audio waveform: The axis we convolve over corresponds to time. We discretize time and measure the amplitude of the waveform once per time step.	Skeleton animation data: Animations of 3-D computer-rendered characters are generated by altering the pose of a “skeleton” over time. At each point in time, the pose of the character is described by a specification of the angles of each of the joints in the character’s skeleton. Each channel in the data we feed to the convolutional model represents the angle about one axis of one joint.
2-D	Audio data that has been preprocessed with a Fourier transform: We can transform the audio waveform into a 2D tensor with different rows corresponding to different frequencies and different columns corresponding to different points in time. Using convolution in the time makes the model equivariant to shifts in time. Using convolution across the frequency axis makes the model equivariant to frequency, so that the same melody played in a different octave produces the same representation but at a different height in the network’s output.	Color image data: One channel contains the red pixels, one the green pixels, and one the blue pixels. The convolution kernel moves over both the horizontal and vertical axes of the image, conferring translation equivariance in both directions.
3-D	Volumetric data: A common source of this kind of data is medical imaging technology, such as CT scans.	Color video data: One axis corresponds to time, one to the height of the video frame, and one to the width of the video frame.

Table 9.1: Examples of different formats of data that can be used with convolutional networks.

Note that the use of convolution for processing variable sized inputs only makes sense for inputs that have variable size because they contain varying amounts of observation of the same kind of thing—different lengths of recordings over time, different widths of observations over space, etc. Convolution does not make sense if the input has variable size because it can optionally include different kinds of observations. For example, if we are processing college applications, and our features consist of both grades and standardized test scores, but not every applicant took the standardized test, then it does not make sense to convolve the same weights over both the features corresponding to the grades and the features corresponding to the test scores.

9.8 Efficient Convolution Algorithms

Modern convolutional network applications often involve networks containing more than one million units. Powerful implementations exploiting parallel computation resources, as discussed in section 12.1, are essential. However, in many cases it is also possible to speed up convolution by selecting an appropriate convolution algorithm.

Convolution is equivalent to converting both the input and the kernel to the frequency domain using a Fourier transform, performing point-wise multiplication of the two signals, and converting back to the time domain using an inverse Fourier transform. For some problem sizes, this can be faster than the naive implementation of discrete convolution.

When a d -dimensional kernel can be expressed as the outer product of d vectors, one vector per dimension, the kernel is called **separable**. When the kernel is separable, naive convolution is inefficient. It is equivalent to compose d one-dimensional convolutions with each of these vectors. The composed approach is significantly faster than performing one d -dimensional convolution with their outer product. The kernel also takes fewer parameters to represent as vectors. If the kernel is w elements wide in each dimension, then naive multidimensional convolution requires $O(w^d)$ runtime and parameter storage space, while separable convolution requires $O(w \times d)$ runtime and parameter storage space. Of course, not every convolution can be represented in this way.

Devising faster ways of performing convolution or approximate convolution without harming the accuracy of the model is an active area of research. Even techniques that improve the efficiency of only forward propagation are useful because in the commercial setting, it is typical to devote more resources to deployment of a network than to its training.

9.9 Random or Unsupervised Features

Typically, the most expensive part of convolutional network training is learning the features. The output layer is usually relatively inexpensive due to the small number of features provided as input to this layer after passing through several layers of pooling. When performing supervised training with gradient descent, every gradient step requires a complete run of forward propagation and backward propagation through the entire network. One way to reduce the cost of convolutional network training is to use features that are not trained in a supervised fashion.

There are three basic strategies for obtaining convolution kernels without supervised training. One is to simply initialize them randomly. Another is to design them by hand, for example by setting each kernel to detect edges at a certain orientation or scale. Finally, one can learn the kernels with an unsupervised criterion. For example, [Coates et al. \(2011\)](#) apply k -means clustering to small image patches, then use each learned centroid as a convolution kernel. Part III describes many more unsupervised learning approaches. Learning the features with an unsupervised criterion allows them to be determined separately from the classifier layer at the top of the architecture. One can then extract the features for the entire training set just once, essentially constructing a new training set for the last layer. Learning the last layer is then typically a convex optimization problem, assuming the last layer is something like logistic regression or an SVM.

Random filters often work surprisingly well in convolutional networks ([Jarrett et al., 2009](#); [Saxe et al., 2011](#); [Pinto et al., 2011](#); [Cox and Pinto, 2011](#)). [Saxe et al. \(2011\)](#) showed that layers consisting of convolution followed by pooling naturally become frequency selective and translation invariant when assigned random weights. They argue that this provides an inexpensive way to choose the architecture of a convolutional network: first evaluate the performance of several convolutional network architectures by training only the last layer, then take the best of these architectures and train the entire architecture using a more expensive approach.

An intermediate approach is to learn the features, but using methods that do not require full forward and back-propagation at every gradient step. As with multilayer perceptrons, we use greedy layer-wise pretraining, to train the first layer in isolation, then extract all features from the first layer only once, then train the second layer in isolation given those features, and so on. Chapter 8 has described how to perform supervised greedy layer-wise pretraining, and part III extends this to greedy layer-wise pretraining using an unsupervised criterion at each layer. The canonical example of greedy layer-wise pretraining of a convolutional model is the convolutional deep belief network ([Lee et al., 2009](#)). Convolutional networks offer

us the opportunity to take the pretraining strategy one step further than is possible with multilayer perceptrons. Instead of training an entire convolutional layer at a time, we can train a model of a small patch, as Coates *et al.* (2011) do with k -means. We can then use the parameters from this patch-based model to define the kernels of a convolutional layer. This means that it is possible to use unsupervised learning to train a convolutional network *without ever using convolution during the training process*. Using this approach, we can train very large models and incur a high computational cost only at inference time (Ranzato *et al.*, 2007b; Jarrett *et al.*, 2009; Kavukcuoglu *et al.*, 2010; Coates *et al.*, 2013). This approach was popular from roughly 2007–2013, when labeled datasets were small and computational power was more limited. Today, most convolutional networks are trained in a purely supervised fashion, using full forward and back-propagation through the entire network on each training iteration.

As with other approaches to unsupervised pretraining, it remains difficult to tease apart the cause of some of the benefits seen with this approach. Unsupervised pretraining may offer some regularization relative to supervised training, or it may simply allow us to train much larger architectures due to the reduced computational cost of the learning rule.

9.10 The Neuroscientific Basis for Convolutional Networks

Convolutional networks are perhaps the greatest success story of biologically inspired artificial intelligence. Though convolutional networks have been guided by many other fields, some of the key design principles of neural networks were drawn from neuroscience.

The history of convolutional networks begins with neuroscientific experiments long before the relevant computational models were developed. Neurophysiologists David Hubel and Torsten Wiesel collaborated for several years to determine many of the most basic facts about how the mammalian vision system works (Hubel and Wiesel, 1959, 1962, 1968). Their accomplishments were eventually recognized with a Nobel prize. Their findings that have had the greatest influence on contemporary deep learning models were based on recording the activity of individual neurons in cats. They observed how neurons in the cat’s brain responded to images projected in precise locations on a screen in front of the cat. Their great discovery was that neurons in the early visual system responded most strongly to very specific patterns of light, such as precisely oriented bars, but responded hardly at all to other patterns.

Their work helped to characterize many aspects of brain function that are beyond the scope of this book. From the point of view of deep learning, we can focus on a simplified, cartoon view of brain function.

In this simplified view, we focus on a part of the brain called V1, also known as the **primary visual cortex**. V1 is the first area of the brain that begins to perform significantly advanced processing of visual input. In this cartoon view, images are formed by light arriving in the eye and stimulating the retina, the light-sensitive tissue in the back of the eye. The neurons in the retina perform some simple preprocessing of the image but do not substantially alter the way it is represented. The image then passes through the optic nerve and a brain region called the lateral geniculate nucleus. The main role, as far as we are concerned here, of both of these anatomical regions is primarily just to carry the signal from the eye to V1, which is located at the back of the head.

A convolutional network layer is designed to capture three properties of V1:

1. V1 is arranged in a spatial map. It actually has a two-dimensional structure mirroring the structure of the image in the retina. For example, light arriving at the lower half of the retina affects only the corresponding half of V1. Convolutional networks capture this property by having their features defined in terms of two dimensional maps.
2. V1 contains many **simple cells**. A simple cell's activity can to some extent be characterized by a linear function of the image in a small, spatially localized receptive field. The detector units of a convolutional network are designed to emulate these properties of simple cells.
3. V1 also contains many **complex cells**. These cells respond to features that are similar to those detected by simple cells, but complex cells are invariant to small shifts in the position of the feature. This inspires the pooling units of convolutional networks. Complex cells are also invariant to some changes in lighting that cannot be captured simply by pooling over spatial locations. These invariances have inspired some of the cross-channel pooling strategies in convolutional networks, such as maxout units ([Goodfellow et al., 2013a](#)).

Though we know the most about V1, it is generally believed that the same basic principles apply to other areas of the visual system. In our cartoon view of the visual system, the basic strategy of detection followed by pooling is repeatedly applied as we move deeper into the brain. As we pass through multiple anatomical layers of the brain, we eventually find cells that respond to some specific concept and are invariant to many transformations of the input. These cells have been

nicknamed “grandmother cells”—the idea is that a person could have a neuron that activates when seeing an image of their grandmother, regardless of whether she appears in the left or right side of the image, whether the image is a close-up of her face or zoomed out shot of her entire body, whether she is brightly lit, or in shadow, etc.

These grandmother cells have been shown to actually exist in the human brain, in a region called the medial temporal lobe (Quiroga *et al.*, 2005). Researchers tested whether individual neurons would respond to photos of famous individuals. They found what has come to be called the “Halle Berry neuron”: an individual neuron that is activated by the concept of Halle Berry. This neuron fires when a person sees a photo of Halle Berry, a drawing of Halle Berry, or even text containing the words “Halle Berry.” Of course, this has nothing to do with Halle Berry herself; other neurons responded to the presence of Bill Clinton, Jennifer Aniston, etc.

These medial temporal lobe neurons are somewhat more general than modern convolutional networks, which would not automatically generalize to identifying a person or object when reading its name. The closest analog to a convolutional network’s last layer of features is a brain area called the inferotemporal cortex (IT). When viewing an object, information flows from the retina, through the LGN, to V1, then onward to V2, then V4, then IT. This happens within the first 100ms of glimpsing an object. If a person is allowed to continue looking at the object for more time, then information will begin to flow backwards as the brain uses top-down feedback to update the activations in the lower level brain areas. However, if we interrupt the person’s gaze, and observe only the firing rates that result from the first 100ms of mostly feedforward activation, then IT proves to be very similar to a convolutional network. Convolutional networks can predict IT firing rates, and also perform very similarly to (time limited) humans on object recognition tasks (DiCarlo, 2013).

That being said, there are many differences between convolutional networks and the mammalian vision system. Some of these differences are well known to computational neuroscientists, but outside the scope of this book. Some of these differences are not yet known, because many basic questions about how the mammalian vision system works remain unanswered. As a brief list:

- The human eye is mostly very low resolution, except for a tiny patch called the **fovea**. The fovea only observes an area about the size of a thumbnail held at arms length. Though we feel as if we can see an entire scene in high resolution, this is an illusion created by the subconscious part of our brain, as it stitches together several glimpses of small areas. Most convolutional networks actually receive large full resolution photographs as input. The human brain makes

several eye movements called **saccades** to glimpse the most visually salient or task-relevant parts of a scene. Incorporating similar attention mechanisms into deep learning models is an active research direction. In the context of deep learning, attention mechanisms have been most successful for natural language processing, as described in section 12.4.5.1. Several visual models with foveation mechanisms have been developed but so far have not become the dominant approach (Larochelle and Hinton, 2010; Denil *et al.*, 2012).

- The human visual system is integrated with many other senses, such as hearing, and factors like our moods and thoughts. Convolutional networks so far are purely visual.
- The human visual system does much more than just recognize objects. It is able to understand entire scenes including many objects and relationships between objects, and processes rich 3-D geometric information needed for our bodies to interface with the world. Convolutional networks have been applied to some of these problems but these applications are in their infancy.
- Even simple brain areas like V1 are heavily impacted by feedback from higher levels. Feedback has been explored extensively in neural network models but has not yet been shown to offer a compelling improvement.
- While feedforward IT firing rates capture much of the same information as convolutional network features, it is not clear how similar the intermediate computations are. The brain probably uses very different activation and pooling functions. An individual neuron’s activation probably is not well-characterized by a single linear filter response. A recent model of V1 involves multiple quadratic filters for each neuron (Rust *et al.*, 2005). Indeed our cartoon picture of “simple cells” and “complex cells” might create a non-existent distinction; simple cells and complex cells might both be the same kind of cell but with their “parameters” enabling a continuum of behaviors ranging from what we call “simple” to what we call “complex.”

It is also worth mentioning that neuroscience has told us relatively little about how to *train* convolutional networks. Model structures with parameter sharing across multiple spatial locations date back to early connectionist models of vision (Marr and Poggio, 1976), but these models did not use the modern back-propagation algorithm and gradient descent. For example, the Neocognitron (Fukushima, 1980) incorporated most of the model architecture design elements of the modern convolutional network but relied on a layer-wise unsupervised clustering algorithm.

Lang and Hinton (1988) introduced the use of back-propagation to train **time-delay neural networks** (TDNNs). To use contemporary terminology, TDNNs are one-dimensional convolutional networks applied to time series. Back-propagation applied to these models was not inspired by any neuroscientific observation and is considered by some to be biologically implausible. Following the success of back-propagation-based training of TDNNs, (LeCun *et al.*, 1989) developed the modern convolutional network by applying the same training algorithm to 2-D convolution applied to images.

So far we have described how simple cells are roughly linear and selective for certain features, complex cells are more nonlinear and become invariant to some transformations of these simple cell features, and stacks of layers that alternate between selectivity and invariance can yield grandmother cells for very specific phenomena. We have not yet described precisely what these individual cells detect. In a deep, nonlinear network, it can be difficult to understand the function of individual cells. Simple cells in the first layer are easier to analyze, because their responses are driven by a linear function. In an artificial neural network, we can just display an image of the convolution kernel to see what the corresponding channel of a convolutional layer responds to. In a biological neural network, we do not have access to the weights themselves. Instead, we put an electrode in the neuron itself, display several samples of white noise images in front of the animal's retina, and record how each of these samples causes the neuron to activate. We can then fit a linear model to these responses in order to obtain an approximation of the neuron's weights. This approach is known as **reverse correlation** (Ringach and Shapley, 2004).

Reverse correlation shows us that most V1 cells have weights that are described by **Gabor functions**. The Gabor function describes the weight at a 2-D point in the image. We can think of an image as being a function of 2-D coordinates, $I(x, y)$. Likewise, we can think of a simple cell as sampling the image at a set of locations, defined by a set of x coordinates \mathbb{X} and a set of y coordinates, \mathbb{Y} , and applying weights that are also a function of the location, $w(x, y)$. From this point of view, the response of a simple cell to an image is given by

$$s(I) = \sum_{x \in \mathbb{X}} \sum_{y \in \mathbb{Y}} w(x, y) I(x, y). \quad (9.15)$$

Specifically, $w(x, y)$ takes the form of a Gabor function:

$$w(x, y; \alpha, \beta_x, \beta_y, f, \phi, x_0, y_0, \tau) = \alpha \exp(-\beta_x x'^2 - \beta_y y'^2) \cos(f x' + \phi), \quad (9.16)$$

where

$$x' = (x - x_0) \cos(\tau) + (y - y_0) \sin(\tau) \quad (9.17)$$

and

$$y' = -(x - x_0) \sin(\tau) + (y - y_0) \cos(\tau). \quad (9.18)$$

Here, α , β_x , β_y , f , ϕ , x_0 , y_0 , and τ are parameters that control the properties of the Gabor function. Figure 9.18 shows some examples of Gabor functions with different settings of these parameters.

The parameters x_0 , y_0 , and τ define a coordinate system. We translate and rotate x and y to form x' and y' . Specifically, the simple cell will respond to image features centered at the point (x_0, y_0) , and it will respond to changes in brightness as we move along a line rotated τ radians from the horizontal.

Viewed as a function of x' and y' , the function w then responds to changes in brightness as we move along the x' axis. It has two important factors: one is a Gaussian function and the other is a cosine function.

The Gaussian factor $\alpha \exp(-\beta_x x'^2 - \beta_y y'^2)$ can be seen as a gating term that ensures the simple cell will only respond to values near where x' and y' are both zero, in other words, near the center of the cell's receptive field. The scaling factor α adjusts the total magnitude of the simple cell's response, while β_x and β_y control how quickly its receptive field falls off.

The cosine factor $\cos(f x' + \phi)$ controls how the simple cell responds to changing brightness along the x' axis. The parameter f controls the frequency of the cosine and ϕ controls its phase offset.

Altogether, this cartoon view of simple cells means that a simple cell responds to a specific spatial frequency of brightness in a specific direction at a specific location. Simple cells are most excited when the wave of brightness in the image has the same phase as the weights. This occurs when the image is bright where the weights are positive and dark where the weights are negative. Simple cells are most inhibited when the wave of brightness is fully out of phase with the weights—when the image is dark where the weights are positive and bright where the weights are negative.

The cartoon view of a complex cell is that it computes the L^2 norm of the 2-D vector containing two simple cells' responses: $c(I) = \sqrt{s_0(I)^2 + s_1(I)^2}$. An important special case occurs when s_1 has all of the same parameters as s_0 except for ϕ , and ϕ is set such that s_1 is one quarter cycle out of phase with s_0 . In this case, s_0 and s_1 form a **quadrature pair**. A complex cell defined in this way responds when the Gaussian reweighted image $I(x, y) \exp(-\beta_x x'^2 - \beta_y y'^2)$ contains a high amplitude sinusoidal wave with frequency f in direction τ near (x_0, y_0) , *regardless of the phase offset of this wave*. In other words, the complex cell is invariant to small translations of the image in direction τ , or to negating the image

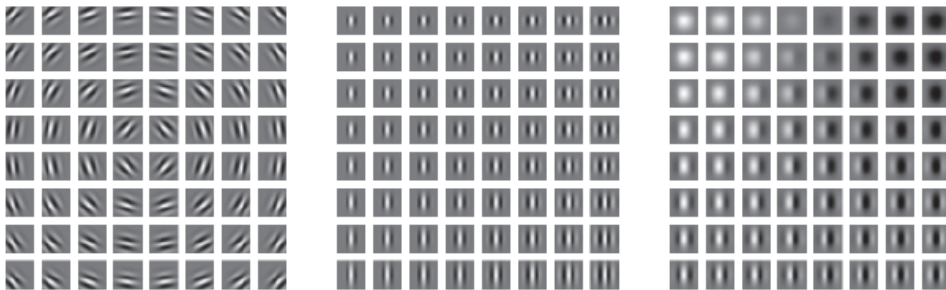


Figure 9.18: Gabor functions with a variety of parameter settings. White indicates large positive weight, black indicates large negative weight, and the background gray corresponds to zero weight. (*Left*)Gabor functions with different values of the parameters that control the coordinate system: x_0 , y_0 , and τ . Each Gabor function in this grid is assigned a value of x_0 and y_0 proportional to its position in its grid, and τ is chosen so that each Gabor filter is sensitive to the direction radiating out from the center of the grid. For the other two plots, x_0 , y_0 , and τ are fixed to zero. (*Center*)Gabor functions with different Gaussian scale parameters β_x and β_y . Gabor functions are arranged in increasing width (decreasing β_x) as we move left to right through the grid, and increasing height (decreasing β_y) as we move top to bottom. For the other two plots, the β values are fixed to $1.5 \times$ the image width. (*Right*)Gabor functions with different sinusoid parameters f and ϕ . As we move top to bottom, f increases, and as we move left to right, ϕ increases. For the other two plots, ϕ is fixed to 0 and f is fixed to $5 \times$ the image width.

(replacing black with white and vice versa).

Some of the most striking correspondences between neuroscience and machine learning come from visually comparing the features learned by machine learning models with those employed by V1. [Olshausen and Field \(1996\)](#) showed that a simple unsupervised learning algorithm, sparse coding, learns features with receptive fields similar to those of simple cells. Since then, we have found that an extremely wide variety of statistical learning algorithms learn features with Gabor-like functions when applied to natural images. This includes most deep learning algorithms, which learn these features in their first layer. Figure 9.19 shows some examples. Because so many different learning algorithms learn edge detectors, it is difficult to conclude that any specific learning algorithm is the “right” model of the brain just based on the features that it learns (though it can certainly be a bad sign if an algorithm does *not* learn some sort of edge detector when applied to natural images). These features are an important part of the statistical structure of natural images and can be recovered by many different approaches to statistical modeling. See [Hyvärinen et al. \(2009\)](#) for a review of the field of natural image statistics.

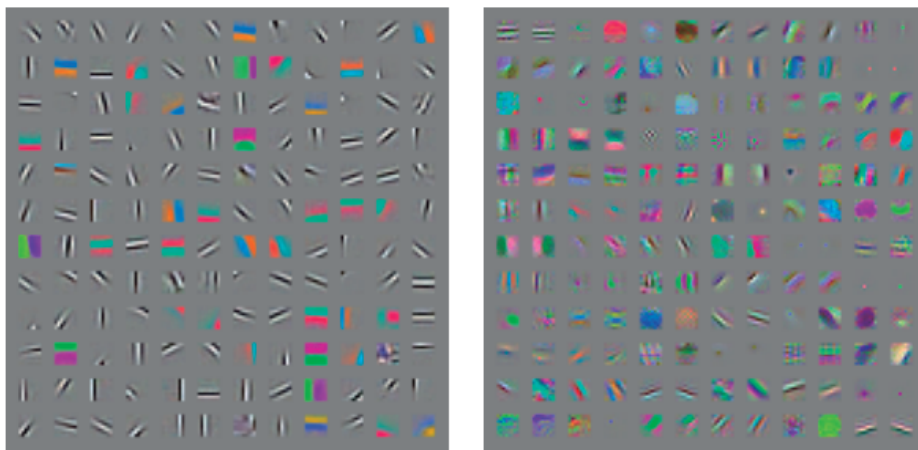


Figure 9.19: Many machine learning algorithms learn features that detect edges or specific colors of edges when applied to natural images. These feature detectors are reminiscent of the Gabor functions known to be present in primary visual cortex. (*Left*)Weights learned by an unsupervised learning algorithm (spike and slab sparse coding) applied to small image patches. (*Right*)Convolution kernels learned by the first layer of a fully supervised convolutional maxout network. Neighboring pairs of filters drive the same maxout unit.

9.11 Convolutional Networks and the History of Deep Learning

Convolutional networks have played an important role in the history of deep learning. They are a key example of a successful application of insights obtained by studying the brain to machine learning applications. They were also some of the first deep models to perform well, long before arbitrary deep models were considered viable. Convolutional networks were also some of the first neural networks to solve important commercial applications and remain at the forefront of commercial applications of deep learning today. For example, in the 1990s, the neural network research group at AT&T developed a convolutional network for reading checks (LeCun *et al.*, 1998b). By the end of the 1990s, this system deployed by NEC was reading over 10% of all the checks in the US. Later, several OCR and handwriting recognition systems based on convolutional nets were deployed by Microsoft (Simard *et al.*, 2003). See chapter 12 for more details on such applications and more modern applications of convolutional networks. See LeCun *et al.* (2010) for a more in-depth history of convolutional networks up to 2010.

Convolutional networks were also used to win many contests. The current intensity of commercial interest in deep learning began when Krizhevsky *et al.* (2012) won the ImageNet object recognition challenge, but convolutional networks

had been used to win other machine learning and computer vision contests with less impact for years earlier.

Convolutional nets were some of the first working deep networks trained with back-propagation. It is not entirely clear why convolutional networks succeeded when general back-propagation networks were considered to have failed. It may simply be that convolutional networks were more computationally efficient than fully connected networks, so it was easier to run multiple experiments with them and tune their implementation and hyperparameters. Larger networks also seem to be easier to train. With modern hardware, large fully connected networks appear to perform reasonably on many tasks, even when using datasets that were available and activation functions that were popular during the times when fully connected networks were believed not to work well. It may be that the primary barriers to the success of neural networks were psychological (practitioners did not expect neural networks to work, so they did not make a serious effort to use neural networks). Whatever the case, it is fortunate that convolutional networks performed well decades ago. In many ways, they carried the torch for the rest of deep learning and paved the way to the acceptance of neural networks in general.

Convolutional networks provide a way to specialize neural networks to work with data that has a clear grid-structured topology and to scale such models to very large size. This approach has been the most successful on a two-dimensional, image topology. To process one-dimensional, sequential data, we turn next to another powerful specialization of the neural networks framework: recurrent neural networks.

Chapter 10

Sequence Modeling: Recurrent and Recursive Nets

Recurrent neural networks or RNNs ([Rumelhart *et al.*, 1986a](#)) are a family of neural networks for processing sequential data. Much as a convolutional network is a neural network that is specialized for processing a grid of values \mathbf{X} such as an image, a recurrent neural network is a neural network that is specialized for processing a sequence of values $\mathbf{x}^{(1)}, \dots, \mathbf{x}^{(\tau)}$. Just as convolutional networks can readily scale to images with large width and height, and some convolutional networks can process images of variable size, recurrent networks can scale to much longer sequences than would be practical for networks without sequence-based specialization. Most recurrent networks can also process sequences of variable length.

To go from multi-layer networks to recurrent networks, we need to take advantage of one of the early ideas found in machine learning and statistical models of the 1980s: sharing parameters across different parts of a model. Parameter sharing makes it possible to extend and apply the model to examples of different forms (different lengths, here) and generalize across them. If we had separate parameters for each value of the time index, we could not generalize to sequence lengths not seen during training, nor share statistical strength across different sequence lengths and across different positions in time. Such sharing is particularly important when a specific piece of information can occur at multiple positions within the sequence. For example, consider the two sentences “I went to Nepal in 2009” and “In 2009, I went to Nepal.” If we ask a machine learning model to read each sentence and extract the year in which the narrator went to Nepal, we would like it to recognize the year 2009 as the relevant piece of information, whether it appears in the sixth

word or the second word of the sentence. Suppose that we trained a feedforward network that processes sentences of fixed length. A traditional fully connected feedforward network would have separate parameters for each input feature, so it would need to learn all of the rules of the language separately at each position in the sentence. By comparison, a recurrent neural network shares the same weights across several time steps.

A related idea is the use of convolution across a 1-D temporal sequence. This convolutional approach is the basis for time-delay neural networks ([Lang and Hinton, 1988](#); [Waibel *et al.*, 1989](#); [Lang *et al.*, 1990](#)). The convolution operation allows a network to share parameters across time, but is shallow. The output of convolution is a sequence where each member of the output is a function of a small number of neighboring members of the input. The idea of parameter sharing manifests in the application of the same convolution kernel at each time step. Recurrent networks share parameters in a different way. Each member of the output is a function of the previous members of the output. Each member of the output is produced using the same update rule applied to the previous outputs. This recurrent formulation results in the sharing of parameters through a very deep computational graph.

For the simplicity of exposition, we refer to RNNs as operating on a sequence that contains vectors $\mathbf{x}^{(t)}$ with the time step index t ranging from 1 to τ . In practice, recurrent networks usually operate on minibatches of such sequences, with a different sequence length τ for each member of the minibatch. We have omitted the minibatch indices to simplify notation. Moreover, the time step index need not literally refer to the passage of time in the real world. Sometimes it refers only to the position in the sequence. RNNs may also be applied in two dimensions across spatial data such as images, and even when applied to data involving time, the network may have connections that go backwards in time, provided that the entire sequence is observed before it is provided to the network.

This chapter extends the idea of a computational graph to include cycles. These cycles represent the influence of the present value of a variable on its own value at a future time step. Such computational graphs allow us to define recurrent neural networks. We then describe many different ways to construct, train, and use recurrent neural networks.

For more information on recurrent neural networks than is available in this chapter, we refer the reader to the textbook of [Graves \(2012\)](#).

10.1 Unfolding Computational Graphs

A computational graph is a way to formalize the structure of a set of computations, such as those involved in mapping inputs and parameters to outputs and loss. Please refer to section 6.5.1 for a general introduction. In this section we explain the idea of **unfolding** a recursive or recurrent computation into a computational graph that has a repetitive structure, typically corresponding to a chain of events. Unfolding this graph results in the sharing of parameters across a deep network structure.

For example, consider the classical form of a dynamical system:

$$\mathbf{s}^{(t)} = f(\mathbf{s}^{(t-1)}; \boldsymbol{\theta}), \quad (10.1)$$

where $\mathbf{s}^{(t)}$ is called the state of the system.

Equation 10.1 is recurrent because the definition of \mathbf{s} at time t refers back to the same definition at time $t - 1$.

For a finite number of time steps τ , the graph can be unfolded by applying the definition $\tau - 1$ times. For example, if we unfold equation 10.1 for $\tau = 3$ time steps, we obtain

$$\mathbf{s}^{(3)} = f(\mathbf{s}^{(2)}; \boldsymbol{\theta}) \quad (10.2)$$

$$= f(f(\mathbf{s}^{(1)}; \boldsymbol{\theta}); \boldsymbol{\theta}) \quad (10.3)$$

Unfolding the equation by repeatedly applying the definition in this way has yielded an expression that does not involve recurrence. Such an expression can now be represented by a traditional directed acyclic computational graph. The unfolded computational graph of equation 10.1 and equation 10.3 is illustrated in figure 10.1.

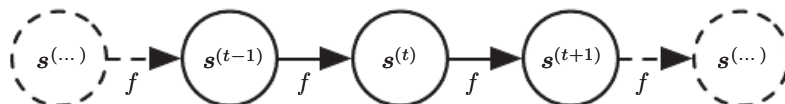


Figure 10.1: The classical dynamical system described by equation 10.1, illustrated as an unfolded computational graph. Each node represents the state at some time t and the function f maps the state at t to the state at $t + 1$. The same parameters (the same value of $\boldsymbol{\theta}$ used to parametrize f) are used for all time steps.

As another example, let us consider a dynamical system driven by an external signal $\mathbf{x}^{(t)}$,

$$\mathbf{s}^{(t)} = f(\mathbf{s}^{(t-1)}, \mathbf{x}^{(t)}; \boldsymbol{\theta}), \quad (10.4)$$

where we see that the state now contains information about the whole past sequence.

Recurrent neural networks can be built in many different ways. Much as almost any function can be considered a feedforward neural network, essentially any function involving recurrence can be considered a recurrent neural network.

Many recurrent neural networks use equation 10.5 or a similar equation to define the values of their hidden units. To indicate that the state is the hidden units of the network, we now rewrite equation 10.4 using the variable \mathbf{h} to represent the state:

$$\mathbf{h}^{(t)} = f(\mathbf{h}^{(t-1)}, \mathbf{x}^{(t)}; \boldsymbol{\theta}), \quad (10.5)$$

illustrated in figure 10.2, typical RNNs will add extra architectural features such as output layers that read information out of the state \mathbf{h} to make predictions.

When the recurrent network is trained to perform a task that requires predicting the future from the past, the network typically learns to use $\mathbf{h}^{(t)}$ as a kind of lossy summary of the task-relevant aspects of the past sequence of inputs up to t . This summary is in general necessarily lossy, since it maps an arbitrary length sequence $(\mathbf{x}^{(t)}, \mathbf{x}^{(t-1)}, \mathbf{x}^{(t-2)}, \dots, \mathbf{x}^{(2)}, \mathbf{x}^{(1)})$ to a fixed length vector $\mathbf{h}^{(t)}$. Depending on the training criterion, this summary might selectively keep some aspects of the past sequence with more precision than other aspects. For example, if the RNN is used in statistical language modeling, typically to predict the next word given previous words, it may not be necessary to store all of the information in the input sequence up to time t , but rather only enough information to predict the rest of the sentence. The most demanding situation is when we ask $\mathbf{h}^{(t)}$ to be rich enough to allow one to approximately recover the input sequence, as in autoencoder frameworks (chapter 14).

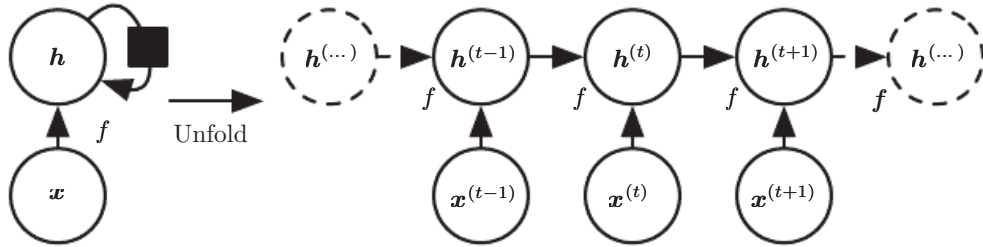


Figure 10.2: A recurrent network with no outputs. This recurrent network just processes information from the input \mathbf{x} by incorporating it into the state \mathbf{h} that is passed forward through time. (*Left*)Circuit diagram. The black square indicates a delay of a single time step. (*Right*)The same network seen as an unfolded computational graph, where each node is now associated with one particular time instance.

Equation 10.5 can be drawn in two different ways. One way to draw the RNN is with a diagram containing one node for every component that might exist in a

physical implementation of the model, such as a biological neural network. In this view, the network defines a circuit that operates in real time, with physical parts whose current state can influence their future state, as in the left of figure 10.2. Throughout this chapter, we use a black square in a circuit diagram to indicate that an interaction takes place with a delay of a single time step, from the state at time t to the state at time $t + 1$. The other way to draw the RNN is as an unfolded computational graph, in which each component is represented by many different variables, with one variable per time step, representing the state of the component at that point in time. Each variable for each time step is drawn as a separate node of the computational graph, as in the right of figure 10.2. What we call unfolding is the operation that maps a circuit as in the left side of the figure to a computational graph with repeated pieces as in the right side. The unfolded graph now has a size that depends on the sequence length.

We can represent the unfolded recurrence after t steps with a function $g^{(t)}$:

$$\mathbf{h}^{(t)} = g^{(t)}(\mathbf{x}^{(t)}, \mathbf{x}^{(t-1)}, \mathbf{x}^{(t-2)}, \dots, \mathbf{x}^{(2)}, \mathbf{x}^{(1)}) \quad (10.6)$$

$$= f(\mathbf{h}^{(t-1)}, \mathbf{x}^{(t)}; \boldsymbol{\theta}) \quad (10.7)$$

The function $g^{(t)}$ takes the whole past sequence $(\mathbf{x}^{(t)}, \mathbf{x}^{(t-1)}, \mathbf{x}^{(t-2)}, \dots, \mathbf{x}^{(2)}, \mathbf{x}^{(1)})$ as input and produces the current state, but the unfolded recurrent structure allows us to factorize $g^{(t)}$ into repeated application of a function f . The unfolding process thus introduces two major advantages:

1. Regardless of the sequence length, the learned model always has the same input size, because it is specified in terms of transition from one state to another state, rather than specified in terms of a variable-length history of states.
2. It is possible to use the *same* transition function f with the same parameters at every time step.

These two factors make it possible to learn a single model f that operates on all time steps and all sequence lengths, rather than needing to learn a separate model $g^{(t)}$ for all possible time steps. Learning a single, shared model allows generalization to sequence lengths that did not appear in the training set, and allows the model to be estimated with far fewer training examples than would be required without parameter sharing.

Both the recurrent graph and the unrolled graph have their uses. The recurrent graph is succinct. The unfolded graph provides an explicit description of which computations to perform. The unfolded graph also helps to illustrate the idea of

information flow forward in time (computing outputs and losses) and backward in time (computing gradients) by explicitly showing the path along which this information flows.

10.2 Recurrent Neural Networks

Armed with the graph unrolling and parameter sharing ideas of section 10.1, we can design a wide variety of recurrent neural networks.

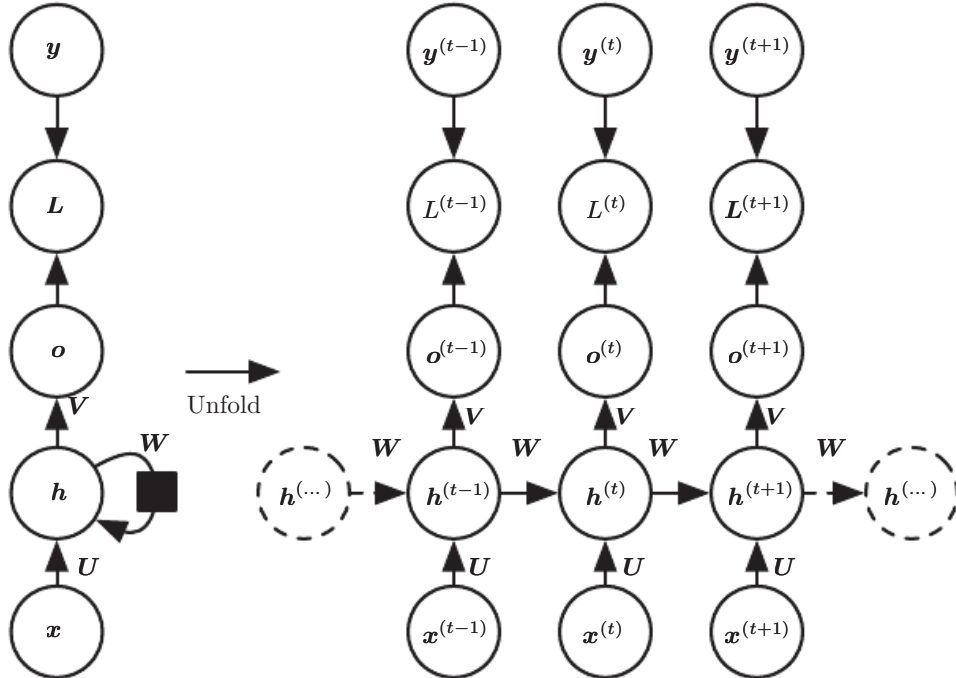


Figure 10.3: The computational graph to compute the training loss of a recurrent network that maps an input sequence of \mathbf{x} values to a corresponding sequence of output \mathbf{o} values. A loss L measures how far each \mathbf{o} is from the corresponding training target \mathbf{y} . When using softmax outputs, we assume \mathbf{o} is the unnormalized log probabilities. The loss L internally computes $\hat{\mathbf{y}} = \text{softmax}(\mathbf{o})$ and compares this to the target \mathbf{y} . The RNN has input to hidden connections parametrized by a weight matrix \mathbf{U} , hidden-to-hidden recurrent connections parametrized by a weight matrix \mathbf{W} , and hidden-to-output connections parametrized by a weight matrix \mathbf{V} . Equation 10.8 defines forward propagation in this model. (*Left*)The RNN and its loss drawn with recurrent connections. (*Right*)The same seen as an time-unfolded computational graph, where each node is now associated with one particular time instance.

Some examples of important design patterns for recurrent neural networks include the following:

- Recurrent networks that produce an output at each time step and have recurrent connections between hidden units, illustrated in figure 10.3.
- Recurrent networks that produce an output at each time step and have recurrent connections only from the output at one time step to the hidden units at the next time step, illustrated in figure 10.4
- Recurrent networks with recurrent connections between hidden units, that read an entire sequence and then produce a single output, illustrated in figure 10.5.

figure 10.3 is a reasonably representative example that we return to throughout most of the chapter.

The recurrent neural network of figure 10.3 and equation 10.8 is universal in the sense that any function computable by a Turing machine can be computed by such a recurrent network of a finite size. The output can be read from the RNN after a number of time steps that is asymptotically linear in the number of time steps used by the Turing machine and asymptotically linear in the length of the input (Siegelmann and Sontag, 1991; Siegelmann, 1995; Siegelmann and Sontag, 1995; Hyötyniemi, 1996). The functions computable by a Turing machine are discrete, so these results regard exact implementation of the function, not approximations. The RNN, when used as a Turing machine, takes a binary sequence as input and its outputs must be discretized to provide a binary output. It is possible to compute all functions in this setting using a single specific RNN of finite size (Siegelmann and Sontag (1995) use 886 units). The “input” of the Turing machine is a specification of the function to be computed, so the same network that simulates this Turing machine is sufficient for all problems. The theoretical RNN used for the proof can simulate an unbounded stack by representing its activations and weights with rational numbers of unbounded precision.

We now develop the forward propagation equations for the RNN depicted in figure 10.3. The figure does not specify the choice of activation function for the hidden units. Here we assume the hyperbolic tangent activation function. Also, the figure does not specify exactly what form the output and loss function take. Here we assume that the output is discrete, as if the RNN is used to predict words or characters. A natural way to represent discrete variables is to regard the output \mathbf{o} as giving the unnormalized log probabilities of each possible value of the discrete variable. We can then apply the softmax operation as a post-processing step to obtain a vector $\hat{\mathbf{y}}$ of normalized probabilities over the output. Forward propagation begins with a specification of the initial state $\mathbf{h}^{(0)}$. Then, for each time step from

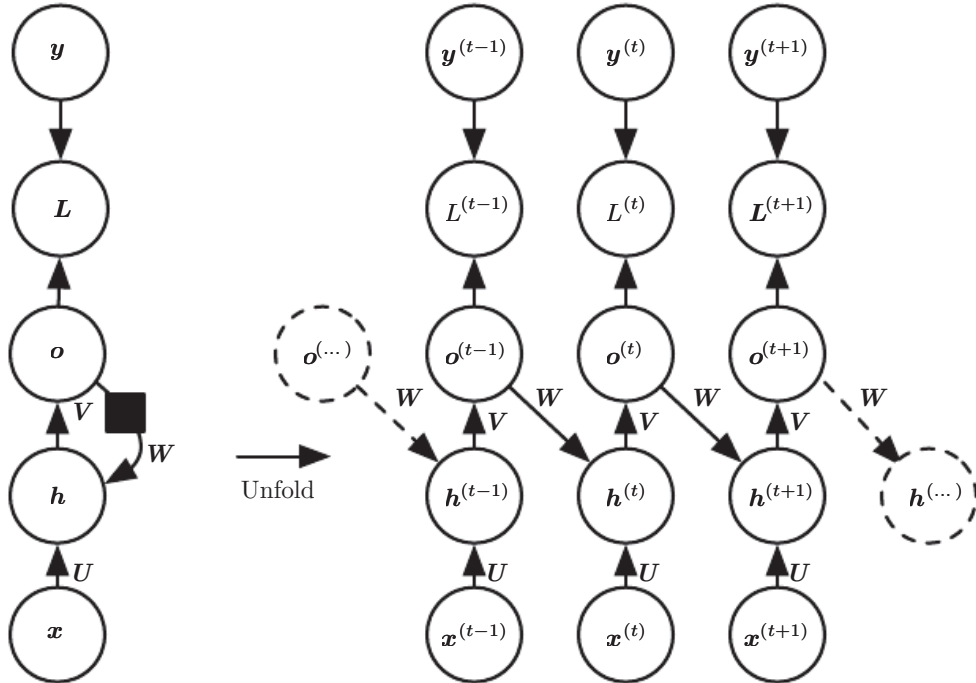


Figure 10.4: An RNN whose only recurrence is the feedback connection from the output to the hidden layer. At each time step t , the input is \mathbf{x}_t , the hidden layer activations are $\mathbf{h}^{(t)}$, the outputs are $\mathbf{o}^{(t)}$, the targets are $\mathbf{y}^{(t)}$ and the loss is $L^{(t)}$. (Left) Circuit diagram. (Right) Unfolded computational graph. Such an RNN is less powerful (can express a smaller set of functions) than those in the family represented by figure 10.3. The RNN in figure 10.3 can choose to put any information it wants about the past into its hidden representation \mathbf{h} and transmit \mathbf{h} to the future. The RNN in this figure is trained to put a specific output value into \mathbf{o} , and \mathbf{o} is the only information it is allowed to send to the future. There are no direct connections from \mathbf{h} going forward. The previous \mathbf{h} is connected to the present only indirectly, via the predictions it was used to produce. Unless \mathbf{o} is very high-dimensional and rich, it will usually lack important information from the past. This makes the RNN in this figure less powerful, but it may be easier to train because each time step can be trained in isolation from the others, allowing greater parallelization during training, as described in section 10.2.1.

$t = 1$ to $t = \tau$, we apply the following update equations:

$$\mathbf{a}^{(t)} = \mathbf{b} + \mathbf{W}\mathbf{h}^{(t-1)} + \mathbf{U}\mathbf{x}^{(t)} \quad (10.8)$$

$$\mathbf{h}^{(t)} = \tanh(\mathbf{a}^{(t)}) \quad (10.9)$$

$$\mathbf{o}^{(t)} = \mathbf{c} + \mathbf{V}\mathbf{h}^{(t)} \quad (10.10)$$

$$\hat{\mathbf{y}}^{(t)} = \text{softmax}(\mathbf{o}^{(t)}) \quad (10.11)$$

where the parameters are the bias vectors \mathbf{b} and \mathbf{c} along with the weight matrices \mathbf{U} , \mathbf{V} and \mathbf{W} , respectively for input-to-hidden, hidden-to-output and hidden-to-hidden connections. This is an example of a recurrent network that maps an input sequence to an output sequence of the same length. The total loss for a given sequence of \mathbf{x} values paired with a sequence of \mathbf{y} values would then be just the sum of the losses over all the time steps. For example, if $L^{(t)}$ is the negative log-likelihood of $y^{(t)}$ given $\mathbf{x}^{(1)}, \dots, \mathbf{x}^{(t)}$, then

$$L\left(\{\mathbf{x}^{(1)}, \dots, \mathbf{x}^{(\tau)}\}, \{\mathbf{y}^{(1)}, \dots, \mathbf{y}^{(\tau)}\}\right) \quad (10.12)$$

$$= \sum_t L^{(t)} \quad (10.13)$$

$$= - \sum_t \log p_{\text{model}}\left(y^{(t)} \mid \{\mathbf{x}^{(1)}, \dots, \mathbf{x}^{(t)}\}\right), \quad (10.14)$$

where $p_{\text{model}}(y^{(t)} \mid \{\mathbf{x}^{(1)}, \dots, \mathbf{x}^{(t)}\})$ is given by reading the entry for $y^{(t)}$ from the model's output vector $\hat{\mathbf{y}}^{(t)}$. Computing the gradient of this loss function with respect to the parameters is an expensive operation. The gradient computation involves performing a forward propagation pass moving left to right through our illustration of the unrolled graph in figure 10.3, followed by a backward propagation pass moving right to left through the graph. The runtime is $O(\tau)$ and cannot be reduced by parallelization because the forward propagation graph is inherently sequential; each time step may only be computed after the previous one. States computed in the forward pass must be stored until they are reused during the backward pass, so the memory cost is also $O(\tau)$. The back-propagation algorithm applied to the unrolled graph with $O(\tau)$ cost is called **back-propagation through time** or BPTT and is discussed further in section 10.2.2. The network with recurrence between hidden units is thus very powerful but also expensive to train. Is there an alternative?

10.2.1 Teacher Forcing and Networks with Output Recurrence

The network with recurrent connections only from the output at one time step to the hidden units at the next time step (shown in figure 10.4) is strictly less powerful

because it lacks hidden-to-hidden recurrent connections. For example, it cannot simulate a universal Turing machine. Because this network lacks hidden-to-hidden recurrence, it requires that the output units capture all of the information about the past that the network will use to predict the future. Because the output units are explicitly trained to match the training set targets, they are unlikely to capture the necessary information about the past history of the input, unless the user knows how to describe the full state of the system and provides it as part of the training set targets. The advantage of eliminating hidden-to-hidden recurrence is that, for any loss function based on comparing the prediction at time t to the training target at time t , all the time steps are decoupled. Training can thus be parallelized, with the gradient for each step t computed in isolation. There is no need to compute the output for the previous time step first, because the training set provides the ideal value of that output.

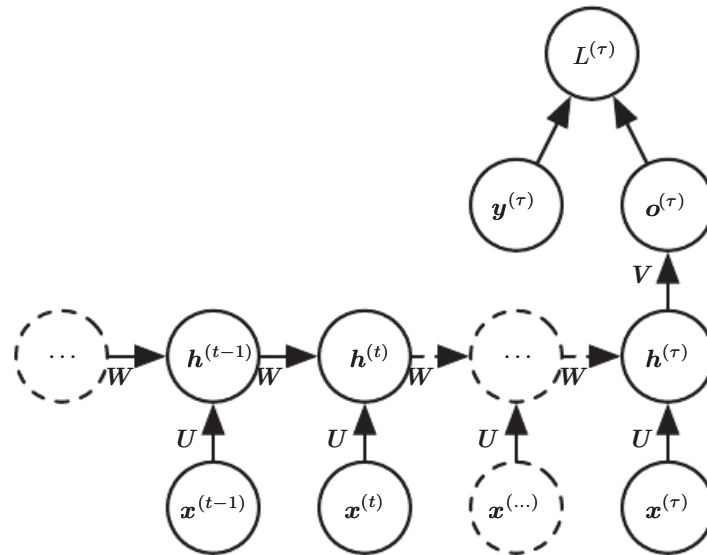


Figure 10.5: Time-unfolded recurrent neural network with a single output at the end of the sequence. Such a network can be used to summarize a sequence and produce a fixed-size representation used as input for further processing. There might be a target right at the end (as depicted here) or the gradient on the output $\mathbf{o}^{(t)}$ can be obtained by back-propagating from further downstream modules.

Models that have recurrent connections from their outputs leading back into the model may be trained with **teacher forcing**. Teacher forcing is a procedure that emerges from the maximum likelihood criterion, in which during training the model receives the ground truth output $y^{(t)}$ as input at time $t + 1$. We can see this by examining a sequence with two time steps. The conditional maximum

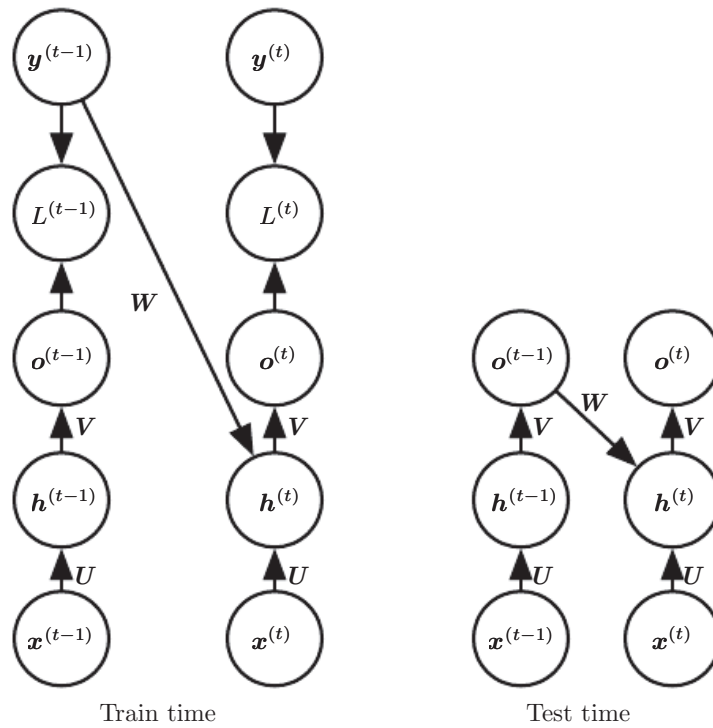


Figure 10.6: Illustration of teacher forcing. Teacher forcing is a training technique that is applicable to RNNs that have connections from their output to their hidden states at the next time step. (*Left*) At train time, we feed the *correct output* $\mathbf{y}^{(t)}$ drawn from the train set as input to $\mathbf{h}^{(t+1)}$. (*Right*) When the model is deployed, the true output is generally not known. In this case, we approximate the correct output $\mathbf{y}^{(t)}$ with the model's output $\mathbf{o}^{(t)}$, and feed the output back into the model.

likelihood criterion is

$$\log p(\mathbf{y}^{(1)}, \mathbf{y}^{(2)} | \mathbf{x}^{(1)}, \mathbf{x}^{(2)}) \quad (10.15)$$

$$= \log p(\mathbf{y}^{(2)} | \mathbf{y}^{(1)}, \mathbf{x}^{(1)}, \mathbf{x}^{(2)}) + \log p(\mathbf{y}^{(1)} | \mathbf{x}^{(1)}, \mathbf{x}^{(2)}) \quad (10.16)$$

In this example, we see that at time $t = 2$, the model is trained to maximize the conditional probability of $\mathbf{y}^{(2)}$ given *both* the \mathbf{x} sequence so far and the previous \mathbf{y} value from the training set. Maximum likelihood thus specifies that during training, rather than feeding the model's own output back into itself, these connections should be fed with the target values specifying what the correct output should be. This is illustrated in figure 10.6.

We originally motivated teacher forcing as allowing us to avoid back-propagation through time in models that lack hidden-to-hidden connections. Teacher forcing may still be applied to models that have hidden-to-hidden connections so long as they have connections from the output at one time step to values computed in the next time step. However, as soon as the hidden units become a function of earlier time steps, the BPTT algorithm is necessary. Some models may thus be trained with both teacher forcing and BPTT.

The disadvantage of strict teacher forcing arises if the network is going to be later used in an **open-loop** mode, with the network outputs (or samples from the output distribution) fed back as input. In this case, the kind of inputs that the network sees during training could be quite different from the kind of inputs that it will see at test time. One way to mitigate this problem is to train with both teacher-forced inputs and with free-running inputs, for example by predicting the correct target a number of steps in the future through the unfolded recurrent output-to-input paths. In this way, the network can learn to take into account input conditions (such as those it generates itself in the free-running mode) not seen during training and how to map the state back towards one that will make the network generate proper outputs after a few steps. Another approach (Bengio *et al.*, 2015b) to mitigate the gap between the inputs seen at train time and the inputs seen at test time randomly chooses to use generated values or actual data values as input. This approach exploits a curriculum learning strategy to gradually use more of the generated values as input.

10.2.2 Computing the Gradient in a Recurrent Neural Network

Computing the gradient through a recurrent neural network is straightforward. One simply applies the generalized back-propagation algorithm of section 6.5.6

to the unrolled computational graph. No specialized algorithms are necessary. Gradients obtained by back-propagation may then be used with any general-purpose gradient-based techniques to train an RNN.

To gain some intuition for how the BPTT algorithm behaves, we provide an example of how to compute gradients by BPTT for the RNN equations above (equation 10.8 and equation 10.12). The nodes of our computational graph include the parameters \mathbf{U} , \mathbf{V} , \mathbf{W} , \mathbf{b} and \mathbf{c} as well as the sequence of nodes indexed by t for $\mathbf{x}^{(t)}$, $\mathbf{h}^{(t)}$, $\mathbf{o}^{(t)}$ and $L^{(t)}$. For each node \mathbf{N} we need to compute the gradient $\nabla_{\mathbf{N}} L$ recursively, based on the gradient computed at nodes that follow it in the graph. We start the recursion with the nodes immediately preceding the final loss

$$\frac{\partial L}{\partial L^{(t)}} = 1. \quad (10.17)$$

In this derivation we assume that the outputs $\mathbf{o}^{(t)}$ are used as the argument to the softmax function to obtain the vector $\hat{\mathbf{y}}$ of probabilities over the output. We also assume that the loss is the negative log-likelihood of the true target $y^{(t)}$ given the input so far. The gradient $\nabla_{\mathbf{o}^{(t)}} L$ on the outputs at time step t , for all i, t , is as follows:

$$(\nabla_{\mathbf{o}^{(t)}} L)_i = \frac{\partial L}{\partial o_i^{(t)}} = \frac{\partial L}{\partial L^{(t)}} \frac{\partial L^{(t)}}{\partial o_i^{(t)}} = \hat{y}_i^{(t)} - \mathbf{1}_{i,y^{(t)}}. \quad (10.18)$$

We work our way backwards, starting from the end of the sequence. At the final time step τ , $\mathbf{h}^{(\tau)}$ only has $\mathbf{o}^{(\tau)}$ as a descendent, so its gradient is simple:

$$\nabla_{\mathbf{h}^{(\tau)}} L = \mathbf{V}^\top \nabla_{\mathbf{o}^{(\tau)}} L. \quad (10.19)$$

We can then iterate backwards in time to back-propagate gradients through time, from $t = \tau - 1$ down to $t = 1$, noting that $\mathbf{h}^{(t)}$ (for $t < \tau$) has as descendants both $\mathbf{o}^{(t)}$ and $\mathbf{h}^{(t+1)}$. Its gradient is thus given by

$$\nabla_{\mathbf{h}^{(t)}} L = \left(\frac{\partial \mathbf{h}^{(t+1)}}{\partial \mathbf{h}^{(t)}} \right)^\top (\nabla_{\mathbf{h}^{(t+1)}} L) + \left(\frac{\partial \mathbf{o}^{(t)}}{\partial \mathbf{h}^{(t)}} \right)^\top (\nabla_{\mathbf{o}^{(t)}} L) \quad (10.20)$$

$$= \mathbf{W}^\top (\nabla_{\mathbf{h}^{(t+1)}} L) \text{diag} \left(1 - (\mathbf{h}^{(t+1)})^2 \right) + \mathbf{V}^\top (\nabla_{\mathbf{o}^{(t)}} L) \quad (10.21)$$

where $\text{diag} \left(1 - (\mathbf{h}^{(t+1)})^2 \right)$ indicates the diagonal matrix containing the elements $1 - (h_i^{(t+1)})^2$. This is the Jacobian of the hyperbolic tangent associated with the hidden unit i at time $t + 1$.

Once the gradients on the internal nodes of the computational graph are obtained, we can obtain the gradients on the parameter nodes. Because the parameters are shared across many time steps, we must take some care when denoting calculus operations involving these variables. The equations we wish to implement use the `bprop` method of section 6.5.6, that computes the contribution of a single edge in the computational graph to the gradient. However, the $\nabla_{\mathbf{W}} f$ operator used in calculus takes into account the contribution of \mathbf{W} to the value of f due to *all* edges in the computational graph. To resolve this ambiguity, we introduce dummy variables $\mathbf{W}^{(t)}$ that are defined to be copies of \mathbf{W} but with each $\mathbf{W}^{(t)}$ used only at time step t . We may then use $\nabla_{\mathbf{W}^{(t)}}$ to denote the contribution of the weights at time step t to the gradient.

Using this notation, the gradient on the remaining parameters is given by:

$$\nabla_{\mathbf{c}} L = \sum_t \left(\frac{\partial \mathbf{o}^{(t)}}{\partial \mathbf{c}} \right)^\top \nabla_{\mathbf{o}^{(t)}} L = \sum_t \nabla_{\mathbf{o}^{(t)}} L \quad (10.22)$$

$$\nabla_{\mathbf{b}} L = \sum_t \left(\frac{\partial \mathbf{h}^{(t)}}{\partial \mathbf{b}^{(t)}} \right)^\top \nabla_{\mathbf{h}^{(t)}} L = \sum_t \text{diag} \left(1 - (\mathbf{h}^{(t)})^2 \right) \nabla_{\mathbf{h}^{(t)}} L \quad (10.23)$$

$$\nabla_{\mathbf{V}} L = \sum_t \sum_i \left(\frac{\partial L}{\partial o_i^{(t)}} \right) \nabla_{\mathbf{V}} o_i^{(t)} = \sum_t (\nabla_{\mathbf{o}^{(t)}} L) \mathbf{h}^{(t)^\top} \quad (10.24)$$

$$\nabla_{\mathbf{W}} L = \sum_t \sum_i \left(\frac{\partial L}{\partial h_i^{(t)}} \right) \nabla_{\mathbf{W}^{(t)}} h_i^{(t)} \quad (10.25)$$

$$= \sum_t \text{diag} \left(1 - (\mathbf{h}^{(t)})^2 \right) (\nabla_{\mathbf{h}^{(t)}} L) \mathbf{h}^{(t-1)^\top} \quad (10.26)$$

$$\nabla_{\mathbf{U}} L = \sum_t \sum_i \left(\frac{\partial L}{\partial h_i^{(t)}} \right) \nabla_{\mathbf{U}^{(t)}} h_i^{(t)} \quad (10.27)$$

$$= \sum_t \text{diag} \left(1 - (\mathbf{h}^{(t)})^2 \right) (\nabla_{\mathbf{h}^{(t)}} L) \mathbf{x}^{(t)^\top} \quad (10.28)$$

We do not need to compute the gradient with respect to $\mathbf{x}^{(t)}$ for training because it does not have any parameters as ancestors in the computational graph defining the loss.

10.2.3 Recurrent Networks as Directed Graphical Models

In the example recurrent network we have developed so far, the losses $L^{(t)}$ were cross-entropies between training targets $\mathbf{y}^{(t)}$ and outputs $\mathbf{o}^{(t)}$. As with a feedforward network, it is in principle possible to use almost any loss with a recurrent network. The loss should be chosen based on the task. As with a feedforward network, we usually wish to interpret the output of the RNN as a probability distribution, and we usually use the cross-entropy associated with that distribution to define the loss. Mean squared error is the cross-entropy loss associated with an output distribution that is a unit Gaussian, for example, just as with a feedforward network.

When we use a predictive log-likelihood training objective, such as equation 10.12, we train the RNN to estimate the conditional distribution of the next sequence element $\mathbf{y}^{(t)}$ given the past inputs. This may mean that we maximize the log-likelihood

$$\log p(\mathbf{y}^{(t)} | \mathbf{x}^{(1)}, \dots, \mathbf{x}^{(t)}), \quad (10.29)$$

or, if the model includes connections from the output at one time step to the next time step,

$$\log p(\mathbf{y}^{(t)} | \mathbf{x}^{(1)}, \dots, \mathbf{x}^{(t)}, \mathbf{y}^{(1)}, \dots, \mathbf{y}^{(t-1)}). \quad (10.30)$$

Decomposing the joint probability over the sequence of \mathbf{y} values as a series of one-step probabilistic predictions is one way to capture the full joint distribution across the whole sequence. When we do not feed past \mathbf{y} values as inputs that condition the next step prediction, the directed graphical model contains no edges from any $\mathbf{y}^{(i)}$ in the past to the current $\mathbf{y}^{(t)}$. In this case, the outputs \mathbf{y} are conditionally independent given the sequence of \mathbf{x} values. When we do feed the actual \mathbf{y} values (not their prediction, but the actual observed or generated values) back into the network, the directed graphical model contains edges from all $\mathbf{y}^{(i)}$ values in the past to the current $y^{(t)}$ value.

As a simple example, let us consider the case where the RNN models only a sequence of scalar random variables $\mathbb{Y} = \{y^{(1)}, \dots, y^{(\tau)}\}$, with no additional inputs \mathbf{x} . The input at time step t is simply the output at time step $t - 1$. The RNN then defines a directed graphical model over the y variables. We parametrize the joint distribution of these observations using the chain rule (equation 3.6) for conditional probabilities:

$$P(\mathbb{Y}) = P(\mathbf{y}^{(1)}, \dots, \mathbf{y}^{(\tau)}) = \prod_{t=1}^{\tau} P(\mathbf{y}^{(t)} | \mathbf{y}^{(t-1)}, \mathbf{y}^{(t-2)}, \dots, \mathbf{y}^{(1)}) \quad (10.31)$$

where the right-hand side of the bar is empty for $t = 1$, of course. Hence the negative log-likelihood of a set of values $\{y^{(1)}, \dots, y^{(\tau)}\}$ according to such a model

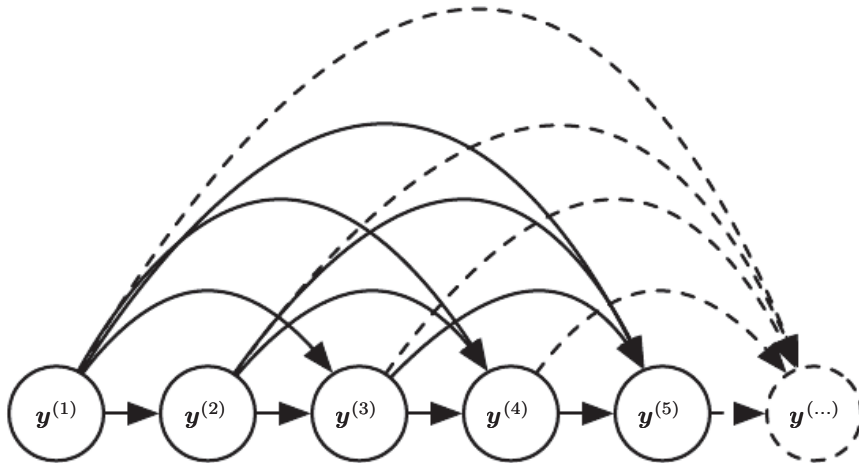


Figure 10.7: Fully connected graphical model for a sequence $y^{(1)}, y^{(2)}, \dots, y^{(t)}, \dots$: every past observation $y^{(i)}$ may influence the conditional distribution of some $y^{(t)}$ (for $t > i$), given the previous values. Parametrizing the graphical model directly according to this graph (as in equation 10.6) might be very inefficient, with an ever growing number of inputs and parameters for each element of the sequence. RNNs obtain the same full connectivity but efficient parametrization, as illustrated in figure 10.8.

is

$$L = \sum_t L^{(t)} \quad (10.32)$$

where

$$L^{(t)} = -\log P(y^{(t)} = y^{(t)} | y^{(t-1)}, y^{(t-2)}, \dots, y^{(1)}). \quad (10.33)$$

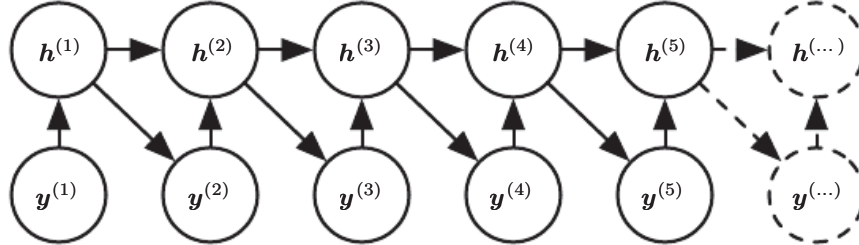


Figure 10.8: Introducing the state variable in the graphical model of the RNN, even though it is a deterministic function of its inputs, helps to see how we can obtain a very efficient parametrization, based on equation 10.5. Every stage in the sequence (for $h^{(t)}$ and $y^{(t)}$) involves the same structure (the same number of inputs for each node) and can share the same parameters with the other stages.

The edges in a graphical model indicate which variables depend directly on other variables. Many graphical models aim to achieve statistical and computational efficiency by omitting edges that do not correspond to strong interactions. For

example, it is common to make the Markov assumption that the graphical model should only contain edges from $\{y^{(t-k)}, \dots, y^{(t-1)}\}$ to $y^{(t)}$, rather than containing edges from the entire past history. However, in some cases, we believe that all past inputs should have an influence on the next element of the sequence. RNNs are useful when we believe that the distribution over $y^{(t)}$ may depend on a value of $y^{(i)}$ from the distant past in a way that is not captured by the effect of $y^{(i)}$ on $y^{(t-1)}$.

One way to interpret an RNN as a graphical model is to view the RNN as defining a graphical model whose structure is the complete graph, able to represent direct dependencies between any pair of y values. The graphical model over the y values with the complete graph structure is shown in figure 10.7. The complete graph interpretation of the RNN is based on ignoring the hidden units $\mathbf{h}^{(t)}$ by marginalizing them out of the model.

It is more interesting to consider the graphical model structure of RNNs that results from regarding the hidden units $\mathbf{h}^{(t)}$ as random variables.¹ Including the hidden units in the graphical model reveals that the RNN provides a very efficient parametrization of the joint distribution over the observations. Suppose that we represented an arbitrary joint distribution over discrete values with a tabular representation—an array containing a separate entry for each possible assignment of values, with the value of that entry giving the probability of that assignment occurring. If y can take on k different values, the tabular representation would have $O(k^T)$ parameters. By comparison, due to parameter sharing, the number of parameters in the RNN is $O(1)$ as a function of sequence length. The number of parameters in the RNN may be adjusted to control model capacity but is not forced to scale with sequence length. Equation 10.5 shows that the RNN parametrizes long-term relationships between variables efficiently, using recurrent applications of the same function f and same parameters θ at each time step. Figure 10.8 illustrates the graphical model interpretation. Incorporating the $\mathbf{h}^{(t)}$ nodes in the graphical model decouples the past and the future, acting as an intermediate quantity between them. A variable $y^{(i)}$ in the distant past may influence a variable $y^{(t)}$ via its effect on \mathbf{h} . The structure of this graph shows that the model can be efficiently parametrized by using the same conditional probability distributions at each time step, and that when the variables are all observed, the probability of the joint assignment of all variables can be evaluated efficiently.

Even with the efficient parametrization of the graphical model, some operations remain computationally challenging. For example, it is difficult to predict missing

¹The conditional distribution over these variables given their parents is deterministic. This is perfectly legitimate, though it is somewhat rare to design a graphical model with such deterministic hidden units.

values in the middle of the sequence.

The price recurrent networks pay for their reduced number of parameters is that *optimizing* the parameters may be difficult.

The parameter sharing used in recurrent networks relies on the assumption that the same parameters can be used for different time steps. Equivalently, the assumption is that the conditional probability distribution over the variables at time $t+1$ given the variables at time t is **stationary**, meaning that the relationship between the previous time step and the next time step does not depend on t . In principle, it would be possible to use t as an extra input at each time step and let the learner discover any time-dependence while sharing as much as it can between different time steps. This would already be much better than using a different conditional probability distribution for each t , but the network would then have to extrapolate when faced with new values of t .

To complete our view of an RNN as a graphical model, we must describe how to draw samples from the model. The main operation that we need to perform is simply to sample from the conditional distribution at each time step. However, there is one additional complication. The RNN must have some mechanism for determining the length of the sequence. This can be achieved in various ways.

In the case when the output is a symbol taken from a vocabulary, one can add a special symbol corresponding to the end of a sequence (Schmidhuber, 2012). When that symbol is generated, the sampling process stops. In the training set, we insert this symbol as an extra member of the sequence, immediately after $\mathbf{x}^{(\tau)}$ in each training example.

Another option is to introduce an extra Bernoulli output to the model that represents the decision to either continue generation or halt generation at each time step. This approach is more general than the approach of adding an extra symbol to the vocabulary, because it may be applied to any RNN, rather than only RNNs that output a sequence of symbols. For example, it may be applied to an RNN that emits a sequence of real numbers. The new output unit is usually a sigmoid unit trained with the cross-entropy loss. In this approach the sigmoid is trained to maximize the log-probability of the correct prediction as to whether the sequence ends or continues at each time step.

Another way to determine the sequence length τ is to add an extra output to the model that predicts the integer τ itself. The model can sample a value of τ and then sample τ steps worth of data. This approach requires adding an extra input to the recurrent update at each time step so that the recurrent update is aware of whether it is near the end of the generated sequence. This extra input can either consist of the value of τ or can consist of $\tau - t$, the number of remaining

time steps. Without this extra input, the RNN might generate sequences that end abruptly, such as a sentence that ends before it is complete. This approach is based on the decomposition

$$P(\mathbf{x}^{(1)}, \dots, \mathbf{x}^{(\tau)}) = P(\tau)P(\mathbf{x}^{(1)}, \dots, \mathbf{x}^{(\tau)} | \tau). \quad (10.34)$$

The strategy of predicting τ directly is used for example by [Goodfellow et al. \(2014d\)](#).

10.2.4 Modeling Sequences Conditioned on Context with RNNs

In the previous section we described how an RNN could correspond to a directed graphical model over a sequence of random variables $y^{(t)}$ with no inputs \mathbf{x} . Of course, our development of RNNs as in equation 10.8 included a sequence of inputs $\mathbf{x}^{(1)}, \mathbf{x}^{(2)}, \dots, \mathbf{x}^{(\tau)}$. In general, RNNs allow the extension of the graphical model view to represent not only a joint distribution over the y variables but also a conditional distribution over y given \mathbf{x} . As discussed in the context of feedforward networks in section 6.2.1.1, any model representing a variable $P(\mathbf{y}; \boldsymbol{\theta})$ can be reinterpreted as a model representing a conditional distribution $P(\mathbf{y}|\boldsymbol{\omega})$ with $\boldsymbol{\omega} = \boldsymbol{\theta}$. We can extend such a model to represent a distribution $P(\mathbf{y} | \mathbf{x})$ by using the same $P(\mathbf{y} | \boldsymbol{\omega})$ as before, but making $\boldsymbol{\omega}$ a function of \mathbf{x} . In the case of an RNN, this can be achieved in different ways. We review here the most common and obvious choices.

Previously, we have discussed RNNs that take a sequence of vectors $\mathbf{x}^{(t)}$ for $t = 1, \dots, \tau$ as input. Another option is to take only a single vector \mathbf{x} as input. When \mathbf{x} is a fixed-size vector, we can simply make it an extra input of the RNN that generates the \mathbf{y} sequence. Some common ways of providing an extra input to an RNN are:

1. as an extra input at each time step, or
2. as the initial state $\mathbf{h}^{(0)}$, or
3. both.

The first and most common approach is illustrated in figure 10.9. The interaction between the input \mathbf{x} and each hidden unit vector $\mathbf{h}^{(t)}$ is parametrized by a newly introduced weight matrix \mathbf{R} that was absent from the model of only the sequence of y values. The same product $\mathbf{x}^\top \mathbf{R}$ is added as additional input to the hidden units at every time step. We can think of the choice of \mathbf{x} as determining the value

of $\mathbf{x}^\top \mathbf{R}$ that is effectively a new bias parameter used for each of the hidden units. The weights remain independent of the input. We can think of this model as taking the parameters θ of the non-conditional model and turning them into ω , where the bias parameters within ω are now a function of the input.

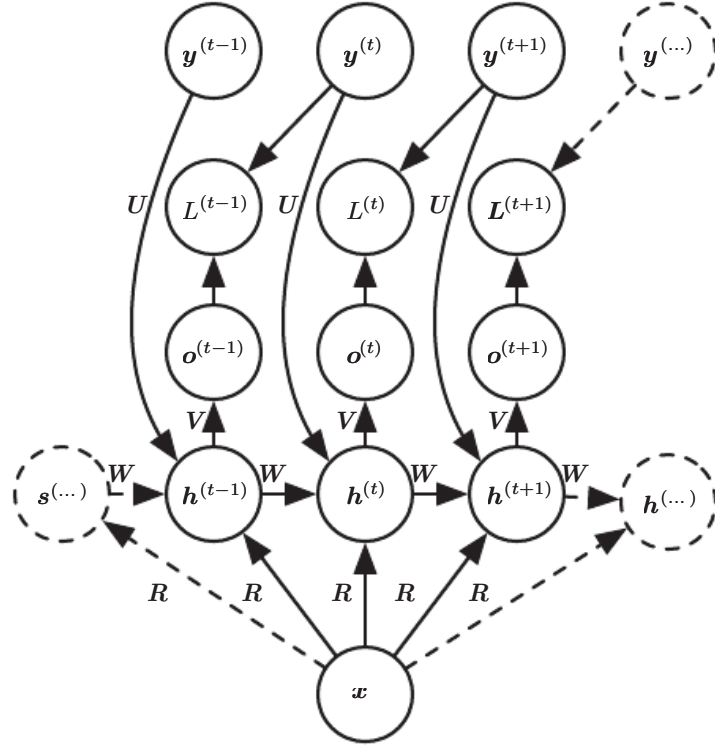


Figure 10.9: An RNN that maps a fixed-length vector \mathbf{x} into a distribution over sequences \mathbf{Y} . This RNN is appropriate for tasks such as image captioning, where a single image is used as input to a model that then produces a sequence of words describing the image. Each element $\mathbf{y}^{(t)}$ of the observed output sequence serves both as input (for the current time step) and, during training, as target (for the previous time step).

Rather than receiving only a single vector \mathbf{x} as input, the RNN may receive a sequence of vectors $\mathbf{x}^{(t)}$ as input. The RNN described in equation 10.8 corresponds to a conditional distribution $P(\mathbf{y}^{(1)}, \dots, \mathbf{y}^{(\tau)} | \mathbf{x}^{(1)}, \dots, \mathbf{x}^{(\tau)})$ that makes a conditional independence assumption that this distribution factorizes as

$$\prod_t P(\mathbf{y}^{(t)} | \mathbf{x}^{(1)}, \dots, \mathbf{x}^{(t)}). \quad (10.35)$$

To remove the conditional independence assumption, we can add connections from the output at time t to the hidden unit at time $t + 1$, as shown in figure 10.10. The model can then represent arbitrary probability distributions over the \mathbf{y} sequence. This kind of model representing a distribution over a sequence given another

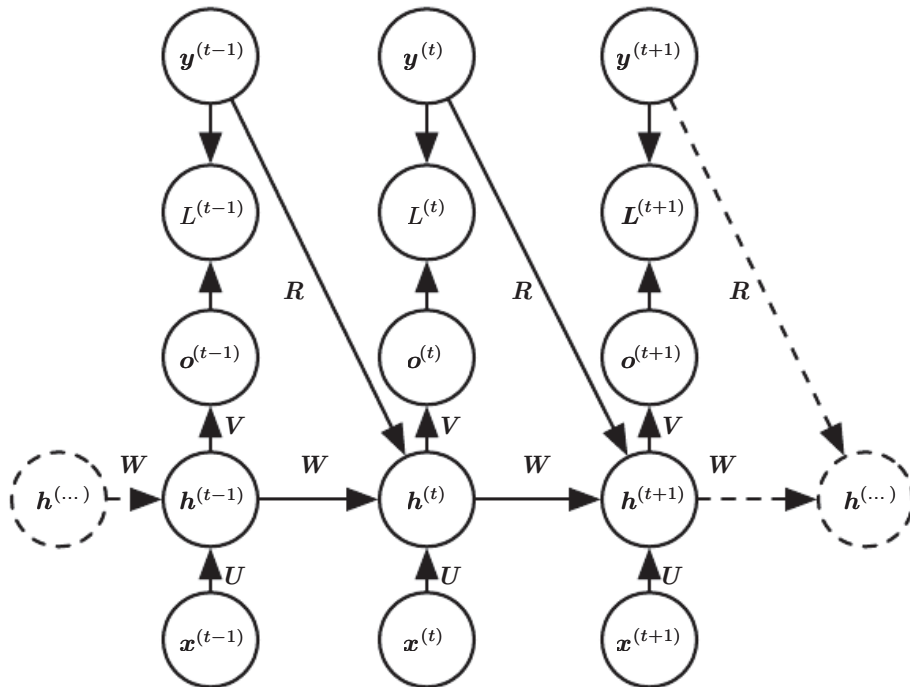


Figure 10.10: A conditional recurrent neural network mapping a variable-length sequence of \mathbf{x} values into a distribution over sequences of \mathbf{y} values of the same length. Compared to figure 10.3, this RNN contains connections from the previous output to the current state. These connections allow this RNN to model an arbitrary distribution over sequences of \mathbf{y} given sequences of \mathbf{x} of the same length. The RNN of figure 10.3 is only able to represent distributions in which the \mathbf{y} values are conditionally independent from each other given the \mathbf{x} values.

sequence still has one restriction, which is that the length of both sequences must be the same. We describe how to remove this restriction in section 10.4.

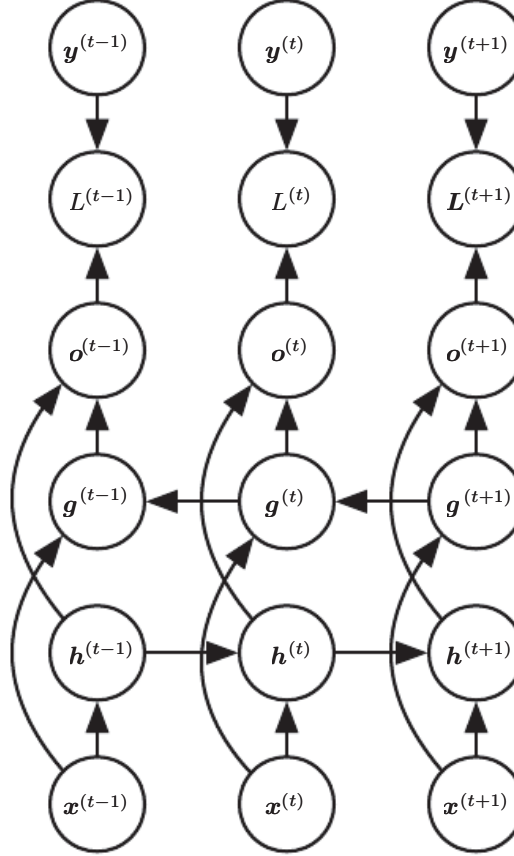


Figure 10.11: Computation of a typical bidirectional recurrent neural network, meant to learn to map input sequences \mathbf{x} to target sequences \mathbf{y} , with loss $L^{(t)}$ at each step t . The \mathbf{h} recurrence propagates information forward in time (towards the right) while the \mathbf{g} recurrence propagates information backward in time (towards the left). Thus at each point t , the output units $\mathbf{o}^{(t)}$ can benefit from a relevant summary of the past in its $\mathbf{h}^{(t)}$ input and from a relevant summary of the future in its $\mathbf{g}^{(t)}$ input.

10.3 Bidirectional RNNs

All of the recurrent networks we have considered up to now have a “causal” structure, meaning that the state at time t only captures information from the past, $\mathbf{x}^{(1)}, \dots, \mathbf{x}^{(t-1)}$, and the present input $\mathbf{x}^{(t)}$. Some of the models we have discussed also allow information from past \mathbf{y} values to affect the current state when the \mathbf{y} values are available.

However, in many applications we want to output a prediction of $\mathbf{y}^{(t)}$ which may

depend on *the whole input sequence*. For example, in speech recognition, the correct interpretation of the current sound as a phoneme may depend on the next few phonemes because of co-articulation and potentially may even depend on the next few words because of the linguistic dependencies between nearby words: if there are two interpretations of the current word that are both acoustically plausible, we may have to look far into the future (and the past) to disambiguate them. This is also true of handwriting recognition and many other sequence-to-sequence learning tasks, described in the next section.

Bidirectional recurrent neural networks (or bidirectional RNNs) were invented to address that need (Schuster and Paliwal, 1997). They have been extremely successful (Graves, 2012) in applications where that need arises, such as handwriting recognition (Graves *et al.*, 2008; Graves and Schmidhuber, 2009), speech recognition (Graves and Schmidhuber, 2005; Graves *et al.*, 2013) and bioinformatics (Baldi *et al.*, 1999).

As the name suggests, bidirectional RNNs combine an RNN that moves forward through time beginning from the start of the sequence with another RNN that moves backward through time beginning from the end of the sequence. Figure 10.11 illustrates the typical bidirectional RNN, with $\mathbf{h}^{(t)}$ standing for the state of the sub-RNN that moves forward through time and $\mathbf{g}^{(t)}$ standing for the state of the sub-RNN that moves backward through time. This allows the output units $\mathbf{o}^{(t)}$ to compute a representation that depends on *both the past and the future* but is most sensitive to the input values around time t , without having to specify a fixed-size window around t (as one would have to do with a feedforward network, a convolutional network, or a regular RNN with a fixed-size look-ahead buffer).

This idea can be naturally extended to 2-dimensional input, such as images, by having *four* RNNs, each one going in one of the four directions: up, down, left, right. At each point (i, j) of a 2-D grid, an output $O_{i,j}$ could then compute a representation that would capture mostly local information but could also depend on long-range inputs, if the RNN is able to learn to carry that information. Compared to a convolutional network, RNNs applied to images are typically more expensive but allow for long-range lateral interactions between features in the same feature map (Visin *et al.*, 2015; Kalchbrenner *et al.*, 2015). Indeed, the forward propagation equations for such RNNs may be written in a form that shows they use a convolution that computes the bottom-up input to each layer, prior to the recurrent propagation across the feature map that incorporates the lateral interactions.

10.4 Encoder-Decoder Sequence-to-Sequence Architectures

We have seen in figure 10.5 how an RNN can map an input sequence to a fixed-size vector. We have seen in figure 10.9 how an RNN can map a fixed-size vector to a sequence. We have seen in figures 10.3, 10.4, 10.10 and 10.11 how an RNN can map an input sequence to an output sequence of the same length.

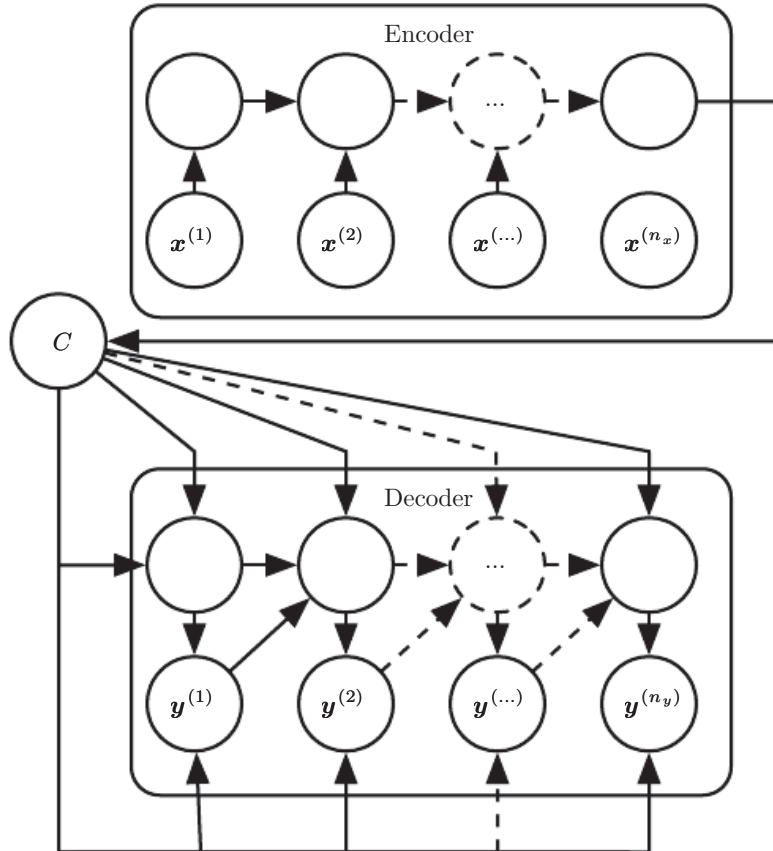


Figure 10.12: Example of an encoder-decoder or sequence-to-sequence RNN architecture, for learning to generate an output sequence $(\mathbf{y}^{(1)}, \dots, \mathbf{y}^{(n_y)})$ given an input sequence $(\mathbf{x}^{(1)}, \mathbf{x}^{(2)}, \dots, \mathbf{x}^{(n_x)})$. It is composed of an encoder RNN that reads the input sequence and a decoder RNN that generates the output sequence (or computes the probability of a given output sequence). The final hidden state of the encoder RNN is used to compute a generally fixed-size context variable C which represents a semantic summary of the input sequence and is given as input to the decoder RNN.

Here we discuss how an RNN can be trained to map an input sequence to an output sequence which is not necessarily of the same length. This comes up in many applications, such as speech recognition, machine translation or question

answering, where the input and output sequences in the training set are generally not of the same length (although their lengths might be related).

We often call the input to the RNN the “context.” We want to produce a representation of this context, C . The context C might be a vector or sequence of vectors that summarize the input sequence $\mathbf{X} = (\mathbf{x}^{(1)}, \dots, \mathbf{x}^{(n_x)})$.

The simplest RNN architecture for mapping a variable-length sequence to another variable-length sequence was first proposed by Cho *et al.* (2014a) and shortly after by Sutskever *et al.* (2014), who independently developed that architecture and were the first to obtain state-of-the-art translation using this approach. The former system is based on scoring proposals generated by another machine translation system, while the latter uses a standalone recurrent network to generate the translations. These authors respectively called this architecture, illustrated in figure 10.12, the encoder-decoder or sequence-to-sequence architecture. The idea is very simple: (1) an **encoder** or **reader** or **input** RNN processes the input sequence. The encoder emits the context C , usually as a simple function of its final hidden state. (2) a **decoder** or **writer** or **output** RNN is conditioned on that fixed-length vector (just like in figure 10.9) to generate the output sequence $\mathbf{Y} = (\mathbf{y}^{(1)}, \dots, \mathbf{y}^{(n_y)})$. The innovation of this kind of architecture over those presented in earlier sections of this chapter is that the lengths n_x and n_y can vary from each other, while previous architectures constrained $n_x = n_y = \tau$. In a sequence-to-sequence architecture, the two RNNs are trained jointly to maximize the average of $\log P(\mathbf{y}^{(1)}, \dots, \mathbf{y}^{(n_y)} | \mathbf{x}^{(1)}, \dots, \mathbf{x}^{(n_x)})$ over all the pairs of \mathbf{x} and \mathbf{y} sequences in the training set. The last state \mathbf{h}_{n_x} of the encoder RNN is typically used as a representation C of the input sequence that is provided as input to the decoder RNN.

If the context C is a vector, then the decoder RNN is simply a vector-to-sequence RNN as described in section 10.2.4. As we have seen, there are at least two ways for a vector-to-sequence RNN to receive input. The input can be provided as the initial state of the RNN, or the input can be connected to the hidden units at each time step. These two ways can also be combined.

There is no constraint that the encoder must have the same size of hidden layer as the decoder.

One clear limitation of this architecture is when the context C output by the encoder RNN has a dimension that is too small to properly summarize a long sequence. This phenomenon was observed by Bahdanau *et al.* (2015) in the context of machine translation. They proposed to make C a variable-length sequence rather than a fixed-size vector. Additionally, they introduced an **attention mechanism** that learns to associate elements of the sequence C to elements of the output

sequence. See section 12.4.5.1 for more details.

10.5 Deep Recurrent Networks

The computation in most RNNs can be decomposed into three blocks of parameters and associated transformations:

1. from the input to the hidden state,
2. from the previous hidden state to the next hidden state, and
3. from the hidden state to the output.

With the RNN architecture of figure 10.3, each of these three blocks is associated with a single weight matrix. In other words, when the network is unfolded, each of these corresponds to a shallow transformation. By a shallow transformation, we mean a transformation that would be represented by a single layer within a deep MLP. Typically this is a transformation represented by a learned affine transformation followed by a fixed nonlinearity.

Would it be advantageous to introduce depth in each of these operations? Experimental evidence ([Graves et al., 2013](#); [Pascanu et al., 2014a](#)) strongly suggests so. The experimental evidence is in agreement with the idea that we need enough depth in order to perform the required mappings. See also [Schmidhuber \(1992\)](#), [El Hihi and Bengio \(1996\)](#), or [Jaeger \(2007a\)](#) for earlier work on deep RNNs.

[Graves et al. \(2013\)](#) were the first to show a significant benefit of decomposing the state of an RNN into multiple layers as in figure 10.13 (left). We can think of the lower layers in the hierarchy depicted in figure 10.13a as playing a role in transforming the raw input into a representation that is more appropriate, at the higher levels of the hidden state. [Pascanu et al. \(2014a\)](#) go a step further and propose to have a separate MLP (possibly deep) for each of the three blocks enumerated above, as illustrated in figure 10.13b. Considerations of representational capacity suggest to allocate enough capacity in each of these three steps, but doing so by adding depth may hurt learning by making optimization difficult. In general, it is easier to optimize shallower architectures, and adding the extra depth of figure 10.13b makes the shortest path from a variable in time step t to a variable in time step $t + 1$ become longer. For example, if an MLP with a single hidden layer is used for the state-to-state transition, we have doubled the length of the shortest path between variables in any two different time steps, compared with the ordinary RNN of figure 10.3. However, as argued by [Pascanu et al. \(2014a\)](#), this

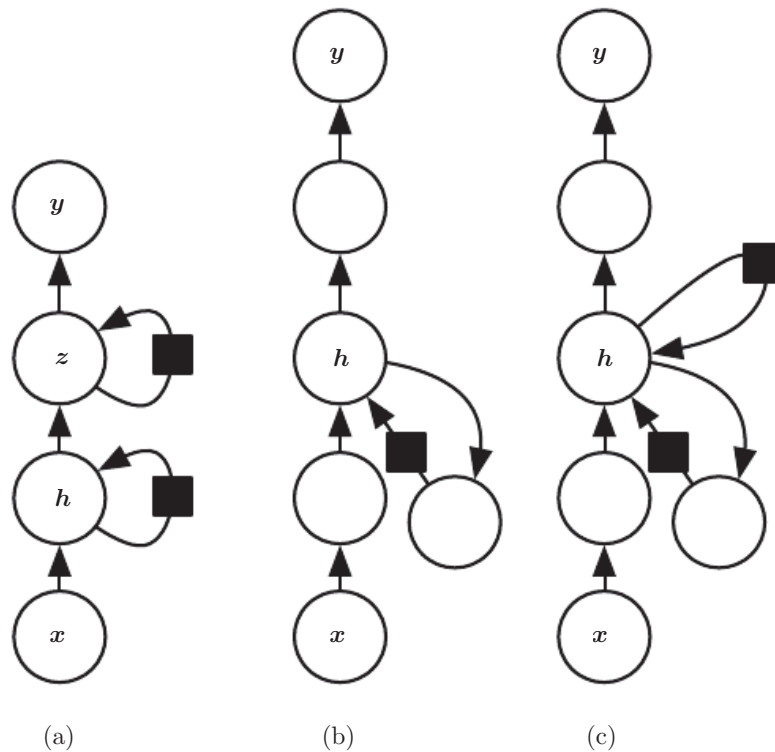


Figure 10.13: A recurrent neural network can be made deep in many ways (Pascanu *et al.*, 2014a). (a)The hidden recurrent state can be broken down into groups organized hierarchically. (b)Deeper computation (e.g., an MLP) can be introduced in the input-to-hidden, hidden-to-hidden and hidden-to-output parts. This may lengthen the shortest path linking different time steps. (c)The path-lengthening effect can be mitigated by introducing skip connections.

can be mitigated by introducing skip connections in the hidden-to-hidden path, as illustrated in figure 10.13c.

10.6 Recursive Neural Networks

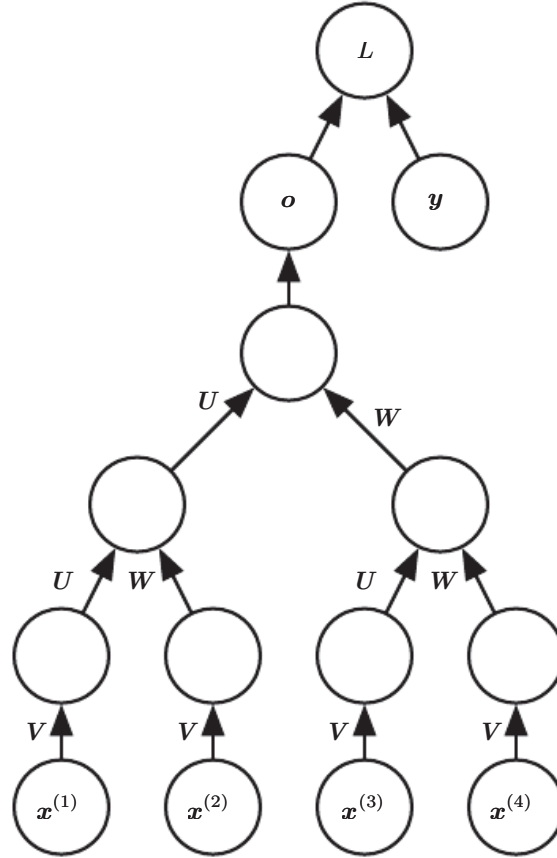


Figure 10.14: A recursive network has a computational graph that generalizes that of the recurrent network from a chain to a tree. A variable-size sequence $\mathbf{x}^{(1)}, \mathbf{x}^{(2)}, \dots, \mathbf{x}^{(t)}$ can be mapped to a fixed-size representation (the output \mathbf{o}), with a fixed set of parameters (the weight matrices $\mathbf{U}, \mathbf{V}, \mathbf{W}$). The figure illustrates a supervised learning case in which some target \mathbf{y} is provided which is associated with the whole sequence.

Recursive neural networks² represent yet another generalization of recurrent networks, with a different kind of computational graph, which is structured as a deep tree, rather than the chain-like structure of RNNs. The typical computational graph for a recursive network is illustrated in figure 10.14. Recursive neural

²We suggest to not abbreviate “recursive neural network” as “RNN” to avoid confusion with “recurrent neural network.”

networks were introduced by [Pollack \(1990\)](#) and their potential use for learning to reason was described by [Bottou \(2011\)](#). Recursive networks have been successfully applied to processing *data structures* as input to neural nets ([Frasconi et al., 1997, 1998](#)), in natural language processing ([Socher et al., 2011a,c, 2013a](#)) as well as in computer vision ([Socher et al., 2011b](#)).

One clear advantage of recursive nets over recurrent nets is that for a sequence of the same length τ , the depth (measured as the number of compositions of nonlinear operations) can be drastically reduced from τ to $O(\log \tau)$, which might help deal with long-term dependencies. An open question is how to best structure the tree. One option is to have a tree structure which does not depend on the data, such as a balanced binary tree. In some application domains, external methods can suggest the appropriate tree structure. For example, when processing natural language sentences, the tree structure for the recursive network can be fixed to the structure of the parse tree of the sentence provided by a natural language parser ([Socher et al., 2011a, 2013a](#)). Ideally, one would like the learner itself to discover and infer the tree structure that is appropriate for any given input, as suggested by [Bottou \(2011\)](#).

Many variants of the recursive net idea are possible. For example, [Frasconi et al. \(1997\)](#) and [Frasconi et al. \(1998\)](#) associate the data with a tree structure, and associate the inputs and targets with individual nodes of the tree. The computation performed by each node does not have to be the traditional artificial neuron computation (affine transformation of all inputs followed by a monotone nonlinearity). For example, [Socher et al. \(2013a\)](#) propose using tensor operations and bilinear forms, which have previously been found useful to model relationships between concepts ([Weston et al., 2010; Bordes et al., 2012](#)) when the concepts are represented by continuous vectors (embeddings).

10.7 The Challenge of Long-Term Dependencies

The mathematical challenge of learning long-term dependencies in recurrent networks was introduced in section [8.2.5](#). The basic problem is that gradients propagated over many stages tend to either vanish (most of the time) or explode (rarely, but with much damage to the optimization). Even if we assume that the parameters are such that the recurrent network is stable (can store memories, with gradients not exploding), the difficulty with long-term dependencies arises from the exponentially smaller weights given to long-term interactions (involving the multiplication of many Jacobians) compared to short-term ones. Many other sources provide a deeper treatment ([Hochreiter, 1991; Doya, 1993; Bengio et al., 1994](#)).

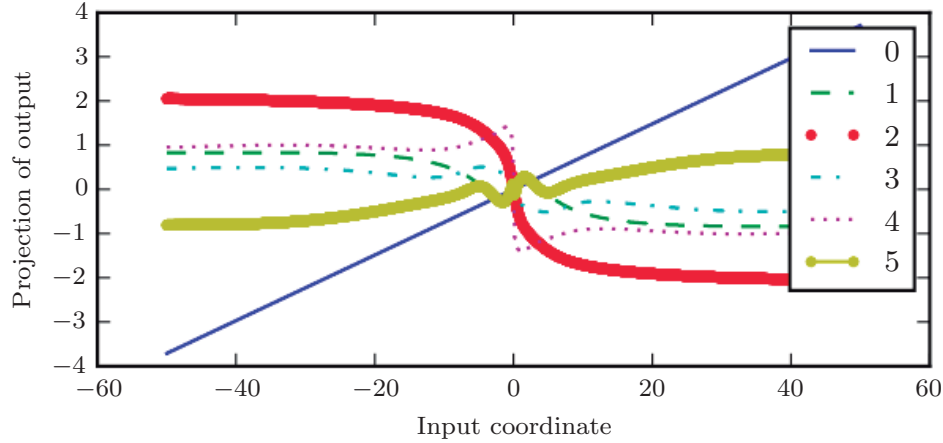


Figure 10.15: When composing many nonlinear functions (like the linear-tanh layer shown here), the result is highly nonlinear, typically with most of the values associated with a tiny derivative, some values with a large derivative, and many alternations between increasing and decreasing. In this plot, we plot a linear projection of a 100-dimensional hidden state down to a single dimension, plotted on the y -axis. The x -axis is the coordinate of the initial state along a random direction in the 100-dimensional space. We can thus view this plot as a linear cross-section of a high-dimensional function. The plots show the function after each time step, or equivalently, after each number of times the transition function has been composed.

1994; Pascanu *et al.*, 2013). In this section, we describe the problem in more detail. The remaining sections describe approaches to overcoming the problem.

Recurrent networks involve the composition of the same function multiple times, once per time step. These compositions can result in extremely nonlinear behavior, as illustrated in figure 10.15.

In particular, the function composition employed by recurrent neural networks somewhat resembles matrix multiplication. We can think of the recurrence relation

$$\mathbf{h}^{(t)} = \mathbf{W}^\top \mathbf{h}^{(t-1)} \quad (10.36)$$

as a very simple recurrent neural network lacking a nonlinear activation function, and lacking inputs \mathbf{x} . As described in section 8.2.5, this recurrence relation essentially describes the power method. It may be simplified to

$$\mathbf{h}^{(t)} = (\mathbf{W}^t)^\top \mathbf{h}^{(0)}, \quad (10.37)$$

and if \mathbf{W} admits an eigendecomposition of the form

$$\mathbf{W} = \mathbf{Q}\Lambda\mathbf{Q}^\top, \quad (10.38)$$

with orthogonal \mathbf{Q} , the recurrence may be simplified further to

$$\mathbf{h}^{(t)} = \mathbf{Q}^\top \boldsymbol{\Lambda}^t \mathbf{Q} \mathbf{h}^{(0)}. \quad (10.39)$$

The eigenvalues are raised to the power of t causing eigenvalues with magnitude less than one to decay to zero and eigenvalues with magnitude greater than one to explode. Any component of $\mathbf{h}^{(0)}$ that is not aligned with the largest eigenvector will eventually be discarded.

This problem is particular to recurrent networks. In the scalar case, imagine multiplying a weight w by itself many times. The product w^t will either vanish or explode depending on the magnitude of w . However, if we make a non-recurrent network that has a different weight $w^{(t)}$ at each time step, the situation is different. If the initial state is given by 1, then the state at time t is given by $\prod_t w^{(t)}$. Suppose that the $w^{(t)}$ values are generated randomly, independently from one another, with zero mean and variance v . The variance of the product is $O(v^n)$. To obtain some desired variance v^* we may choose the individual weights with variance $v = \sqrt[n]{v^*}$. Very deep feedforward networks with carefully chosen scaling can thus avoid the vanishing and exploding gradient problem, as argued by [Sussillo \(2014\)](#).

The vanishing and exploding gradient problem for RNNs was independently discovered by separate researchers ([Hochreiter, 1991](#); [Bengio et al., 1993, 1994](#)). One may hope that the problem can be avoided simply by staying in a region of parameter space where the gradients do not vanish or explode. Unfortunately, in order to store memories in a way that is robust to small perturbations, the RNN must enter a region of parameter space where gradients vanish ([Bengio et al., 1993, 1994](#)). Specifically, whenever the model is able to represent long term dependencies, the gradient of a long term interaction has exponentially smaller magnitude than the gradient of a short term interaction. It does not mean that it is impossible to learn, but that it might take a very long time to learn long-term dependencies, because the signal about these dependencies will tend to be hidden by the smallest fluctuations arising from short-term dependencies. In practice, the experiments in [Bengio et al. \(1994\)](#) show that as we increase the span of the dependencies that need to be captured, gradient-based optimization becomes increasingly difficult, with the probability of successful training of a traditional RNN via SGD rapidly reaching 0 for sequences of only length 10 or 20.

For a deeper treatment of recurrent networks as dynamical systems, see [Doya \(1993\)](#), [Bengio et al. \(1994\)](#) and [Siegelmann and Sontag \(1995\)](#), with a review in [Pascanu et al. \(2013\)](#). The remaining sections of this chapter discuss various approaches that have been proposed to reduce the difficulty of learning long-term dependencies (in some cases allowing an RNN to learn dependencies across

hundreds of steps), but the problem of learning long-term dependencies remains one of the main challenges in deep learning.

10.8 Echo State Networks

The recurrent weights mapping from $\mathbf{h}^{(t-1)}$ to $\mathbf{h}^{(t)}$ and the input weights mapping from $\mathbf{x}^{(t)}$ to $\mathbf{h}^{(t)}$ are some of the most difficult parameters to learn in a recurrent network. One proposed (Jaeger, 2003; Maass *et al.*, 2002; Jaeger and Haas, 2004; Jaeger, 2007b) approach to avoiding this difficulty is to set the recurrent weights such that the recurrent hidden units do a good job of capturing the history of past inputs, and *learn only the output weights*. This is the idea that was independently proposed for **echo state networks** or ESNs (Jaeger and Haas, 2004; Jaeger, 2007b) and **liquid state machines** (Maass *et al.*, 2002). The latter is similar, except that it uses spiking neurons (with binary outputs) instead of the continuous-valued hidden units used for ESNs. Both ESNs and liquid state machines are termed **reservoir computing** (Lukoševičius and Jaeger, 2009) to denote the fact that the hidden units form of reservoir of temporal features which may capture different aspects of the history of inputs.

One way to think about these reservoir computing recurrent networks is that they are similar to kernel machines: they map an arbitrary length sequence (the history of inputs up to time t) into a fixed-length vector (the recurrent state $\mathbf{h}^{(t)}$), on which a linear predictor (typically a linear regression) can be applied to solve the problem of interest. The training criterion may then be easily designed to be convex as a function of the output weights. For example, if the output consists of linear regression from the hidden units to the output targets, and the training criterion is mean squared error, then it is convex and may be solved reliably with simple learning algorithms (Jaeger, 2003).

The important question is therefore: how do we set the input and recurrent weights so that a rich set of histories can be represented in the recurrent neural network state? The answer proposed in the reservoir computing literature is to view the recurrent net as a dynamical system, and set the input and recurrent weights such that the dynamical system is near the edge of stability.

The original idea was to make the eigenvalues of the Jacobian of the state-to-state transition function be close to 1. As explained in section 8.2.5, an important characteristic of a recurrent network is the eigenvalue spectrum of the Jacobians $\mathbf{J}^{(t)} = \frac{\partial s^{(t)}}{\partial s^{(t-1)}}$. Of particular importance is the **spectral radius** of $\mathbf{J}^{(t)}$, defined to be the maximum of the absolute values of its eigenvalues.

To understand the effect of the spectral radius, consider the simple case of back-propagation with a Jacobian matrix \mathbf{J} that does not change with t . This case happens, for example, when the network is purely linear. Suppose that \mathbf{J} has an eigenvector \mathbf{v} with corresponding eigenvalue λ . Consider what happens as we propagate a gradient vector backwards through time. If we begin with a gradient vector \mathbf{g} , then after one step of back-propagation, we will have $\mathbf{J}\mathbf{g}$, and after n steps we will have $\mathbf{J}^n\mathbf{g}$. Now consider what happens if we instead back-propagate a perturbed version of \mathbf{g} . If we begin with $\mathbf{g} + \delta\mathbf{v}$, then after one step, we will have $\mathbf{J}(\mathbf{g} + \delta\mathbf{v})$. After n steps, we will have $\mathbf{J}^n(\mathbf{g} + \delta\mathbf{v})$. From this we can see that back-propagation starting from \mathbf{g} and back-propagation starting from $\mathbf{g} + \delta\mathbf{v}$ diverge by $\delta\mathbf{J}^n\mathbf{v}$ after n steps of back-propagation. If \mathbf{v} is chosen to be a unit eigenvector of \mathbf{J} with eigenvalue λ , then multiplication by the Jacobian simply scales the difference at each step. The two executions of back-propagation are separated by a distance of $\delta|\lambda|^n$. When \mathbf{v} corresponds to the largest value of $|\lambda|$, this perturbation achieves the widest possible separation of an initial perturbation of size δ .

When $|\lambda| > 1$, the deviation size $\delta|\lambda|^n$ grows exponentially large. When $|\lambda| < 1$, the deviation size becomes exponentially small.

Of course, this example assumed that the Jacobian was the same at every time step, corresponding to a recurrent network with no nonlinearity. When a nonlinearity is present, the derivative of the nonlinearity will approach zero on many time steps, and help to prevent the explosion resulting from a large spectral radius. Indeed, the most recent work on echo state networks advocates using a spectral radius much larger than unity (Yildiz *et al.*, 2012; Jaeger, 2012).

Everything we have said about back-propagation via repeated matrix multiplication applies equally to forward propagation in a network with no nonlinearity, where the state $\mathbf{h}^{(t+1)} = \mathbf{h}^{(t)\top}\mathbf{W}$.

When a linear map \mathbf{W}^\top always shrinks \mathbf{h} as measured by the L^2 norm, then we say that the map is **contractive**. When the spectral radius is less than one, the mapping from $\mathbf{h}^{(t)}$ to $\mathbf{h}^{(t+1)}$ is contractive, so a small change becomes smaller after each time step. This necessarily makes the network forget information about the past when we use a finite level of precision (such as 32 bit integers) to store the state vector.

The Jacobian matrix tells us how a small change of $\mathbf{h}^{(t)}$ propagates one step forward, or equivalently, how the gradient on $\mathbf{h}^{(t+1)}$ propagates one step backward, during back-propagation. Note that neither \mathbf{W} nor \mathbf{J} need to be symmetric (although they are square and real), so they can have complex-valued eigenvalues and eigenvectors, with imaginary components corresponding to potentially oscillatory

behavior (if the same Jacobian was applied iteratively). Even though $\mathbf{h}^{(t)}$ or a small variation of $\mathbf{h}^{(t)}$ of interest in back-propagation are real-valued, they can be expressed in such a complex-valued basis. What matters is what happens to the magnitude (complex absolute value) of these possibly complex-valued basis coefficients, when we multiply the matrix by the vector. An eigenvalue with magnitude greater than one corresponds to magnification (exponential growth, if applied iteratively) or shrinking (exponential decay, if applied iteratively).

With a nonlinear map, the Jacobian is free to change at each step. The dynamics therefore become more complicated. However, it remains true that a small initial variation can turn into a large variation after several steps. One difference between the purely linear case and the nonlinear case is that the use of a squashing nonlinearity such as tanh can cause the recurrent dynamics to become bounded. Note that it is possible for back-propagation to retain unbounded dynamics even when forward propagation has bounded dynamics, for example, when a sequence of tanh units are all in the middle of their linear regime and are connected by weight matrices with spectral radius greater than 1. However, it is rare for all of the tanh units to simultaneously lie at their linear activation point.

The strategy of echo state networks is simply to fix the weights to have some spectral radius such as 3, where information is carried forward through time but does not explode due to the stabilizing effect of saturating nonlinearities like tanh.

More recently, it has been shown that the techniques used to set the weights in ESNs could be used to *initialize* the weights in a fully trainable recurrent network (with the hidden-to-hidden recurrent weights trained using back-propagation through time), helping to learn long-term dependencies ([Sutskever, 2012](#); [Sutskever et al., 2013](#)). In this setting, an initial spectral radius of 1.2 performs well, combined with the sparse initialization scheme described in section 8.4.

10.9 Leaky Units and Other Strategies for Multiple Time Scales

One way to deal with long-term dependencies is to design a model that operates at multiple time scales, so that some parts of the model operate at fine-grained time scales and can handle small details, while other parts operate at coarse time scales and transfer information from the distant past to the present more efficiently. Various strategies for building both fine and coarse time scales are possible. These include the addition of skip connections across time, “leaky units” that integrate signals with different time constants, and the removal of some of the connections

used to model fine-grained time scales.

10.9.1 Adding Skip Connections through Time

One way to obtain coarse time scales is to add direct connections from variables in the distant past to variables in the present. The idea of using such skip connections dates back to [Lin et al. \(1996\)](#) and follows from the idea of incorporating delays in feedforward neural networks ([Lang and Hinton, 1988](#)). In an ordinary recurrent network, a recurrent connection goes from a unit at time t to a unit at time $t + 1$. It is possible to construct recurrent networks with longer delays ([Bengio, 1991](#)).

As we have seen in section [8.2.5](#), gradients may vanish or explode exponentially *with respect to the number of time steps*. [Lin et al. \(1996\)](#) introduced recurrent connections with a time-delay of d to mitigate this problem. Gradients now diminish exponentially as a function of $\frac{\tau}{d}$ rather than τ . Since there are both delayed and single step connections, gradients may still explode exponentially in τ . This allows the learning algorithm to capture longer dependencies although not all long-term dependencies may be represented well in this way.

10.9.2 Leaky Units and a Spectrum of Different Time Scales

Another way to obtain paths on which the product of derivatives is close to one is to have units with *linear* self-connections and a weight near one on these connections.

When we accumulate a running average $\mu^{(t)}$ of some value $v^{(t)}$ by applying the update $\mu^{(t)} \leftarrow \alpha\mu^{(t-1)} + (1 - \alpha)v^{(t)}$ the α parameter is an example of a linear self-connection from $\mu^{(t-1)}$ to $\mu^{(t)}$. When α is near one, the running average remembers information about the past for a long time, and when α is near zero, information about the past is rapidly discarded. Hidden units with linear self-connections can behave similarly to such running averages. Such hidden units are called **leaky units**.

Skip connections through d time steps are a way of ensuring that a unit can always learn to be influenced by a value from d time steps earlier. The use of a linear self-connection with a weight near one is a different way of ensuring that the unit can access values from the past. The linear self-connection approach allows this effect to be adapted more smoothly and flexibly by adjusting the real-valued α rather than by adjusting the integer-valued skip length.

These ideas were proposed by [Mozer \(1992\)](#) and by [El Hihi and Bengio \(1996\)](#). Leaky units were also found to be useful in the context of echo state networks ([Jaeger et al., 2007](#)).

There are two basic strategies for setting the time constants used by leaky units. One strategy is to manually fix them to values that remain constant, for example by sampling their values from some distribution once at initialization time. Another strategy is to make the time constants free parameters and learn them. Having such leaky units at different time scales appears to help with long-term dependencies (Mozer, 1992; Pascanu *et al.*, 2013).

10.9.3 Removing Connections

Another approach to handle long-term dependencies is the idea of organizing the state of the RNN at multiple time-scales (El Hihi and Bengio, 1996), with information flowing more easily through long distances at the slower time scales.

This idea differs from the skip connections through time discussed earlier because it involves actively *removing* length-one connections and replacing them with longer connections. Units modified in such a way are forced to operate on a long time scale. Skip connections through time *add* edges. Units receiving such new connections may learn to operate on a long time scale but may also choose to focus on their other short-term connections.

There are different ways in which a group of recurrent units can be forced to operate at different time scales. One option is to make the recurrent units leaky, but to have different groups of units associated with different fixed time scales. This was the proposal in Mozer (1992) and has been successfully used in Pascanu *et al.* (2013). Another option is to have explicit and discrete updates taking place at different times, with a different frequency for different groups of units. This is the approach of El Hihi and Bengio (1996) and Koutnik *et al.* (2014). It worked well on a number of benchmark datasets.

10.10 The Long Short-Term Memory and Other Gated RNNs

As of this writing, the most effective sequence models used in practical applications are called **gated RNNs**. These include the **long short-term memory** and networks based on the **gated recurrent unit**.

Like leaky units, gated RNNs are based on the idea of creating paths through time that have derivatives that neither vanish nor explode. Leaky units did this with connection weights that were either manually chosen constants or were parameters. Gated RNNs generalize this to connection weights that may change

at each time step.

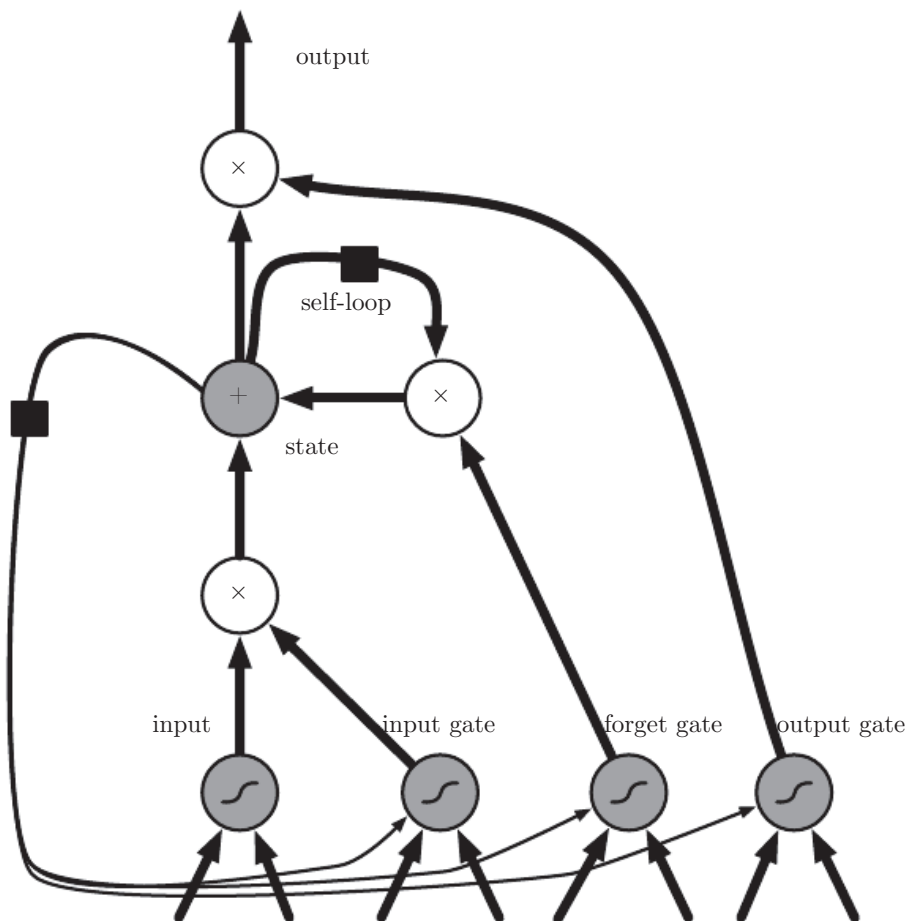


Figure 10.16: Block diagram of the LSTM recurrent network “cell.” Cells are connected recurrently to each other, replacing the usual hidden units of ordinary recurrent networks. An input feature is computed with a regular artificial neuron unit. Its value can be accumulated into the state if the sigmoidal input gate allows it. The state unit has a linear self-loop whose weight is controlled by the forget gate. The output of the cell can be shut off by the output gate. All the gating units have a sigmoid nonlinearity, while the input unit can have any squashing nonlinearity. The state unit can also be used as an extra input to the gating units. The black square indicates a delay of a single time step.

Leaky units allow the network to *accumulate* information (such as evidence for a particular feature or category) over a long duration. However, once that information has been used, it might be useful for the neural network to *forget* the old state. For example, if a sequence is made of sub-sequences and we want a leaky unit to accumulate evidence inside each sub-subsequence, we need a mechanism to forget the old state by setting it to zero. Instead of manually deciding when to clear the state, we want the neural network to learn to decide when to do it. This

is what gated RNNs do.

10.10.1 LSTM

The clever idea of introducing self-loops to produce paths where the gradient can flow for long durations is a core contribution of the initial **long short-term memory (LSTM)** model (Hochreiter and Schmidhuber, 1997). A crucial addition has been to make the weight on this self-loop conditioned on the context, rather than fixed (Gers *et al.*, 2000). By making the weight of this self-loop gated (controlled by another hidden unit), the time scale of integration can be changed dynamically. In this case, we mean that even for an LSTM with fixed parameters, the time scale of integration can change based on the input sequence, because the time constants are output by the model itself. The LSTM has been found extremely successful in many applications, such as unconstrained handwriting recognition (Graves *et al.*, 2009), speech recognition (Graves *et al.*, 2013; Graves and Jaitly, 2014), handwriting generation (Graves, 2013), machine translation (Sutskever *et al.*, 2014), image captioning (Kiros *et al.*, 2014b; Vinyals *et al.*, 2014b; Xu *et al.*, 2015) and parsing (Vinyals *et al.*, 2014a).

The LSTM block diagram is illustrated in figure 10.16. The corresponding forward propagation equations are given below, in the case of a shallow recurrent network architecture. Deeper architectures have also been successfully used (Graves *et al.*, 2013; Pascanu *et al.*, 2014a). Instead of a unit that simply applies an element-wise nonlinearity to the affine transformation of inputs and recurrent units, LSTM recurrent networks have “LSTM cells” that have an internal recurrence (a self-loop), in addition to the outer recurrence of the RNN. Each cell has the same inputs and outputs as an ordinary recurrent network, but has more parameters and a system of gating units that controls the flow of information. The most important component is the state unit $s_i^{(t)}$ that has a linear self-loop similar to the leaky units described in the previous section. However, here, the self-loop weight (or the associated time constant) is controlled by a **forget gate** unit $f_i^{(t)}$ (for time step t and cell i), that sets this weight to a value between 0 and 1 via a sigmoid unit:

$$f_i^{(t)} = \sigma \left(b_i^f + \sum_j U_{i,j}^f x_j^{(t)} + \sum_j W_{i,j}^f h_j^{(t-1)} \right), \quad (10.40)$$

where $\mathbf{x}^{(t)}$ is the current input vector and $\mathbf{h}^{(t)}$ is the current hidden layer vector, containing the outputs of all the LSTM cells, and \mathbf{b}^f , \mathbf{U}^f , \mathbf{W}^f are respectively biases, input weights and recurrent weights for the forget gates. The LSTM cell

internal state is thus updated as follows, but with a conditional self-loop weight $f_i^{(t)}$:

$$s_i^{(t)} = f_i^{(t)} s_i^{(t-1)} + g_i^{(t)} \sigma \left(b_i + \sum_j U_{i,j} x_j^{(t)} + \sum_j W_{i,j} h_j^{(t-1)} \right), \quad (10.41)$$

where \mathbf{b} , \mathbf{U} and \mathbf{W} respectively denote the biases, input weights and recurrent weights into the LSTM cell. The **external input gate** unit $g_i^{(t)}$ is computed similarly to the forget gate (with a sigmoid unit to obtain a gating value between 0 and 1), but with its own parameters:

$$g_i^{(t)} = \sigma \left(b_i^g + \sum_j U_{i,j}^g x_j^{(t)} + \sum_j W_{i,j}^g h_j^{(t-1)} \right). \quad (10.42)$$

The output $h_i^{(t)}$ of the LSTM cell can also be shut off, via the **output gate** $q_i^{(t)}$, which also uses a sigmoid unit for gating:

$$h_i^{(t)} = \tanh(s_i^{(t)}) q_i^{(t)} \quad (10.43)$$

$$q_i^{(t)} = \sigma \left(b_i^o + \sum_j U_{i,j}^o x_j^{(t)} + \sum_j W_{i,j}^o h_j^{(t-1)} \right) \quad (10.44)$$

which has parameters \mathbf{b}^o , \mathbf{U}^o , \mathbf{W}^o for its biases, input weights and recurrent weights, respectively. Among the variants, one can choose to use the cell state $s_i^{(t)}$ as an extra input (with its weight) into the three gates of the i -th unit, as shown in figure 10.16. This would require three additional parameters.

LSTM networks have been shown to learn long-term dependencies more easily than the simple recurrent architectures, first on artificial data sets designed for testing the ability to learn long-term dependencies (Bengio *et al.*, 1994; Hochreiter and Schmidhuber, 1997; Hochreiter *et al.*, 2001), then on challenging sequence processing tasks where state-of-the-art performance was obtained (Graves, 2012; Graves *et al.*, 2013; Sutskever *et al.*, 2014). Variants and alternatives to the LSTM have been studied and used and are discussed next.

10.10.2 Other Gated RNNs

Which pieces of the LSTM architecture are actually necessary? What other successful architectures could be designed that allow the network to dynamically control the time scale and forgetting behavior of different units?

Some answers to these questions are given with the recent work on gated RNNs, whose units are also known as gated recurrent units or GRUs ([Cho et al., 2014b](#); [Chung et al., 2014, 2015a](#); [Jozefowicz et al., 2015](#); [Chrupala et al., 2015](#)). The main difference with the LSTM is that a single gating unit simultaneously controls the forgetting factor and the decision to update the state unit. The update equations are the following:

$$h_i^{(t)} = u_i^{(t-1)} h_i^{(t-1)} + (1 - u_i^{(t-1)}) \sigma \left(b_i + \sum_j U_{i,j} x_j^{(t-1)} + \sum_j W_{i,j} r_j^{(t-1)} h_j^{(t-1)} \right), \quad (10.45)$$

where \mathbf{u} stands for “update” gate and \mathbf{r} for “reset” gate. Their value is defined as usual:

$$u_i^{(t)} = \sigma \left(b_i^u + \sum_j U_{i,j}^u x_j^{(t)} + \sum_j W_{i,j}^u h_j^{(t)} \right) \quad (10.46)$$

and

$$r_i^{(t)} = \sigma \left(b_i^r + \sum_j U_{i,j}^r x_j^{(t)} + \sum_j W_{i,j}^r h_j^{(t)} \right). \quad (10.47)$$

The reset and updates gates can individually “ignore” parts of the state vector. The update gates act like conditional leaky integrators that can linearly gate any dimension, thus choosing to copy it (at one extreme of the sigmoid) or completely ignore it (at the other extreme) by replacing it by the new “target state” value (towards which the leaky integrator wants to converge). The reset gates control which parts of the state get used to compute the next target state, introducing an additional nonlinear effect in the relationship between past state and future state.

Many more variants around this theme can be designed. For example the reset gate (or forget gate) output could be shared across multiple hidden units. Alternately, the product of a global gate (covering a whole group of units, such as an entire layer) and a local gate (per unit) could be used to combine global control and local control. However, several investigations over architectural variations of the LSTM and GRU found no variant that would clearly beat both of these across a wide range of tasks ([Greff et al., 2015](#); [Jozefowicz et al., 2015](#)). Greff *et al.* (2015) found that a crucial ingredient is the forget gate, while Jozefowicz *et al.* (2015) found that adding a bias of 1 to the LSTM forget gate, a practice advocated by Gers *et al.* (2000), makes the LSTM as strong as the best of the explored architectural variants.

10.11 Optimization for Long-Term Dependencies

Section 8.2.5 and section 10.7 have described the vanishing and exploding gradient problems that occur when optimizing RNNs over many time steps.

An interesting idea proposed by [Martens and Sutskever \(2011\)](#) is that second derivatives may vanish at the same time that first derivatives vanish. Second-order optimization algorithms may roughly be understood as dividing the first derivative by the second derivative (in higher dimension, multiplying the gradient by the inverse Hessian). If the second derivative shrinks at a similar rate to the first derivative, then the ratio of first and second derivatives may remain relatively constant. Unfortunately, second-order methods have many drawbacks, including high computational cost, the need for a large minibatch, and a tendency to be attracted to saddle points. [Martens and Sutskever \(2011\)](#) found promising results using second-order methods. Later, [Sutskever et al. \(2013\)](#) found that simpler methods such as Nesterov momentum with careful initialization could achieve similar results. See [Sutskever \(2012\)](#) for more detail. Both of these approaches have largely been replaced by simply using SGD (even without momentum) applied to LSTMs. This is part of a continuing theme in machine learning that it is often much easier to design a model that is easy to optimize than it is to design a more powerful optimization algorithm.

10.11.1 Clipping Gradients

As discussed in section 8.2.4, strongly nonlinear functions such as those computed by a recurrent net over many time steps tend to have derivatives that can be either very large or very small in magnitude. This is illustrated in figure 8.3 and figure 10.17, in which we see that the objective function (as a function of the parameters) has a “landscape” in which one finds “cliffs”: wide and rather flat regions separated by tiny regions where the objective function changes quickly, forming a kind of cliff.

The difficulty that arises is that when the parameter gradient is very large, a gradient descent parameter update could throw the parameters very far, into a region where the objective function is larger, undoing much of the work that had been done to reach the current solution. The gradient tells us the direction that corresponds to the steepest descent within an infinitesimal region surrounding the current parameters. Outside of this infinitesimal region, the cost function may begin to curve back upwards. The update must be chosen to be small enough to avoid traversing too much upward curvature. We typically use learning rates that

decay slowly enough that consecutive steps have approximately the same learning rate. A step size that is appropriate for a relatively linear part of the landscape is often inappropriate and causes uphill motion if we enter a more curved part of the landscape on the next step.

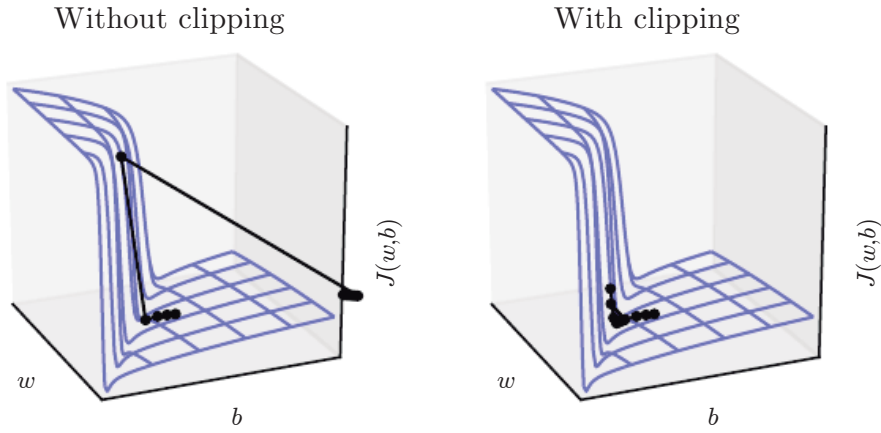


Figure 10.17: Example of the effect of gradient clipping in a recurrent network with two parameters \mathbf{w} and \mathbf{b} . Gradient clipping can make gradient descent perform more reasonably in the vicinity of extremely steep cliffs. These steep cliffs commonly occur in recurrent networks near where a recurrent network behaves approximately linearly. The cliff is exponentially steep in the number of time steps because the weight matrix is multiplied by itself once for each time step. (*Left*)Gradient descent without gradient clipping overshoots the bottom of this small ravine, then receives a very large gradient from the cliff face. The large gradient catastrophically propels the parameters outside the axes of the plot. (*Right*)Gradient descent with gradient clipping has a more moderate reaction to the cliff. While it does ascend the cliff face, the step size is restricted so that it cannot be propelled away from steep region near the solution. Figure adapted with permission from [Pascanu et al. \(2013\)](#).

A simple type of solution has been in use by practitioners for many years: **clipping the gradient**. There are different instances of this idea ([Mikolov, 2012](#); [Pascanu et al., 2013](#)). One option is to clip the parameter gradient from a minibatch *element-wise* ([Mikolov, 2012](#)) just before the parameter update. Another is to *clip the norm* $\|\mathbf{g}\|$ of the gradient \mathbf{g} ([Pascanu et al., 2013](#)) just before the parameter update:

$$\text{if } \|\mathbf{g}\| > v \quad (10.48)$$

$$\mathbf{g} \leftarrow \frac{\mathbf{g}v}{\|\mathbf{g}\|} \quad (10.49)$$

where v is the norm threshold and \mathbf{g} is used to update parameters. Because the gradient of all the parameters (including different groups of parameters, such as weights and biases) is renormalized jointly with a single scaling factor, the latter method has the advantage that it guarantees that each step is still in the gradient direction, but experiments suggest that both forms work similarly. Although the parameter update has the same direction as the true gradient, with gradient norm clipping, the parameter update vector norm is now bounded. This bounded gradient avoids performing a detrimental step when the gradient explodes. In fact, even simply taking a *random step* when the gradient magnitude is above a threshold tends to work almost as well. If the explosion is so severe that the gradient is numerically `Inf` or `Nan` (considered infinite or not-a-number), then a random step of size v can be taken and will typically move away from the numerically unstable configuration. Clipping the gradient norm per-minibatch will not change the direction of the gradient for an individual minibatch. However, taking the average of the norm-clipped gradient from many minibatches is not equivalent to clipping the norm of the true gradient (the gradient formed from using all examples). Examples that have large gradient norm, as well as examples that appear in the same minibatch as such examples, will have their contribution to the final direction diminished. This stands in contrast to traditional minibatch gradient descent, where the true gradient direction is equal to the average over all minibatch gradients. Put another way, traditional stochastic gradient descent uses an unbiased estimate of the gradient, while gradient descent with norm clipping introduces a heuristic bias that we know empirically to be useful. With element-wise clipping, the direction of the update is not aligned with the true gradient or the minibatch gradient, but it is still a descent direction. It has also been proposed (Graves, 2013) to clip the back-propagated gradient (with respect to hidden units) but no comparison has been published between these variants; we conjecture that all these methods behave similarly.

10.11.2 Regularizing to Encourage Information Flow

Gradient clipping helps to deal with exploding gradients, but it does not help with vanishing gradients. To address vanishing gradients and better capture long-term dependencies, we discussed the idea of creating paths in the computational graph of the unfolded recurrent architecture along which the product of gradients associated with arcs is near 1. One approach to achieve this is with LSTMs and other self-loops and gating mechanisms, described above in section 10.10. Another idea is to regularize or constrain the parameters so as to encourage “information flow.” In particular, we would like the gradient vector $\nabla_{\mathbf{h}^{(t)}} L$ being back-propagated to

maintain its magnitude, even if the loss function only penalizes the output at the end of the sequence. Formally, we want

$$(\nabla_{\mathbf{h}^{(t)}} L) \frac{\partial \mathbf{h}^{(t)}}{\partial \mathbf{h}^{(t-1)}} \quad (10.50)$$

to be as large as

$$\nabla_{\mathbf{h}^{(t)}} L. \quad (10.51)$$

With this objective, [Pascanu et al. \(2013\)](#) propose the following regularizer:

$$\Omega = \sum_t \left(\frac{\left| (\nabla_{\mathbf{h}^{(t)}} L) \frac{\partial \mathbf{h}^{(t)}}{\partial \mathbf{h}^{(t-1)}} \right|}{\|\nabla_{\mathbf{h}^{(t)}} L\|} - 1 \right)^2. \quad (10.52)$$

Computing the gradient of this regularizer may appear difficult, but [Pascanu et al. \(2013\)](#) propose an approximation in which we consider the back-propagated vectors $\nabla_{\mathbf{h}^{(t)}} L$ as if they were constants (for the purpose of this regularizer, so that there is no need to back-propagate through them). The experiments with this regularizer suggest that, if combined with the norm clipping heuristic (which handles gradient explosion), the regularizer can considerably increase the span of the dependencies that an RNN can learn. Because it keeps the RNN dynamics on the edge of explosive gradients, the gradient clipping is particularly important. Without gradient clipping, gradient explosion prevents learning from succeeding.

A key weakness of this approach is that it is not as effective as the LSTM for tasks where data is abundant, such as language modeling.

10.12 Explicit Memory

Intelligence requires knowledge and acquiring knowledge can be done via learning, which has motivated the development of large-scale deep architectures. However, there are different kinds of knowledge. Some knowledge can be implicit, subconscious, and difficult to verbalize—such as how to walk, or how a dog looks different from a cat. Other knowledge can be explicit, declarative, and relatively straightforward to put into words—every day commonsense knowledge, like “a cat is a kind of animal,” or very specific facts that you need to know to accomplish your current goals, like “the meeting with the sales team is at 3:00 PM in room 141.”

Neural networks excel at storing implicit knowledge. However, they struggle to memorize facts. Stochastic gradient descent requires many presentations of the

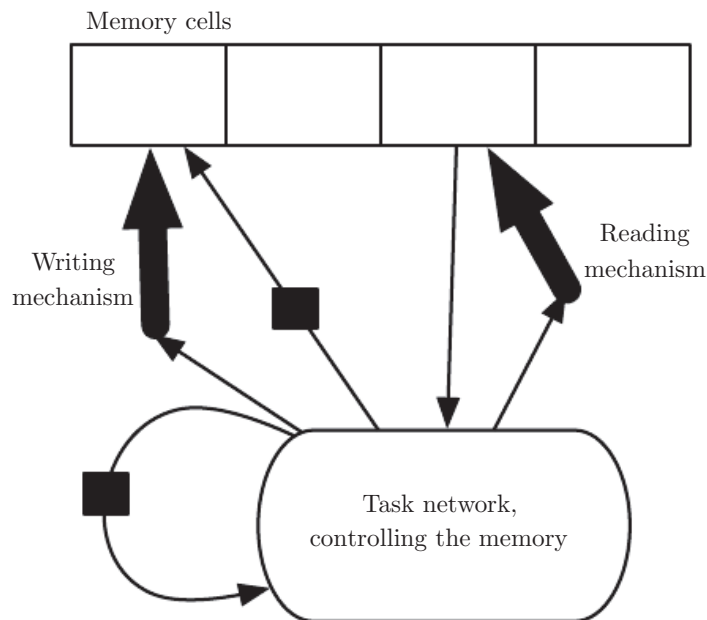


Figure 10.18: A schematic of an example of a network with an explicit memory, capturing some of the key design elements of the neural Turing machine. In this diagram we distinguish the “representation” part of the model (the “task network,” here a recurrent net in the bottom) from the “memory” part of the model (the set of cells), which can store facts. The task network learns to “control” the memory, deciding where to read from and where to write to within the memory (through the reading and writing mechanisms, indicated by bold arrows pointing at the reading and writing addresses).

same input before it can be stored in a neural network parameters, and even then, that input will not be stored especially precisely. [Graves et al. \(2014b\)](#) hypothesized that this is because neural networks lack the equivalent of the **working memory** system that allows human beings to explicitly hold and manipulate pieces of information that are relevant to achieving some goal. Such explicit memory components would allow our systems not only to rapidly and “intentionally” store and retrieve specific facts but also to sequentially reason with them. The need for neural networks that can process information in a sequence of steps, changing the way the input is fed into the network at each step, has long been recognized as important for the ability to reason rather than to make automatic, intuitive responses to the input ([Hinton, 1990](#)).

To resolve this difficulty, [Weston et al. \(2014\)](#) introduced **memory networks** that include a set of memory cells that can be accessed via an addressing mechanism. Memory networks originally required a supervision signal instructing them how to use their memory cells. [Graves et al. \(2014b\)](#) introduced the **neural Turing machine**, which is able to learn to read from and write arbitrary content to memory cells without explicit supervision about which actions to undertake, and allowed end-to-end training without this supervision signal, via the use of a content-based soft attention mechanism (see [Bahdanau et al. \(2015\)](#) and section 12.4.5.1). This soft addressing mechanism has become standard with other related architectures emulating algorithmic mechanisms in a way that still allows gradient-based optimization ([Sukhbaatar et al., 2015](#); [Joulin and Mikolov, 2015](#); [Kumar et al., 2015](#); [Vinyals et al., 2015a](#); [Grefenstette et al., 2015](#)).

Each memory cell can be thought of as an extension of the memory cells in LSTMs and GRUs. The difference is that the network outputs an internal state that chooses which cell to read from or write to, just as memory accesses in a digital computer read from or write to a specific address.

It is difficult to optimize functions that produce exact, integer addresses. To alleviate this problem, NTMs actually read to or write from many memory cells simultaneously. To read, they take a weighted average of many cells. To write, they modify multiple cells by different amounts. The coefficients for these operations are chosen to be focused on a small number of cells, for example, by producing them via a softmax function. Using these weights with non-zero derivatives allows the functions controlling access to the memory to be optimized using gradient descent. The gradient on these coefficients indicates whether each of them should be increased or decreased, but the gradient will typically be large only for those memory addresses receiving a large coefficient.

These memory cells are typically augmented to contain a vector, rather than

the single scalar stored by an LSTM or GRU memory cell. There are two reasons to increase the size of the memory cell. One reason is that we have increased the cost of accessing a memory cell. We pay the computational cost of producing a coefficient for many cells, but we expect these coefficients to cluster around a small number of cells. By reading a vector value, rather than a scalar value, we can offset some of this cost. Another reason to use vector-valued memory cells is that they allow for **content-based addressing**, where the weight used to read to or write from a cell is a function of that cell. Vector-valued cells allow us to retrieve a complete vector-valued memory if we are able to produce a pattern that matches some but not all of its elements. This is analogous to the way that people can recall the lyrics of a song based on a few words. We can think of a content-based read instruction as saying, “Retrieve the lyrics of the song that has the chorus ‘We all live in a yellow submarine.’” Content-based addressing is more useful when we make the objects to be retrieved large—if every letter of the song was stored in a separate memory cell, we would not be able to find them this way. By comparison, **location-based addressing** is not allowed to refer to the content of the memory. We can think of a location-based read instruction as saying “Retrieve the lyrics of the song in slot 347.” Location-based addressing can often be a perfectly sensible mechanism even when the memory cells are small.

If the content of a memory cell is copied (not forgotten) at most time steps, then the information it contains can be propagated forward in time and the gradients propagated backward in time without either vanishing or exploding.

The explicit memory approach is illustrated in figure 10.18, where we see that a “task neural network” is coupled with a memory. Although that task neural network could be feedforward or recurrent, the overall system is a recurrent network. The task network can choose to read from or write to specific memory addresses. Explicit memory seems to allow models to learn tasks that ordinary RNNs or LSTM RNNs cannot learn. One reason for this advantage may be because information and gradients can be propagated (forward in time or backwards in time, respectively) for very long durations.

As an alternative to back-propagation through weighted averages of memory cells, we can interpret the memory addressing coefficients as probabilities and stochastically read just one cell (Zaremba and Sutskever, 2015). Optimizing models that make discrete decisions requires specialized optimization algorithms, described in section 20.9.1. So far, training these stochastic architectures that make discrete decisions remains harder than training deterministic algorithms that make soft decisions.

Whether it is soft (allowing back-propagation) or stochastic and hard, the

mechanism for choosing an address is in its form identical to the **attention mechanism** which had been previously introduced in the context of machine translation ([Bahdanau et al., 2015](#)) and discussed in section [12.4.5.1](#). The idea of attention mechanisms for neural networks was introduced even earlier, in the context of handwriting generation ([Graves, 2013](#)), with an attention mechanism that was constrained to move only forward in time through the sequence. In the case of machine translation and memory networks, at each step, the focus of attention can move to a completely different place, compared to the previous step.

Recurrent neural networks provide a way to extend deep learning to sequential data. They are the last major tool in our deep learning toolbox. Our discussion now moves to how to choose and use these tools and how to apply them to real-world tasks.

Chapter 11

Practical Methodology

Successfully applying deep learning techniques requires more than just a good knowledge of what algorithms exist and the principles that explain how they work. A good machine learning practitioner also needs to know how to choose an algorithm for a particular application and how to monitor and respond to feedback obtained from experiments in order to improve a machine learning system. During day to day development of machine learning systems, practitioners need to decide whether to gather more data, increase or decrease model capacity, add or remove regularizing features, improve the optimization of a model, improve approximate inference in a model, or debug the software implementation of the model. All of these operations are at the very least time-consuming to try out, so it is important to be able to determine the right course of action rather than blindly guessing.

Most of this book is about different machine learning models, training algorithms, and objective functions. This may give the impression that the most important ingredient to being a machine learning expert is knowing a wide variety of machine learning techniques and being good at different kinds of math. In practice, one can usually do much better with a correct application of a commonplace algorithm than by sloppily applying an obscure algorithm. Correct application of an algorithm depends on mastering some fairly simple methodology. Many of the recommendations in this chapter are adapted from [Ng \(2015\)](#).

We recommend the following practical design process:

- Determine your goals—what error metric to use, and your target value for this error metric. These goals and error metrics should be driven by the problem that the application is intended to solve.
- Establish a working end-to-end pipeline as soon as possible, including the

estimation of the appropriate performance metrics.

- Instrument the system well to determine bottlenecks in performance. Diagnose which components are performing worse than expected and whether it is due to overfitting, underfitting, or a defect in the data or software.
- Repeatedly make incremental changes such as gathering new data, adjusting hyperparameters, or changing algorithms, based on specific findings from your instrumentation.

As a running example, we will use Street View address number transcription system ([Goodfellow et al., 2014d](#)). The purpose of this application is to add buildings to Google Maps. Street View cars photograph the buildings and record the GPS coordinates associated with each photograph. A convolutional network recognizes the address number in each photograph, allowing the Google Maps database to add that address in the correct location. The story of how this commercial application was developed gives an example of how to follow the design methodology we advocate.

We now describe each of the steps in this process.

11.1 Performance Metrics

Determining your goals, in terms of which error metric to use, is a necessary first step because your error metric will guide all of your future actions. You should also have an idea of what level of performance you desire.

Keep in mind that for most applications, it is impossible to achieve absolute zero error. The Bayes error defines the minimum error rate that you can hope to achieve, even if you have infinite training data and can recover the true probability distribution. This is because your input features may not contain complete information about the output variable, or because the system might be intrinsically stochastic. You will also be limited by having a finite amount of training data.

The amount of training data can be limited for a variety of reasons. When your goal is to build the best possible real-world product or service, you can typically collect more data but must determine the value of reducing error further and weigh this against the cost of collecting more data. Data collection can require time, money, or human suffering (for example, if your data collection process involves performing invasive medical tests). When your goal is to answer a scientific question about which algorithm performs better on a fixed benchmark, the benchmark

specification usually determines the training set and you are not allowed to collect more data.

How can one determine a reasonable level of performance to expect? Typically, in the academic setting, we have some estimate of the error rate that is attainable based on previously published benchmark results. In the real-word setting, we have some idea of the error rate that is necessary for an application to be safe, cost-effective, or appealing to consumers. Once you have determined your realistic desired error rate, your design decisions will be guided by reaching this error rate.

Another important consideration besides the target value of the performance metric is the choice of which metric to use. Several different performance metrics may be used to measure the effectiveness of a complete application that includes machine learning components. These performance metrics are usually different from the cost function used to train the model. As described in section 5.1.2, it is common to measure the accuracy, or equivalently, the error rate, of a system.

However, many applications require more advanced metrics.

Sometimes it is much more costly to make one kind of a mistake than another. For example, an e-mail spam detection system can make two kinds of mistakes: incorrectly classifying a legitimate message as spam, and incorrectly allowing a spam message to appear in the inbox. It is much worse to block a legitimate message than to allow a questionable message to pass through. Rather than measuring the error rate of a spam classifier, we may wish to measure some form of total cost, where the cost of blocking legitimate messages is higher than the cost of allowing spam messages.

Sometimes we wish to train a binary classifier that is intended to detect some rare event. For example, we might design a medical test for a rare disease. Suppose that only one in every million people has this disease. We can easily achieve 99.9999% accuracy on the detection task, by simply hard-coding the classifier to always report that the disease is absent. Clearly, accuracy is a poor way to characterize the performance of such a system. One way to solve this problem is to instead measure **precision** and **recall**. Precision is the fraction of detections reported by the model that were correct, while recall is the fraction of true events that were detected. A detector that says no one has the disease would achieve perfect precision, but zero recall. A detector that says everyone has the disease would achieve perfect recall, but precision equal to the percentage of people who have the disease (0.0001% in our example of a disease that only one people in a million have). When using precision and recall, it is common to plot a **PR curve**, with precision on the *y*-axis and recall on the *x*-axis. The classifier generates a score that is higher if the event to be detected occurred. For example, a feedforward

network designed to detect a disease outputs $\hat{y} = P(y = 1 \mid \mathbf{x})$, estimating the probability that a person whose medical results are described by features \mathbf{x} has the disease. We choose to report a detection whenever this score exceeds some threshold. By varying the threshold, we can trade precision for recall. In many cases, we wish to summarize the performance of the classifier with a single number rather than a curve. To do so, we can convert precision p and recall r into an **F-score** given by

$$F = \frac{2pr}{p + r}. \quad (11.1)$$

Another option is to report the total area lying beneath the PR curve.

In some applications, it is possible for the machine learning system to refuse to make a decision. This is useful when the machine learning algorithm can estimate how confident it should be about a decision, especially if a wrong decision can be harmful and if a human operator is able to occasionally take over. The Street View transcription system provides an example of this situation. The task is to transcribe the address number from a photograph in order to associate the location where the photo was taken with the correct address in a map. Because the value of the map degrades considerably if the map is inaccurate, it is important to add an address only if the transcription is correct. If the machine learning system thinks that it is less likely than a human being to obtain the correct transcription, then the best course of action is to allow a human to transcribe the photo instead. Of course, the machine learning system is only useful if it is able to dramatically reduce the amount of photos that the human operators must process. A natural performance metric to use in this situation is **coverage**. Coverage is the fraction of examples for which the machine learning system is able to produce a response. It is possible to trade coverage for accuracy. One can always obtain 100% accuracy by refusing to process any example, but this reduces the coverage to 0%. For the Street View task, the goal for the project was to reach human-level transcription accuracy while maintaining 95% coverage. Human-level performance on this task is 98% accuracy.

Many other metrics are possible. We can for example, measure click-through rates, collect user satisfaction surveys, and so on. Many specialized application areas have application-specific criteria as well.

What is important is to determine which performance metric to improve ahead of time, then concentrate on improving this metric. Without clearly defined goals, it can be difficult to tell whether changes to a machine learning system make progress or not.

11.2 Default Baseline Models

After choosing performance metrics and goals, the next step in any practical application is to establish a reasonable end-to-end system as soon as possible. In this section, we provide recommendations for which algorithms to use as the first baseline approach in various situations. Keep in mind that deep learning research progresses quickly, so better default algorithms are likely to become available soon after this writing.

Depending on the complexity of your problem, you may even want to begin without using deep learning. If your problem has a chance of being solved by just choosing a few linear weights correctly, you may want to begin with a simple statistical model like logistic regression.

If you know that your problem falls into an “AI-complete” category like object recognition, speech recognition, machine translation, and so on, then you are likely to do well by beginning with an appropriate deep learning model.

First, choose the general category of model based on the structure of your data. If you want to perform supervised learning with fixed-size vectors as input, use a feedforward network with fully connected layers. If the input has known topological structure (for example, if the input is an image), use a convolutional network. In these cases, you should begin by using some kind of piecewise linear unit (ReLUs or their generalizations like Leaky ReLUs, PreLus and maxout). If your input or output is a sequence, use a gated recurrent net (LSTM or GRU).

A reasonable choice of optimization algorithm is SGD with momentum with a decaying learning rate (popular decay schemes that perform better or worse on different problems include decaying linearly until reaching a fixed minimum learning rate, decaying exponentially, or decreasing the learning rate by a factor of 2-10 each time validation error plateaus). Another very reasonable alternative is Adam. Batch normalization can have a dramatic effect on optimization performance, especially for convolutional networks and networks with sigmoidal nonlinearities. While it is reasonable to omit batch normalization from the very first baseline, it should be introduced quickly if optimization appears to be problematic.

Unless your training set contains tens of millions of examples or more, you should include some mild forms of regularization from the start. Early stopping should be used almost universally. Dropout is an excellent regularizer that is easy to implement and compatible with many models and training algorithms. Batch normalization also sometimes reduces generalization error and allows dropout to be omitted, due to the noise in the estimate of the statistics used to normalize each variable.

If your task is similar to another task that has been studied extensively, you will probably do well by first copying the model and algorithm that is already known to perform best on the previously studied task. You may even want to copy a trained model from that task. For example, it is common to use the features from a convolutional network trained on ImageNet to solve other computer vision tasks (Girshick *et al.*, 2015).

A common question is whether to begin by using unsupervised learning, described further in part III. This is somewhat domain specific. Some domains, such as natural language processing, are known to benefit tremendously from unsupervised learning techniques such as learning unsupervised word embeddings. In other domains, such as computer vision, current unsupervised learning techniques do not bring a benefit, except in the semi-supervised setting, when the number of labeled examples is very small (Kingma *et al.*, 2014; Rasmus *et al.*, 2015). If your application is in a context where unsupervised learning is known to be important, then include it in your first end-to-end baseline. Otherwise, only use unsupervised learning in your first attempt if the task you want to solve is unsupervised. You can always try adding unsupervised learning later if you observe that your initial baseline overfits.

11.3 Determining Whether to Gather More Data

After the first end-to-end system is established, it is time to measure the performance of the algorithm and determine how to improve it. Many machine learning novices are tempted to make improvements by trying out many different algorithms. However, it is often much better to gather more data than to improve the learning algorithm.

How does one decide whether to gather more data? First, determine whether the performance on the training set is acceptable. If performance on the training set is poor, the learning algorithm is not using the training data that is already available, so there is no reason to gather more data. Instead, try increasing the size of the model by adding more layers or adding more hidden units to each layer. Also, try improving the learning algorithm, for example by tuning the learning rate hyperparameter. If large models and carefully tuned optimization algorithms do not work well, then the problem might be the *quality* of the training data. The data may be too noisy or may not include the right inputs needed to predict the desired outputs. This suggests starting over, collecting cleaner data or collecting a richer set of features.

If the performance on the training set is acceptable, then measure the per-

formance on a test set. If the performance on the test set is also acceptable, then there is nothing left to be done. If test set performance is much worse than training set performance, then gathering more data is one of the most effective solutions. The key considerations are the cost and feasibility of gathering more data, the cost and feasibility of reducing the test error by other means, and the amount of data that is expected to be necessary to improve test set performance significantly. At large internet companies with millions or billions of users, it is feasible to gather large datasets, and the expense of doing so can be considerably less than the other alternatives, so the answer is almost always to gather more training data. For example, the development of large labeled datasets was one of the most important factors in solving object recognition. In other contexts, such as medical applications, it may be costly or infeasible to gather more data. A simple alternative to gathering more data is to reduce the size of the model or improve regularization, by adjusting hyperparameters such as weight decay coefficients, or by adding regularization strategies such as dropout. If you find that the gap between train and test performance is still unacceptable even after tuning the regularization hyperparameters, then gathering more data is advisable.

When deciding whether to gather more data, it is also necessary to decide how much to gather. It is helpful to plot curves showing the relationship between training set size and generalization error, like in figure 5.4. By extrapolating such curves, one can predict how much additional training data would be needed to achieve a certain level of performance. Usually, adding a small fraction of the total number of examples will not have a noticeable impact on generalization error. It is therefore recommended to experiment with training set sizes on a logarithmic scale, for example doubling the number of examples between consecutive experiments.

If gathering much more data is not feasible, the only other way to improve generalization error is to improve the learning algorithm itself. This becomes the domain of research and not the domain of advice for applied practitioners.

11.4 Selecting Hyperparameters

Most deep learning algorithms come with many hyperparameters that control many aspects of the algorithm's behavior. Some of these hyperparameters affect the time and memory cost of running the algorithm. Some of these hyperparameters affect the quality of the model recovered by the training process and its ability to infer correct results when deployed on new inputs.

There are two basic approaches to choosing these hyperparameters: choosing them manually and choosing them automatically. Choosing the hyperparameters

manually requires understanding what the hyperparameters do and how machine learning models achieve good generalization. Automatic hyperparameter selection algorithms greatly reduce the need to understand these ideas, but they are often much more computationally costly.

11.4.1 Manual Hyperparameter Tuning

To set hyperparameters manually, one must understand the relationship between hyperparameters, training error, generalization error and computational resources (memory and runtime). This means establishing a solid foundation on the fundamental ideas concerning the effective capacity of a learning algorithm from chapter 5.

The goal of manual hyperparameter search is usually to find the lowest generalization error subject to some runtime and memory budget. We do not discuss how to determine the runtime and memory impact of various hyperparameters here because this is highly platform-dependent.

The primary goal of manual hyperparameter search is to adjust the effective capacity of the model to match the complexity of the task. Effective capacity is constrained by three factors: the representational capacity of the model, the ability of the learning algorithm to successfully minimize the cost function used to train the model, and the degree to which the cost function and training procedure regularize the model. A model with more layers and more hidden units per layer has higher representational capacity—it is capable of representing more complicated functions. It can not necessarily actually learn all of these functions though, if the training algorithm cannot discover that certain functions do a good job of minimizing the training cost, or if regularization terms such as weight decay forbid some of these functions.

The generalization error typically follows a U-shaped curve when plotted as a function of one of the hyperparameters, as in figure 5.3. At one extreme, the hyperparameter value corresponds to low capacity, and generalization error is high because training error is high. This is the underfitting regime. At the other extreme, the hyperparameter value corresponds to high capacity, and the generalization error is high because the gap between training and test error is high. Somewhere in the middle lies the optimal model capacity, which achieves the lowest possible generalization error, by adding a medium generalization gap to a medium amount of training error.

For some hyperparameters, overfitting occurs when the value of the hyperparameter is large. The number of hidden units in a layer is one such example,

because increasing the number of hidden units increases the capacity of the model. For some hyperparameters, overfitting occurs when the value of the hyperparameter is small. For example, the smallest allowable weight decay coefficient of zero corresponds to the greatest effective capacity of the learning algorithm.

Not every hyperparameter will be able to explore the entire U-shaped curve. Many hyperparameters are discrete, such as the number of units in a layer or the number of linear pieces in a maxout unit, so it is only possible to visit a few points along the curve. Some hyperparameters are binary. Usually these hyperparameters are switches that specify whether or not to use some optional component of the learning algorithm, such as a preprocessing step that normalizes the input features by subtracting their mean and dividing by their standard deviation. These hyperparameters can only explore two points on the curve. Other hyperparameters have some minimum or maximum value that prevents them from exploring some part of the curve. For example, the minimum weight decay coefficient is zero. This means that if the model is underfitting when weight decay is zero, we can not enter the overfitting region by modifying the weight decay coefficient. In other words, some hyperparameters can only subtract capacity.

The learning rate is perhaps the most important hyperparameter. If you have time to tune only one hyperparameter, tune the learning rate. It controls the effective capacity of the model in a more complicated way than other hyperparameters—the effective capacity of the model is highest when the learning rate is *correct* for the optimization problem, not when the learning rate is especially large or especially small. The learning rate has a U-shaped curve for *training* error, illustrated in figure 11.1. When the learning rate is too large, gradient descent can inadvertently increase rather than decrease the training error. In the idealized quadratic case, this occurs if the learning rate is at least twice as large as its optimal value (LeCun *et al.*, 1998a). When the learning rate is too small, training is not only slower, but may become permanently stuck with a high training error. This effect is poorly understood (it would not happen for a convex loss function).

Tuning the parameters other than the learning rate requires monitoring both training and test error to diagnose whether your model is overfitting or underfitting, then adjusting its capacity appropriately.

If your error on the training set is higher than your target error rate, you have no choice but to increase capacity. If you are not using regularization and you are confident that your optimization algorithm is performing correctly, then you must add more layers to your network or add more hidden units. Unfortunately, this increases the computational costs associated with the model.

If your error on the test set is higher than than your target error rate, you can

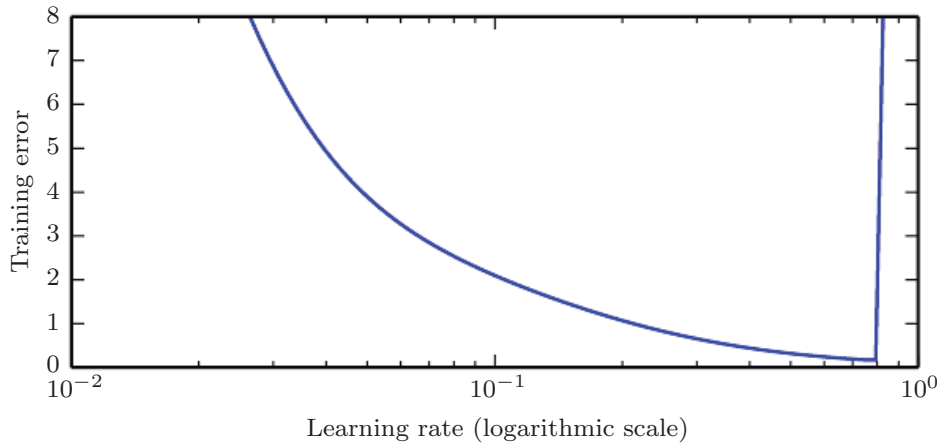


Figure 11.1: Typical relationship between the learning rate and the training error. Notice the sharp rise in error when the learning is above an optimal value. This is for a fixed training time, as a smaller learning rate may sometimes only slow down training by a factor proportional to the learning rate reduction. Generalization error can follow this curve or be complicated by regularization effects arising out of having a too large or too small learning rates, since poor optimization can, to some degree, reduce or prevent overfitting, and even points with equivalent training error can have different generalization error.

now take two kinds of actions. The test error is the sum of the training error and the gap between training and test error. The optimal test error is found by trading off these quantities. Neural networks typically perform best when the training error is very low (and thus, when capacity is high) and the test error is primarily driven by the gap between train and test error. Your goal is to reduce this gap without increasing training error faster than the gap decreases. To reduce the gap, change regularization hyperparameters to reduce effective model capacity, such as by adding dropout or weight decay. Usually the best performance comes from a large model that is regularized well, for example by using dropout.

Most hyperparameters can be set by reasoning about whether they increase or decrease model capacity. Some examples are included in Table 11.1.

While manually tuning hyperparameters, do not lose sight of your end goal: good performance on the test set. Adding regularization is only one way to achieve this goal. As long as you have low training error, you can always reduce generalization error by collecting more training data. The brute force way to practically guarantee success is to continually increase model capacity and training set size until the task is solved. This approach does of course increase the computational cost of training and inference, so it is only feasible given appropriate resources. In

Hyperparameter	Increases capacity when...	Reason	Caveats
Number of hidden units	increased	Increasing the number of hidden units increases the representational capacity of the model.	Increasing the number of hidden units increases both the time and memory cost of essentially every operation on the model.
Learning rate	tuned optimally	An improper learning rate, whether too high or too low, results in a model with low effective capacity due to optimization failure	
Convolution kernel width	increased	Increasing the kernel width increases the number of parameters in the model	A wider kernel results in a narrower output dimension, reducing model capacity unless you use implicit zero padding to reduce this effect. Wider kernels require more memory for parameter storage and increase runtime, but a narrower output reduces memory cost.
Implicit zero padding	increased	Adding implicit zeros before convolution keeps the representation size large	Increased time and memory cost of most operations.
Weight decay coefficient	decreased	Decreasing the weight decay coefficient frees the model parameters to become larger	
Dropout rate	decreased	Dropping units less often gives the units more opportunities to “conspire” with each other to fit the training set	

Table 11.1: The effect of various hyperparameters on model capacity.

principle, this approach could fail due to optimization difficulties, but for many problems optimization does not seem to be a significant barrier, provided that the model is chosen appropriately.

11.4.2 Automatic Hyperparameter Optimization Algorithms

The ideal learning algorithm just takes a dataset and outputs a function, without requiring hand-tuning of hyperparameters. The popularity of several learning algorithms such as logistic regression and SVMs stems in part from their ability to perform well with only one or two tuned hyperparameters. Neural networks can sometimes perform well with only a small number of tuned hyperparameters, but often benefit significantly from tuning of forty or more hyperparameters. Manual hyperparameter tuning can work very well when the user has a good starting point, such as one determined by others having worked on the same type of application and architecture, or when the user has months or years of experience in exploring hyperparameter values for neural networks applied to similar tasks. However, for many applications, these starting points are not available. In these cases, automated algorithms can find useful values of the hyperparameters.

If we think about the way in which the user of a learning algorithm searches for good values of the hyperparameters, we realize that an optimization is taking place: we are trying to find a value of the hyperparameters that optimizes an objective function, such as validation error, sometimes under constraints (such as a budget for training time, memory or recognition time). It is therefore possible, in principle, to develop **hyperparameter optimization** algorithms that wrap a learning algorithm and choose its hyperparameters, thus hiding the hyperparameters of the learning algorithm from the user. Unfortunately, hyperparameter optimization algorithms often have their own hyperparameters, such as the range of values that should be explored for each of the learning algorithm's hyperparameters. However, these secondary hyperparameters are usually easier to choose, in the sense that acceptable performance may be achieved on a wide range of tasks using the same secondary hyperparameters for all tasks.

11.4.3 Grid Search

When there are three or fewer hyperparameters, the common practice is to perform **grid search**. For each hyperparameter, the user selects a small finite set of values to explore. The grid search algorithm then trains a model for every joint specification of hyperparameter values in the Cartesian product of the set of values for each individual hyperparameter. The experiment that yields the best validation

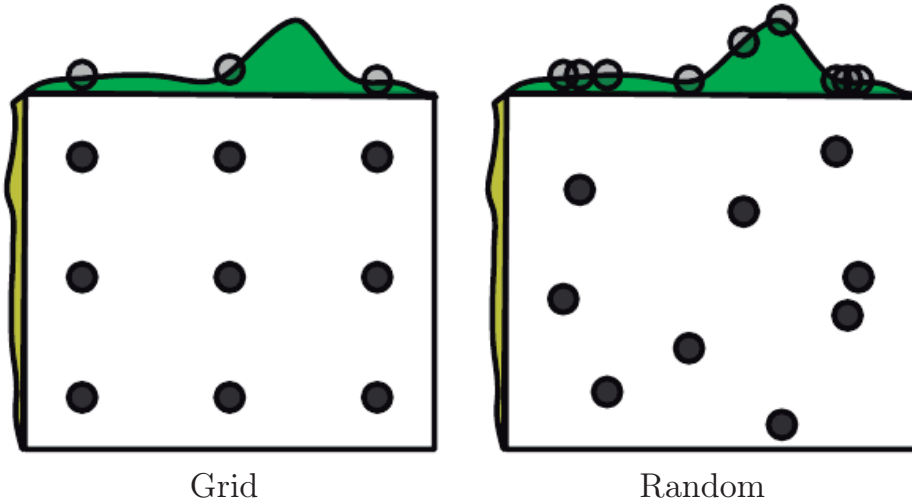


Figure 11.2: Comparison of grid search and random search. For illustration purposes we display two hyperparameters but we are typically interested in having many more. (*Left*) To perform grid search, we provide a set of values for each hyperparameter. The search algorithm runs training for every joint hyperparameter setting in the cross product of these sets. (*Right*) To perform random search, we provide a probability distribution over joint hyperparameter configurations. Usually most of these hyperparameters are independent from each other. Common choices for the distribution over a single hyperparameter include uniform and log-uniform (to sample from a log-uniform distribution, take the exp of a sample from a uniform distribution). The search algorithm then randomly samples joint hyperparameter configurations and runs training with each of them. Both grid search and random search evaluate the validation set error and return the best configuration. The figure illustrates the typical case where only some hyperparameters have a significant influence on the result. In this illustration, only the hyperparameter on the horizontal axis has a significant effect. Grid search wastes an amount of computation that is exponential in the number of non-influential hyperparameters, while random search tests a unique value of every influential hyperparameter on nearly every trial. Figure reproduced with permission from [Bergstra and Bengio \(2012\)](#).

set error is then chosen as having found the best hyperparameters. See the left of figure 11.2 for an illustration of a grid of hyperparameter values.

How should the lists of values to search over be chosen? In the case of numerical (ordered) hyperparameters, the smallest and largest element of each list is chosen conservatively, based on prior experience with similar experiments, to make sure that the optimal value is very likely to be in the selected range. Typically, a grid search involves picking values approximately on a *logarithmic scale*, e.g., a learning rate taken within the set $\{.1, .01, 10^{-3}, 10^{-4}, 10^{-5}\}$, or a number of hidden units taken with the set $\{50, 100, 200, 500, 1000, 2000\}$.

Grid search usually performs best when it is performed repeatedly. For example, suppose that we ran a grid search over a hyperparameter α using values of $\{-1, 0, 1\}$. If the best value found is 1, then we underestimated the range in which the best α lies and we should shift the grid and run another search with α in, for example, $\{1, 2, 3\}$. If we find that the best value of α is 0, then we may wish to refine our estimate by zooming in and running a grid search over $\{-1, 0, 1\}$.

The obvious problem with grid search is that its computational cost grows exponentially with the number of hyperparameters. If there are m hyperparameters, each taking at most n values, then the number of training and evaluation trials required grows as $O(n^m)$. The trials may be run in parallel and exploit loose parallelism (with almost no need for communication between different machines carrying out the search). Unfortunately, due to the exponential cost of grid search, even parallelization may not provide a satisfactory size of search.

11.4.4 Random Search

Fortunately, there is an alternative to grid search that is as simple to program, more convenient to use, and converges much faster to good values of the hyperparameters: random search (Bergstra and Bengio, 2012).

A random search proceeds as follows. First we define a marginal distribution for each hyperparameter, e.g., a Bernoulli or multinoulli for binary or discrete hyperparameters, or a uniform distribution on a log-scale for positive real-valued hyperparameters. For example,

$$\text{log_learning_rate} \sim u(-1, -5) \tag{11.2}$$

$$\text{learning_rate} = 10^{\text{log_learning_rate}}. \tag{11.3}$$

where $u(a, b)$ indicates a sample of the uniform distribution in the interval (a, b) . Similarly the `log_number_of_hidden_units` may be sampled from $u(\log(50), \log(2000))$.

Unlike in the case of a grid search, one *should not discretize* or bin the values of the hyperparameters. This allows one to explore a larger set of values, and does not incur additional computational cost. In fact, as illustrated in figure 11.2, a random search can be exponentially more efficient than a grid search, when there are several hyperparameters that do not strongly affect the performance measure. This is studied at length in [Bergstra and Bengio \(2012\)](#), who found that random search reduces the validation set error much faster than grid search, in terms of the number of trials run by each method.

As with grid search, one may often want to run repeated versions of random search, to refine the search based on the results of the first run.

The main reason why random search finds good solutions faster than grid search is that there are no wasted experimental runs, unlike in the case of grid search, when two values of a hyperparameter (given values of the other hyperparameters) would give the same result. In the case of grid search, the other hyperparameters would have the same values for these two runs, whereas with random search, they would usually have different values. Hence if the change between these two values does not marginally make much difference in terms of validation set error, grid search will unnecessarily repeat two equivalent experiments while random search will still give two independent explorations of the other hyperparameters.

11.4.5 Model-Based Hyperparameter Optimization

The search for good hyperparameters can be cast as an optimization problem. The decision variables are the hyperparameters. The cost to be optimized is the validation set error that results from training using these hyperparameters. In simplified settings where it is feasible to compute the gradient of some differentiable error measure on the validation set with respect to the hyperparameters, we can simply follow this gradient ([Bengio et al., 1999](#); [Bengio, 2000](#); [Maclaurin et al., 2015](#)). Unfortunately, in most practical settings, this gradient is unavailable, either due to its high computation and memory cost, or due to hyperparameters having intrinsically non-differentiable interactions with the validation set error, as in the case of discrete-valued hyperparameters.

To compensate for this lack of a gradient, we can build a model of the validation set error, then propose new hyperparameter guesses by performing optimization within this model. Most model-based algorithms for hyperparameter search use a Bayesian regression model to estimate both the expected value of the validation set error for each hyperparameter and the uncertainty around this expectation. Optimization thus involves a tradeoff between exploration (proposing hyperparameters

for which there is high uncertainty, which may lead to a large improvement but may also perform poorly) and exploitation (proposing hyperparameters which the model is confident will perform as well as any hyperparameters it has seen so far—usually hyperparameters that are very similar to ones it has seen before). Contemporary approaches to hyperparameter optimization include Spearmint ([Snoek et al., 2012](#)), TPE ([Bergstra et al., 2011](#)) and SMAC ([Hutter et al., 2011](#)).

Currently, we cannot unambiguously recommend Bayesian hyperparameter optimization as an established tool for achieving better deep learning results or for obtaining those results with less effort. Bayesian hyperparameter optimization sometimes performs comparably to human experts, sometimes better, but fails catastrophically on other problems. It may be worth trying to see if it works on a particular problem but is not yet sufficiently mature or reliable. That being said, hyperparameter optimization is an important field of research that, while often driven primarily by the needs of deep learning, holds the potential to benefit not only the entire field of machine learning but the discipline of engineering in general.

One drawback common to most hyperparameter optimization algorithms with more sophistication than random search is that they require for a training experiment to run to completion before they are able to extract any information from the experiment. This is much less efficient, in the sense of how much information can be gleaned early in an experiment, than manual search by a human practitioner, since one can usually tell early on if some set of hyperparameters is completely pathological. [Swersky et al. \(2014\)](#) have introduced an early version of an algorithm that maintains a set of multiple experiments. At various time points, the hyperparameter optimization algorithm can choose to begin a new experiment, to “freeze” a running experiment that is not promising, or to “thaw” and resume an experiment that was earlier frozen but now appears promising given more information.

11.5 Debugging Strategies

When a machine learning system performs poorly, it is usually difficult to tell whether the poor performance is intrinsic to the algorithm itself or whether there is a bug in the implementation of the algorithm. Machine learning systems are difficult to debug for a variety of reasons.

In most cases, we do not know *a priori* what the intended behavior of the algorithm is. In fact, the entire point of using machine learning is that it will discover useful behavior that we were not able to specify ourselves. If we train a

neural network on a *new* classification task and it achieves 5% test error, we have no straightforward way of knowing if this is the expected behavior or sub-optimal behavior.

A further difficulty is that most machine learning models have multiple parts that are each adaptive. If one part is broken, the other parts can adapt and still achieve roughly acceptable performance. For example, suppose that we are training a neural net with several layers parametrized by weights \mathbf{W} and biases \mathbf{b} . Suppose further that we have manually implemented the gradient descent rule for each parameter separately, and we made an error in the update for the biases:

$$\mathbf{b} \leftarrow \mathbf{b} - \alpha \quad (11.4)$$

where α is the learning rate. This erroneous update does not use the gradient at all. It causes the biases to constantly become negative throughout learning, which is clearly not a correct implementation of any reasonable learning algorithm. The bug may not be apparent just from examining the output of the model though. Depending on the distribution of the input, the weights may be able to adapt to compensate for the negative biases.

Most debugging strategies for neural nets are designed to get around one or both of these two difficulties. Either we design a case that is so simple that the correct behavior actually can be predicted, or we design a test that exercises one part of the neural net implementation in isolation.

Some important debugging tests include:

Visualize the model in action : When training a model to detect objects in images, view some images with the detections proposed by the model displayed superimposed on the image. When training a generative model of speech, listen to some of the speech samples it produces. This may seem obvious, but it is easy to fall into the practice of only looking at quantitative performance measurements like accuracy or log-likelihood. Directly observing the machine learning model performing its task will help to determine whether the quantitative performance numbers it achieves seem reasonable. Evaluation bugs can be some of the most devastating bugs because they can mislead you into believing your system is performing well when it is not.

Visualize the worst mistakes : Most models are able to output some sort of confidence measure for the task they perform. For example, classifiers based on a softmax output layer assign a probability to each class. The probability assigned to the most likely class thus gives an estimate of the confidence the model has in its classification decision. Typically, maximum likelihood training results in these values being overestimates rather than accurate probabilities of correct prediction,

but they are somewhat useful in the sense that examples that are actually less likely to be correctly labeled receive smaller probabilities under the model. By viewing the training set examples that are the hardest to model correctly, one can often discover problems with the way the data has been preprocessed or labeled. For example, the Street View transcription system originally had a problem where the address number detection system would crop the image too tightly and omit some of the digits. The transcription network then assigned very low probability to the correct answer on these images. Sorting the images to identify the most confident mistakes showed that there was a systematic problem with the cropping. Modifying the detection system to crop much wider images resulted in much better performance of the overall system, even though the transcription network needed to be able to process greater variation in the position and scale of the address numbers.

Reasoning about software using train and test error: It is often difficult to determine whether the underlying software is correctly implemented. Some clues can be obtained from the train and test error. If training error is low but test error is high, then it is likely that the training procedure works correctly, and the model is overfitting for fundamental algorithmic reasons. An alternative possibility is that the test error is measured incorrectly due to a problem with saving the model after training then reloading it for test set evaluation, or if the test data was prepared differently from the training data. If both train and test error are high, then it is difficult to determine whether there is a software defect or whether the model is underfitting due to fundamental algorithmic reasons. This scenario requires further tests, described next.

Fit a tiny dataset: If you have high error on the training set, determine whether it is due to genuine underfitting or due to a software defect. Usually even small models can be guaranteed to be able fit a sufficiently small dataset. For example, a classification dataset with only one example can be fit just by setting the biases of the output layer correctly. Usually if you cannot train a classifier to correctly label a single example, an autoencoder to successfully reproduce a single example with high fidelity, or a generative model to consistently emit samples resembling a single example, there is a software defect preventing successful optimization on the training set. This test can be extended to a small dataset with few examples.

Compare back-propagated derivatives to numerical derivatives: If you are using a software framework that requires you to implement your own gradient computations, or if you are adding a new operation to a differentiation library and must define its `bprop` method, then a common source of error is implementing this gradient expression incorrectly. One way to verify that these derivatives are correct

is to compare the derivatives computed by your implementation of automatic differentiation to the derivatives computed by a **finite differences**. Because

$$f'(x) = \lim_{\epsilon \rightarrow 0} \frac{f(x + \epsilon) - f(x)}{\epsilon}, \quad (11.5)$$

we can approximate the derivative by using a small, finite ϵ :

$$f'(x) \approx \frac{f(x + \epsilon) - f(x)}{\epsilon}. \quad (11.6)$$

We can improve the accuracy of the approximation by using the **centered difference**:

$$f'(x) \approx \frac{f(x + \frac{1}{2}\epsilon) - f(x - \frac{1}{2}\epsilon)}{\epsilon}. \quad (11.7)$$

The perturbation size ϵ must chosen to be large enough to ensure that the perturbation is not rounded down too much by finite-precision numerical computations.

Usually, we will want to test the gradient or Jacobian of a vector-valued function $g : \mathbb{R}^m \rightarrow \mathbb{R}^n$. Unfortunately, finite differencing only allows us to take a single derivative at a time. We can either run finite differencing mn times to evaluate all of the partial derivatives of g , or we can apply the test to a new function that uses random projections at both the input and output of g . For example, we can apply our test of the implementation of the derivatives to $f(x)$ where $f(x) = \mathbf{u}^T g(\mathbf{v}x)$, where \mathbf{u} and \mathbf{v} are randomly chosen vectors. Computing $f'(x)$ correctly requires being able to back-propagate through g correctly, yet is efficient to do with finite differences because f has only a single input and a single output. It is usually a good idea to repeat this test for more than one value of \mathbf{u} and \mathbf{v} to reduce the chance that the test overlooks mistakes that are orthogonal to the random projection.

If one has access to numerical computation on complex numbers, then there is a very efficient way to numerically estimate the gradient by using complex numbers as input to the function ([Squire and Trapp, 1998](#)). The method is based on the observation that

$$f(x + i\epsilon) = f(x) + i\epsilon f'(x) + O(\epsilon^2) \quad (11.8)$$

$$\text{real}(f(x + i\epsilon)) = f(x) + O(\epsilon^2), \quad \text{imag}\left(\frac{f(x + i\epsilon)}{\epsilon}\right) = f'(x) + O(\epsilon^2), \quad (11.9)$$

where $i = \sqrt{-1}$. Unlike in the real-valued case above, there is no cancellation effect due to taking the difference between the value of f at different points. This allows the use of tiny values of ϵ like $\epsilon = 10^{-150}$, which make the $O(\epsilon^2)$ error insignificant for all practical purposes.

Monitor histograms of activations and gradient: It is often useful to visualize statistics of neural network activations and gradients, collected over a large amount of training iterations (maybe one epoch). The pre-activation value of hidden units can tell us if the units saturate, or how often they do. For example, for rectifiers, how often are they off? Are there units that are always off? For tanh units, the average of the absolute value of the pre-activations tells us how saturated the unit is. In a deep network where the propagated gradients quickly grow or quickly vanish, optimization may be hampered. Finally, it is useful to compare the magnitude of parameter gradients to the magnitude of the parameters themselves. As suggested by Bottou (2015), we would like the magnitude of parameter updates over a minibatch to represent something like 1% of the magnitude of the parameter, not 50% or 0.001% (which would make the parameters move too slowly). It may be that some groups of parameters are moving at a good pace while others are stalled. When the data is sparse (like in natural language), some parameters may be very rarely updated, and this should be kept in mind when monitoring their evolution.

Finally, many deep learning algorithms provide some sort of guarantee about the results produced at each step. For example, in part III, we will see some approximate inference algorithms that work by using algebraic solutions to optimization problems. Typically these can be debugged by testing each of their guarantees. Some guarantees that some optimization algorithms offer include that the objective function will never increase after one step of the algorithm, that the gradient with respect to some subset of variables will be zero after each step of the algorithm, and that the gradient with respect to all variables will be zero at convergence. Usually due to rounding error, these conditions will not hold exactly in a digital computer, so the debugging test should include some tolerance parameter.

11.6 Example: Multi-Digit Number Recognition

To provide an end-to-end description of how to apply our design methodology in practice, we present a brief account of the Street View transcription system, from the point of view of designing the deep learning components. Obviously, many other components of the complete system, such as the Street View cars, the database infrastructure, and so on, were of paramount importance.

From the point of view of the machine learning task, the process began with data collection. The cars collected the raw data and human operators provided labels. The transcription task was preceded by a significant amount of dataset curation, including using other machine learning techniques to *detect* the house

numbers prior to transcribing them.

The transcription project began with a choice of performance metrics and desired values for these metrics. An important general principle is to tailor the choice of metric to the business goals for the project. Because maps are only useful if they have high accuracy, it was important to set a high accuracy requirement for this project. Specifically, the goal was to obtain human-level, 98% accuracy. This level of accuracy may not always be feasible to obtain. In order to reach this level of accuracy, the Street View transcription system sacrifices coverage. Coverage thus became the main performance metric optimized during the project, with accuracy held at 98%. As the convolutional network improved, it became possible to reduce the confidence threshold below which the network refuses to transcribe the input, eventually exceeding the goal of 95% coverage.

After choosing quantitative goals, the next step in our recommended methodology is to rapidly establish a sensible baseline system. For vision tasks, this means a convolutional network with rectified linear units. The transcription project began with such a model. At the time, it was not common for a convolutional network to output a sequence of predictions. In order to begin with the simplest possible baseline, the first implementation of the output layer of the model consisted of n different softmax units to predict a sequence of n characters. These softmax units were trained exactly the same as if the task were classification, with each softmax unit trained independently.

Our recommended methodology is to iteratively refine the baseline and test whether each change makes an improvement. The first change to the Street View transcription system was motivated by a theoretical understanding of the coverage metric and the structure of the data. Specifically, the network refuses to classify an input \mathbf{x} whenever the probability of the output sequence $p(\mathbf{y} \mid \mathbf{x}) < t$ for some threshold t . Initially, the definition of $p(\mathbf{y} \mid \mathbf{x})$ was ad-hoc, based on simply multiplying all of the softmax outputs together. This motivated the development of a specialized output layer and cost function that actually computed a principled log-likelihood. This approach allowed the example rejection mechanism to function much more effectively.

At this point, coverage was still below 90%, yet there were no obvious theoretical problems with the approach. Our methodology therefore suggests to instrument the train and test set performance in order to determine whether the problem is underfitting or overfitting. In this case, train and test set error were nearly identical. Indeed, the main reason this project proceeded so smoothly was the availability of a dataset with tens of millions of labeled examples. Because train and test set error were so similar, this suggested that the problem was either due

to underfitting or due to a problem with the training data. One of the debugging strategies we recommend is to visualize the model’s worst errors. In this case, that meant visualizing the incorrect training set transcriptions that the model gave the highest confidence. These proved to mostly consist of examples where the input image had been cropped too tightly, with some of the digits of the address being removed by the cropping operation. For example, a photo of an address “1849” might be cropped too tightly, with only the “849” remaining visible. This problem could have been resolved by spending weeks improving the accuracy of the address number detection system responsible for determining the cropping regions. Instead, the team took a much more practical decision, to simply expand the width of the crop region to be systematically wider than the address number detection system predicted. This single change added ten percentage points to the transcription system’s coverage.

Finally, the last few percentage points of performance came from adjusting hyperparameters. This mostly consisted of making the model larger while maintaining some restrictions on its computational cost. Because train and test error remained roughly equal, it was always clear that any performance deficits were due to underfitting, as well as due to a few remaining problems with the dataset itself.

Overall, the transcription project was a great success, and allowed hundreds of millions of addresses to be transcribed both faster and at lower cost than would have been possible via human effort.

We hope that the design principles described in this chapter will lead to many other similar successes.

Chapter 12

Applications

In this chapter, we describe how to use deep learning to solve applications in computer vision, speech recognition, natural language processing, and other application areas of commercial interest. We begin by discussing the large scale neural network implementations required for most serious AI applications. Next, we review several specific application areas that deep learning has been used to solve. While one goal of deep learning is to design algorithms that are capable of solving a broad variety of tasks, so far some degree of specialization is needed. For example, vision tasks require processing a large number of input features (pixels) per example. Language tasks require modeling a large number of possible values (words in the vocabulary) per input feature.

12.1 Large-Scale Deep Learning

Deep learning is based on the philosophy of connectionism: while an individual biological neuron or an individual feature in a machine learning model is not intelligent, a large population of these neurons or features acting together can exhibit intelligent behavior. It truly is important to emphasize the fact that the number of neurons must be *large*. One of the key factors responsible for the improvement in neural network's accuracy and the improvement of the complexity of tasks they can solve between the 1980s and today is the dramatic increase in the size of the networks we use. As we saw in section 1.2.3, network sizes have grown exponentially for the past three decades, yet artificial neural networks are only as large as the nervous systems of insects.

Because the size of neural networks is of paramount importance, deep learning

requires high performance hardware and software infrastructure.

12.1.1 Fast CPU Implementations

Traditionally, neural networks were trained using the CPU of a single machine. Today, this approach is generally considered insufficient. We now mostly use GPU computing or the CPUs of many machines networked together. Before moving to these expensive setups, researchers worked hard to demonstrate that CPUs could not manage the high computational workload required by neural networks.

A description of how to implement efficient numerical CPU code is beyond the scope of this book, but we emphasize here that careful implementation for specific CPU families can yield large improvements. For example, in 2011, the best CPUs available could run neural network workloads faster when using fixed-point arithmetic rather than floating-point arithmetic. By creating a carefully tuned fixed-point implementation, [Vanhoucke *et al.* \(2011\)](#) obtained a threefold speedup over a strong floating-point system. Each new model of CPU has different performance characteristics, so sometimes floating-point implementations can be faster too. The important principle is that careful specialization of numerical computation routines can yield a large payoff. Other strategies, besides choosing whether to use fixed or floating point, include optimizing data structures to avoid cache misses and using vector instructions. Many machine learning researchers neglect these implementation details, but when the performance of an implementation restricts the size of the model, the accuracy of the model suffers.

12.1.2 GPU Implementations

Most modern neural network implementations are based on graphics processing units. Graphics processing units (GPUs) are specialized hardware components that were originally developed for graphics applications. The consumer market for video gaming systems spurred development of graphics processing hardware. The performance characteristics needed for good video gaming systems turn out to be beneficial for neural networks as well.

Video game rendering requires performing many operations in parallel quickly. Models of characters and environments are specified in terms of lists of 3-D coordinates of vertices. Graphics cards must perform matrix multiplication and division on many vertices in parallel to convert these 3-D coordinates into 2-D on-screen coordinates. The graphics card must then perform many computations at each pixel in parallel to determine the color of each pixel. In both cases, the

computations are fairly simple and do not involve much branching compared to the computational workload that a CPU usually encounters. For example, each vertex in the same rigid object will be multiplied by the same matrix; there is no need to evaluate an if statement per-vertex to determine which matrix to multiply by. The computations are also entirely independent of each other, and thus may be parallelized easily. The computations also involve processing massive buffers of memory, containing bitmaps describing the texture (color pattern) of each object to be rendered. Together, this results in graphics cards having been designed to have a high degree of parallelism and high memory bandwidth, at the cost of having a lower clock speed and less branching capability relative to traditional CPUs.

Neural network algorithms require the same performance characteristics as the real-time graphics algorithms described above. Neural networks usually involve large and numerous buffers of parameters, activation values, and gradient values, each of which must be completely updated during every step of training. These buffers are large enough to fall outside the cache of a traditional desktop computer so the memory bandwidth of the system often becomes the rate limiting factor. GPUs offer a compelling advantage over CPUs due to their high memory bandwidth. Neural network training algorithms typically do not involve much branching or sophisticated control, so they are appropriate for GPU hardware. Since neural networks can be divided into multiple individual “neurons” that can be processed independently from the other neurons in the same layer, neural networks easily benefit from the parallelism of GPU computing.

GPU hardware was originally so specialized that it could only be used for graphics tasks. Over time, GPU hardware became more flexible, allowing custom subroutines to be used to transform the coordinates of vertices or assign colors to pixels. In principle, there was no requirement that these pixel values actually be based on a rendering task. These GPUs could be used for scientific computing by writing the output of a computation to a buffer of pixel values. [Steinkrau et al. \(2005\)](#) implemented a two-layer fully connected neural network on a GPU and reported a threefold speedup over their CPU-based baseline. Shortly thereafter, [Chellapilla et al. \(2006\)](#) demonstrated that the same technique could be used to accelerate supervised convolutional networks.

The popularity of graphics cards for neural network training exploded after the advent of **general purpose GPUs**. These GP-GPUs could execute arbitrary code, not just rendering subroutines. NVIDIA’s CUDA programming language provided a way to write this arbitrary code in a C-like language. With their relatively convenient programming model, massive parallelism, and high memory

bandwidth, GP-GPUs now offer an ideal platform for neural network programming. This platform was rapidly adopted by deep learning researchers soon after it became available (Raina *et al.*, 2009; Ciresan *et al.*, 2010).

Writing efficient code for GP-GPUs remains a difficult task best left to specialists. The techniques required to obtain good performance on GPU are very different from those used on CPU. For example, good CPU-based code is usually designed to read information from the cache as much as possible. On GPU, most writable memory locations are not cached, so it can actually be faster to compute the same value twice, rather than compute it once and read it back from memory. GPU code is also inherently multi-threaded and the different threads must be coordinated with each other carefully. For example, memory operations are faster if they can be **coalesced**. Coalesced reads or writes occur when several threads can each read or write a value that they need simultaneously, as part of a single memory transaction. Different models of GPUs are able to coalesce different kinds of read or write patterns. Typically, memory operations are easier to coalesce if among n threads, thread i accesses byte $i + j$ of memory, and j is a multiple of some power of 2. The exact specifications differ between models of GPU. Another common consideration for GPUs is making sure that each thread in a group executes the same instruction simultaneously. This means that branching can be difficult on GPU. Threads are divided into small groups called **warps**. Each thread in a warp executes the same instruction during each cycle, so if different threads within the same warp need to execute different code paths, these different code paths must be traversed sequentially rather than in parallel.

Due to the difficulty of writing high performance GPU code, researchers should structure their workflow to avoid needing to write new GPU code in order to test new models or algorithms. Typically, one can do this by building a software library of high performance operations like convolution and matrix multiplication, then specifying models in terms of calls to this library of operations. For example, the machine learning library Pylearn2 (Goodfellow *et al.*, 2013c) specifies all of its machine learning algorithms in terms of calls to Theano (Bergstra *et al.*, 2010; Bastien *et al.*, 2012) and cuda-convnet (Krizhevsky, 2010), which provide these high-performance operations. This factored approach can also ease support for multiple kinds of hardware. For example, the same Theano program can run on either CPU or GPU, without needing to change any of the calls to Theano itself. Other libraries like TensorFlow (Abadi *et al.*, 2015) and Torch (Collobert *et al.*, 2011b) provide similar features.

12.1.3 Large-Scale Distributed Implementations

In many cases, the computational resources available on a single machine are insufficient. We therefore want to distribute the workload of training and inference across many machines.

Distributing inference is simple, because each input example we want to process can be run by a separate machine. This is known as **data parallelism**.

It is also possible to get **model parallelism**, where multiple machines work together on a single datapoint, with each machine running a different part of the model. This is feasible for both inference and training.

Data parallelism during training is somewhat harder. We can increase the size of the minibatch used for a single SGD step, but usually we get less than linear returns in terms of optimization performance. It would be better to allow multiple machines to compute multiple gradient descent steps in parallel. Unfortunately, the standard definition of gradient descent is as a completely sequential algorithm: the gradient at step t is a function of the parameters produced by step $t - 1$.

This can be solved using **asynchronous stochastic gradient descent** (Bengio *et al.*, 2001; Recht *et al.*, 2011). In this approach, several processor cores share the memory representing the parameters. Each core reads parameters without a lock, then computes a gradient, then increments the parameters without a lock. This reduces the average amount of improvement that each gradient descent step yields, because some of the cores overwrite each other's progress, but the increased rate of production of steps causes the learning process to be faster overall. Dean *et al.* (2012) pioneered the multi-machine implementation of this lock-free approach to gradient descent, where the parameters are managed by a **parameter server** rather than stored in shared memory. Distributed asynchronous gradient descent remains the primary strategy for training large deep networks and is used by most major deep learning groups in industry (Chilimbi *et al.*, 2014; Wu *et al.*, 2015). Academic deep learning researchers typically cannot afford the same scale of distributed learning systems but some research has focused on how to build distributed networks with relatively low-cost hardware available in the university setting (Coates *et al.*, 2013).

12.1.4 Model Compression

In many commercial applications, it is much more important that the time and memory cost of running inference in a machine learning model be low than that the time and memory cost of training be low. For applications that do not require

personalization, it is possible to train a model once, then deploy it to be used by billions of users. In many cases, the end user is more resource-constrained than the developer. For example, one might train a speech recognition network with a powerful computer cluster, then deploy it on mobile phones.

A key strategy for reducing the cost of inference is **model compression** ([Buciluă et al., 2006](#)). The basic idea of model compression is to replace the original, expensive model with a smaller model that requires less memory and runtime to store and evaluate.

Model compression is applicable when the size of the original model is driven primarily by a need to prevent overfitting. In most cases, the model with the lowest generalization error is an ensemble of several independently trained models. Evaluating all n ensemble members is expensive. Sometimes, even a single model generalizes better if it is large (for example, if it is regularized with dropout).

These large models learn some function $f(\mathbf{x})$, but do so using many more parameters than are necessary for the task. Their size is necessary only due to the limited number of training examples. As soon as we have fit this function $f(\mathbf{x})$, we can generate a training set containing infinitely many examples, simply by applying f to randomly sampled points \mathbf{x} . We then train the new, smaller, model to match $f(\mathbf{x})$ on these points. In order to most efficiently use the capacity of the new, small model, it is best to sample the new \mathbf{x} points from a distribution resembling the actual test inputs that will be supplied to the model later. This can be done by corrupting training examples or by drawing points from a generative model trained on the original training set.

Alternatively, one can train the smaller model only on the original training points, but train it to copy other features of the model, such as its posterior distribution over the incorrect classes ([Hinton et al., 2014, 2015](#)).

12.1.5 Dynamic Structure

One strategy for accelerating data processing systems in general is to build systems that have **dynamic structure** in the graph describing the computation needed to process an input. Data processing systems can dynamically determine which subset of many neural networks should be run on a given input. Individual neural networks can also exhibit dynamic structure internally by determining which subset of features (hidden units) to compute given information from the input. This form of dynamic structure inside neural networks is sometimes called **conditional computation** ([Bengio, 2013; Bengio et al., 2013b](#)). Since many components of the architecture may be relevant only for a small amount of possible inputs, the

system can run faster by computing these features only when they are needed.

Dynamic structure of computations is a basic computer science principle applied generally throughout the software engineering discipline. The simplest versions of dynamic structure applied to neural networks are based on determining which subset of some group of neural networks (or other machine learning models) should be applied to a particular input.

A venerable strategy for accelerating inference in a classifier is to use a **cascade** of classifiers. The cascade strategy may be applied when the goal is to detect the presence of a rare object (or event). To know for sure that the object is present, we must use a sophisticated classifier with high capacity, that is expensive to run. However, because the object is rare, we can usually use much less computation to reject inputs as not containing the object. In these situations, we can train a sequence of classifiers. The first classifiers in the sequence have low capacity, and are trained to have high recall. In other words, they are trained to make sure we do not wrongly reject an input when the object is present. The final classifier is trained to have high precision. At test time, we run inference by running the classifiers in a sequence, abandoning any example as soon as any one element in the cascade rejects it. Overall, this allows us to verify the presence of objects with high confidence, using a high capacity model, but does not force us to pay the cost of full inference for every example. There are two different ways that the cascade can achieve high capacity. One way is to make the later members of the cascade individually have high capacity. In this case, the system as a whole obviously has high capacity, because some of its individual members do. It is also possible to make a cascade in which every individual model has low capacity but the system as a whole has high capacity due to the combination of many small models. [Viola and Jones \(2001\)](#) used a cascade of boosted decision trees to implement a fast and robust face detector suitable for use in handheld digital cameras. Their classifier localizes a face using essentially a sliding window approach in which many windows are examined and rejected if they do not contain faces. Another version of cascades uses the earlier models to implement a sort of hard attention mechanism: the early members of the cascade localize an object and later members of the cascade perform further processing given the location of the object. For example, Google transcribes address numbers from Street View imagery using a two-step cascade that first locates the address number with one machine learning model and then transcribes it with another ([Goodfellow et al., 2014d](#)).

Decision trees themselves are an example of dynamic structure, because each node in the tree determines which of its subtrees should be evaluated for each input. A simple way to accomplish the union of deep learning and dynamic structure

is to train a decision tree in which each node uses a neural network to make the splitting decision (Guo and Gelfand, 1992), though this has typically not been done with the primary goal of accelerating inference computations.

In the same spirit, one can use a neural network, called the **gater** to select which one out of several **expert networks** will be used to compute the output, given the current input. The first version of this idea is called the **mixture of experts** (Nowlan, 1990; Jacobs *et al.*, 1991), in which the gater outputs a set of probabilities or weights (obtained via a softmax nonlinearity), one per expert, and the final output is obtained by the weighted combination of the output of the experts. In that case, the use of the gater does not offer a reduction in computational cost, but if a single expert is chosen by the gater for each example, we obtain the **hard mixture of experts** (Collobert *et al.*, 2001, 2002), which can considerably accelerate training and inference time. This strategy works well when the number of gating decisions is small because it is not combinatorial. But when we want to select different subsets of units or parameters, it is not possible to use a “soft switch” because it requires enumerating (and computing outputs for) all the gater configurations. To deal with this problem, several approaches have been explored to train combinatorial gaters. Bengio *et al.* (2013b) experiment with several estimators of the gradient on the gating probabilities, while Bacon *et al.* (2015) and Bengio *et al.* (2015a) use reinforcement learning techniques (policy gradient) to learn a form of conditional dropout on blocks of hidden units and get an actual reduction in computational cost without impacting negatively on the quality of the approximation.

Another kind of dynamic structure is a switch, where a hidden unit can receive input from different units depending on the context. This dynamic routing approach can be interpreted as an attention mechanism (Olshausen *et al.*, 1993). So far, the use of a hard switch has not proven effective on large-scale applications. Contemporary approaches instead use a weighted average over many possible inputs, and thus do not achieve all of the possible computational benefits of dynamic structure. Contemporary attention mechanisms are described in section 12.4.5.1.

One major obstacle to using dynamically structured systems is the decreased degree of parallelism that results from the system following different code branches for different inputs. This means that few operations in the network can be described as matrix multiplication or batch convolution on a minibatch of examples. We can write more specialized sub-routines that convolve each example with different kernels or multiply each row of a design matrix by a different set of columns of weights. Unfortunately, these more specialized subroutines are difficult to implement efficiently. CPU implementations will be slow due to the lack of cache

coherence and GPU implementations will be slow due to the lack of coalesced memory transactions and the need to serialize warps when members of a warp take different branches. In some cases, these issues can be mitigated by partitioning the examples into groups that all take the same branch, and processing these groups of examples simultaneously. This can be an acceptable strategy for minimizing the time required to process a fixed amount of examples in an offline setting. In a real-time setting where examples must be processed continuously, partitioning the workload can result in load-balancing issues. For example, if we assign one machine to process the first step in a cascade and another machine to process the last step in a cascade, then the first will tend to be overloaded and the last will tend to be underloaded. Similar issues arise if each machine is assigned to implement different nodes of a neural decision tree.

12.1.6 Specialized Hardware Implementations of Deep Networks

Since the early days of neural networks research, hardware designers have worked on specialized hardware implementations that could speed up training and/or inference of neural network algorithms. See early and more recent reviews of specialized hardware for deep networks (Lindsey and Lindblad, 1994; Beiu *et al.*, 2003; Misra and Saha, 2010).

Different forms of specialized hardware (Graf and Jackel, 1989; Mead and Ismail, 2012; Kim *et al.*, 2009; Pham *et al.*, 2012; Chen *et al.*, 2014a,b) have been developed over the last decades, either with ASICs (application-specific integrated circuit), either with digital (based on binary representations of numbers), analog (Graf and Jackel, 1989; Mead and Ismail, 2012) (based on physical implementations of continuous values as voltages or currents) or hybrid implementations (combining digital and analog components). In recent years more flexible FPGA (field programmable gated array) implementations (where the particulars of the circuit can be written on the chip after it has been built) have been developed.

Though software implementations on general-purpose processing units (CPUs and GPUs) typically use 32 or 64 bits of precision to represent floating point numbers, it has long been known that it was possible to use less precision, at least at inference time (Holt and Baker, 1991; Holi and Hwang, 1993; Presley and Haggard, 1994; Simard and Graf, 1994; Wawrzynek *et al.*, 1996; Savich *et al.*, 2007). This has become a more pressing issue in recent years as deep learning has gained in popularity in industrial products, and as the great impact of faster hardware was demonstrated with GPUs. Another factor that motivates current research on specialized hardware for deep networks is that the rate of progress of a single CPU or GPU core has slowed down, and most recent improvements in

computing speed have come from parallelization across cores (either in CPUs or GPUs). This is very different from the situation of the 1990s (the previous neural network era) where the hardware implementations of neural networks (which might take two years from inception to availability of a chip) could not keep up with the rapid progress and low prices of general-purpose CPUs. Building specialized hardware is thus a way to push the envelope further, at a time when new hardware designs are being developed for low-power devices such as phones, aiming for general-public applications of deep learning (e.g., with speech, computer vision or natural language).

Recent work on low-precision implementations of backprop-based neural nets ([Vanhoucke et al., 2011](#); [Courbariaux et al., 2015](#); [Gupta et al., 2015](#)) suggests that between 8 and 16 bits of precision can suffice for using or training deep neural networks with back-propagation. What is clear is that more precision is required during training than at inference time, and that some forms of dynamic fixed point representation of numbers can be used to reduce how many bits are required per number. Traditional fixed point numbers are restricted to a fixed range (which corresponds to a given exponent in a floating point representation). Dynamic fixed point representations share that range among a set of numbers (such as all the weights in one layer). Using fixed point rather than floating point representations and using less bits per number reduces the hardware surface area, power requirements and computing time needed for performing multiplications, and multiplications are the most demanding of the operations needed to use or train a modern deep network with backprop.

12.2 Computer Vision

Computer vision has traditionally been one of the most active research areas for deep learning applications, because vision is a task that is effortless for humans and many animals but challenging for computers ([Ballard et al., 1983](#)). Many of the most popular standard benchmark tasks for deep learning algorithms are forms of object recognition or optical character recognition.

Computer vision is a very broad field encompassing a wide variety of ways of processing images, and an amazing diversity of applications. Applications of computer vision range from reproducing human visual abilities, such as recognizing faces, to creating entirely new categories of visual abilities. As an example of the latter category, one recent computer vision application is to recognize sound waves from the vibrations they induce in objects visible in a video ([Davis et al., 2014](#)). Most deep learning research on computer vision has not focused on such

exotic applications that expand the realm of what is possible with imagery but rather a small core of AI goals aimed at replicating human abilities. Most deep learning for computer vision is used for object recognition or detection of some form, whether this means reporting which object is present in an image, annotating an image with bounding boxes around each object, transcribing a sequence of symbols from an image, or labeling each pixel in an image with the identity of the object it belongs to. Because generative modeling has been a guiding principle of deep learning research, there is also a large body of work on image synthesis using deep models. While image synthesis *ex nihilo* is usually not considered a computer vision endeavor, models capable of image synthesis are usually useful for image restoration, a computer vision task involving repairing defects in images or removing objects from images.

12.2.1 Preprocessing

Many application areas require sophisticated preprocessing because the original input comes in a form that is difficult for many deep learning architectures to represent. Computer vision usually requires relatively little of this kind of preprocessing. The images should be standardized so that their pixels all lie in the same, reasonable range, like $[0,1]$ or $[-1, 1]$. Mixing images that lie in $[0,1]$ with images that lie in $[0, 255]$ will usually result in failure. Formatting images to have the same scale is the only kind of preprocessing that is strictly necessary. Many computer vision architectures require images of a standard size, so images must be cropped or scaled to fit that size. Even this rescaling is not always strictly necessary. Some convolutional models accept variably-sized inputs and dynamically adjust the size of their pooling regions to keep the output size constant ([Waibel et al., 1989](#)). Other convolutional models have variable-sized output that automatically scales in size with the input, such as models that denoise or label each pixel in an image ([Hadsell et al., 2007](#)).

Dataset augmentation may be seen as a way of preprocessing the training set only. Dataset augmentation is an excellent way to reduce the generalization error of most computer vision models. A related idea applicable at test time is to show the model many different versions of the same input (for example, the same image cropped at slightly different locations) and have the different instantiations of the model vote to determine the output. This latter idea can be interpreted as an ensemble approach, and helps to reduce generalization error.

Other kinds of preprocessing are applied to both the train and the test set with the goal of putting each example into a more canonical form in order to reduce the amount of variation that the model needs to account for. Reducing the amount of

variation in the data can both reduce generalization error and reduce the size of the model needed to fit the training set. Simpler tasks may be solved by smaller models, and simpler solutions are more likely to generalize well. Preprocessing of this kind is usually designed to remove some kind of variability in the input data that is easy for a human designer to describe and that the human designer is confident has no relevance to the task. When training with large datasets and large models, this kind of preprocessing is often unnecessary, and it is best to just let the model learn which kinds of variability it should become invariant to. For example, the AlexNet system for classifying ImageNet only has one preprocessing step: subtracting the mean across training examples of each pixel (Krizhevsky *et al.*, 2012).

12.2.1.1 Contrast Normalization

One of the most obvious sources of variation that can be safely removed for many tasks is the amount of contrast in the image. Contrast simply refers to the magnitude of the difference between the bright and the dark pixels in an image. There are many ways of quantifying the contrast of an image. In the context of deep learning, contrast usually refers to the standard deviation of the pixels in an image or region of an image. Suppose we have an image represented by a tensor $\mathbf{X} \in \mathbb{R}^{r \times c \times 3}$, with $X_{i,j,1}$ being the red intensity at row i and column j , $X_{i,j,2}$ giving the green intensity and $X_{i,j,3}$ giving the blue intensity. Then the contrast of the entire image is given by

$$\sqrt{\frac{1}{3rc} \sum_{i=1}^r \sum_{j=1}^c \sum_{k=1}^3 (X_{i,j,k} - \bar{\mathbf{X}})^2} \quad (12.1)$$

where $\bar{\mathbf{X}}$ is the mean intensity of the entire image:

$$\bar{\mathbf{X}} = \frac{1}{3rc} \sum_{i=1}^r \sum_{j=1}^c \sum_{k=1}^3 X_{i,j,k}. \quad (12.2)$$

Global contrast normalization (GCN) aims to prevent images from having varying amounts of contrast by subtracting the mean from each image, then rescaling it so that the standard deviation across its pixels is equal to some constant s . This approach is complicated by the fact that no scaling factor can change the contrast of a zero-contrast image (one whose pixels all have equal intensity). Images with very low but non-zero contrast often have little information content. Dividing by the true standard deviation usually accomplishes nothing

more than amplifying sensor noise or compression artifacts in such cases. This motivates introducing a small, positive regularization parameter λ to bias the estimate of the standard deviation. Alternately, one can constrain the denominator to be at least ϵ . Given an input image \mathbf{X} , GCN produces an output image \mathbf{X}' , defined such that

$$\mathbf{X}'_{i,j,k} = s \frac{\mathbf{X}_{i,j,k} - \bar{\mathbf{X}}}{\max \left\{ \epsilon, \sqrt{\lambda + \frac{1}{3rc} \sum_{i=1}^r \sum_{j=1}^c \sum_{k=1}^3 (\mathbf{X}_{i,j,k} - \bar{\mathbf{X}})^2} \right\}}. \quad (12.3)$$

Datasets consisting of large images cropped to interesting objects are unlikely to contain any images with nearly constant intensity. In these cases, it is safe to practically ignore the small denominator problem by setting $\lambda = 0$ and avoid division by 0 in extremely rare cases by setting ϵ to an extremely low value like 10^{-8} . This is the approach used by [Goodfellow et al. \(2013a\)](#) on the CIFAR-10 dataset. Small images cropped randomly are more likely to have nearly constant intensity, making aggressive regularization more useful. [Coates et al. \(2011\)](#) used $\epsilon = 0$ and $\lambda = 10$ on small, randomly selected patches drawn from CIFAR-10.

The scale parameter s can usually be set to 1, as done by [Coates et al. \(2011\)](#), or chosen to make each individual pixel have standard deviation across examples close to 1, as done by [Goodfellow et al. \(2013a\)](#).

The standard deviation in equation 12.3 is just a rescaling of the L^2 norm of the image (assuming the mean of the image has already been removed). It is preferable to define GCN in terms of standard deviation rather than L^2 norm because the standard deviation includes division by the number of pixels, so GCN based on standard deviation allows the same s to be used regardless of image size. However, the observation that the L^2 norm is proportional to the standard deviation can help build a useful intuition. One can understand GCN as mapping examples to a spherical shell. See figure 12.1 for an illustration. This can be a useful property because neural networks are often better at responding to directions in space rather than exact locations. Responding to multiple distances in the same direction requires hidden units with collinear weight vectors but different biases. Such coordination can be difficult for the learning algorithm to discover. Additionally, many shallow graphical models have problems with representing multiple separated modes along the same line. GCN avoids these problems by reducing each example to a direction rather than a direction and a distance.

Counterintuitively, there is a preprocessing operation known as **sphering** and it is not the same operation as GCN. Sphering does not refer to making the data lie on a spherical shell, but rather to rescaling the principal components to have

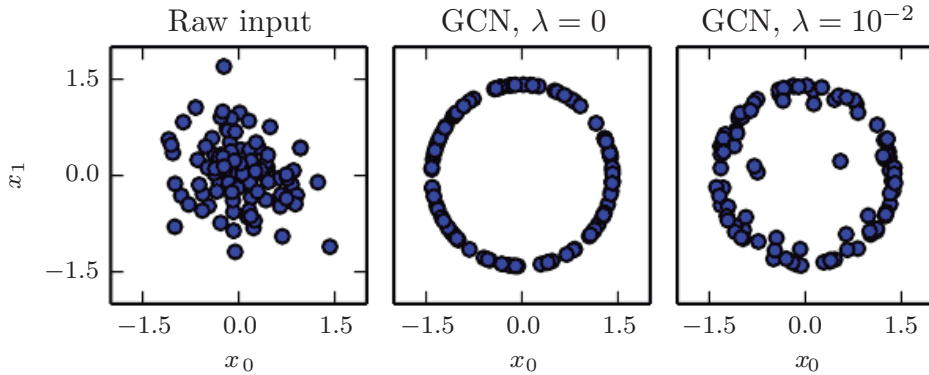


Figure 12.1: GCN maps examples onto a sphere. (*Left*) Raw input data may have any norm. (*Center*) GCN with $\lambda = 0$ maps all non-zero examples perfectly onto a sphere. Here we use $s = 1$ and $\epsilon = 10^{-8}$. Because we use GCN based on normalizing the standard deviation rather than the L^2 norm, the resulting sphere is not the unit sphere. (*Right*) Regularized GCN, with $\lambda > 0$, draws examples toward the sphere but does not completely discard the variation in their norm. We leave s and ϵ the same as before.

equal variance, so that the multivariate normal distribution used by PCA has spherical contours. Spherling is more commonly known as **whitening**.

Global contrast normalization will often fail to highlight image features we would like to stand out, such as edges and corners. If we have a scene with a large dark area and a large bright area (such as a city square with half the image in the shadow of a building) then global contrast normalization will ensure there is a large difference between the brightness of the dark area and the brightness of the light area. It will not, however, ensure that edges within the dark region stand out.

This motivates **local contrast normalization**. Local contrast normalization ensures that the contrast is normalized across each small window, rather than over the image as a whole. See figure 12.2 for a comparison of global and local contrast normalization.

Various definitions of local contrast normalization are possible. In all cases, one modifies each pixel by subtracting a mean of nearby pixels and dividing by a standard deviation of nearby pixels. In some cases, this is literally the mean and standard deviation of all pixels in a rectangular window centered on the pixel to be modified (Pinto *et al.*, 2008). In other cases, this is a weighted mean and weighted standard deviation using Gaussian weights centered on the pixel to be modified. In the case of color images, some strategies process different color

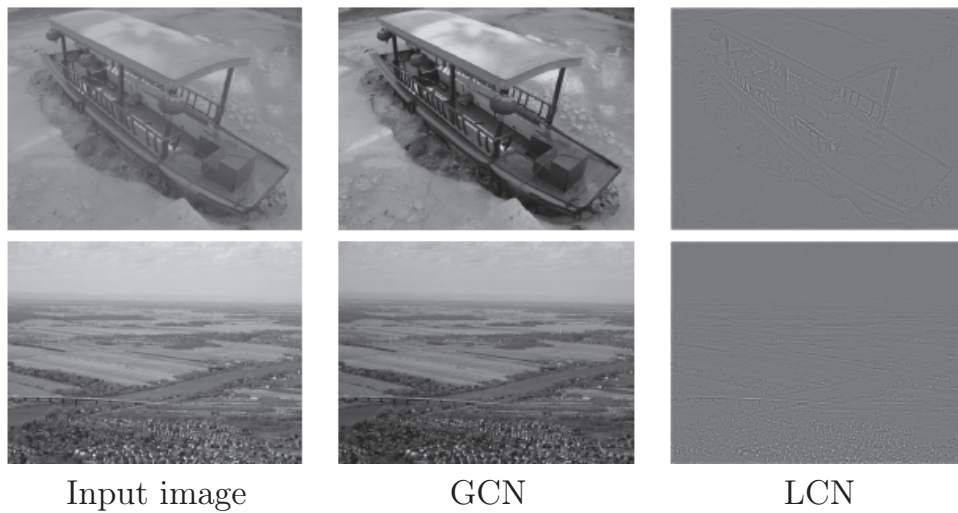


Figure 12.2: A comparison of global and local contrast normalization. Visually, the effects of global contrast normalization are subtle. It places all images on roughly the same scale, which reduces the burden on the learning algorithm to handle multiple scales. Local contrast normalization modifies the image much more, discarding all regions of constant intensity. This allows the model to focus on just the edges. Regions of fine texture, such as the houses in the second row, may lose some detail due to the bandwidth of the normalization kernel being too high.

channels separately while others combine information from different channels to normalize each pixel ([Sermanet *et al.*, 2012](#)).

Local contrast normalization can usually be implemented efficiently by using separable convolution (see section 9.8) to compute feature maps of local means and local standard deviations, then using element-wise subtraction and element-wise division on different feature maps.

Local contrast normalization is a differentiable operation and can also be used as a nonlinearity applied to the hidden layers of a network, as well as a preprocessing operation applied to the input.

As with global contrast normalization, we typically need to regularize local contrast normalization to avoid division by zero. In fact, because local contrast normalization typically acts on smaller windows, it is even more important to regularize. Smaller windows are more likely to contain values that are all nearly the same as each other, and thus more likely to have zero standard deviation.

12.2.1.2 Dataset Augmentation

As described in section 7.4, it is easy to improve the generalization of a classifier by increasing the size of the training set by adding extra copies of the training examples that have been modified with transformations that do not change the class. Object recognition is a classification task that is especially amenable to this form of dataset augmentation because the class is invariant to so many transformations and the input can be easily transformed with many geometric operations. As described before, classifiers can benefit from random translations, rotations, and in some cases, flips of the input to augment the dataset. In specialized computer vision applications, more advanced transformations are commonly used for dataset augmentation. These schemes include random perturbation of the colors in an image (Krizhevsky *et al.*, 2012) and nonlinear geometric distortions of the input (LeCun *et al.*, 1998b).

12.3 Speech Recognition

The task of speech recognition is to map an acoustic signal containing a spoken natural language utterance into the corresponding sequence of words intended by the speaker. Let $\mathbf{X} = (\mathbf{x}^{(1)}, \mathbf{x}^{(2)}, \dots, \mathbf{x}^{(T)})$ denote the sequence of acoustic input vectors (traditionally produced by splitting the audio into 20ms frames). Most speech recognition systems preprocess the input using specialized hand-designed features, but some (Jaitly and Hinton, 2011) deep learning systems learn features from raw input. Let $\mathbf{y} = (y_1, y_2, \dots, y_N)$ denote the target output sequence (usually a sequence of words or characters). The **automatic speech recognition** (ASR) task consists of creating a function f_{ASR}^* that computes the most probable linguistic sequence \mathbf{y} given the acoustic sequence \mathbf{X} :

$$f_{\text{ASR}}^*(\mathbf{X}) = \arg \max_{\mathbf{y}} P^*(\mathbf{y} \mid \mathbf{X} = \mathbf{X}) \quad (12.4)$$

where P^* is the true conditional distribution relating the inputs \mathbf{X} to the targets \mathbf{y} .

Since the 1980s and until about 2009–2012, state-of-the art speech recognition systems primarily combined hidden Markov models (HMMs) and Gaussian mixture models (GMMs). GMMs modeled the association between acoustic features and phonemes (Bahl *et al.*, 1987), while HMMs modeled the sequence of phonemes. The GMM-HMM model family treats acoustic waveforms as being generated by the following process: first an HMM generates a sequence of phonemes and discrete sub-phonemic states (such as the beginning, middle, and end of each

phoneme), then a GMM transforms each discrete symbol into a brief segment of audio waveform. Although GMM-HMM systems dominated ASR until recently, speech recognition was actually one of the first areas where neural networks were applied, and numerous ASR systems from the late 1980s and early 1990s used neural nets (Bourlard and Wellekens, 1989; Waibel *et al.*, 1989; Robinson and Fallside, 1991; Bengio *et al.*, 1991, 1992; Konig *et al.*, 1996). At the time, the performance of ASR based on neural nets approximately matched the performance of GMM-HMM systems. For example, Robinson and Fallside (1991) achieved 26% phoneme error rate on the TIMIT (Garofolo *et al.*, 1993) corpus (with 39 phonemes to discriminate between), which was better than or comparable to HMM-based systems. Since then, TIMIT has been a benchmark for phoneme recognition, playing a role similar to the role MNIST plays for object recognition. However, because of the complex engineering involved in software systems for speech recognition and the effort that had been invested in building these systems on the basis of GMM-HMMs, the industry did not see a compelling argument for switching to neural networks. As a consequence, until the late 2000s, both academic and industrial research in using neural nets for speech recognition mostly focused on using neural nets to learn extra features for GMM-HMM systems.

Later, with *much larger and deeper models* and much larger datasets, recognition accuracy was dramatically improved by using neural networks to replace GMMs for the task of associating acoustic features to phonemes (or sub-phonemic states). Starting in 2009, speech researchers applied a form of deep learning based on unsupervised learning to speech recognition. This approach to deep learning was based on training undirected probabilistic models called restricted Boltzmann machines (RBMs) to model the input data. RBMs will be described in part III.

To solve speech recognition tasks, unsupervised pretraining was used to build deep feedforward networks whose layers were each initialized by training an RBM. These networks take spectral acoustic representations in a fixed-size input window (around a center frame) and predict the conditional probabilities of HMM states for that center frame. Training such deep networks helped to significantly improve the recognition rate on TIMIT (Mohamed *et al.*, 2009, 2012a), bringing down the phoneme error rate from about 26% to 20.7%. See Mohamed *et al.* (2012b) for an analysis of reasons for the success of these models. Extensions to the basic phone recognition pipeline included the addition of speaker-adaptive features (Mohamed *et al.*, 2011) that further reduced the error rate. This was quickly followed up by work to expand the architecture from phoneme recognition (which is what TIMIT is focused on) to large-vocabulary speech recognition (Dahl *et al.*, 2012), which involves not just recognizing phonemes but also recognizing sequences of words from a large vocabulary. Deep networks for speech recognition eventually

shifted from being based on pretraining and Boltzmann machines to being based on techniques such as rectified linear units and dropout (Zeiler *et al.*, 2013; Dahl *et al.*, 2013). By that time, several of the major speech groups in industry had started exploring deep learning in collaboration with academic researchers. Hinton *et al.* (2012a) describe the breakthroughs achieved by these collaborators, which are now deployed in products such as mobile phones.

Later, as these groups explored larger and larger labeled datasets and incorporated some of the methods for initializing, training, and setting up the architecture of deep nets, they realized that the unsupervised pretraining phase was either unnecessary or did not bring any significant improvement.

These breakthroughs in recognition performance for word error rate in speech recognition were unprecedented (around 30% improvement) and were following a long period of about ten years during which error rates did not improve much with the traditional GMM-HMM technology, in spite of the continuously growing size of training sets (see figure 2.4 of Deng and Yu (2014)). This created a rapid shift in the speech recognition community towards deep learning. In a matter of roughly two years, most of the industrial products for speech recognition incorporated deep neural networks and this success spurred a new wave of research into deep learning algorithms and architectures for ASR, which is still ongoing today.

One of these innovations was the use of convolutional networks (Sainath *et al.*, 2013) that replicate weights across time and frequency, improving over the earlier time-delay neural networks that replicated weights only across time. The new two-dimensional convolutional models regard the input spectrogram not as one long vector but as an image, with one axis corresponding to time and the other to frequency of spectral components.

Another important push, still ongoing, has been towards end-to-end deep learning speech recognition systems that completely remove the HMM. The first major breakthrough in this direction came from Graves *et al.* (2013) who trained a deep LSTM RNN (see section 10.10), using MAP inference over the frame-to-phoneme alignment, as in LeCun *et al.* (1998b) and in the CTC framework (Graves *et al.*, 2006; Graves, 2012). A deep RNN (Graves *et al.*, 2013) has state variables from several layers at each time step, giving the unfolded graph two kinds of depth: ordinary depth due to a stack of layers, and depth due to time unfolding. This work brought the phoneme error rate on TIMIT to a record low of 17.7%. See Pascanu *et al.* (2014a) and Chung *et al.* (2014) for other variants of deep RNNs, applied in other settings.

Another contemporary step toward end-to-end deep learning ASR is to let the system learn how to “align” the acoustic-level information with the phonetic-level

information (Chorowski *et al.*, 2014; Lu *et al.*, 2015).

12.4 Natural Language Processing

Natural language processing (NLP) is the use of human languages, such as English or French, by a computer. Computer programs typically read and emit specialized languages designed to allow efficient and unambiguous parsing by simple programs. More naturally occurring languages are often ambiguous and defy formal description. Natural language processing includes applications such as machine translation, in which the learner must read a sentence in one human language and emit an equivalent sentence in another human language. Many NLP applications are based on language models that define a probability distribution over sequences of words, characters or bytes in a natural language.

As with the other applications discussed in this chapter, very generic neural network techniques can be successfully applied to natural language processing. However, to achieve excellent performance and to scale well to large applications, some domain-specific strategies become important. To build an efficient model of natural language, we must usually use techniques that are specialized for processing sequential data. In many cases, we choose to regard natural language as a sequence of words, rather than a sequence of individual characters or bytes. Because the total number of possible words is so large, word-based language models must operate on an extremely high-dimensional and sparse discrete space. Several strategies have been developed to make models of such a space efficient, both in a computational and in a statistical sense.

12.4.1 *n*-grams

A **language model** defines a probability distribution over sequences of tokens in a natural language. Depending on how the model is designed, a token may be a word, a character, or even a byte. Tokens are always discrete entities. The earliest successful language models were based on models of fixed-length sequences of tokens called *n*-grams. An *n*-gram is a sequence of *n* tokens.

Models based on *n*-grams define the conditional probability of the *n*-th token given the preceding $n - 1$ tokens. The model uses products of these conditional distributions to define the probability distribution over longer sequences:

$$P(x_1, \dots, x_\tau) = P(x_1, \dots, x_{n-1}) \prod_{t=n}^{\tau} P(x_t | x_{t-n+1}, \dots, x_{t-1}). \quad (12.5)$$

This decomposition is justified by the chain rule of probability. The probability distribution over the initial sequence $P(x_1, \dots, x_{n-1})$ may be modeled by a different model with a smaller value of n .

Training n -gram models is straightforward because the maximum likelihood estimate can be computed simply by counting how many times each possible n gram occurs in the training set. Models based on n -grams have been the core building block of statistical language modeling for many decades (Jelinek and Mercer, 1980; Katz, 1987; Chen and Goodman, 1999).

For small values of n , models have particular names: **unigram** for $n=1$, **bigram** for $n=2$, and **trigram** for $n=3$. These names derive from the Latin prefixes for the corresponding numbers and the Greek suffix “-gram” denoting something that is written.

Usually we train both an n -gram model and an $n-1$ gram model simultaneously. This makes it easy to compute

$$P(x_t | x_{t-n+1}, \dots, x_{t-1}) = \frac{P_n(x_{t-n+1}, \dots, x_t)}{P_{n-1}(x_{t-n+1}, \dots, x_{t-1})} \quad (12.6)$$

simply by looking up two stored probabilities. For this to exactly reproduce inference in P_n , we must omit the final character from each sequence when we train P_{n-1} .

As an example, we demonstrate how a trigram model computes the probability of the sentence “THE DOG RAN AWAY.” The first words of the sentence cannot be handled by the default formula based on conditional probability because there is no context at the beginning of the sentence. Instead, we must use the marginal probability over words at the start of the sentence. We thus evaluate $P_3(\text{THE DOG RAN})$. Finally, the last word may be predicted using the typical case, of using the conditional distribution $P(\text{AWAY} | \text{DOG RAN})$. Putting this together with equation 12.6, we obtain:

$$P(\text{THE DOG RAN AWAY}) = P_3(\text{THE DOG RAN})P_3(\text{DOG RAN AWAY})/P_2(\text{DOG RAN}). \quad (12.7)$$

A fundamental limitation of maximum likelihood for n -gram models is that P_n as estimated from training set counts is very likely to be zero in many cases, even though the tuple (x_{t-n+1}, \dots, x_t) may appear in the test set. This can cause two different kinds of catastrophic outcomes. When P_{n-1} is zero, the ratio is undefined, so the model does not even produce a sensible output. When P_{n-1} is non-zero but P_n is zero, the test log-likelihood is $-\infty$. To avoid such catastrophic outcomes, most n -gram models employ some form of **smoothing**. Smoothing techniques

shift probability mass from the observed tuples to unobserved ones that are similar. See [Chen and Goodman \(1999\)](#) for a review and empirical comparisons. One basic technique consists of adding non-zero probability mass to all of the possible next symbol values. This method can be justified as Bayesian inference with a uniform or Dirichlet prior over the count parameters. Another very popular idea is to form a mixture model containing higher-order and lower-order n -gram models, with the higher-order models providing more capacity and the lower-order models being more likely to avoid counts of zero. **Back-off methods** look-up the lower-order n -grams if the frequency of the context $x_{t-1}, \dots, x_{t-n+1}$ is too small to use the higher-order model. More formally, they estimate the distribution over x_t by using contexts $x_{t-n+k}, \dots, x_{t-1}$, for increasing k , until a sufficiently reliable estimate is found.

Classical n -gram models are particularly vulnerable to the curse of dimensionality. There are $|\mathbb{V}|^n$ possible n -grams and $|\mathbb{V}|$ is often very large. Even with a massive training set and modest n , most n -grams will not occur in the training set. One way to view a classical n -gram model is that it is performing nearest-neighbor lookup. In other words, it can be viewed as a local non-parametric predictor, similar to k -nearest neighbors. The statistical problems facing these extremely local predictors are described in section [5.11.2](#). The problem for a language model is even more severe than usual, because any two different words have the same distance from each other in one-hot vector space. It is thus difficult to leverage much information from any “neighbors”—only training examples that repeat literally the same context are useful for local generalization. To overcome these problems, a language model must be able to share knowledge between one word and other semantically similar words.

To improve the statistical efficiency of n -gram models, **class-based language models** ([Brown et al., 1992](#); [Ney and Kneser, 1993](#); [Niesler et al., 1998](#)) introduce the notion of word categories and then share statistical strength between words that are in the same category. The idea is to use a clustering algorithm to partition the set of words into clusters or classes, based on their co-occurrence frequencies with other words. The model can then use word class IDs rather than individual word IDs to represent the context on the right side of the conditioning bar. Composite models combining word-based and class-based models via mixing or back-off are also possible. Although word classes provide a way to generalize between sequences in which some word is replaced by another of the same class, much information is lost in this representation.

12.4.2 Neural Language Models

Neural language models or NLMs are a class of language model designed to overcome the curse of dimensionality problem for modeling natural language sequences by using a distributed representation of words (Bengio *et al.*, 2001). Unlike class-based n -gram models, neural language models are able to recognize that two words are similar without losing the ability to encode each word as distinct from the other. Neural language models share statistical strength between one word (and its context) and other similar words and contexts. The distributed representation the model learns for each word enables this sharing by allowing the model to treat words that have features in common similarly. For example, if the word `dog` and the word `cat` map to representations that share many attributes, then sentences that contain the word `cat` can inform the predictions that will be made by the model for sentences that contain the word `dog`, and vice-versa. Because there are many such attributes, there are many ways in which generalization can happen, transferring information from each training sentence to an exponentially large number of semantically related sentences. The curse of dimensionality requires the model to generalize to a number of sentences that is exponential in the sentence length. The model counters this curse by relating each training sentence to an exponential number of similar sentences.

We sometimes call these word representations **word embeddings**. In this interpretation, we view the raw symbols as points in a space of dimension equal to the vocabulary size. The word representations embed those points in a feature space of lower dimension. In the original space, every word is represented by a one-hot vector, so every pair of words is at Euclidean distance $\sqrt{2}$ from each other. In the embedding space, words that frequently appear in similar contexts (or any pair of words sharing some “features” learned by the model) are close to each other. This often results in words with similar meanings being neighbors. Figure 12.3 zooms in on specific areas of a learned word embedding space to show how semantically similar words map to representations that are close to each other.

Neural networks in other domains also define embeddings. For example, a hidden layer of a convolutional network provides an “image embedding.” Usually NLP practitioners are much more interested in this idea of embeddings because natural language does not originally lie in a real-valued vector space. The hidden layer has provided a more qualitatively dramatic change in the way the data is represented.

The basic idea of using distributed representations to improve models for natural language processing is not restricted to neural networks. It may also be used with graphical models that have distributed representations in the form of

multiple latent variables (Mnih and Hinton, 2007).

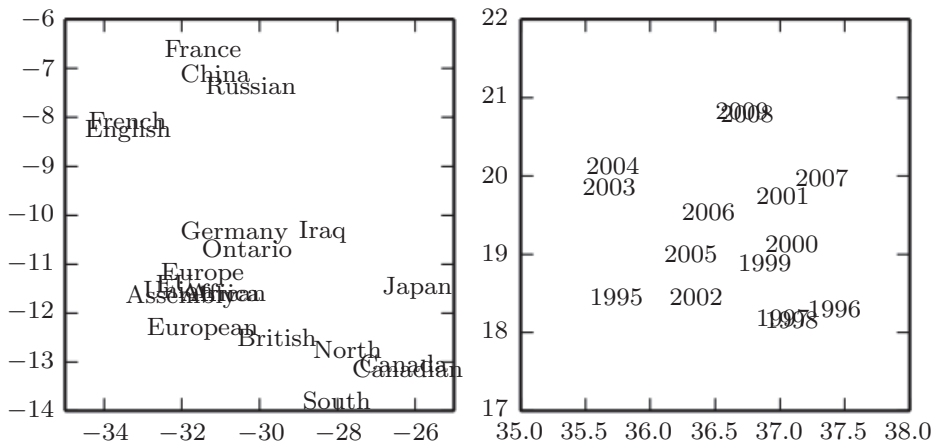


Figure 12.3: Two-dimensional visualizations of word embeddings obtained from a neural machine translation model (Bahdanau *et al.*, 2015), zooming in on specific areas where semantically related words have embedding vectors that are close to each other. Countries appear on the left and numbers on the right. Keep in mind that these embeddings are 2-D for the purpose of visualization. In real applications, embeddings typically have higher dimensionality and can simultaneously capture many kinds of similarity between words.

12.4.3 High-Dimensional Outputs

In many natural language applications, we often want our models to produce words (rather than characters) as the fundamental unit of the output. For large vocabularies, it can be very computationally expensive to represent an output distribution over the choice of a word, because the vocabulary size is large. In many applications, \mathbb{V} contains hundreds of thousands of words. The naive approach to representing such a distribution is to apply an affine transformation from a hidden representation to the output space, then apply the softmax function. Suppose we have a vocabulary \mathbb{V} with size $|\mathbb{V}|$. The weight matrix describing the linear component of this affine transformation is very large, because its output dimension is $|\mathbb{V}|$. This imposes a high memory cost to represent the matrix, and a high computational cost to multiply by it. Because the softmax is normalized across all $|\mathbb{V}|$ outputs, it is necessary to perform the full matrix multiplication at training time as well as test time—we cannot calculate only the dot product with the weight vector for the correct output. The high computational costs of the output layer thus arise both at training time (to compute the likelihood and its gradient) and at test time (to compute probabilities for all or selected words). For specialized

loss functions, the gradient can be computed efficiently (Vincent *et al.*, 2015), but the standard cross-entropy loss applied to a traditional softmax output layer poses many difficulties.

Suppose that \mathbf{h} is the top hidden layer used to predict the output probabilities $\hat{\mathbf{y}}$. If we parametrize the transformation from \mathbf{h} to $\hat{\mathbf{y}}$ with learned weights \mathbf{W} and learned biases \mathbf{b} , then the affine-softmax output layer performs the following computations:

$$a_i = b_i + \sum_j W_{ij} h_j \quad \forall i \in \{1, \dots, |\mathbb{V}|\}, \quad (12.8)$$

$$\hat{y}_i = \frac{e^{a_i}}{\sum_{i'=1}^{|\mathbb{V}|} e^{a_{i'}}}. \quad (12.9)$$

If \mathbf{h} contains n_h elements then the above operation is $O(|\mathbb{V}|n_h)$. With n_h in the thousands and $|\mathbb{V}|$ in the hundreds of thousands, this operation dominates the computation of most neural language models.

12.4.3.1 Use of a Short List

The first neural language models (Bengio *et al.*, 2001, 2003) dealt with the high cost of using a softmax over a large number of output words by limiting the vocabulary size to 10,000 or 20,000 words. Schwenk and Gauvain (2002) and Schwenk (2007) built upon this approach by splitting the vocabulary \mathbb{V} into a **shortlist** \mathbb{L} of most frequent words (handled by the neural net) and a tail $\mathbb{T} = \mathbb{V} \setminus \mathbb{L}$ of more rare words (handled by an n -gram model). To be able to combine the two predictions, the neural net also has to predict the probability that a word appearing after context C belongs to the tail list. This may be achieved by adding an extra sigmoid output unit to provide an estimate of $P(i \in \mathbb{T} | C)$. The extra output can then be used to achieve an estimate of the probability distribution over all words in \mathbb{V} as follows:

$$\begin{aligned} P(y = i | C) &= 1_{i \in \mathbb{L}} P(y = i | C, i \in \mathbb{L}) (1 - P(i \in \mathbb{T} | C)) \\ &\quad + 1_{i \in \mathbb{T}} P(y = i | C, i \in \mathbb{T}) P(i \in \mathbb{T} | C) \end{aligned} \quad (12.10)$$

where $P(y = i | C, i \in \mathbb{L})$ is provided by the neural language model and $P(y = i | C, i \in \mathbb{T})$ is provided by the n -gram model. With slight modification, this approach can also work using an extra output value in the neural language model's softmax layer, rather than a separate sigmoid unit.

An obvious disadvantage of the short list approach is that the potential generalization advantage of the neural language models is limited to the most frequent

words, where, arguably, it is the least useful. This disadvantage has stimulated the exploration of alternative methods to deal with high-dimensional outputs, described below.

12.4.3.2 Hierarchical Softmax

A classical approach (Goodman, 2001) to reducing the computational burden of high-dimensional output layers over large vocabulary sets \mathbb{V} is to decompose probabilities hierarchically. Instead of necessitating a number of computations proportional to $|\mathbb{V}|$ (and also proportional to the number of hidden units, n_h), the $|\mathbb{V}|$ factor can be reduced to as low as $\log |\mathbb{V}|$. Bengio (2002) and Morin and Bengio (2005) introduced this factorized approach to the context of neural language models.

One can think of this hierarchy as building categories of words, then categories of categories of words, then categories of categories of categories of words, etc. These nested categories form a tree, with words at the leaves. In a balanced tree, the tree has depth $O(\log |\mathbb{V}|)$. The probability of choosing a word is given by the product of the probabilities of choosing the branch leading to that word at every node on a path from the root of the tree to the leaf containing the word. Figure 12.4 illustrates a simple example. Mnih and Hinton (2009) also describe how to use multiple paths to identify a single word in order to better model words that have multiple meanings. Computing the probability of a word then involves summation over all of the paths that lead to that word.

To predict the conditional probabilities required at each node of the tree, we typically use a logistic regression model at each node of the tree, and provide the same context C as input to all of these models. Because the correct output is encoded in the training set, we can use supervised learning to train the logistic regression models. This is typically done using a standard cross-entropy loss, corresponding to maximizing the log-likelihood of the correct sequence of decisions.

Because the output log-likelihood can be computed efficiently (as low as $\log |\mathbb{V}|$ rather than $|\mathbb{V}|$), its gradients may also be computed efficiently. This includes not only the gradient with respect to the output parameters but also the gradients with respect to the hidden layer activations.

It is possible but usually not practical to optimize the tree structure to minimize the expected number of computations. Tools from information theory specify how to choose the optimal binary code given the relative frequencies of the words. To do so, we could structure the tree so that the number of bits associated with a word is approximately equal to the logarithm of the frequency of that word. However, in

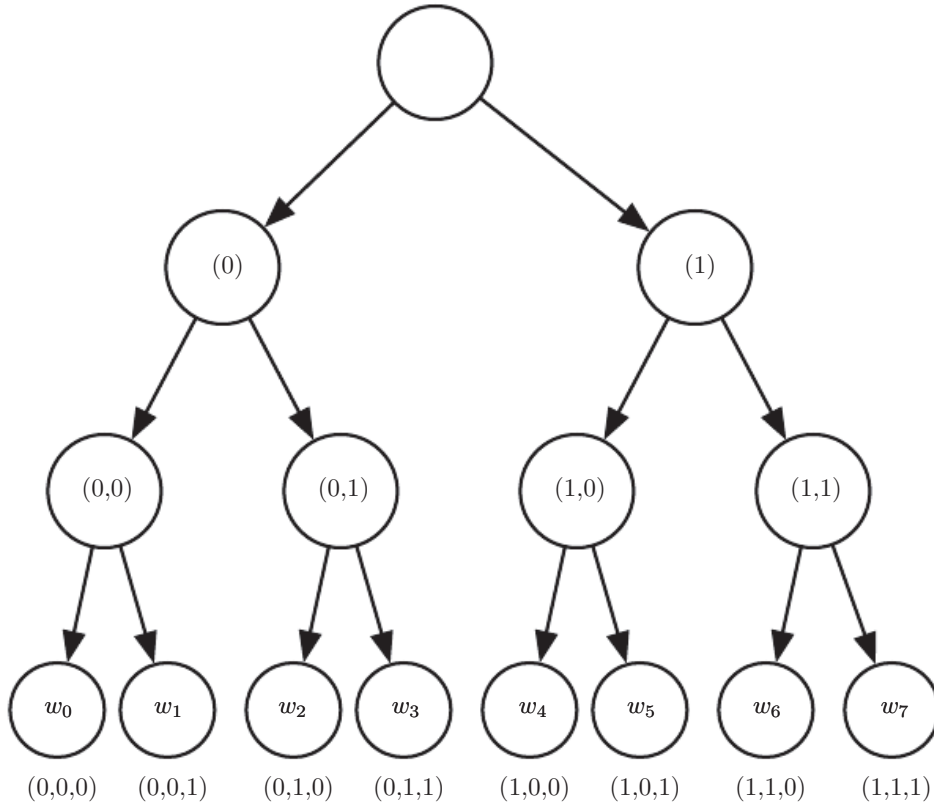


Figure 12.4: Illustration of a simple hierarchy of word categories, with 8 words w_0, \dots, w_7 organized into a three level hierarchy. The leaves of the tree represent actual specific words. Internal nodes represent groups of words. Any node can be indexed by the sequence of binary decisions (0=left, 1=right) to reach the node from the root. Super-class (0) contains the classes (0, 0) and (0, 1), which respectively contain the sets of words $\{w_0, w_1\}$ and $\{w_2, w_3\}$, and similarly super-class (1) contains the classes (1, 0) and (1, 1), which respectively contain the words (w_4, w_5) and (w_6, w_7) . If the tree is sufficiently balanced, the maximum depth (number of binary decisions) is on the order of the logarithm of the number of words $|\mathbb{V}|$: the choice of one out of $|\mathbb{V}|$ words can be obtained by doing $O(\log |\mathbb{V}|)$ operations (one for each of the nodes on the path from the root). In this example, computing the probability of a word y can be done by multiplying three probabilities, associated with the binary decisions to move left or right at each node on the path from the root to a node y . Let $b_i(y)$ be the i -th binary decision when traversing the tree towards the value y . The probability of sampling an output y decomposes into a product of conditional probabilities, using the chain rule for conditional probabilities, with each node indexed by the prefix of these bits. For example, node (1, 0) corresponds to the prefix $(b_0(w_4) = 1, b_1(w_4) = 0)$, and the probability of w_4 can be decomposed as follows:

$$P(y = w_4) = P(b_0 = 1, b_1 = 0, b_2 = 0) \quad (12.11)$$

$$= P(b_0 = 1)P(b_1 = 0 | b_0 = 1)P(b_2 = 0 | b_0 = 1, b_1 = 0). \quad (12.12)$$

practice, the computational savings are typically not worth the effort because the computation of the output probabilities is only one part of the total computation in the neural language model. For example, suppose there are l fully connected hidden layers of width n_h . Let n_b be the weighted average of the number of bits required to identify a word, with the weighting given by the frequency of these words. In this example, the number of operations needed to compute the hidden activations grows as $O(ln_h^2)$ while the output computations grow as $O(n_h n_b)$. As long as $n_b \leq ln_h$, we can reduce computation more by shrinking n_h than by shrinking n_b . Indeed, n_b is often small. Because the size of the vocabulary rarely exceeds a million words and $\log_2(10^6) \approx 20$, it is possible to reduce n_b to about 20, but n_h is often much larger, around 10^3 or more. Rather than carefully optimizing a tree with a branching factor of 2, one can instead define a tree with depth two and a branching factor of $\sqrt{|\mathbb{V}|}$. Such a tree corresponds to simply defining a set of mutually exclusive word classes. The simple approach based on a tree of depth two captures most of the computational benefit of the hierarchical strategy.

One question that remains somewhat open is how to best define these word classes, or how to define the word hierarchy in general. Early work used existing hierarchies ([Morin and Bengio, 2005](#)) but the hierarchy can also be learned, ideally jointly with the neural language model. Learning the hierarchy is difficult. An exact optimization of the log-likelihood appears intractable because the choice of a word hierarchy is a discrete one, not amenable to gradient-based optimization. However, one could use discrete optimization to approximately optimize the partition of words into word classes.

An important advantage of the hierarchical softmax is that it brings computational benefits both at training time and at test time, if at test time we want to compute the probability of specific words.

Of course, computing the probability of all $|\mathbb{V}|$ words will remain expensive even with the hierarchical softmax. Another important operation is selecting the most likely word in a given context. Unfortunately the tree structure does not provide an efficient and exact solution to this problem.

A disadvantage is that in practice the hierarchical softmax tends to give worse test results than sampling-based methods we will describe next. This may be due to a poor choice of word classes.

12.4.3.3 Importance Sampling

One way to speed up the training of neural language models is to avoid explicitly computing the contribution of the gradient from all of the words that do not appear

in the next position. Every incorrect word should have low probability under the model. It can be computationally costly to enumerate all of these words. Instead, it is possible to sample only a subset of the words. Using the notation introduced in equation 12.8, the gradient can be written as follows:

$$\frac{\partial \log P(y | C)}{\partial \theta} = \frac{\partial \log \text{softmax}_y(\mathbf{a})}{\partial \theta} \quad (12.13)$$

$$= \frac{\partial}{\partial \theta} \log \frac{e^{a_y}}{\sum_i e^{a_i}} \quad (12.14)$$

$$= \frac{\partial}{\partial \theta} (a_y - \log \sum_i e^{a_i}) \quad (12.15)$$

$$= \frac{\partial a_y}{\partial \theta} - \sum_i P(y = i | C) \frac{\partial a_i}{\partial \theta} \quad (12.16)$$

where \mathbf{a} is the vector of pre-softmax activations (or scores), with one element per word. The first term is the **positive phase** term (pushing a_y up) while the second term is the **negative phase** term (pushing a_i down for all i , with weight $P(i | C)$). Since the negative phase term is an expectation, we can estimate it with a Monte Carlo sample. However, that would require sampling from the model itself. Sampling from the model requires computing $P(i | C)$ for all i in the vocabulary, which is precisely what we are trying to avoid.

Instead of sampling from the model, one can sample from another distribution, called the proposal distribution (denoted q), and use appropriate weights to correct for the bias introduced by sampling from the wrong distribution (Bengio and Sénecal, 2003; Bengio and Sénecal, 2008). This is an application of a more general technique called **importance sampling**, which will be described in more detail in section 17.2. Unfortunately, even exact importance sampling is not efficient because it requires computing weights p_i/q_i , where $p_i = P(i | C)$, which can only be computed if all the scores a_i are computed. The solution adopted for this application is called **biased importance sampling**, where the importance weights are normalized to sum to 1. When negative word n_i is sampled, the associated gradient is weighted by

$$w_i = \frac{p_{n_i}/q_{n_i}}{\sum_{j=1}^N p_{n_j}/q_{n_j}}. \quad (12.17)$$

These weights are used to give the appropriate importance to the m negative samples from q used to form the estimated negative phase contribution to the

gradient:

$$\sum_{i=1}^{|V|} P(i \mid C) \frac{\partial a_i}{\partial \theta} \approx \frac{1}{m} \sum_{i=1}^m w_i \frac{\partial a_{n_i}}{\partial \theta}. \quad (12.18)$$

A unigram or a bigram distribution works well as the proposal distribution q . It is easy to estimate the parameters of such a distribution from data. After estimating the parameters, it is also possible to sample from such a distribution very efficiently.

Importance sampling is not only useful for speeding up models with large softmax outputs. More generally, it is useful for accelerating training with large sparse output layers, where the output is a sparse vector rather than a 1-of- n choice. An example is a **bag of words**. A bag of words is a sparse vector \mathbf{v} where v_i indicates the presence or absence of word i from the vocabulary in the document. Alternately, v_i can indicate the number of times that word i appears. Machine learning models that emit such sparse vectors can be expensive to train for a variety of reasons. Early in learning, the model may not actually choose to make the output truly sparse. Moreover, the loss function we use for training might most naturally be described in terms of comparing every element of the output to every element of the target. This means that it is not always clear that there is a computational benefit to using sparse outputs, because the model may choose to make the majority of the output non-zero and all of these non-zero values need to be compared to the corresponding training target, even if the training target is zero. [Dauphin et al. \(2011\)](#) demonstrated that such models can be accelerated using importance sampling. The efficient algorithm minimizes the loss reconstruction for the “positive words” (those that are non-zero in the target) and an equal number of “negative words.” The negative words are chosen randomly, using a heuristic to sample words that are more likely to be mistaken. The bias introduced by this heuristic oversampling can then be corrected using importance weights.

In all of these cases, the computational complexity of gradient estimation for the output layer is reduced to be proportional to the number of negative samples rather than proportional to the size of the output vector.

12.4.3.4 Noise-Contrastive Estimation and Ranking Loss

Other approaches based on sampling have been proposed to reduce the computational cost of training neural language models with large vocabularies. An early example is the ranking loss proposed by [Collobert and Weston \(2008a\)](#), which views the output of the neural language model for each word as a score and tries to make the score of the correct word a_y be ranked high in comparison to the other

scores a_i . The ranking loss proposed then is

$$L = \sum_i \max(0, 1 - a_y + a_i). \quad (12.19)$$

The gradient is zero for the i -th term if the score of the observed word, a_y , is greater than the score of the negative word a_i by a margin of 1. One issue with this criterion is that it does not provide estimated conditional probabilities, which are useful in some applications, including speech recognition and text generation (including conditional text generation tasks such as translation).

A more recently used training objective for neural language model is noise-contrastive estimation, which is introduced in section 18.6. This approach has been successfully applied to neural language models (Mnih and Teh, 2012; Mnih and Kavukcuoglu, 2013).

12.4.4 Combining Neural Language Models with n -grams

A major advantage of n -gram models over neural networks is that n -gram models achieve high model capacity (by storing the frequencies of very many tuples) while requiring very little computation to process an example (by looking up only a few tuples that match the current context). If we use hash tables or trees to access the counts, the computation used for n -grams is almost independent of capacity. In comparison, doubling a neural network’s number of parameters typically also roughly doubles its computation time. Exceptions include models that avoid using all parameters on each pass. Embedding layers index only a single embedding in each pass, so we can increase the vocabulary size without increasing the computation time per example. Some other models, such as tiled convolutional networks, can add parameters while reducing the degree of parameter sharing in order to maintain the same amount of computation. However, typical neural network layers based on matrix multiplication use an amount of computation proportional to the number of parameters.

One easy way to add capacity is thus to combine both approaches in an ensemble consisting of a neural language model and an n -gram language model (Bengio *et al.*, 2001, 2003). As with any ensemble, this technique can reduce test error if the ensemble members make independent mistakes. The field of ensemble learning provides many ways of combining the ensemble members’ predictions, including uniform weighting and weights chosen on a validation set. Mikolov *et al.* (2011a) extended the ensemble to include not just two models but a large array of models. It is also possible to pair a neural network with a maximum entropy model and train both jointly (Mikolov *et al.*, 2011b). This approach can be viewed as training

a neural network with an extra set of inputs that are connected directly to the output, and not connected to any other part of the model. The extra inputs are indicators for the presence of particular n -grams in the input context, so these variables are very high-dimensional and very sparse. The increase in model capacity is huge—the new portion of the architecture contains up to $|sV|^n$ parameters—but the amount of added computation needed to process an input is minimal because the extra inputs are very sparse.

12.4.5 Neural Machine Translation

Machine translation is the task of reading a sentence in one natural language and emitting a sentence with the equivalent meaning in another language. Machine translation systems often involve many components. At a high level, there is often one component that proposes many candidate translations. Many of these translations will not be grammatical due to differences between the languages. For example, many languages put adjectives after nouns, so when translated to English directly they yield phrases such as “apple red.” The proposal mechanism suggests many variants of the suggested translation, ideally including “red apple.” A second component of the translation system, a language model, evaluates the proposed translations, and can score “red apple” as better than “apple red.”

The earliest use of neural networks for machine translation was to upgrade the language model of a translation system by using a neural language model ([Schwenk et al., 2006; Schwenk, 2010](#)). Previously, most machine translation systems had used an n -gram model for this component. The n -gram based models used for machine translation include not just traditional back-off n -gram models ([Jelinek and Mercer, 1980; Katz, 1987; Chen and Goodman, 1999](#)) but also **maximum entropy language models** ([Berger et al., 1996](#)), in which an affine-softmax layer predicts the next word given the presence of frequent n -grams in the context.

Traditional language models simply report the probability of a natural language sentence. Because machine translation involves producing an output sentence given an input sentence, it makes sense to extend the natural language model to be conditional. As described in section 6.2.1.1, it is straightforward to extend a model that defines a marginal distribution over some variable to define a conditional distribution over that variable given a context C , where C might be a single variable or a list of variables. [Devlin et al. \(2014\)](#) beat the state-of-the-art in some statistical machine translation benchmarks by using an MLP to score a phrase t_1, t_2, \dots, t_k in the target language given a phrase s_1, s_2, \dots, s_n in the source language. The MLP estimates $P(t_1, t_2, \dots, t_k | s_1, s_2, \dots, s_n)$. The estimate formed by this MLP replaces the estimate provided by conditional n -gram models.

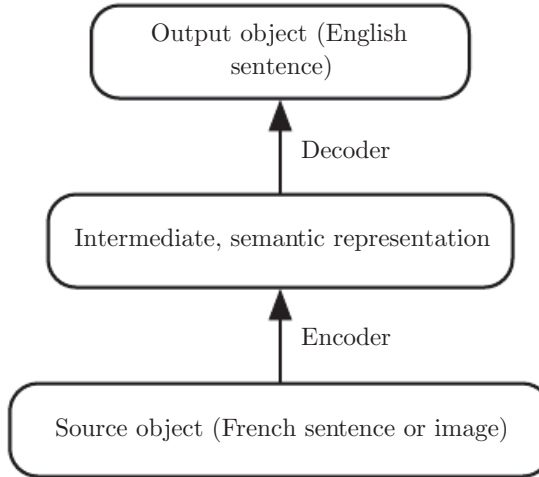


Figure 12.5: The encoder-decoder architecture to map back and forth between a surface representation (such as a sequence of words or an image) and a semantic representation. By using the output of an encoder of data from one modality (such as the encoder mapping from French sentences to hidden representations capturing the meaning of sentences) as the input to a decoder for another modality (such as the decoder mapping from hidden representations capturing the meaning of sentences to English), we can train systems that translate from one modality to another. This idea has been applied successfully not just to machine translation but also to caption generation from images.

A drawback of the MLP-based approach is that it requires the sequences to be preprocessed to be of fixed length. To make the translation more flexible, we would like to use a model that can accommodate variable length inputs and variable length outputs. An RNN provides this ability. Section 10.2.4 describes several ways of constructing an RNN that represents a conditional distribution over a sequence given some input, and section 10.4 describes how to accomplish this conditioning when the input is a sequence. In all cases, one model first reads the input sequence and emits a data structure that summarizes the input sequence. We call this summary the “context” C . The context C may be a list of vectors, or it may be a vector or tensor. The model that reads the input to produce C may be an RNN (Cho *et al.*, 2014a; Sutskever *et al.*, 2014; Jean *et al.*, 2014) or a convolutional network (Kalchbrenner and Blunsom, 2013). A second model, usually an RNN, then reads the context C and generates a sentence in the target language. This general idea of an encoder-decoder framework for machine translation is illustrated in figure 12.5.

In order to generate an entire sentence conditioned on the source sentence, the model must have a way to represent the entire source sentence. Earlier models were only able to represent individual words or phrases. From a representation

learning point of view, it can be useful to learn a representation in which sentences that have the same meaning have similar representations regardless of whether they were written in the source language or the target language. This strategy was explored first using a combination of convolutions and RNNs ([Kalchbrenner and Blunsom, 2013](#)). Later work introduced the use of an RNN for scoring proposed translations ([Cho et al., 2014a](#)) and for generating translated sentences ([Sutskever et al., 2014](#)). [Jean et al. \(2014\)](#) scaled these models to larger vocabularies.

12.4.5.1 Using an Attention Mechanism and Aligning Pieces of Data

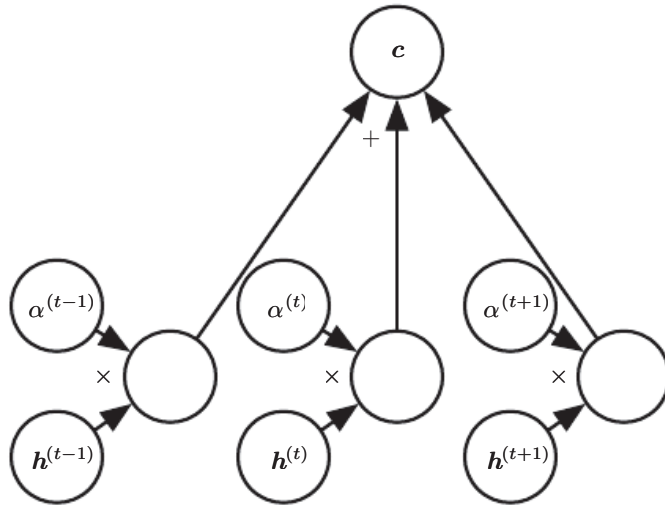


Figure 12.6: A modern attention mechanism, as introduced by [Bahdanau et al. \(2015\)](#), is essentially a weighted average. A context vector c is formed by taking a weighted average of feature vectors $\mathbf{h}^{(t)}$ with weights $\alpha^{(t)}$. In some applications, the feature vectors \mathbf{h} are hidden units of a neural network, but they may also be raw input to the model. The weights $\alpha^{(t)}$ are produced by the model itself. They are usually values in the interval $[0, 1]$ and are intended to concentrate around just one $\mathbf{h}^{(t)}$ so that the weighted average approximates reading that one specific time step precisely. The weights $\alpha^{(t)}$ are usually produced by applying a softmax function to relevance scores emitted by another portion of the model. The attention mechanism is more expensive computationally than directly indexing the desired $\mathbf{h}^{(t)}$, but direct indexing cannot be trained with gradient descent. The attention mechanism based on weighted averages is a smooth, differentiable approximation that can be trained with existing optimization algorithms.

Using a fixed-size representation to capture all the semantic details of a very long sentence of say 60 words is very difficult. It can be achieved by training a sufficiently large RNN well enough and for long enough, as demonstrated by [Cho et al. \(2014a\)](#) and [Sutskever et al. \(2014\)](#). However, a more efficient approach is to read the whole sentence or paragraph (to get the context and the gist of what

is being expressed), then produce the translated words one at a time, each time focusing on a different part of the input sentence in order to gather the semantic details that are required to produce the next output word. That is exactly the idea that Bahdanau *et al.* (2015) first introduced. The attention mechanism used to focus on specific parts of the input sequence at each time step is illustrated in figure 12.6.

We can think of an attention-based system as having three components:

1. A process that “*reads*” raw data (such as source words in a source sentence), and converts them into distributed representations, with one feature vector associated with each word position.
2. A list of feature vectors storing the output of the reader. This can be understood as a “*memory*” containing a sequence of facts, which can be retrieved later, not necessarily in the same order, without having to visit all of them.
3. A process that “*exploits*” the content of the memory to sequentially perform a task, at each time step having the ability put attention on the content of one memory element (or a few, with a different weight).

The third component generates the translated sentence.

When words in a sentence written in one language are aligned with corresponding words in a translated sentence in another language, it becomes possible to relate the corresponding word embeddings. Earlier work showed that one could learn a kind of translation matrix relating the word embeddings in one language with the word embeddings in another (Kočiský *et al.*, 2014), yielding lower alignment error rates than traditional approaches based on the frequency counts in the phrase table. There is even earlier work on learning cross-lingual word vectors (Klementiev *et al.*, 2012). Many extensions to this approach are possible. For example, more efficient cross-lingual alignment (Gouws *et al.*, 2014) allows training on larger datasets.

12.4.6 Historical Perspective

The idea of distributed representations for symbols was introduced by Rumelhart *et al.* (1986a) in one of the first explorations of back-propagation, with symbols corresponding to the identity of family members and the neural network capturing the relationships between family members, with training examples forming triplets such as (Colin, Mother, Victoria). The first layer of the neural network learned a representation of each family member. For example, the features for Colin

might represent which family tree Colin was in, what branch of that tree he was in, what generation he was from, etc. One can think of the neural network as computing learned rules relating these attributes together in order to obtain the desired predictions. The model can then make predictions such as inferring who is the mother of Colin.

The idea of forming an embedding for a symbol was extended to the idea of an embedding for a word by [Deerwester *et al.* \(1990\)](#). These embeddings were learned using the SVD. Later, embeddings would be learned by neural networks.

The history of natural language processing is marked by transitions in the popularity of different ways of representing the input to the model. Following this early work on symbols or words, some of the earliest applications of neural networks to NLP ([Miikkulainen and Dyer, 1991](#); [Schmidhuber, 1996](#)) represented the input as a sequence of characters.

[Bengio *et al.* \(2001\)](#) returned the focus to modeling words and introduced neural language models, which produce interpretable word embeddings. These neural models have scaled up from defining representations of a small set of symbols in the 1980s to millions of words (including proper nouns and misspellings) in modern applications. This computational scaling effort led to the invention of the techniques described above in section [12.4.3](#).

Initially, the use of words as the fundamental units of language models yielded improved language modeling performance ([Bengio *et al.*, 2001](#)). To this day, new techniques continually push both character-based models ([Sutskever *et al.*, 2011](#)) and word-based models forward, with recent work ([Gillick *et al.*, 2015](#)) even modeling individual bytes of Unicode characters.

The ideas behind neural language models have been extended into several natural language processing applications, such as parsing ([Henderson, 2003, 2004](#); [Collobert, 2011](#)), part-of-speech tagging, semantic role labeling, chunking, etc, sometimes using a single multi-task learning architecture ([Collobert and Weston, 2008a](#); [Collobert *et al.*, 2011a](#)) in which the word embeddings are shared across tasks.

Two-dimensional visualizations of embeddings became a popular tool for analyzing language models following the development of the t-SNE dimensionality reduction algorithm ([van der Maaten and Hinton, 2008](#)) and its high-profile application to visualization word embeddings by Joseph Turian in 2009.

12.5 Other Applications

In this section we cover a few other types of applications of deep learning that are different from the standard object recognition, speech recognition and natural language processing tasks discussed above. Part III of this book will expand that scope even further to tasks that remain primarily research areas.

12.5.1 Recommender Systems

One of the major families of applications of machine learning in the information technology sector is the ability to make recommendations of items to potential users or customers. Two major types of applications can be distinguished: online advertising and item recommendations (often these recommendations are still for the purpose of selling a product). Both rely on predicting the association between a user and an item, either to predict the probability of some action (the user buying the product, or some proxy for this action) or the expected gain (which may depend on the value of the product) if an ad is shown or a recommendation is made regarding that product to that user. The internet is currently financed in great part by various forms of online advertising. There are major parts of the economy that rely on online shopping. Companies including Amazon and eBay use machine learning, including deep learning, for their product recommendations. Sometimes, the items are not products that are actually for sale. Examples include selecting posts to display on social network news feeds, recommending movies to watch, recommending jokes, recommending advice from experts, matching players for video games, or matching people in dating services.

Often, this association problem is handled like a supervised learning problem: given some information about the item and about the user, predict the proxy of interest (user clicks on ad, user enters a rating, user clicks on a “like” button, user buys product, user spends some amount of money on the product, user spends time visiting a page for the product, etc). This often ends up being either a regression problem (predicting some conditional expected value) or a probabilistic classification problem (predicting the conditional probability of some discrete event).

The early work on recommender systems relied on minimal information as inputs for these predictions: the user ID and the item ID. In this context, the only way to generalize is to rely on the similarity between the patterns of values of the target variable for different users or for different items. Suppose that user 1 and user 2 both like items A, B and C. From this, we may infer that user 1 and

user 2 have similar tastes. If user 1 likes item D, then this should be a strong cue that user 2 will also like D. Algorithms based on this principle come under the name of **collaborative filtering**. Both non-parametric approaches (such as nearest-neighbor methods based on the estimated similarity between patterns of preferences) and parametric methods are possible. Parametric methods often rely on learning a distributed representation (also called an embedding) for each user and for each item. Bilinear prediction of the target variable (such as a rating) is a simple parametric method that is highly successful and often found as a component of state-of-the-art systems. The prediction is obtained by the dot product between the user embedding and the item embedding (possibly corrected by constants that depend only on either the user ID or the item ID). Let $\hat{\mathbf{R}}$ be the matrix containing our predictions, \mathbf{A} a matrix with user embeddings in its rows and \mathbf{B} a matrix with item embeddings in its columns. Let \mathbf{b} and \mathbf{c} be vectors that contain respectively a kind of bias for each user (representing how grumpy or positive that user is in general) and for each item (representing its general popularity). The bilinear prediction is thus obtained as follows:

$$\hat{R}_{u,i} = b_u + c_i + \sum_j A_{u,j} B_{j,i}. \quad (12.20)$$

Typically one wants to minimize the squared error between predicted ratings $\hat{R}_{u,i}$ and actual ratings $R_{u,i}$. User embeddings and item embeddings can then be conveniently visualized when they are first reduced to a low dimension (two or three), or they can be used to compare users or items against each other, just like word embeddings. One way to obtain these embeddings is by performing a singular value decomposition of the matrix \mathbf{R} of actual targets (such as ratings). This corresponds to factorizing $\mathbf{R} = \mathbf{UDV}'$ (or a normalized variant) into the product of two factors, the lower rank matrices $\mathbf{A} = \mathbf{UD}$ and $\mathbf{B} = \mathbf{V}'$. One problem with the SVD is that it treats the missing entries in an arbitrary way, as if they corresponded to a target value of 0. Instead we would like to avoid paying any cost for the predictions made on missing entries. Fortunately, the sum of squared errors on the observed ratings can also be easily minimized by gradient-based optimization. The SVD and the bilinear prediction of equation 12.20 both performed very well in the competition for the Netflix prize ([Bennett and Lanning, 2007](#)), aiming at predicting ratings for films, based only on previous ratings by a large set of anonymous users. Many machine learning experts participated in this competition, which took place between 2006 and 2009. It raised the level of research in recommender systems using advanced machine learning and yielded improvements in recommender systems. Even though it did not win by itself, the simple bilinear prediction or SVD was a component of the ensemble models

presented by most of the competitors, including the winners ([Töscher et al., 2009](#); [Koren, 2009](#)).

Beyond these bilinear models with distributed representations, one of the first uses of neural networks for collaborative filtering is based on the RBM undirected probabilistic model ([Salakhutdinov et al., 2007](#)). RBMs were an important element of the ensemble of methods that won the Netflix competition ([Töscher et al., 2009](#); [Koren, 2009](#)). More advanced variants on the idea of factorizing the ratings matrix have also been explored in the neural networks community ([Salakhutdinov and Mnih, 2008](#)).

However, there is a basic limitation of collaborative filtering systems: when a new item or a new user is introduced, its lack of rating history means that there is no way to evaluate its similarity with other items or users (respectively), or the degree of association between, say, that new user and existing items. This is called the problem of cold-start recommendations. A general way of solving the cold-start recommendation problem is to introduce extra information about the individual users and items. For example, this extra information could be user profile information or features of each item. Systems that use such information are called **content-based recommender systems**. The mapping from a rich set of user features or item features to an embedding can be learned through a deep learning architecture ([Huang et al., 2013](#); [Elkahky et al., 2015](#)).

Specialized deep learning architectures such as convolutional networks have also been applied to learn to extract features from rich content such as from musical audio tracks, for music recommendation ([van den Oörd et al., 2013](#)). In that work, the convolutional net takes acoustic features as input and computes an embedding for the associated song. The dot product between this song embedding and the embedding for a user is then used to predict whether a user will listen to the song.

12.5.1.1 Exploration Versus Exploitation

When making recommendations to users, an issue arises that goes beyond ordinary supervised learning and into the realm of reinforcement learning. Many recommendation problems are most accurately described theoretically as **contextual bandits** ([Langford and Zhang, 2008](#); [Lu et al., 2010](#)). The issue is that when we use the recommendation system to collect data, we get a biased and incomplete view of the preferences of users: we only see the responses of users to the items they were recommended and not to the other items. In addition, in some cases we may not get any information on users for whom no recommendation has been made (for example, with ad auctions, it may be that the price proposed for an

ad was below a minimum price threshold, or does not win the auction, so the ad is not shown at all). More importantly, we get no information about what outcome would have resulted from recommending any of the other items. This would be like training a classifier by picking one class \hat{y} for each training example x (typically the class with the highest probability according to the model) and then only getting as feedback whether this was the correct class or not. Clearly, each example conveys less information than in the supervised case where the true label y is directly accessible, so more examples are necessary. Worse, if we are not careful, we could end up with a system that continues picking the wrong decisions even as more and more data is collected, because the correct decision initially had a very low probability: until the learner picks that correct decision, it does not learn about the correct decision. This is similar to the situation in reinforcement learning where only the reward for the selected action is observed. In general, reinforcement learning can involve a sequence of many actions and many rewards. The bandits scenario is a special case of reinforcement learning, in which the learner takes only a single action and receives a single reward. The bandit problem is easier in the sense that the learner knows which reward is associated with which action. In the general reinforcement learning scenario, a high reward or a low reward might have been caused by a recent action or by an action in the distant past. The term **contextual** bandits refers to the case where the action is taken in the context of some input variable that can inform the decision. For example, we at least know the user identity, and we want to pick an item. The mapping from context to action is also called a **policy**. The feedback loop between the learner and the data distribution (which now depends on the actions of the learner) is a central research issue in the reinforcement learning and bandits literature.

Reinforcement learning requires choosing a tradeoff between **exploration** and **exploitation**. Exploitation refers to taking actions that come from the current, best version of the learned policy—actions that we know will achieve a high reward. Exploration refers to taking actions specifically in order to obtain more training data. If we know that given context x , action a gives us a reward of 1, we do not know whether that is the best possible reward. We may want to exploit our current policy and continue taking action a in order to be relatively sure of obtaining a reward of 1. However, we may also want to explore by trying action a' . We do not know what will happen if we try action a' . We hope to get a reward of 2, but we run the risk of getting a reward of 0. Either way, we at least gain some knowledge.

Exploration can be implemented in many ways, ranging from occasionally taking random actions intended to cover the entire space of possible actions, to model-based approaches that compute a choice of action based on its expected reward and the model’s amount of uncertainty about that reward.

Many factors determine the extent to which we prefer exploration or exploitation. One of the most prominent factors is the time scale we are interested in. If the agent has only a short amount of time to accrue reward, then we prefer more exploitation. If the agent has a long time to accrue reward, then we begin with more exploration so that future actions can be planned more effectively with more knowledge. As time progresses and our learned policy improves, we move toward more exploitation.

Supervised learning has no tradeoff between exploration and exploitation because the supervision signal always specifies which output is correct for each input. There is no need to try out different outputs to determine if one is better than the model’s current output—we always know that the label is the best output.

Another difficulty arising in the context of reinforcement learning, besides the exploration-exploitation trade-off, is the difficulty of evaluating and comparing different policies. Reinforcement learning involves interaction between the learner and the environment. This feedback loop means that it is not straightforward to evaluate the learner’s performance using a fixed set of test set input values. The policy itself determines which inputs will be seen. [Dudik *et al.* \(2011\)](#) present techniques for evaluating contextual bandits.

12.5.2 Knowledge Representation, Reasoning and Question Answering

Deep learning approaches have been very successful in language modeling, machine translation and natural language processing due to the use of embeddings for symbols ([Rumelhart *et al.*, 1986a](#)) and words ([Deerwester *et al.*, 1990; Bengio *et al.*, 2001](#)). These embeddings represent semantic knowledge about individual words and concepts. A research frontier is to develop embeddings for phrases and for relations between words and facts. Search engines already use machine learning for this purpose but much more remains to be done to improve these more advanced representations.

12.5.2.1 Knowledge, Relations and Question Answering

One interesting research direction is determining how distributed representations can be trained to capture the **relations** between two entities. These relations allow us to formalize facts about objects and how objects interact with each other.

In mathematics, a **binary relation** is a set of ordered pairs of objects. Pairs that are in the set are said to have the relation while those who are not in the set

do not. For example, we can define the relation “is less than” on the set of entities $\{1, 2, 3\}$ by defining the set of ordered pairs $S = \{(1, 2), (1, 3), (2, 3)\}$. Once this relation is defined, we can use it like a verb. Because $(1, 2) \in S$, we say that 1 is less than 2. Because $(2, 1) \notin S$, we can not say that 2 is less than 1. Of course, the entities that are related to one another need not be numbers. We could define a relation `is_a_type_of` containing tuples like `(dog, mammal)`.

In the context of AI, we think of a relation as a sentence in a syntactically simple and highly structured language. The relation plays the role of a verb, while two arguments to the relation play the role of its subject and object. These sentences take the form of a triplet of tokens

$$(\text{subject}, \text{verb}, \text{object}) \quad (12.21)$$

with values

$$(\text{entity}_i, \text{relation}_j, \text{entity}_k). \quad (12.22)$$

We can also define an **attribute**, a concept analogous to a relation, but taking only one argument:

$$(\text{entity}_i, \text{attribute}_j). \quad (12.23)$$

For example, we could define the `has_fur` attribute, and apply it to entities like `dog`.

Many applications require representing relations and reasoning about them. How should we best do this within the context of neural networks?

Machine learning models of course require training data. We can infer relations between entities from training datasets consisting of unstructured natural language. There are also structured databases that identify relations explicitly. A common structure for these databases is the **relational database**, which stores this same kind of information, albeit not formatted as three token sentences. When a database is intended to convey commonsense knowledge about everyday life or expert knowledge about an application area to an artificial intelligence system, we call the database a **knowledge base**. Knowledge bases range from general ones like Freebase, OpenCyc, WordNet, or Wikibase,¹ etc. to more specialized knowledge bases, like GeneOntology.² Representations for entities and relations can be learned by considering each triplet in a knowledge base as a training example and maximizing a training objective that captures their joint distribution ([Bordes et al., 2013a](#)).

¹Respectively available from these web sites: [freebase.com](#), [cyc.com/opencyc](#), [wordnet.princeton.edu](#), [wikiba.se](#)

²[geneontology.org](#)

In addition to training data, we also need to define a model family to train. A common approach is to extend neural language models to model entities and relations. Neural language models learn a vector that provides a distributed representation of each word. They also learn about interactions between words, such as which word is likely to come after a sequence of words, by learning functions of these vectors. We can extend this approach to entities and relations by learning an embedding vector for each relation. In fact, the parallel between modeling language and modeling knowledge encoded as relations is so close that researchers have trained representations of such entities by using *both* knowledge bases *and* natural language sentences (Bordes *et al.*, 2011, 2012; Wang *et al.*, 2014a) or combining data from multiple relational databases (Bordes *et al.*, 2013b). Many possibilities exist for the particular parametrization associated with such a model. Early work on learning about relations between entities (Paccanaro and Hinton, 2000) posited highly constrained parametric forms (“linear relational embeddings”), often using a different form of representation for the relation than for the entities. For example, Paccanaro and Hinton (2000) and Bordes *et al.* (2011) used vectors for entities and matrices for relations, with the idea that a relation acts like an operator on entities. Alternatively, relations can be considered as any other entity (Bordes *et al.*, 2012), allowing us to make statements about relations, but more flexibility is put in the machinery that combines them in order to model their joint distribution.

A practical short-term application of such models is **link prediction**: predicting missing arcs in the knowledge graph. This is a form of generalization to new facts, based on old facts. Most of the knowledge bases that currently exist have been constructed through manual labor, which tends to leave many and probably the majority of true relations absent from the knowledge base. See Wang *et al.* (2014b), Lin *et al.* (2015) and Garcia-Duran *et al.* (2015) for examples of such an application.

Evaluating the performance of a model on a link prediction task is difficult because we have only a dataset of positive examples (facts that are known to be true). If the model proposes a fact that is not in the dataset, we are unsure whether the model has made a mistake or discovered a new, previously unknown fact. The metrics are thus somewhat imprecise and are based on testing how the model ranks a held-out set of known true positive facts compared to other facts that are less likely to be true. A common way to construct interesting examples that are probably negative (facts that are probably false) is to begin with a true fact and create corrupted versions of that fact, for example by replacing one entity in the relation with a different entity selected at random. The popular precision at 10% metric counts how many times the model ranks a “correct” fact among the top 10% of all corrupted versions of that fact.

Another application of knowledge bases and distributed representations for them is **word-sense disambiguation** (Navigli and Velardi, 2005; Bordes *et al.*, 2012), which is the task of deciding which of the senses of a word is the appropriate one, in some context.

Eventually, knowledge of relations combined with a reasoning process and understanding of natural language could allow us to build a general question answering system. A general question answering system must be able to process input information and remember important facts, organized in a way that enables it to retrieve and reason about them later. This remains a difficult open problem which can only be solved in restricted “toy” environments. Currently, the best approach to remembering and retrieving specific declarative facts is to use an explicit memory mechanism, as described in section 10.12. Memory networks were first proposed to solve a toy question answering task (Weston *et al.*, 2014). Kumar *et al.* (2015) have proposed an extension that uses GRU recurrent nets to read the input into the memory and to produce the answer given the contents of the memory.

Deep learning has been applied to many other applications besides the ones described here, and will surely be applied to even more after this writing. It would be impossible to describe anything remotely resembling a comprehensive coverage of such a topic. This survey provides a representative sample of what is possible as of this writing.

This concludes part II, which has described modern practices involving deep networks, comprising all of the most successful methods. Generally speaking, these methods involve using the gradient of a cost function to find the parameters of a model that approximates some desired function. With enough training data, this approach is extremely powerful. We now turn to part III, in which we step into the territory of research—methods that are designed to work with less training data or to perform a greater variety of tasks, where the challenges are more difficult and not as close to being solved as the situations we have described so far.